DESIGN AND SYNTHESIS OF NEW ULK1/2 INHIBITOR AS ANTICANCER AGENT

A Thesis submitted to Gujarat Technological University

for the Award of

DOCTOR OF PHILOSOPHY

in

Pharmacy Discipline

By

Sidat Parin Salim

[189999901017]

Under supervision of

Dr. Malleshappa N. Noolvi

GUJARAT TECHNOLOGICAL UNIVERSITY
AHMADABAD

[March-2024]

DECLARATION

I declare that the thesis entitled **"Design and Synthesis of New ULK1/2 inhibitor as Anticancer Agent"** submitted by me for the degree of Doctor of Philosophy is the record of research work carried out by me during the period from **June 2018 to March 2024** under the supervision of **Dr. Malleshappa N. Noolvi** and this has not formed the basis for the award of any degree, diploma, associateship, fellowship, titles in this or any other University or other institution of higher learning.

I further declare that the material obtained from other sources has been duly acknowledged in the thesis. I shall be solely responsible for any plagiarism or other irregularities, if noticed in the thesis.

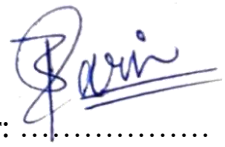

Signature of the Research Scholar: …… Date: 11-03-2024

Name of Research Scholar: **Ms. Parin S. Sidat**

Place: Ahmedabad

CERTIFICATE

I certify that the work incorporated in the thesis **"Design and Synthesis of New ULK1/2 inhibitor as Anticancer Agent"** submitted by **Ms. Parin S. Sidat** was carried out by the candidate under my supervision/guidance. To the best of my knowledge: (i) the candidate has not submitted the same research work to any other institution for any degree/diploma, Associateship, Fellowship or other similar titles (ii) the thesis submitted is a record of original research work done by the Research Scholar during the period of study under my supervision, and (iii) the thesis represents independent research work on the part of the Research Scholar.

Signature of Supervisor: 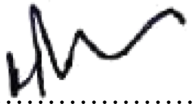 Date: 11-03-2024

Name of Supervisor: **Dr. Malleshappa N. Noolvi**

Place: Ahmedabad

Course-work Completion Certificate

This is to certify that **Ms. Parin S. Sidat** enrolment no. **189999901017** is enrolled for PhD program in the branch **Pharmacy** of Gujarat Technological University, Ahmedabad.

(Please tick the relevant option(s))

☐ He/She has been exempted from the course-work (successfully completed during M.PhilCourse)

☐ He/She has been exempted from Research Methodology Course only (successfully completed during M.Phil Course)

☑ He/She has successfully completed the PhD course work for the partial requirement for theaward of PhD Degree. His/ Her performance in the course work is as follows-

Grade Obtained in Research Methodology [PH001]	Grade Obtained in Self-Study Course/ Contact Program [PHD22-03]
BB	**AB**

Supervisor's Sign: 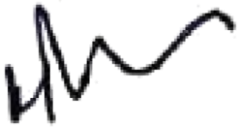

Name of Supervisor: **Dr. Malleshappa N. Noolvi**

DrillBit

The Report is Generated by DrillBit Plagiarism Detection Software

Submission Information

Author Name	Sidat Parin Salim
Title	“Design and Synthesis of new ULK1/2 inhibitor..
Paper/Submission ID	1077310
Submitted by	parinsidat12@gmail.com
Submission Date	2023-11-03 13:56:57
Total Pages	259
Document type	Thesis

Result Information

Similarity **9 %**

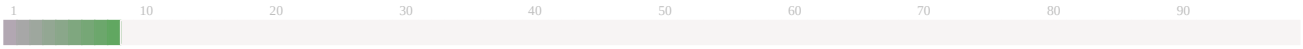

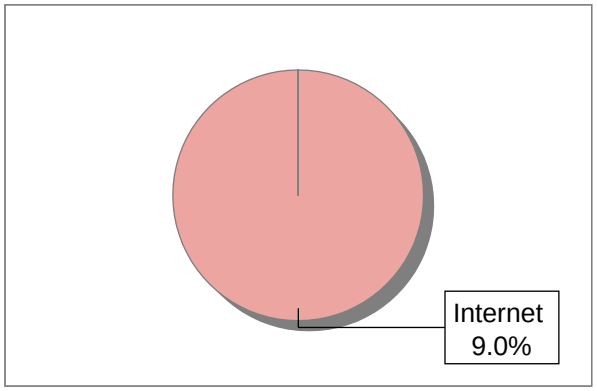

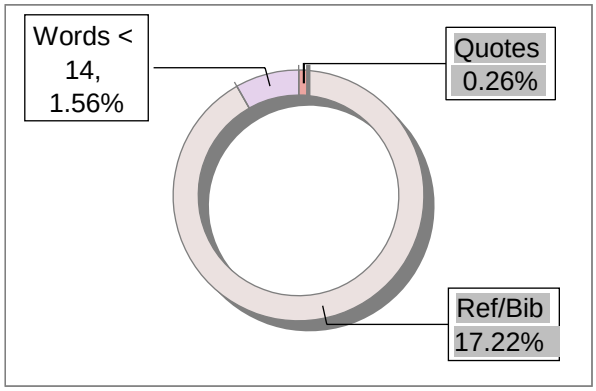

Exclude Information

Quotes	Not Excluded
References/Bibliography	Not Excluded
Sources: Less than 14 Words Similarity	Not Excluded
Excluded Source	**0 %**
Excluded Phrases	Not Excluded

A Unique QR Code use to View/Download/Share Pdf File

Research Scholar: .....

Dr. Malleshappa N. Noolvi

Originality Report Certificate

It is certified that PhD Thesis titled **"Design and Synthesis of New ULK1/2 inhibitor as Anticancer Agent"** by **Ms. Parin S. Sidat** has been examined by us. We undertake the following:

a. Thesis has significant new work / knowledge as compared already published or are under consideration to be published elsewhere. No sentence, equation, diagram, table, paragraph or section has been copied verbatim from previous work unless itis placed under quotation marks and duly referenced.

b. The work presented is original and own work of the author (i.e. there is no plagiarism). No ideas, processes, results or words of others have been presented as Author own work.

c. There is no fabrication of data or results which have been compiled / analyzed.

d. There is no falsification by manipulating research materials, equipment or processes, or changing or omitting data or results such that the research is not accurately represented in the research record.

e. The thesis has been checked using **DrillBit Software** (copy of originality report attached) and found within limits as per GTU Plagiarism Policy and instructions issued from time to time (i.e. permitted similarityindex <=10%).

Signature of the Research Scholar: ..... Date: 11-03-2024

Name of Research Scholar: **Ms. Parin S. Sidat**

Signature of Supervisor: ..... Date: 11-03-2024

Name of Supervisor: **Dr. Malleshappa N. Noolvi**

Place: Ahmedabad.....

Ph.D. Thesis Non-Exclusive License to
GUJARAT TECHNOLOGICAL UNIVERSITY

In consideration of being a Research Scholar at Gujarat Technological University, and in the interests of the facilitation of research at the University and elsewhere, I, **Ms. Parin S. Sidat** having (Enrollment No.) **189999901017** hereby grant a non-exclusive, royalty free and perpetual license to the University on the following terms:

a. The University is permitted to archive, reproduce and distribute my thesis, in whole or in part, and/or my abstract, in whole or in part (referred to collectively as the "Work") anywhere in the world, for non-commercial purposes, in all forms of media;
b. The University is permitted to authorize, sub-lease, sub-contract or procure any of theacts mentioned in paragraph (a);
c. The University is authorized to submit the Work at any National / International Library,under the authority of their "Thesis Non-Exclusive License";
d. The Universal Copyright Notice (©) shall appear on all copies made under the authorityof this license;
e. I undertake to submit my thesis, through my University, to any Library and Archives. Any abstract submitted with the thesis will be considered to form part of the thesis.
f. I represent that my thesis is my original work, does not infringe any rights of others, including privacy rights, and that I have the right to make the grant conferred by this non-exclusive license.
g. If third party copyrighted material was included in my thesis for which, under the terms of the Copyright Act, written permission from the copyright owners is required, I haveobtained such permission from the copyright owners to do the acts mentioned in paragraph (a) above for the full term of copyright protection.
h. I understand that the responsibility for the matter as mentioned in the paragraph (g) rests with the authors / me solely. In no case shall GTU have any liability for any acts/ omissions / errors / copyright infringement from the publication of the said thesis or otherwise.

i. I retain copyright ownership and moral rights in my thesis, and may deal with the copyright in my thesis, in any way consistent with rights granted by me to my University in this non-exclusive license.

j. GTU logo shall not be used /printed in the book (in any manner whatsoever) being published or any promotional or marketing materials or any such similar documents.

k. The following statement shall be included appropriately and displayed prominently inthe book or any material being published anywhere: "The content of the publishedwork is part of the thesis submitted in partial fulfilment for the award of the degree of Ph.D.in **Pharmacy** of the Gujarat Technological University".

l. I further promise to inform any person to whom I may hereafter assign or license my copyright in my thesis of the rights granted by me to my University in this nonexclusivelicense. I shall keep GTU indemnified from any and all claims from the Publisher(s) orany third parties at all times resulting or arising from the publishing or use or intendeuse of the book / such similar document or its contents.

m. I am aware of and agree to accept the conditions and regulations of Ph.D. including allpolicy matters related to authorship and plagiarism.

Date: 11-03-2024

Place: ..... Ahmedabad

Signature of the Research Scholar :……..

Recommendation of the Supervisor: ……..

Thesis Approval Form

The viva-voce of the PhD Thesis submitted by **Ms. Parin S. Sidat (Enrollment No.189999901017)** entitled **"Design and Synthesis of New ULK1/2 inhibitor as Anticancer Agent"** was conducted on 11-03-2024. at Gujarat Technological University.

(Please tick any one of the following options)

☑ The performance of the candidate was satisfactory. We recommend that he/she be awarded the PhD degree.

☐ Any further modifications in research work recommended by the panel after 3 months from the date of first viva-voce upon request of the Supervisor or request of Independent Research Scholar after which viva-voce can be re-conducted by the same panel again.

(briefly specify the modifications suggested by the panel)

☐ The performance of the candidate was unsatisfactory. We recommend that he/she should not be awarded the PhD degree.

(The panel must give justifications for rejecting the research work)

Dr. Malleshappa N. Noolvi
.....
Name and Signature of Supervisor with Seal

Dr. Srinivas Joshi
.....
1) (External Examiner-1) Name and Signature

Dr. Veeresh Virapur
.....
2) (External Examiner-1) Name and Signature

"Design and Synthesis of New ULK1/2 Inhibitor as Anticancer Agent"

Submitted By
Sidat Parin Salim
Supervised By
DR. M. N. NOOLVI **M. Pharma; Ph. D**
Professor and PG Coordinator.

ABSTRACT

Autophagy initiation kinase 1 and 2 (also known as ULK1/2 in humans) is a protein kinase that plays a key role in the initiation of the autophagy process. Autophagy is a cellular process in which the cell breaks down and recycles its components, such as damaged or unnecessary proteins and organelles. This process helps the cell to maintain homeostasis and can also play a role in response to stress, such as starvation. In autophagy machinery various genes and enzymes are involved, among the most promising enzymes is ULK1 (Unc-51-like autophagy activating kinase 1). ULK1 is activated by various stress signals, such as nutrient deprivation, and phosphorylates other proteins to initiate the formation of the autophagosome, which is the membrane-bound structure that encloses the material to be degraded during autophagy. ULK1 has been found to play a role in the development and progression of non-small cell lung cancer (NSCLC). Research has shown that ULK1 is involved in promoting tumor cell proliferation, invasion, and resistance to chemotherapy and radiation therapy. ULK2 (Unc-51 like autophagy activating kinase 2) may have additional functions beyond autophagy regulation, such as in cell migration, embryonic development, and neuronal survival. Inhibiting ULK1 has been found to sensitize NSCLC cells to chemotherapy and radiation, suggesting that targeting ULK1 may be a promising strategy for treating NSCLC. In the present research proposal aims at the design of new series of heterocyclic rings like Thiadiazole, quinazoline, benzimidazole, pyrimidine and aniline derivatives as ULK ½ inhibitors. Initial *In-silico* studies of Ligand based pharmacophore modelling, Molecular docking, Molecular dynamic simulation, DFT and Drug-likeness assessment were done to strengthen the rationale of the study. Based on the literature

review different synthetic routes were adopted to synthesize the a for mentioned heterocyclic compounds. A new series of nitrogen and sulfur-containing heterocyclic compounds were synthesized and characterized by using spectral analysis such as IR, ^{1}H NMR, and MASS. The synthesized compounds were tested for *In-vitro* 96 well MTT assay on the A549 cell line (NSCLC) with Cisplatin as positive control. Compounds **12(b-IV), 12(c-II), 12(b-I), 12(d-IV), 12(f-IV)** and **12(a-II)** showed maximum inhibition IC_{50} values respectively (12.2 μM, 16.35 μM, 20.61 μM, 20.76 μM, 22.01 μM, and 32.04 μM) against Non-small cell lung cancer (A549) cell line, which is more potent or equivalent to Cisplatin (33.09 μM) as standard drug.

Keywords: Anticancer, Autophagy 1,3,4-Thiadiazole analogs, ULK inhibitors, MTT Assay.

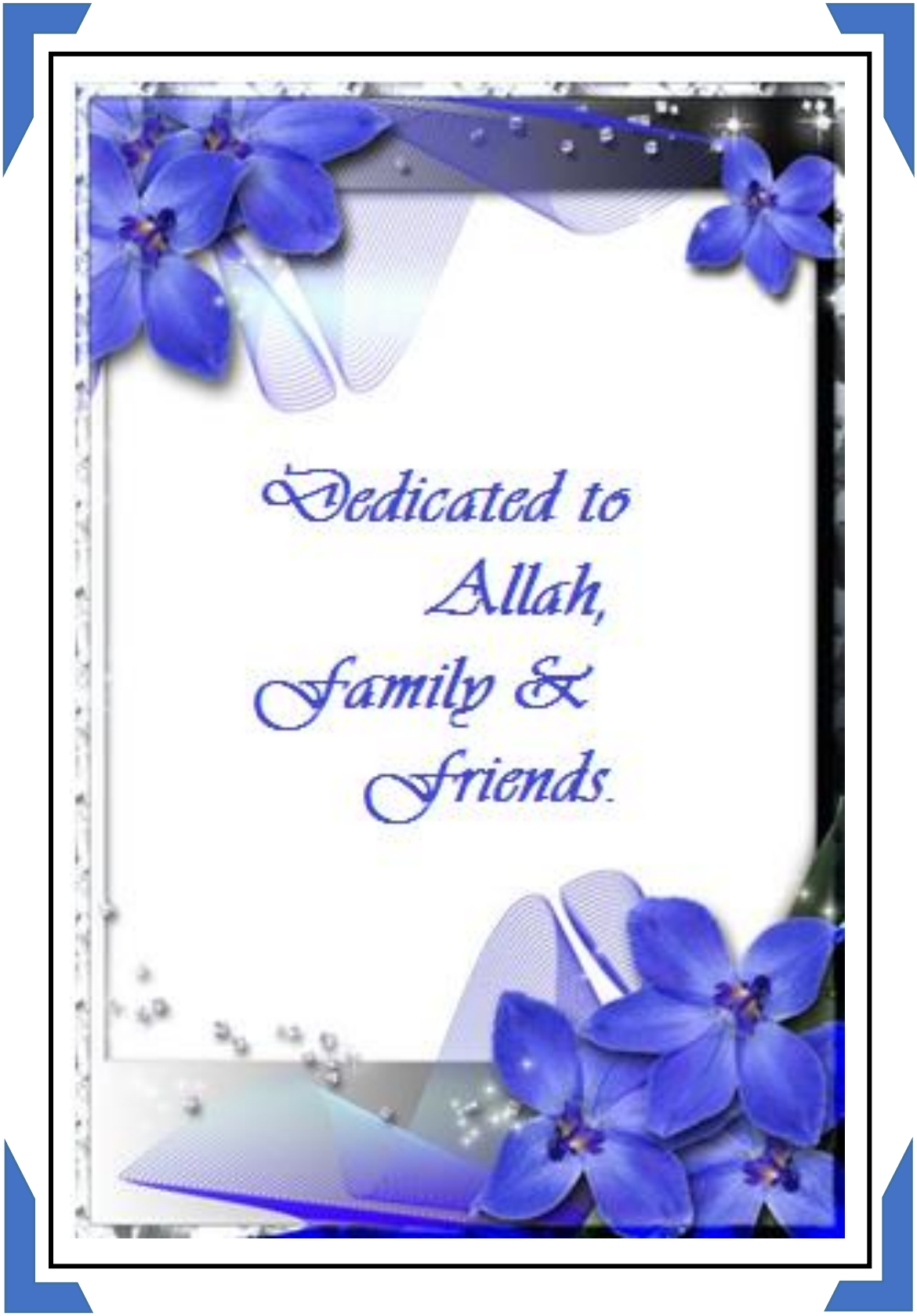
Dedicated to
Allah,
family &
friends.

ACKNOWLEDGEMENT

Any successful task is not an individual's effort but it is a joint venture of many people who put in their mind and soul for the completion of that work and it would not be justifiable to forget those people's dedication and efforts while sailing in the boat of success, so here I would like to thank those sailors who have kept my spirits up to sail in even through the stormy sea making my task to end up safely on the shore of success. Above all I am thankful to the Supreme Power, God, for giving me strength and patience to carry out this piece of work.

I offer flowers of gratitude to the almighty ***Allah*** *who has been the source of strength in my life.*

Thanks, are the small word for my beloved parents, Mr. Salim Sidat and Mrs. Hawa Sidat, and my brother Salman, Sajid, Samir, Sarfraz and my sister Dr. Farah, My Jiju Mr. Habib, and all my family members who not only supported me but also inspired me during the course of my study.

I am indebted to the deep inspirer and my esteemed guide ***Dr. M. N. Noolvi,*** *Professor, Head of Department of Pharmaceutical Chemistry. Their words of advice have been etched in my heart and I will always endeavor to hold up her ideas. Their simplicity, untiring and meticulous guidance, caring attitude and provision of fearless work environment will be cherished in all walks of my life. I thank to both of them for bringing out the best in me. I would heartily thanks to my DPC Member* ***Dr. Anuradha Gajjar*** ***and*** ***Dr. D. B. Mesharam*** *for guided me suggest me and correct me. I have never forgot their advices during my whole journey of Ph. D.*

My heartfelt thanks to ***Dr. M. N. Noolvi*** *Principal, Shree Dhanvantary Pharmacy College, Kim, Surat for providing all the required infrastructure and facilities needed to complete my work and post-graduation. I express my profound sense of gratitude to Research Scholar, Shree Dhanvantary Pharmaceutical Analysis & Research center (SDPARC), Kim, Surat for helping me during my project. I am extremely grateful to him.*

I am also thankful to our college professor ***Dr. Uttam More, Dr. Anand Deshmukh, Dr. Manish Goyani, Dr Pallavi K.J.*** *I would like to pay my humble and an authentic credit regards to the noble support provided by library staff especially Dr. Dilip*

Vasava of Shree Dhanvantary Pharmacy College, Kim.

*The buddy system is essential to your survival. thanks for tolerating my idiosyncrasies and crazy habits. I owe special thanks to my friends Hina, Velenti, Sagufta, Goshiya, Vijay Sir, Rahul Sir, Sanket Sir, Vishal Sir, Rohan Sir, Safwan, Azmin, Rozina, Tasnim, Anjum, Payal. and My dear students Aishiq, Kaleem, Kaif, Meet, Jhanvi, and Feni. I would like to special thanks to **Fazal (Patel Saheb)** who always encourage me.*

I would also like thanks to my bachelor degree college staff especially Mr. Sitansu, Mr. Hiten Yadav, Mr. Tularam, Mr. Arindam Paul, Mrs. Madhuri, Mrs. Rupa, Ms. Alisha and my friends, Hemantika, Sahbnam of Rofel College of Pharmacy. For helping me throughout my project work in all type of phases which I have faced during my work. Moments of joy shared with all of them will remain fresh in my memory.

I would like thanks to all lab technician. I would like to thank Nistha madam and all masi for their helpful approach.

Besides this, I Thank several people have knowingly and unknowingly helped me in the successful completion of this project.

Parin Salim Sidat.

TABLE OF CONTENT

LIST OF ABBREVIATION

Sr. No.	Abbreviation	Full Name
1	Ar	Aromatic
2	%w/v	Percentage weight by volume
3	%w/w	Percentage weight by weight
4	^{0}C	Degree centigrade (Unit of temperature)
5	GI_{50}	50% growth inhibition
6	IC_{50}	50% inhibitory concentration
7	CCl_4	Carbon Tetrachloride
8	V	Voltage
9	Rb	Retinoblastoma
10	UV	Ultra-violate
11	DNA	Deoxyribonucleic acid
12	RNA	Ribonucleic Acid
13	SV 40	Simian Virus 40
14	ULK	Human Autophagy initiation kinase
15	TLC	Thin Layer Chromatography
16	MP	Melting Point
17	^{1}H NMR	Proton nuclear magnetic resonance
18	DIEM	N, N Diethyl isopropyl ethylamine

19	THF	Tetrahydrofuran
20	KBr	Potassium Bromide
21	ppm	Parts per Million
22	EtOH	Ethanol
23	NaOH	Sodium Hydroxide
24	μg	Microgram
25	nM	Nanometer
26	TMS	Trimethyl Silane

LIST OF FIGURE

LIST OF TABLE

1. Introduction

Medicinal chemistry is a science that combines chemistry, particularly synthetic organic chemistry, pharmacology, and numerous other biological specialties, and is concerned with the molecular elements of drug action, such as interactions with drug targets from both the drug and the target's perspectives, the link of drug chemical structure to drug action, and the impact of metabolism on drug structure and hence action. "In the field of medicinal chemistry, which predominantly revolves around small organic compounds, it encompasses synthetic organic chemistry, exploration of natural products, and extensive utilization of computational chemistry. These endeavours are closely intertwined with chemical biology, enzymology, and structural biology, all with a shared objective of unearthing and advancing novel therapeutic agents. In practical terms, this discipline involves the chemical facets of identification, followed by the systematic and comprehensive synthetic alteration of emerging chemical entities to render them suitable for therapeutic use." It encompasses the synthetic and computational aspects of investigating existing medications and substances to enhance their biological activities and attributes, specifically by comprehending their structure-activity relationships (SAR). Pharmaceutical chemistry is primarily concerned with ensuring the quality of drugs and the suitability of pharmaceutical products for their intended applications. Within the realm of biological interfaces, medicinal chemistry merges as part of a multidisciplinary field, with a focus on organic, physical, and computational sciences, in conjunction with biological disciplines such as biochemistry, molecular biology, pharmacognosy, pharmacology, toxicology, as well as veterinary and human medicine. Additionally, project management, statistical analysis, and pharmaceutical business practices play a pivotal role in the systematic modification of identified chemical compounds. Consequently, medicinal chemistry occupies a central position and is poised to continue its essential role in the process of discovering new drugs.

Few medical diagnoses evoke as much fear as cancer does in most individuals. Cancer is often perceived as a disease that is difficult to treat, characterized by severe pain and often considered incurable. This perspective of cancer, although prevalent, is overstated and over-generalized. Cancer is unquestionably a serious and potentially fatal disease. For example, it is the leading cause of death in those under the age of 85 worldwide, and the second greatest cause of death in people over the age of 85. In the following year, there will be 1.3 billion new cases of cancer, with over 500,000 fatalities as a result. However, it is a common fallacy that all types of cancer are incurable and fatal. The truth is that there are many different varieties of cancer, many of which can now be properly treated in order

to eliminate, lessen, or slow the effects of disease on people' lives. While a cancer diagnosis can still leave patients feeling helpless and out of control, there are many reasons for hope today rather than despondency. Despite advances in diagnosis and treatment, overall patient survival remains low. Until recently, patients' typical treatment options included surgery, chemotherapy, radiation, and endocrine therapy. Three types of pathways are mostly involved in cancer cell killing. Apoptosis, necrosis, and autophagy all play important roles in the cell death process. Aside from that, autophagic cell death is quite useful in nutrient-depleted environments. Some kind of target is required for autophagy induction. ULK1/2 inhibitors are the most useful targets in autophagic processes. At the moment, this target is mostly employed to activate autophagy. Under starvation conditions, the mTOR inhibitor is inactive while ULK ("Human autophagy initiation kinase") is active. The primary goal of this research is to design and synthesize some new ULK1/2 inhibitors as anti-cancer medicines. Here, we are proposed Some heterocyclic moieties contain molecules. We are using Thiadiazole, Quinazoline, Benzimidazole, and some other aniline derivatives for proposing a novel molecule. Before, synthesizing the molecule we used some computational approaches for finding stable ligands. We found a better ligand by using an ***In silico*** study. From that, we are performing Pharmacophore modeling, MD Simulation, and Docking. Pharmacophore models can be employed to identify possible drug interactions with drug-metabolizing enzymes by comparing the similar chemical groups in test compounds to those found in drug molecules with established ADME-toxicity profiles. Molecular dynamics (MD) is another approach for the investigation of the atom's location in space. MD, or Molecular Dynamics, is commonly utilized to model the time-evolving movements (trajectories) of biological macromolecules, such as proteins and RNAs. Forces operating on atoms (particles) in standard MD implementations are calculated as derivatives of potentials. The technique of molecular docking is employed to replicate the interaction between a small molecule and a protein at the atomic scale. This approach enables us to understand the behaviour of small molecules within binding sites of target proteins and uncover essential biochemical processes. All factors are quite useful in determining ligand stability and potency. Drug ability indicators such as Lipinski and bioactivity score are also used in this study.

1. INTRODUCTION

1.1 Cancer

The field of oncology, which encompasses the study of cancer, represents the collective efforts of numerous doctors and scientists worldwide, delving into disciplines such as anatomy, physiology, chemistry, and epidemiology. The term "cancer" traces its origins back to the ancient Greek physician Hippocrates, often revered as the "Father of Medicine." Hippocrates employed the words "carcinons" and "carcinomas" to distinguish between non-ulcer forming and ulcer-forming tumors.

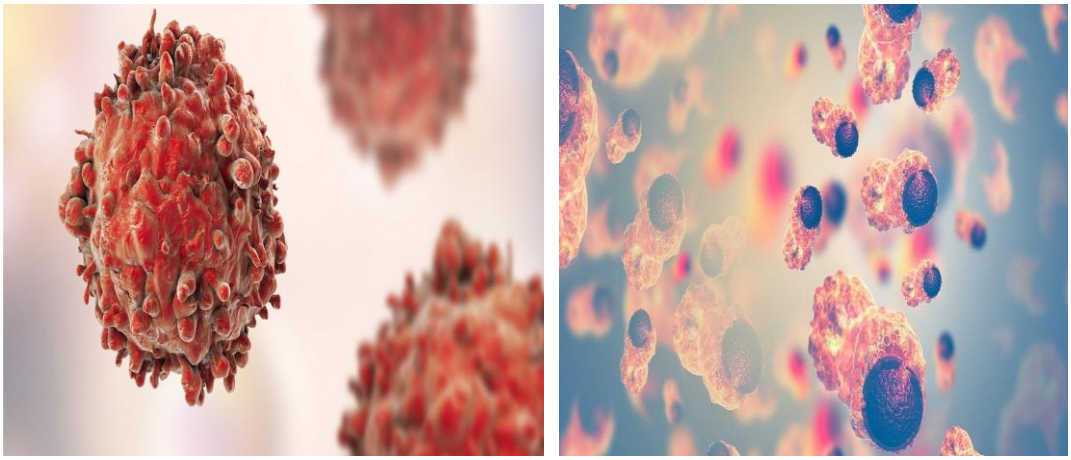

Fig.1. Cancer Cell

In developed countries, cancer stands as the second leading cause of death. In 2020, it was projected that there would be 1,685,210 new cases of cancer, with 595,690 resulting in fatalities globally. Oncogenes and tumour suppressor genes.

- **Oncogenes** These genes lead to uncontrolled cell growth and the development of cancerous cells.
- **Tumour suppressor** genes these genes are typically healthy genes responsible for regulating cell division, correcting DNA errors, and signaling when a cell should undergo apoptosis (cell death). When tumor suppressor genes malfunction, cells may proliferate uncontrollably, potentially resulting in the development of cancer.

Although the cancer cell cycle utilizes the same mechanisms as a regular cell, this procedure experiences profound dysregulation. The standard mammalian cell cycle encompasses five phases, interspersed with interphases lasting at least 12 hours. These so-called "resting" phases or gap stages are misleadingly named, as they involve periods of intense protein synthesis. Proteins are crucial, as they ensure the isolating

cell attains sufficient size for division. Interphase recurs four times in a cycle - Gaps 0, 1, and 2, as well as the Synthesis (S) phase.

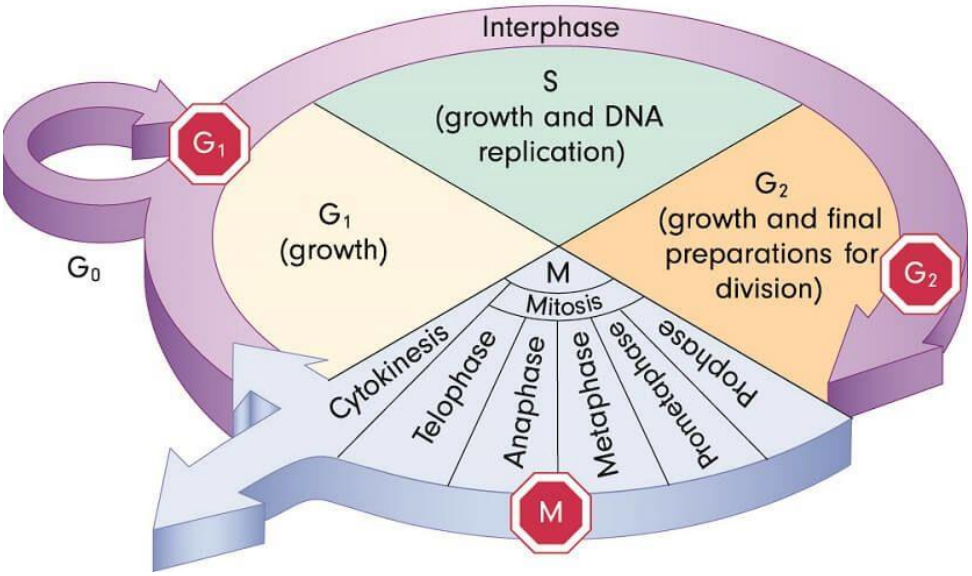

Fig.2. Cell Cycle

- During Gap 0 (G0), the cell is considered out of the cycle, constituting the sole "resting" interphase. The duration of a cell's stay in this quiescent period is dictated by our non-coding DNA. Non-replicating cells may either temporarily (quiescent cells) or permanently (senescent cells) refrain from dividing.
- In Gap 1 (G1), cells enlarge and generate more proteins. A G1/S checkpoint ensures the cell is prepared to progress to the subsequent phase - Synthesis.
- Synthesis phase (S), the cell must duplicate its DNA, as it will divide to yield two daughter cells, each requiring a complete set of chromosomes for survival.
- Gap 2 (G2) marks the conclusion of DNA replication and provides another interval for additional protein production, affording the cell another opportunity to increase in size. Another checkpoint verifies the cell's readiness to divide, which occurs in the M phase.
- Mitosis (M) is the phase where the cell stops growing and directs its resources toward dividing into two daughter cells with identical genetic material. This phase involves a series of steps, including prophase, prometaphase, metaphase, anaphase, telophase, and cytokinesis. In the presence of errors detected at the checkpoints, a healthy cell typically undergoes apoptosis, leading to self-destruction. Mitosis in

mammals lasts only an hour or two and includes a metaphase checkpoint to ensure smooth progress. In the event of discrepancies at these checkpoints, a normal cell generally undergoes apoptosis and self-destructs. However, cancer cell partition does not adhere to the controlling checkpoint norms.

In most cancer cases, genetic mutations occur in genes responsible for encoding regulatory proteins that control the cell cycle. A prominent example is the malfunction of the p53 protein, which happens in more than 60% of cancers. Other regulatory molecules, like cyclin-dependent kinases, interact with proteins called cyclins and, by doing so, either start or halt the cell cycle. An illustration of the cancer cell cycle would reveal irregularities in checkpoints, growth, division, and cell death (apoptosis). A gene that interferes with the production of regulatory proteins can result in unceasing cell division and the incapacity of a compromised cell to undergo self-destruction. Given that all daughter cells inherit the same DNA, a cascading effect ensues. Cancer cells do not proliferate more rapidly than normal cells, but they lack self-destruct mechanisms and exhibit unrestricted division potential.

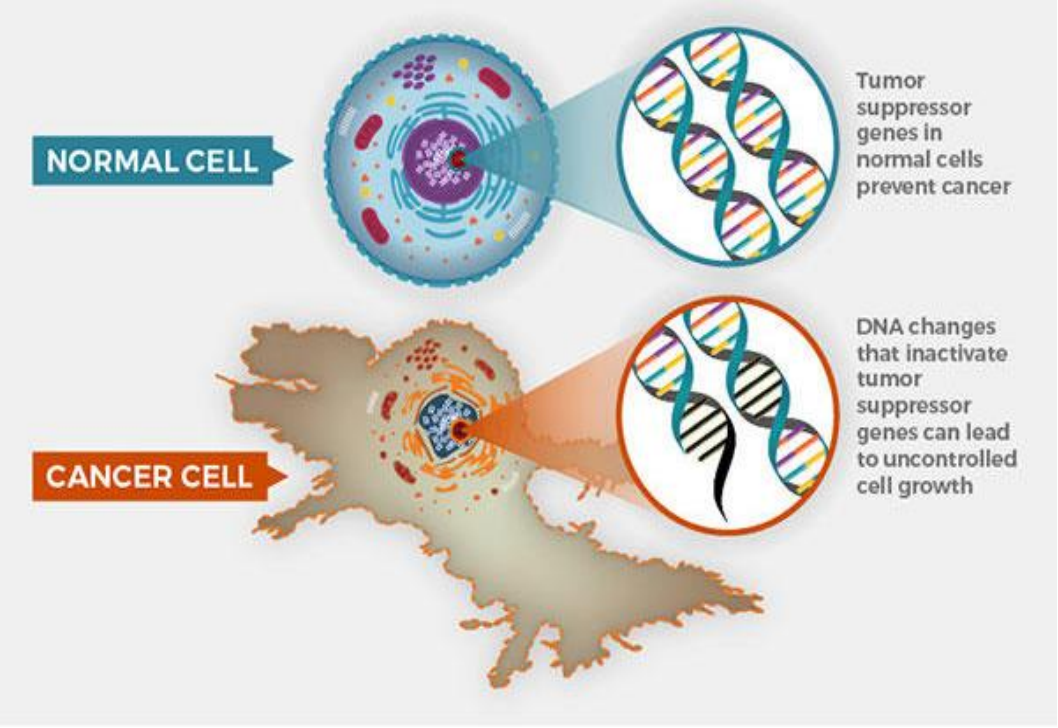

Fig.3. Cell Differentiation

Some types of cancer cells divide and grow in a typical fashion but possess significantly prolonged lifespans compared to their usual duration. Cell division is the process through which a cell transmits its genetic material to its two offspring cells,

effectively creating clones or duplicates of itself. Occasionally, this process goes awry, resulting in genetic variations or issues in DNA replication during cell division. Cancer or neoplasm manifests as the formation of a tumor. A tumor constitutes an abnormal mass of tissue; its growth is disorganized and persists even after the cessation of the stimulus that incited the change. Tumors can arise in any part of the body. (1)

1.1.1 Tumours are of two kinds.

1.1.1.1 Benign tumours (Non-malignant tumours)

1.1.1.2 Cancerous tumours (malignant tumours)

1.1.1.1 Benign tumours (Non-malignant tumours)

Benign tumours exhibit slow growth. They remain localized at their point of origin within the body and do not metastasize to other regions. The growth of these tumours can lead to compression of adjacent organs, potentially causing discomfort or pain. It's worth noting that benign tumours have the potential to transform into malignant tumours. They are typically easily detected and can be surgically removed.

1.1.1.2 Cancerous tumours (malignant tumours)

Initially, cancerous tumours grow slowly and may not manifest noticeable symptoms. At this stage, their presence may go unnoticed. However, as they progress, these tumours demonstrate the capacity for uncontrolled proliferation, spreading to various parts of the body, and infiltrating surrounding tissues much like the roots of a tree. This leads to the formation of secondary tumours and further complications. Ultimately, these tumours can be fatal, as they interfere with the body's essential life processes, contributing to the person's demise.

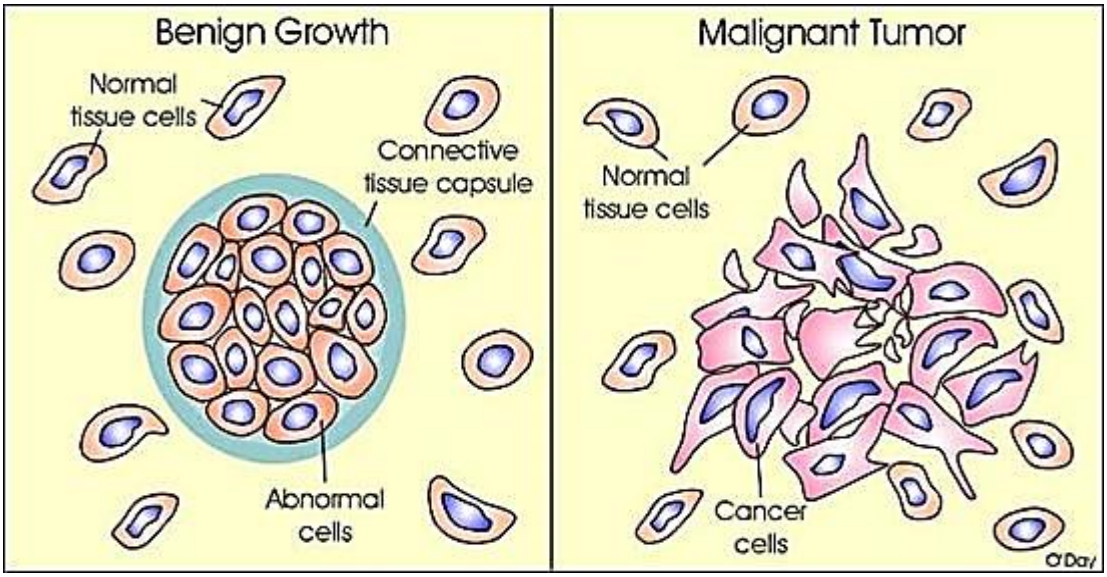

Fig.4. Types of Tumor

1.1.2 Sign and symptoms of cancer

1. A sore that does not heal.
2. Change in bowel or bladder habits.
3. Cough and hoarseness.
4. Unexpected weight loss.
5. Loss of appetite.
6. Low grade fever persists.
7. A hard tissue (lump) which grows larger, changes its size.
8. Unusual bleeding or discharge.
9. Indigestion or difficulty swallowing
10. Excessive loss of blood during menstruation period in women.

1.1.3 Causes of cancer

Cancer is neither hereditary nor contagious. It is influenced by factors known as carcinogens. Identifying the specific cause of cancer in an individual is often challenging because most cancers have multiple contributing factors. While cancer is not an infectious disease that can be transmitted by proximity to an affected person, certain oncoviruses and cancer-causing bacteria can contribute to its development. (2-5)

Fig.5.Causes of Cancer

1.1.3.1 Chemicals

Various chemicals are implicated in cancer development, including nicotine, caffeine, pesticides, asbestos, nickel, dyes, and artificial sweeteners. Consuming alcohol and exposure to substances like Benzene, Dioxane, CCl4, Clofibrate, and Aniline can elevate cancer risks.

1.1.3.2 Radiations

Radiation exposure is another cancer-causing factor. This encompasses X-rays, ionizing radiation, nonionizing ultraviolet radiation, Gamma radiation, and Nuclear fission. Radiation energy induces chromosomal alterations, such as breakage, translocations, and point mutations. Ionizing radiation activates oncogenes while deactivating the Rb tumor suppressor gene. Free radicals generated by X-rays and gamma rays lead to molecular damage, contributing to their carcinogenic effects. Natural UV radiation from the sun can result in skin cancer.

1.1.3.3 Smoking

Tobacco smoking is associated with many types of cancer, and causes 90% of lung cancer. Daily long-term vamping with a high voltage (5.0 V) electronic cigarette may form formaldehyde-forming chemicals at a greater level than smoking, which was determined to be a lifetime cancer risk of approximately 5 to 15 times greater than smoking.

1.1.3.4 Tobacco chewing

Tobacco use in different forms can lead to cancer in the lungs, larynx, mouth, pharynx, esophagus, bladder, pancreas, and potentially the kidney.

1.1.3.5 Diet and exercises

Diet, physical inactivity, and obesity contribute to roughly 30-35% of cancer-related deaths. More than half of this effect is attributed to overconsumption rather than insufficient intake of nutritious foods. Diets low in vegetables, fruits, and whole grains, coupled with high consumption of processed or red meats, are linked to several types of cancer.

1.1.3.6 Hormones

Hormones play a role in cancer development by promoting cell proliferation. Insulin-like growth factors and their binding proteins are pivotal in cancer cell processes like proliferation, differentiation, and apoptosis, suggesting their

potential involvement in carcinogenesis. Hormones also feature prominently in sex-related cancers, such as those of the ovary, testis, thyroid, and bone.

1.1.3.7 Viruses

Oncogenic viruses possess either DNA or RNA genomes. Viruses like 'polyoma virus' and 'SV 40' are significant in cancer induction. These small viruses code for approximately 5-6 proteins within their circular genomes. Infection of susceptible cells by these viruses can result in malignant transformation. Virus infection heightens the risk of cervical and liver cancers. Additionally, bacterial infection may elevate cancer risk.

1.1.3.8 Foods

Many foods are responsible for causing cancer, they all are enlist as below;

- Genetically Modified Foods, Microwave Popcorn, Canned goods
- Grilled Red Meat, Refined Sugar
- Salted, Pickled, and Smoked foods, Soda and Carbonated Beverages
- White Flour, Farmed Fish, Hydrogenated Oils

1.1.4 Types of Cancer

Carcinomas	Sarcomas	Lymphomas	Leukemia	Adenomas
			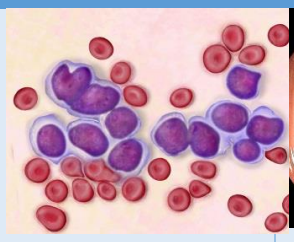	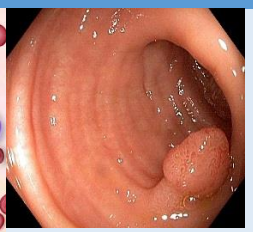
These are characterized by cancer cells that cover internal and external parts of the body such as lung, breast and colon.	These are characterized by cancer cells that are located in bone, cartilage, fat, connective tissue, muscle and other supportive tissues.	These are cancers that begin in the lymph nodes and immune system tissues	These are cancers that begin in the bone marrow and often accumulate in the blood stream.	These are cancers that arise in the thyroid, pituitary gland, adrenal gland and other glandular tissues.

Fig.6. Types of Cancer

1.1.5 Treatment of Cancer

A wide array of cancer treatments is accessible worldwide, with the selection depending on the specific type of cancer. While some individuals may undergo a singular form of treatment, most often, a combination of approaches is employed. Options may involve surgical interventions in combination with chemotherapy, immunotherapy, targeted therapy, radiation therapy, and hormone therapy. Chemotherapy, in a broader context, refers to the use of drugs in treating various diseases. However, within the realm of cancer treatment, the term is commonly associated with medications designed specifically for combating cancer. This is frequently abbreviated as "chemo". Unlike surgery and radiation therapy, which target cancer cells within a localized area, chemotherapy operates throughout the entire body. When used in conjunction with other treatments, chemotherapy serves several key purposes: reducing tumor size prior to surgery or radiation therapy, and eradicating any residual cancer cells post-treatment.(6–8) Despite its effectiveness, chemotherapy can have detrimental effects due to its toxic nature. There are three primary objectives associated with the application of anticancer drugs:

1. Disrupt the DNA of the cancerous cells.
2. Inhibition of the synthesis of the new DNA strands which stop the cell from replicating, because the replication of the cells is allows to formation of tumour.
3. Stop the actual mitosis of the original cell into two new cells.

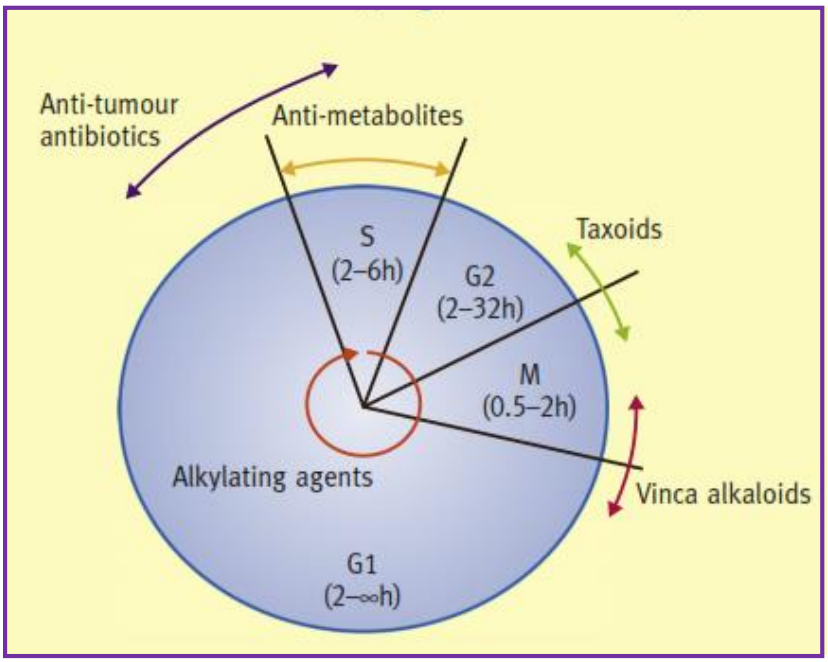

Fig.7.Action of Chemotherapeutic agents in cell cycle

1.1.6 Types of Cell death

They may be three types:

- **Necrosis**

  The demise of a significant portion or the entirety of cells within an organ or tissue caused by disease, injury, or a lack of adequate blood supply**.**

- **Autophagy**

  Autophagy, also known as autophagocytosis, is the intrinsic and controlled process within the cell that deconstructs superfluous or malfunctioning components

- **Apoptosis**

  Cell death that takes place as a routine and orchestrated aspect of an organism's growth and development

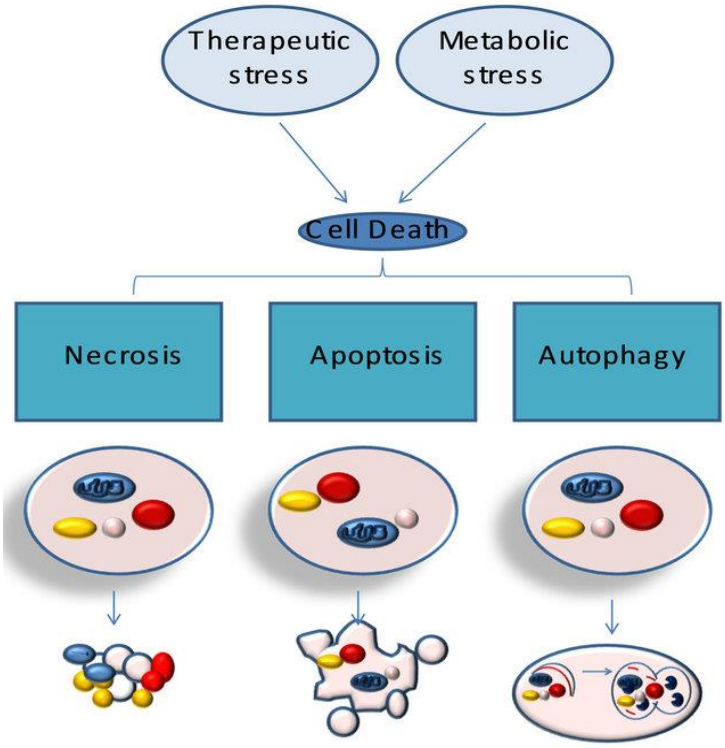

Fig.8. Cell death Process

The interplay between necrosis, autophagy, and apoptosis is crucial. Metabolic and therapeutic stress conditions result in a sudden depletion of NAD+ and ATP, accompanied by elevated levels of intracellular calcium and ROS. Cells unable to adapt to these changes undergo necrotic cell death.

The activation of stress-responsive mechanisms, such as AMPK, allows cells to adapt to these shifts. AMPK-driven phosphorylation inhibits the mammalian target of rapamycin,

leading to autophagy suppression. It also triggers p53, which can initiate either autophagy or apoptosis.

In contrast to apoptosis or necrosis, stress-induced autophagy can lead to autophagic cell death or cell survival

1.1.7 Autophagy and Cancer

Autophagy is a dynamic process of self-eating involving the degradation of proteins. Coined by French physiologist M. Anselmier in 1859, it was not until 1963, during a symposium on lysosomes, that Christian De Duve elucidated its mechanistic intricacies.

Today, a PubMed search yields over 30,000 scientific articles featuring the term "autophagy," underscoring its profound significance in life sciences. This culminated in the 2016 Nobel Prize in Medicine and Physiology awarded to Professor Y. Oshumi for his pioneering discovery of ATG genes (autophagy-related genes) in the early '90s, which govern and regulate autophagy in yeasts.

Autophagy comprises three distinct mechanistic pathways by which cellular components are delivered to lysosomes for breakdown by lysosomal enzymes. This process yields macromolecular components like amino acids and fatty acids are subsequently recycled to synthesize new macromolecules or serve as fuel for metabolic pathways. Moreover, it has recently emerged that the autophagy-controlling machinery also participates in non-degradative processes, including cellular secretion and the regulation of signal transduction pathways. Furthermore, it has become evident in recent times that the apparatus regulating autophagy also plays a role in non-degradative functions, such as cellular secretion and the regulation of signal transduction pathways (9)**.**

Autophagy responds to various physiological and pathological cues and can be influenced positively or negatively by drugs initially designed for other purposes. For instance, conditions like nutrient deprivation, starvation, hypoxia, hypothermia, re-warming, glucose deprivation, and redox stress, among others, have all been shown to induce autophagy.

1.1.7.1 Mechanism of Autophagy

The process of autophagy contains distinct stages: initiation (membrane isolation), nucleation (elongation), maturation, fusion, and degradation. Autophagy's capacity to recycle macromolecules provides cells with a survival advantage, particularly in stressful conditions like carbohydrate deficiency, oxidative stress, hypoxia, ER stress, and metabolic stress (10). Numerous genes and proteins play pivotal roles in autophagy's mechanism. For instance, FIP200, ULK1 & 2, BECN1, BCL-2, ATG 13, UVRAG, AMBRAN1, VPS34, BCL-XL, VPS34, ATG14, VPS15, ATG101, and RUBICON assist

in induction and nucleation. During the elongation phase, proteins like ATG3, ATG5, LC3-PE, ATG16, ATG7, ATG12, ATG48, and ATG10 are involved. In the final fusion process, proteins such as STX17, LAMP2, ATG2A, RAB7, and ATG2b play crucial roles. Collectively, they form an integral part of the intricate autophagic process.

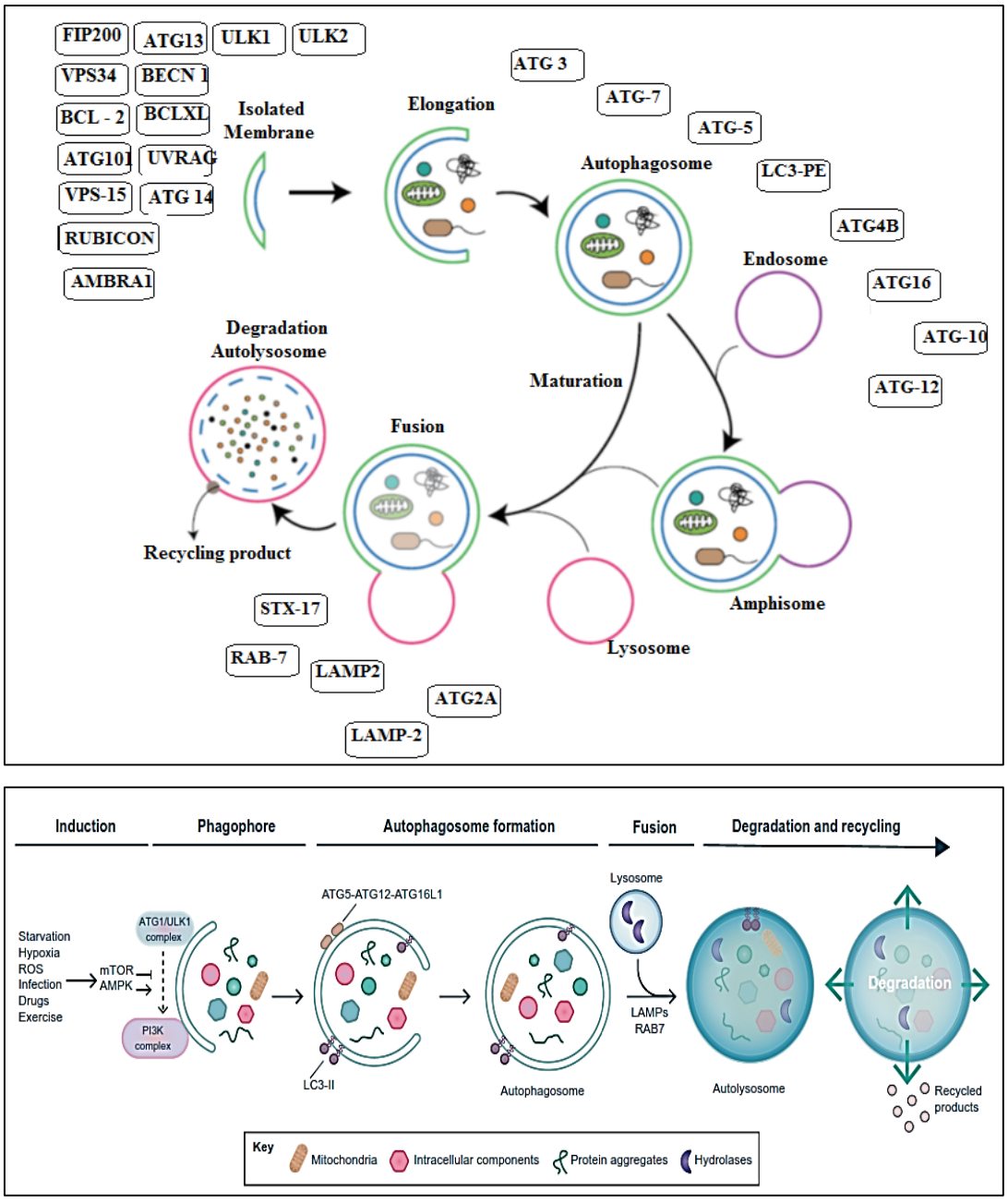

Fig 9: Mechanism and Regulation of autophagy process

Initiation Stage

Autophagy initiation involves various factors including small molecules, protein components, and modulation points. At this point, the mammalian target of Rapamycin (mTOR) plays a central role in relaying activating signals. It triggers the activation of

serine/threonine Unc-51-like kinases 1 and 2 (ULK1 and ULK2), which are the mammalian equivalents of ATG1. In mammals, mTOR exists in two distinct complexes: mTOR complex1 (mTORC1) and mTOR complex2 (mTORC2)(11–13). These complexes have a vital function in harmonizing signaling pathways that control the balance of cellular energy by managing both anabolic and catabolic processes. Specifically, mTORC1 complexes inhibit autophagy under conditions of nutrient abundance by deactivating the ULK1/2 complex. This complex comprises ULK1 or ULK2 kinase, ATG13 (family interacting protein of 200 kDa), FIP200 (the mammalian equivalent of ATG17), and ATG101 (also known as C12orf44). Activation of the ULK1/2 complex occurs when mTORC1 dissociates, typically in response to nutrient scarcity. This activation subsequently initiates autophagy through the class III phosphatidylinositol 3-kinase (PI3K) complex, which is also referred to as vacuolar protein sorting 34 (Vps34). The PI3K complex comprises VPS34, ATG14 L, VPS15, also known as PI3K regulatory subunit 4, and PIK3R4. This intricate process underscores the critical role of mTOR in the regulation of autophagy initiation.(12,15,16).

Nucleation stage

The nucleation of autophagic membranes is primarily orchestrated by a class III phosphatidylinositol PI3K complex. To generate phagophores (early structures of autophagosomes), various proteins, including VPS34, Beclin-1, AMBRA1, and mATG9, have been identified as essential regulatory elements (17,18). Beclin-1, a central protein in membrane nucleation, interacts with BCL2, which acts as an inhibitor of autophagy. Interfering with this interaction leads to Beclin-1 binding to the lipid kinase VPS34, subsequently facilitating the initiation of membrane nucleation (19). VPS34-mediated enzymatic generation of phosphatidylinositol 3-phosphate (PtdIns3P) provides the foundation for autophagy proteins with PI3P binding domains, including WIPI1–4 and DFCP1(12,20). The initiation complex, also known as the class III PI-3K complex, is activated through the pre-initiation complex by phosphorylation of the protein sorting by vacuolar protein 34 (VPS34) and Beclin-1 (17). Regulation of the initiation complex directly impacts the development of phosphatidylinositol-3-phosphate (PI3P). Cellular pools of the precursor phosphatidylinositol (PI) are essential for isolating membrane nucleation. This detailed process underscores the critical role of various proteins and complexes in the nucleation phase of autophagy (21).

Maturation

During the maturation phase of autophagy, two crucial ubiquitin-like conjugation systems come into play to facilitate the elongation and maturation of autophagosomes. The first involves the complex formation of ATG5 and ATG12, which then conjugate with ATG16L1. Simultaneously, microtubule-associated protein 1 light chain 3 (MAP1LC3, commonly known as LC3) also plays a pivotal role (12,13) At the site of membrane nucleation, the accumulation of proteins with PI3P-binding domains leads to the binding of additional ATGs. These ATGs are essential for the elongation and eventual closure of the autophagosome membrane (22). The ubiquitin-like protein ATG12 undergoes a covalent connection with ATG5 through a sequential process catalysed by the E1-like enzyme ATG7 and the E2-like enzyme ATG10. The resulting ATG5-ATG12 complex is recruited to the autophagic membrane, where it facilitates elongation by interacting with ATG16L1. This interaction leads to the creation of the ATG12-ATG5-ATG16L1 complex, which functions in a manner similar to an E3 enzyme in the second ubiquitin-like conjugation system (12,13,23,24)

In the second system, the LC3 protein is linked to a lipid molecule called phosphatidylethanolamine (PE). The cellular levels of the initiation complex are further controlled through a ubiquitination cascade, which is overseen by the deubiquitinating peptidases USP10 and USP13. The expansion of emerging precursor vesicles relies on microtubule-associated proteins 1A/1B light chain 3B (LC3). In this process, the conjugated LC3 form, referred to as LC3-II, plays a pivotal role. Initially, cytosolic LC3-I is formed through the cleavage of LC3 by ATG4. Following conjugation to phosphatidylethanolamine (PE), LC3-I transforms into LC3-II, a well-established marker for assessing autophagic activity. This cleavage reveals the glycine residue at the C-terminal domain, facilitating PE conjugation and making LC3-II the only protein stably associated with mature autophagosome membranes during the maturation process (12,24–26)

Fusion and Degradation

After the autophagic membrane is established, the autophagic vesicles are conveyed to the lysosomes for degradation. During this process, LC3-associated autophagosome proteins undergo de-lipidation and recycling before fusion (27). Several SNARE proteins, such as STX17 and WAMP8, as well as lysosomal integral protein LAMP2 and RAB proteins, play crucial roles in mediating the fusion between autophagosomes and lysosomes (28). Finally, autolysosomes are formed by the fusion of autophagosomes with

lysosomes, in which lysosomal proteases degrade cargo. The degradation products such as amino acids and fatty acids are then returned to the cytosol for further reuse in different metabolic processes (29). This process has been associated with the development of a range of diseases, including cancer, neurodegenerative disorders, cardiovascular diseases, metabolic disorders, and immune-related conditions. (30).

1.1.8 Autophagy-mediated cancer regulation

In a pivotal development in 1999, Beth Levine's research group first proposed a direct link between autophagy and cancer. They demonstrated that monoallelic deletions of the BECN1/ATG6 genes in human cells could lead to both in vitro malignancies and in vivo tumor formation (31) and in vivo (32). Contemporary research suggests that ATGs and related pathways interact with oncogenes and/or tumor suppressors. However, accumulated data support the idea that autophagy's role in malignant transformation is complex and can have opposing effects depending on the cellular background and type (33,34). Autophagy has been identified as a beneficial mechanism in suppressing multi-stage cancer development. It accomplishes this by playing established roles in preserving genomic stability, eliminating internal sources of reactive oxygen species (ROS), supporting bioenergetic functions, breaking down oncogenic proteins, and instigating immune response mechanisms against malignant changes (35). The autophagic process involves numerous genes and proteins, each performing distinct functions at different stages of autophagy (36). All genes and proteins are described in the table with their specific function.

Table 1: Regulation of autophagy through proteins and genes.

Regulation of autophagy			
Sr. No.	**Protein/Genes involved in autophagy**	**Role of proteins and genes**	**Reference**
1.	FIP200	Part of the ULK1/2 complex, responsible for initiating autophagosome formation in the early stages.	(37)
2.	5 AMPK	An enzyme that plays a crucial role in the regulation of ATP production and the maintenance of cell homeostasis.	(38)

3.	mTOR (Mammalian target of rapamycin)	Autophagy is triggered during senescence, and its activation is associated with negative feedback in the rapamycin (mTOR) pathway PI3K – mammalian target. PIKK family serine/threonine-protein kinase controlling various cellular processes including metabolism, cell growth and autophagy.	(39)
4.	ULK1/2 (Unc-51-like autophagy activating kinase ½)	Two similar ATG1 serine/threonine kinase homologues essential for autophagy signaling. ULK1 specifically phosphorylate mAtg13 and FIP200, thus providing clear roles in autophagy for the most reliable evidence of Atg1 substrates to date.	(40,41)
5.	VPS34 (Vacuolar protein sorting protein 34)	A Class III PI3K protein that plays a role in phosphorylating phosphatidylinositol to generate phosphatidylinositol (3)-phosphate (PI3P), which is essential for autophagosome formation. In vivo, when VPS34 activity is inhibited, the affinity purification of the ubiquitin proteome reveals various autophagic substrates, including NCOA4. NCOA4 physically interacts with the ferritin protein complex and guides it to auto lysosomal degradation	(42,43)
6.	ATG7 (Autophagy-related protein 7)	A homologous ubiquitin-activating enzyme E1binds and activates LC3 for conjugation.	(44)(45)
7.	ATG13 (Autophagy-related protein 13)	Autophagy protein targets mTOR signalling pathway, which controls the creation of autophagosomes by phosphorylation.	(46)
8.	ATG3 (Autophagy-related protein 3)	A related ubiquitin-conjugating enzyme E2 facilitates the attachment of LC3-I to phosphatidylethanolamine subsequent to the activation of LC3 by ATG7.	(47)

9.	ATG4B (Autophagy-related protein 4B)	A cysteine peptidase enzyme, akin to ATG4, participates in the final residue cleavage of proLC3. This cleavage activates LC3-I, allowing it to link with phospholipids and facilitating autophagosome formation.	(37)
10.	LC3 Microtubule-associated proteins 1A/1 B light chain 3B (LC3)	Ubiquitin-like protein (LC3-I) that combines LC3-II with phospholipid phosphatidyl-ethanolamine and is involved in autophagosome formation.	(48)
11.	PI3K (Phosphoinositide 3-kinase)	A signal transducer enzyme class inside cells that regulates cellular function through phosphorylation of the lipids associated with a phosphatidylinositol (PI).	(49)
12.	P62	Protein kinase C-interacting protein is used to signal and activate the mTOR pathway; destroyed by autophagy. P62 itself is a scaffold protein binding essential signaling intermediaries across various domains.	(50,51)
13.	BECL1	A major PI3 K protein that interacts with BCL-2 or Pl3 K and plays a crucial role in activating and controlling autophagy and apoptosis.	(52)

Table 2: Role of autophagy proteins in cancer

Cancer type	**Protein**	**Phase of autophagy**	**Status in cancer**	**Reference**
Colorectal carcinomas	AMBRA1	Initiation	Mutated	(53)
Breast carcinomas	FIP200	Initiation	Mutated	(54)
Breast carcinomas	BECN1	Initiation	Decreased	(55)
Colorectal and gastric carcinomas	BECN1	Initiation	Increased	(56)

Melanoma	ATG5	Elongation	Decreased	(57)
Benign liver tumour	ATG5	Elongation	Decreased	(58)
Colorectal and gastric carcinomas	ATG5	Elongation	Mutated	(59)
Fibrosarcomas	ATG4C	Elongation	Decreased	(57)
Leukaemia	RAB7A	Fusion	Mutated	(60)
Hepatocellular carcinomas	ULK1	Initiation	Increased	(61)
Breast carcinomas	ULK1	Initiation	Increased	(62)

Table 3: Some Selected ULK1/2 containing Compounds That Modulate Autophagy

Compound	**Chemical structure**	**Target**	**Novel features**	**Potency/Selectivity**
Compound 1	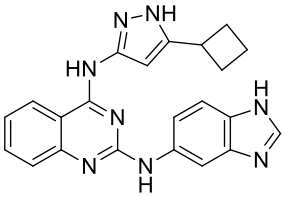	ULK1 and ULK2	Inhibitor Pyrazole amino quinazoline scaffold Crystal structure obtained with ULK1	ULK1: IC50 of 5.3 nM; ULK2: IC50 of 13 nM; PDPK1: IC50 of 420 nM
Compound 3	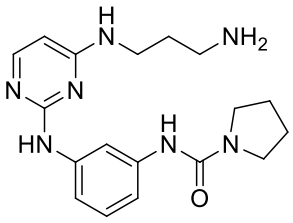	ULK1 Inhibitor	Pyrimidine scaffold Crystal structure obtained with ULK1	ULK1: IC50 of 120 nM; ULK2: IC50 of 360 nM; PDPK1: IC50 of 710 nM

SBI-0206965	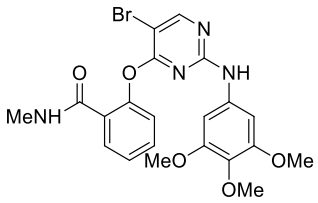	ULK1 and ULK2	Selective inhibitor Pyrimidine scaffold Suppresses ULK1 downstream phosphorylation of VPS34 and Beclin-1 Induces apoptosis in NSCLC cells by destabilizing Bcl2 and Bclxl	ULK1: IC50 of 108 nM; ULK2: IC50 of 711 nM
MRT67307	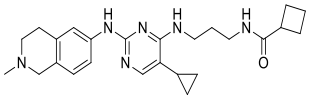	ULK1 and ULK2	In vitro inhibitor Pyrimidine scaffold Also targets TBK1 and AMPK-related kinases	ULK1: IC50 of 45 nM; ULK2: IC50 of 38 nM
MRT68921	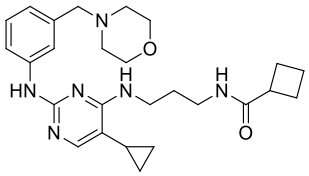	ULK1 and ULK2	In vitro inhibitor Pyrimidine scaffold Also targets TBK1 and AMPK-related kinases	ULK1: IC50 of 2.9 nM; ULK2: IC50 of 1.1 nM
SR-17398	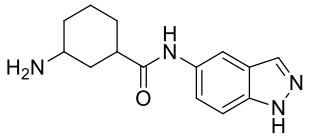	ULK1	Indazole-derived inhibitor Mixture of four stereoisomers	ULK1: IC50 of 22 mM
SR-20295	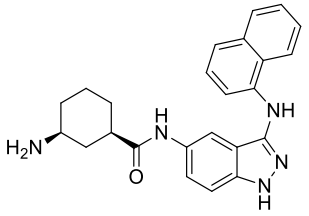	ULK1	Indazole-derived inhibitor	ULK1: IC50 of 45 nM, In vitro microsome

1.2 Rational Behind Development of Anticancer Agents.

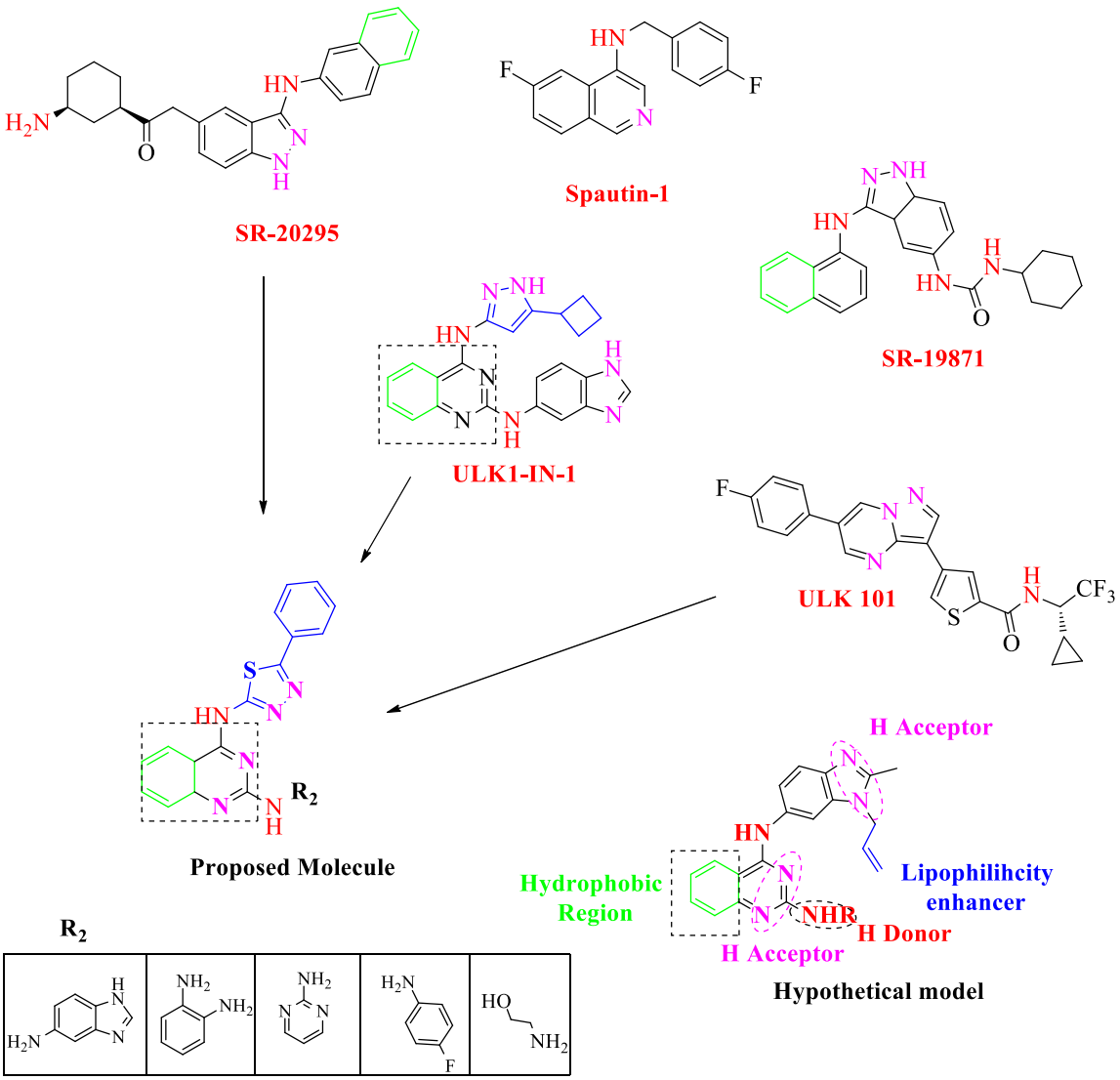

Fig.10. Design Strategy of Proposed Molecule

Wood and colleagues discovered a promising ULK inhibitor. All of them have a low IC_{50} value for the ULK protein(63). ULK protein has two terminal lobes, one on the N side chain and one on the C side chain, which are very specific for binding to the active side. The N-chain contains a serine-proline-rich region, which is the site of numerous regulatory phosphorylation by both mTORC1 and AMPK, which act as negative and positive regulators of ULK1 activity, respectively(64). Some amino acids, such as CYS95, TYR94, GLU93, LYS38, and MET92, are required to initiate phosphorylation. All amino acids interact with ULK at the hinge region, causing the confirmation to change from inactive to active. These ULK play an essential role in the autophagy mechanism by inhibiting it via an active site containing the NH group of the benzimidazole moiety, which

interacts with GLN142, and other benzene ring fragments, which interact with GLY98. In ULK-LN-1, the NH group between pyrazol and quinazoline forms an H bonding interaction with the carbonyl group of CYS95 amino acid. GLU93 and LYS38 were mutated at the N terminal side chain, and LYS162 is adjacent to this C terminal patch and is a known ULK1 regulatory site via acetylation by TIP60(34,65). The cyclopropyl substituent in the STD compound fits into a pocket adjacent to the gatekeeper methionine. This is the most fundamental pharmacophoric requirement for ULK inhibitory activity(66). We intend to design a proposed molecule containing thiadiazole, quinazoline, benzimidazole, and some aniline derivatives that fulfil all pharmacophoric requirements in the current research. The thiadiazole ring was selected for its dynamic role in pharmacokinetic and dynamic properties. Thiadiazole contains two N atoms with a high electron-donating ability and the ability to form H bonding interactions with ASN143 and GLN142, causing GLN142 to shift in position and reducing the transactivation mediated side effect.

1.2.1 ULK (Human autophagic initiating kinase) inhibitor

Autophagy initiation kinase (also known as ULK1 in humans) is a protein kinase that plays a key role in the initiation of the autophagy process. ULK1 is activated by various stress signals, such as nutrient deprivation, and phosphorylates other proteins to initiate the formation of the autophagosome, which is the membrane-bound structure that encloses the material to be degraded during autophagy (65)(67). Mutations in the ULK1 gene have been found in several human diseases, including cancer, and it is considered as a potential therapeutic target. Some studies have shown that inhibition of ULK1 can lead to increased sensitivity to chemotherapy and radiation therapy in cancer cells, but more research is needed to fully understand its role in human diseases and develop effective strategies targeting ULK1(68)(69)(70)(71).

ULK1, found in mammals, and Atg1 in yeast, share similarities in their roles in autophagy. There are five homologues of ULK1 (ULK1, ULK2, ULK3, ULK4, and STK36, also known as serine/threonine kinase 36), but it is established that only ULK1 and ULK2 are engaged in conventional autophagy signalling (72). In most cell lines, loss of ULK1 is enough to interrupt autophagy; however, in this pathway, ULK2 is thought to be functioning with a degree of redundancy. This redundancy is demonstrated by the need to knock out ULK1 and ULK2 in mice to show the same neonatal lethality as other essential autophagy genes such as ATG5 and ATG7 (73)(74). As anticipated for a protein kinase, the kinase function of ULK1 is essential for instigating autophagy. Mutants of

ULK1 lacking kinase activity and the chemical inhibition of ULK1's enzymatic function both lead to the obstruction of autophagic flux (75). Unc-51-like protein kinase 1 (ULK1), the mammalian counterpart of Atg1, serves as the primary protein in the autophagic process and is the sole serine/threonine kinase recognized within the core autophagic pathway (76). ULK1 activation through upstream signals, including AMPK and mTOR, can cause autophagy under various stress conditions. ULK1, FIP200, mAtg13, and Atg101 form a complex of proteins that can be regulated by post-translational changes, such as phosphorylation and acetylation. Ironically, both ULK1's transcriptional and posttranscriptional modifications vary in different cancers, making ULK1 a promising therapeutic target and a diagnostic marker(77). ATG1 is the first known autophagy-related gene (ATG) in yeast. It has been described as a phosphorylation-dependent regulatory mechanism, including Atg1 and seven other interacting proteins (34,78). The Atg1 non-coordinated-51 (Unc-51) nematode homolog has a corresponding and additional neuronal role. Vertebrate genomes encode five kinases closely related to Atg1, but only Unc-51-like protein kinase 1 ULK1 and ULK2 have autophagic functions and a new vesicular transport mechanism unique to neurons (69). In the context of autophagy, molecular regulation involves three key components: the ULK1 complex in pre-initiation, the class III phosphatidylinositol 3-kinase complex in initiation, and two protein conjugation systems that resemble ubiquitin (Ub-like). The pre-initiation complex is formed by ULK1, mAtg13, Focal Adhesion Kinase (FAK) of 200 kDa (FIP200), and Atg101-interacting protein. It can be triggered by stress signals, such as amino acid or serum deficiency, low energy levels, and glucose scarcity. Notably, Atg13 and FIP200 play crucial roles in facilitating the localization of autophagosomes from ULK1 to the isolation membrane; the absence of either component disrupts this process. Homeostatic regulators like mammalian TOR complex 1 (mTORC1) and AMP-activated kinase (AMPK) activate ULK1 through post-translational modifications (79). MTOR is one of the ULK1 complex's most prestigious regulators; it phosphorylated ULK1 directly and thus inactivated. Also, mTORC1 regulates trafficking in Atg9, which is the only autophagic multiple membrane proteins that spans (40) as an energy sensor AMPK can induce ULK1 activity by inhibiting mTORC1 and phosphorylating ULK1 directly under hunger stress (80).

1.2.2 The Structure of ULK1

Atg1, originally identified through genetic screens in Saccharomyces cerevisiae, plays a critical downstream role for the nutrient-sensing protein mTOR. Atg1 interacts with several binding partners, including Atg13, Atg15, Atg17, Atg20, Atg24, Atg29, Atg31, and

others. Notably, both Atg1 and Atg13 have functions in autophagy and the autophagy-related targeting (Cvt) processes, mediating the transfer of cytoplasmic material to the vacuole. By contrast, Atg17, Atg29, and Atg31 function directly in autophagy, while Atg11, Atg20, and Atg24 function only in Cvt pathways (67). There are five Atg1 orthologs encoded by vertebrate genomes, ULK1/2/3/4 and STK36, and only ULK1 and ULK2 are available for autophagy control(81). Human ULK1 shares a 41% overall similarity with Unc-51, its homolog in Caenorhabditis elegans, and a 29% similarity with Atg1. In contrast to other related kinases like ULK3, ULK4, and STK36, where the similarity is primarily limited to the catalytic N-terminal domain, the likeness between ULK1 and Atg1 extends across the entire protein, encompassing the catalytic N-terminal domain (NTD), the central proline/serine-rich (PS) domain, and the C-terminal domain (CTD) (34). The ULK1 domain N-terminal kinase (residue 16–278) and CTD (residue 833–1050) are highly conserved in Homo sapiens. And a PS region, which contains post-translational modification sites, locates between the kinase domain and CTD. ULK2 has a combined association of 52% of amino acids with ULK1; it is therefore accused of compensating for ULK1 functions or playing its roles in initiating autophagy (82). Furthermore, the knockdown of ULK1 or the use of dominant-negative mutants can result in the inhibition of autophagy, underscoring the essential role of ULK1 as a protein kinase in the autophagic process (83). Moreover, the C-terminal domain (CTD), known for its high conservation, could potentially serve other crucial roles. Alterations in autophosphorylation, conformational changes upon CTD treatment, and the delineation of regions directly involved in membrane association and the interaction between ULK1 and mAtg13 have elucidated the dominant-negative behavior of a 7-residue motif in the kinase-dead mutants within the CTD. This suggests that CTD's work It may not restrict binding with mAtg13, but may also interact with other functions. Some studies have shown that inhibition of ULK1 can lead to increased sensitivity to chemotherapy and radiation therapy in cancer cells, but more research is needed to fully understand its role in human diseases and develop effective strategies targeting ULK1(79).

The kinase domain of ULK1 contains the Conserved residues that are essential for kinase activity, including the catalytic lysine residue, which is responsible for the transfer of the phosphoryl group from ATP to the substrate protein. The central serine/threonine-rich domain of ULK1 is thought to be involved in the regulation of its activity and localization, while the carboxy-terminal domain is thought to be involved in the binding of other proteins and the regulation of autophagosome formation.

ULK1 also has several domains that allow it to interact with other proteins, including the FIP200 domain is a binding site for other proteins involved in the initiation of autophagy, such as Atg13 and FIP200. The interaction of ULK1 with these Proteins are important for the formation of the autophagosome.

In addition, ULK1 also contains a phosphorylation site (Ser757) that is critical for its activity and targeting it could be a promising strategy for treating non-small cell lung cancer (NSCLC) and other diseases in which ULK1 is overactive.

The active site of ULK1, also known as autophagy initiation kinase, is the region of the protein where the substrate (usually other proteins) binds And undergoes phosphorylation. The active site of ULK1 is made up of several amino acids that form the binding pocket for the substrate.

The specific amino acids That make up the active site of ULK1 are not well characterized, but it is known that the kinase domain of ULK1 contains the conserved residues that are essential for kinase activity, including the catalytic lysine residue, which is responsible for the transfer of the phosphoryl group from ATP to the substrate protein.

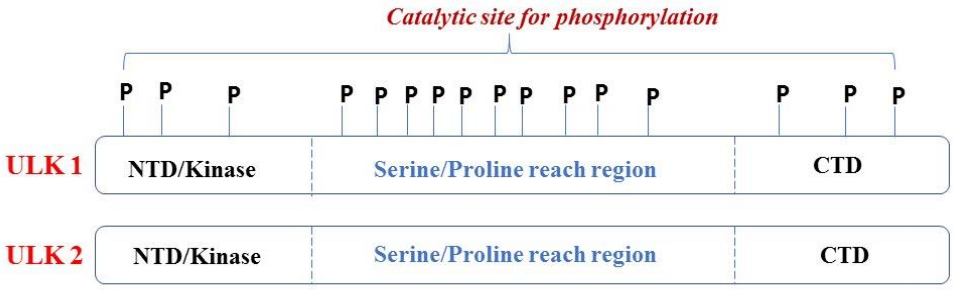

Fig 11: Structure of ULK1 and ULK2 (NTD/Kinase- N Terminal kinase domain, CTD-C Terminal Kinase domain)

Phosphorylation is a process in which a phosphate group is added to a protein by a protein kinase, such as ULK1. Phosphorylation can change the activity or localization of a protein and is a key mechanism of regulation in many cellular processes, including autophagy. In the case of ULK1, phosphorylation plays a key role in the initiation of autophagy. The phosphorylation of ULK1 by an upstream kinase, such as AMPK, leads to its activation and the phosphorylation of other proteins, including Beclin-1 and Atg13, which in turn leads to the formation of the autophagosome.

Phosphorylation of ULK1 also regulates its localization and stability. The phosphorylation of specific amino acids in the active site of ULK1 is thought to play a key role in the regulation of autophagy.

In cancer, ULK1 is hyperactive, and this hyperactivity has been linked to cancer cell proliferation and resistance to therapy. Targeting the phosphorylation process of ULK1 has been proposed as a potential strategy to treat cancer. Inhibiting the kinases that phosphorylate ULK1, or developing drugs that target the active site of ULK1 and disrupt its phosphorylation process, could be a promising approach to inhibit ULK1 activity and induce cancer cell death.

1.2.3 Mechanism of ULK in cancer cell death

The mechanism by which ULK1 (Unc-51-like kinase 1) contributes to cancer cell death is not fully understood, but several potential mechanisms have been proposed.

One of the main mechanisms is that ULK1 can promote autophagy, which is a cellular process that allows the cell to break down and recycle its own components, such as damaged or unnecessary proteins and organelles. In cancer, autophagy can promote cell survival and resistance to chemotherapy and radiation therapy. Inhibiting ULK1 activity can inhibit autophagy and promote cancer cell death.

Another mechanism is related to the role of ULK1 in regulating the cytoskeleton, which is the network of proteins that gives cells their shape and enables them to move. ULK1 can interact with cytoskeleton-associated proteins, such as actin and tubulin, and regulate their polymerization. This can lead to the formation of filopodia, which are small protrusions that can promote cell migration, invasion, and resistance to therapy. Inhibiting ULK1 can disrupt cytoskeleton organization and lead to cancer cell death.

ULK1 can also regulate the activity of other proteins that are important for cancer cell survival. For example, ULK1 can promote the activity of the protein mTOR, which can promote cancer cell growth and survival. Inhibiting ULK1 can inhibit mTOR activity and promote cancer cell death.

Finally, ULK1 can also regulate the activity of other proteins that are important for cancer cell death. For example, ULK1 can promote the activity of the protein p53, which is a tumour suppressor protein that can induce cancer cell death. Inhibiting ULK1 can inhibit p53 activity and promote cancer cell survival.

It's important to note that these mechanisms are not mutually exclusive, and ULK1 can regulate multiple pathways that contribute to cancer cell death. Additionally, the specific mechanism of ULK1 in cancer cell death may vary depending on the cancer type and stage of the disease.

1.2.4 Basic pharmacophoric requirements for activation of ULK

Pharmacophoric requirements refer to the specific chemical features or groups that a molecule must possess in order to bind to and activate a target protein, such as ULK1. The specific pharmacophoric requirements for ULK1 activation have not been fully characterized, but some general information is accessible.

ULK1 is a protein kinase, so it requires a small molecule that can bind to the ATP-binding site of the kinase domain, and mimic the structure of ATP. This usually includes a molecule with a high electron density, like a phospho group or a similar group, that can mimic the phosphate group of ATPs.

Also, ULK1 has a large hydrophobic pocket that can accommodate a small lipophilic group. This pocket is thought to be important for the binding of ULK1 inhibitors, which is why small lipophilic groups are considered as a basic pharmacophoric requirement for ULK1 activation.

Additionally, ULK1 has a Serine/Threonine rich domain, which means that its activation requires a molecule that can bind to this domain, that could be a molecule containing a hydroxyl or amine group, also considered as a basic pharmacophoric requirement.

It's important to note that these are general requirements and the specific pharmacophoric requirements for ULK1 activation may vary depending on the specific small molecule and the stage of the autophagic process targeted.

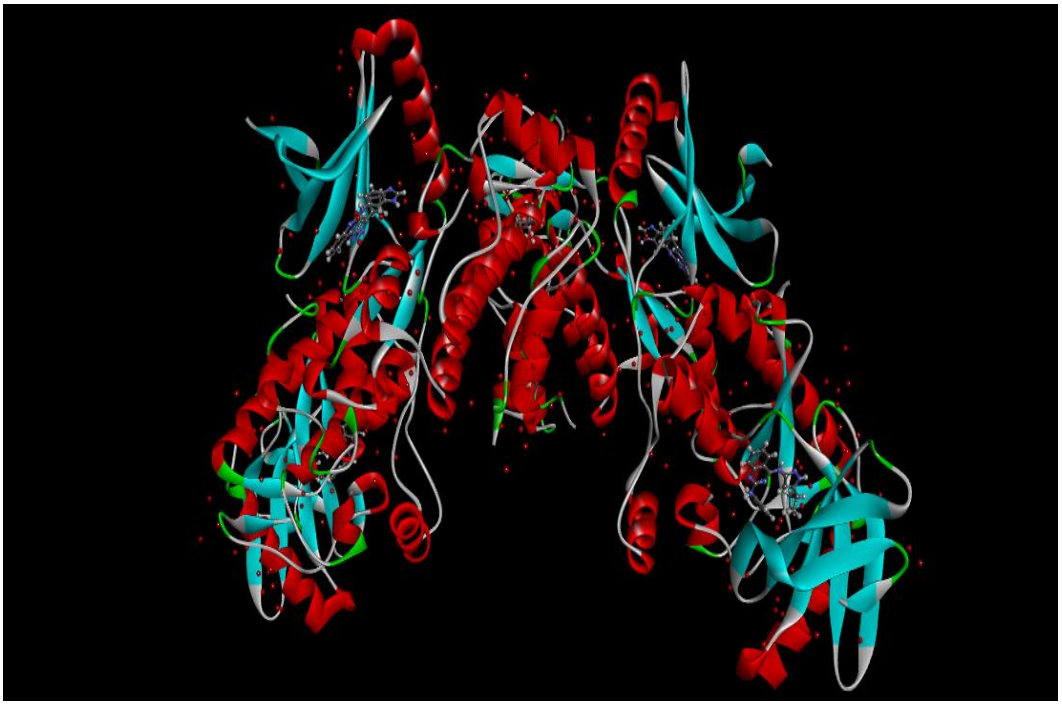

Fig.12. High resolution X-ray structure of Human Autophagy initiating kinase (PDB code 4WNP, resolution 2.90 Å

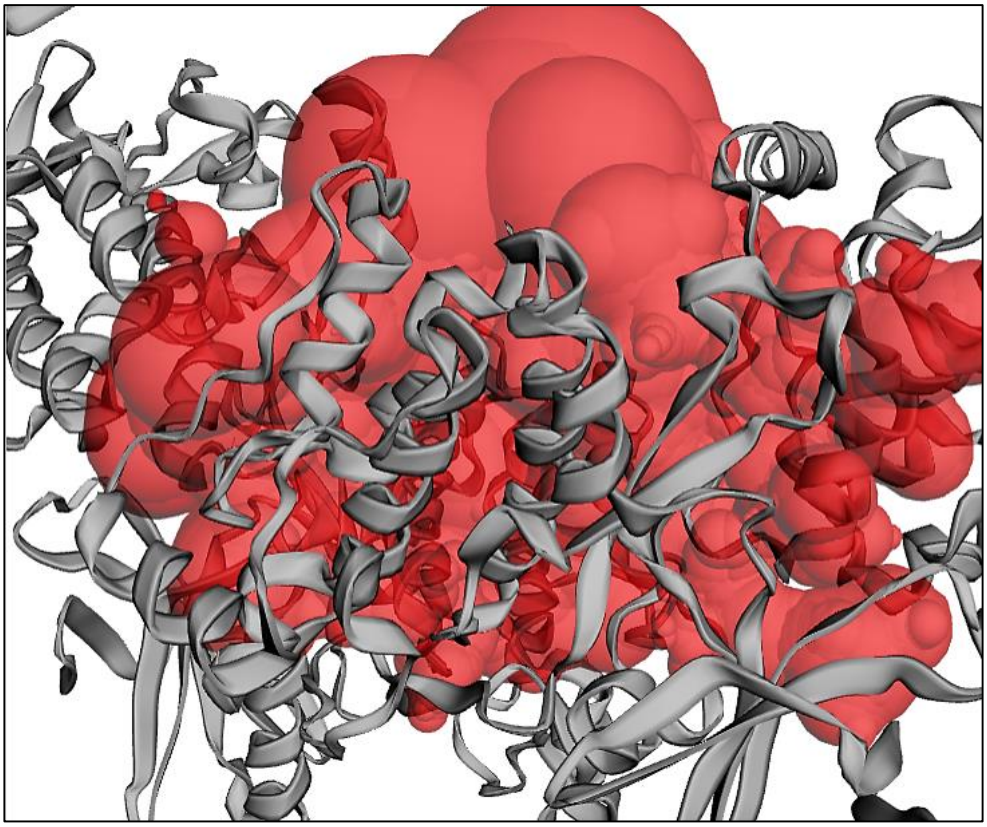

Fig.13. Binding pocket (red) of 4WNP observed from CASTp server

1.3. Profile of Heterocyclic Moiety

1.3.1. Thiadiazole

Thiadiazole is a class of heterocyclic compounds characterized by a five-membered ring containing three nitrogen and two sulfur atoms.

Here are some key features of thiadiazole:

Heterocyclic Structure: Thiadiazole possesses a unique heterocyclic structure, which includes three nitrogen atoms and two sulfur atoms. The presence of both nitrogen and sulfur in the ring contributes to the compound's distinct chemical and biological properties.

Isomers: Thiadiazole can exist in various isomeric forms, depending on the arrangement of the atoms within the five-membered ring. The two most common isomers are 1,2,3-thiadiazole and 1,2,4-thiadiazole, differing in the position of the sulfur atom relative to the nitrogen atoms.

Versatile Substituent Positions: The positions on the thiadiazole ring can be substituted with different chemical groups, leading to a wide range of derivatives. These substitutions significantly influence the compound's reactivity and biological activities.

Biological Activities: Many thiadiazole derivatives exhibit diverse biological activities, such as antimicrobial, antiviral, antifungal, anti-inflammatory, and anticancer properties. These properties have led to significant interest in their potential use as therapeutic agents.

Drug Development: Due to their broad range of biological activities, some thiadiazole derivatives have been studied as potential drug candidates in pharmaceutical research.

Synthetic Versatility: Thiadiazole can be synthesized through various chemical reactions, making it easily accessible for medicinal and industrial applications.

Coordination Chemistry: Thiadiazole derivatives can act as ligands in coordination complexes with transition metal ions, showing interesting coordination and catalytic properties.

Pharmacophore: The thiadiazole ring system can serve as a pharmacophore, a crucial part of a molecule responsible for its biological activity. By modifying the substituents on the ring, chemists can optimize the biological activity of the compound.

1.3.1.1 Synthesis of Thiadiazole

a. Oxidative cyclization of N'- imidoylthiohydrazide with bromine in the presence of pyridine gave 2,5-diphenyl-1,3,4-thiadiazole along with the 3,6-diphenyl-4H-1,2,4,5-thiatriazine.

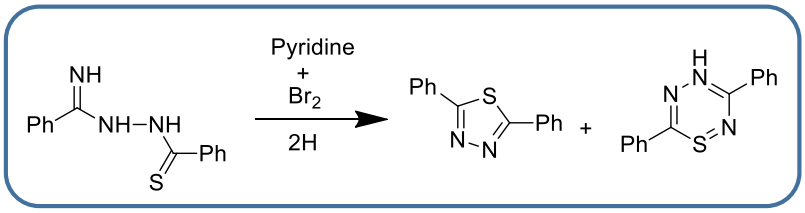

b. Frund and Meinecke have shown that thiosemicarbazide cyclized directly to the 2-amino-5-methyl-1,3,4-thiadiazole with acetyl chloride. This method is simple route for the synthesis. R may be ethyl, norhydnocarpyl, cyclopropyl, benzyl etc.

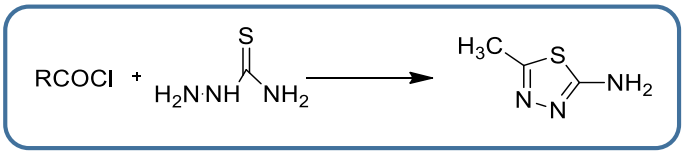

c. Pulvermacher observed that formic acid cyclized the alkanoyl halides by acylation. He found that 4-phenylthiosemicarbazide react with formic acid which give 2-anilino-1,3,4-thiadiazole.

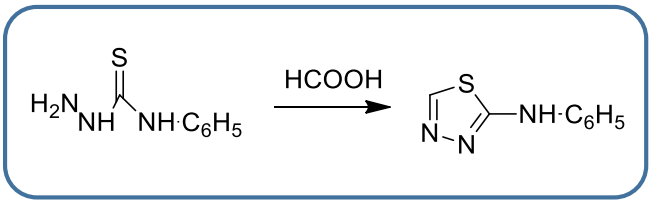

d. Preparation of 2-amino-5-mercapto-1,3,4-thiadiazole was developed by Guha. When thiosemicarbazide react with carbon disulphide and potassium hydroxide, the potassium salt of thiosemicarbazide-4-dithiocarboxylic acid was formed. Heating this potassium salt of thiosemicarbazide-4-dithiocarboxylic acid to 180^0 causes cyclization of salt to 2-amino-5-mercapto-1,3,4-thiadiazole.

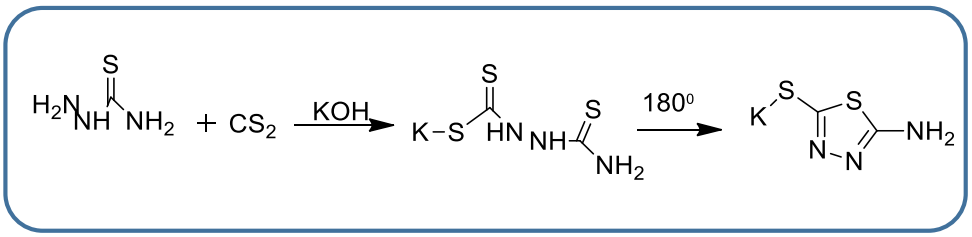

e. Synthesis of 1,3,4-thiadiazole via substituted dithiocarbazide acid and their esters. In this reaction, formation of 2,5-dimercapto-1,3,4-thiadiazole by action of carbon disulphide on hydrazine in basic medium.

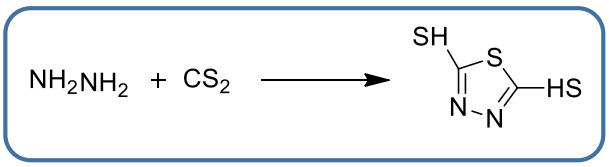

f. Synthesis of 1,3,4-thiadiazole by benzoic acid. Reaction of benzoic acid and thiosemicarbazide in the presence of Conc.H_2SO_4 and ethanol and it give 5-phenuyl-1,3,4-thiadiazole-2-amine.

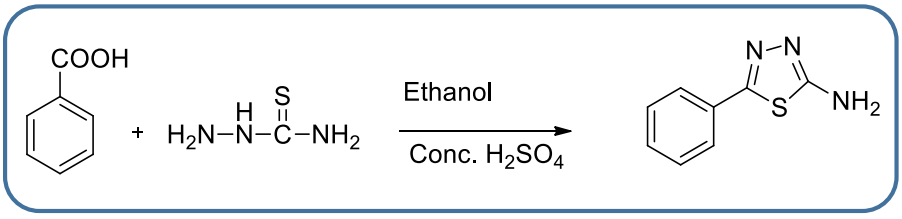

1.3.2 Benzimidazole

Benzimidazole is a heterocyclic compound with the chemical formula C7H6N2. It is a bicyclic compound consisting of a benzene ring fused with an imidazole ring. The imidazole ring is a five-membered ring containing two nitrogen atoms.

Key features of benzimidazole:

Heterocyclic Structure: Benzimidazole contains two different types of rings—benzene and imidazole—which are fused together, resulting in a heterocyclic compound.

Aromaticity: Both the benzene ring and the imidazole ring in benzimidazole are aromatic, making the compound stable and exhibiting resonance effects in chemical reactions.

Versatile Substitution: The benzimidazole ring can be substituted at various positions with different chemical groups, leading to the formation of various derivatives with unique properties.

Medicinal Significance: Benzimidazole and its derivatives have been extensively studied in medicinal chemistry due to their diverse biological activities. Some benzimidazole-based drugs are used to treat conditions such as parasitic infections and peptic ulcers.

Antifungal and Antihelminthic Agents: Benzimidazole derivatives are commonly used as antifungal and antihelminthic agents in both human and veterinary medicine.

Coordination Chemistry: Benzimidazole can act as a ligand in coordination complexes with transition metal ions, leading to interesting coordination chemistry and catalytic properties.

Synthetic Accessibility: Benzimidazole derivatives can be synthesized through various chemical reactions, making them readily accessible for medicinal and industrial applications.

1.3.2.1 Synthesis of Benzimidazole

a. Benzimidazoles are produced in good yields when different o-phenylenediamines and N-substituted formamides are used as C1 sources during a zinc-catalyzed cyclization in the presence of poly(methylhydrosiloxane). Derivates of benzoxazole and benzothiazole can also be produced synthetically.

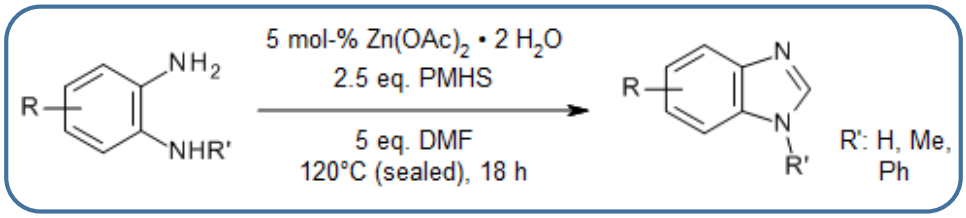

b. O-iodoanilines or electron-rich aromatic amines can be used to produce 2-unsubstituted benzothiazoles in good isolated yields with good functional group tolerance through a three-component reaction with K2S and DMSO. O-phenylenediamines underwent a similar reaction to produce 2-unsubstituted benzimidazoles devoid of K2S. DMSO serves as a carbon source, solvent, and oxidant, three crucial functions.

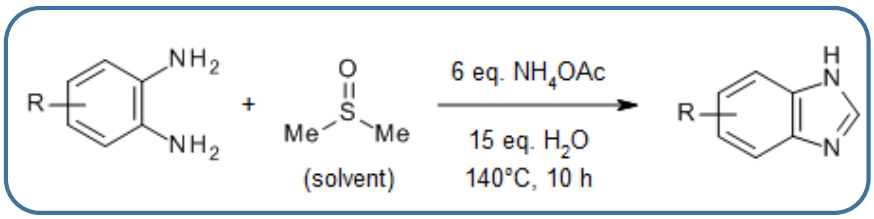

c. Through an effective copper-catalyzed amination of N-aryl imines, in which the imine acts as a directing group by chelating to the metal centre, it is possible to convert commercial aryl amines, aldehydes, and azides into valuable benzimidazole structural units with a wide substrate scope and diversity.

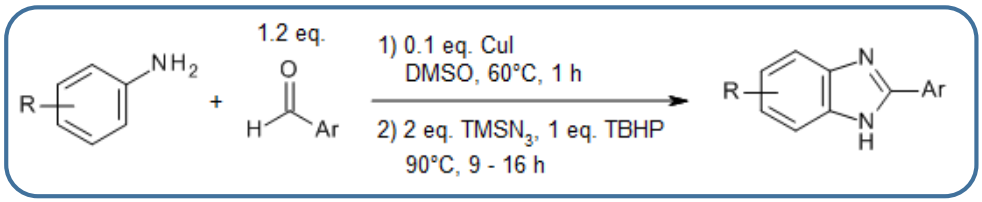

d. Under "metal-free" conditions in a mixed aqueous medium, supramolecular nanoassemblies of an AIEE-ICT-active pyrazine derivative (TETPY) with strong absorption in the visible region catalyse the synthesis of a wide range of benzimidazoles, benzothiazoles, and quinazolines in excellent yields.

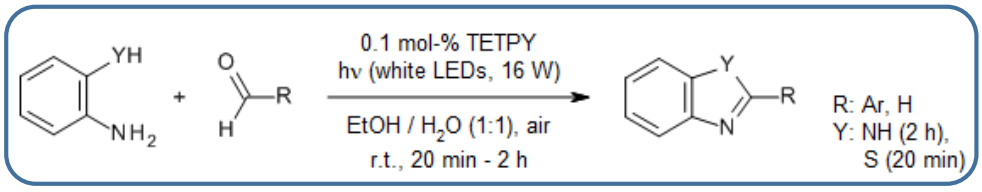

e. O-nitroanilines and alcohols undergo an unbalanced redox condensation reaction that results in benzimidazole and quinoxaline heterocycles when sodium sulphide and iron (III) chloride hexahydrate are present. Hydrated

sodium sulphide serves as a precursor for an iron-sulfur catalyst in addition to being a great non-competitive, multi-electron reducer.

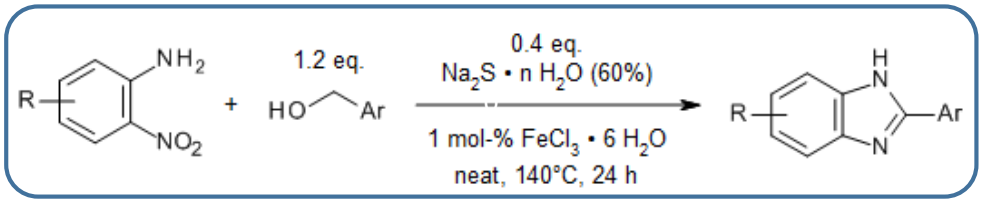

1.3.3 Pyrimidine

Pyrimidine is a heterocyclic aromatic compound that plays a crucial role in various biological processes and is a fundamental building block in the structure of important biomolecules.

Here are some key features of pyrimidine:

Structure: Pyrimidine is a six-membered ring composed of four carbon atoms and two nitrogen atoms. The ring has alternating single and double bonds, making it aromatic.

Nucleobases: Pyrimidine serves as the core structure for two of the four nitrogenous bases found in DNA and RNA: cytosine (C) and thymine (T) in DNA, and cytosine (C) and uracil (U) in RNA. These bases are essential for encoding genetic information and regulating gene expression.

Complementary Base Pairing: In DNA, pyrimidine bases (cytosine and thymine) form complementary base pairs with purine bases (guanine and adenine) through hydrogen bonding. This pairing is critical for the double-stranded structure and replication of DNA.

Biosynthesis: Pyrimidines are synthesized de novo in living organisms to produce the nucleotides required for nucleic acid synthesis. The synthesis of pyrimidine nucleotides involves a series of enzymatic reactions, leading to the formation of cytosine, thymine, and uracil nucleotides.

Antimetabolites: Certain drugs and compounds can interfere with pyrimidine biosynthesis and function, acting as antimetabolites. They disrupt DNA and RNA synthesis and are used as chemotherapy agents to treat cancer and other diseases.

Pharmaceutical Applications: Several drugs and pharmaceutical agents contain pyrimidine moieties as part of their chemical structure. Examples include antiviral drugs, antifungal agents, antimalarials, and antihypertensive medications.

Plant Defence: Pyrimidine derivatives can play a role in plant defense against pathogens, acting as chemical compounds that protect plants from various stresses and infections.

Synthetic Chemistry: Pyrimidine derivatives can be synthesized through various chemical reactions, allowing for the incorporation of different substituents and functional groups, leading to compounds with diverse properties and applications.

DNA Repair: Pyrimidine dimers, formed by ultraviolet radiation-induced covalent bonding of adjacent pyrimidine bases in DNA, are a common type of DNA damage. Cells have DNA repair mechanisms to correct these dimers and maintain genomic integrity.

Photochemistry: Pyrimidines are involved in various photochemical reactions and are relevant in studies of atmospheric and environmental chemistry.

1.3.3.1 Synthesis of Pyrimidine

a. 4-arylquinolines are produced by an oxidative annulation involving anilines, aryl ketones, and DMSO as a methine (=CH) equivalent supported by K2S2O8, whereas 4-arylpyrimidines are produced by activating acetophenone-formamide conjugates.

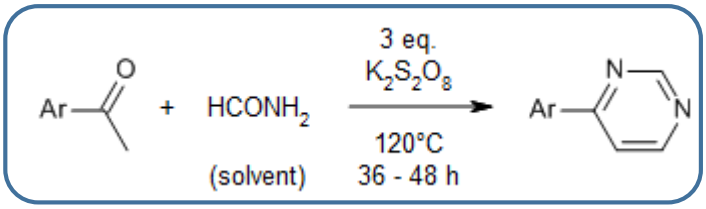

b. Different pyrimidine derivatives with broad functional group tolerance are produced by an operationally straightforward, regioselective reaction of ketones, aldehydes, or esters with amidines in the presence of TEMPO and an in situ prepared recyclable iron (II)-complex. The reactions will likely follow a sequence of TEMPO complexation, enamine addition, temporary occupancy, TEMPO elimination, and cyclization.

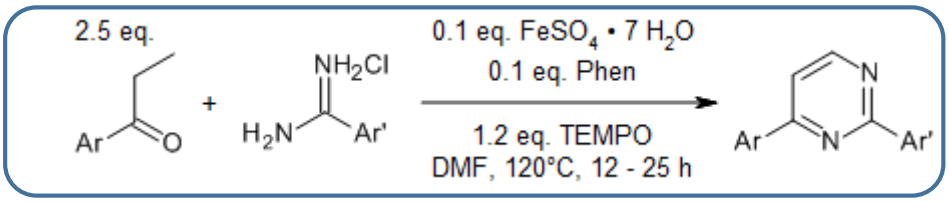

c. In the presence of O2 as the only oxidant, polysubstituted pyrimidines can be formed smoothly by base-promoted intermolecular oxidation of allylic C(sp3)-H and vinylic C(sp2)-H of allyllic compounds with amidines. This protocol has

benefits for the environment, good functional group tolerance, high atom economy, and protection of group-free nitrogen sources.

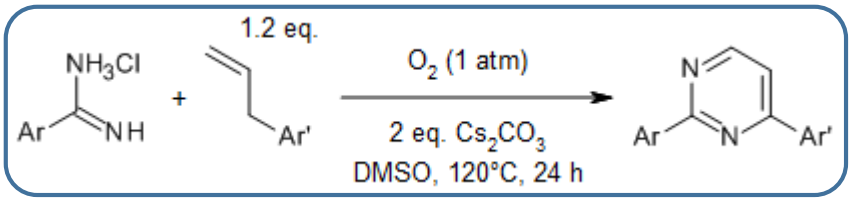

d. Under basic conditions, pyrimidines with a variety of functionalities can be easily, broadly, and cheaply synthesised through a copper-catalyzed cyclization of ketones with nitriles. The reaction has a wide range of acceptable substrates and accepts a number of significant functional groups.

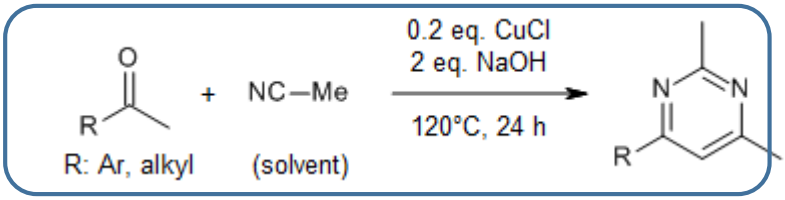

e. An oxidative [3 + 2 + 1] three-component annulation using amidines, ketones, and N, N-dimethylaminoethanol as the sole carbon source yields an effective, simple, and environmentally friendly way to make pyrimidine derivatives. The reaction accepts a variety of significant functional groups.

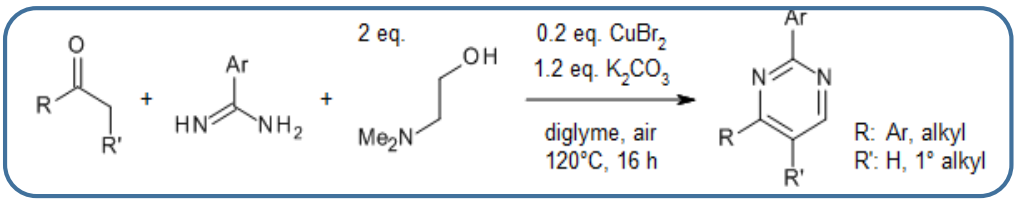

f. The reaction of trifluorinated 2-bromoenones with aryl- and alkylamidines provides trifluoromethylated pyrimidines in very good yields via an aza-Michael addition-intramolecular cyclization-dehydrohalogenation/dehydration cascade reaction. This strategy offers high selectivity and mild reaction conditions.

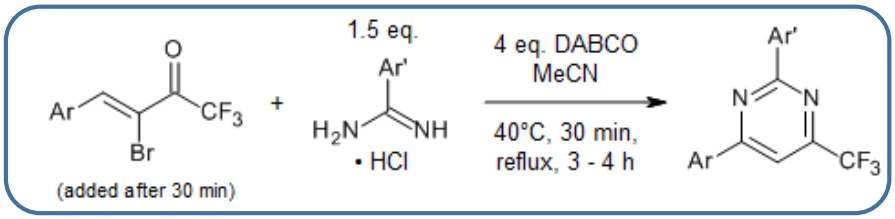

1.3.4 Quinazoline

Quinazoline is a heterocyclic organic compound with the chemical formula C8H6N2. It is a bicyclic ring system consisting of two fused rings—a benzene ring fused with a pyrimidine ring. The pyrimidine ring in quinazoline contains two nitrogen atoms and four carbon atoms.

Key features of quinazoline:

Bicyclic Structure: Quinazoline has a unique bicyclic structure, with a benzene ring fused to a pyrimidine ring. This gives quinazoline a combination of aromatic properties from both rings.

Aromaticity: Both the benzene and pyrimidine rings in quinazoline are aromatic, resulting in enhanced stability and reactivity of the compound.

Isomers: Quinazoline exists in two main isomeric forms—2-quinazolinone and 4-quinazolinone—differing in the position of the nitrogen atom in the pyrimidine ring relative to the benzene ring.

Medicinal Significance: Quinazoline and its derivatives have been studied in medicinal chemistry due to their diverse biological activities. Some quinazoline-based drugs are used to treat cancer and respiratory disorders.

Anticancer Agents: Several quinazoline derivatives have been developed as anticancer agents, particularly as receptor tyrosine kinase inhibitors, targeting specific signalling pathways involved in cancer growth and metastasis.

Synthetic Accessibility: Quinazoline derivatives can be synthesized through various chemical reactions, allowing for the incorporation of different substituents and functional groups, leading to compounds with diverse properties and applications.

1.3.4.1 Synthesis of Quinazoline

a. When 2-aminobenzaldehydes and 2-aminobenzophenones are combined with benzylamines, molecular iodine catalyses the formation of quinazolines in excellent yields. The methodology is environmentally friendly and cost-effective due to the use of oxygen as an oxidant and the absence of transition metals, additives, and solvents. Starting materials can also include 2-aminobenzyl alcohols.

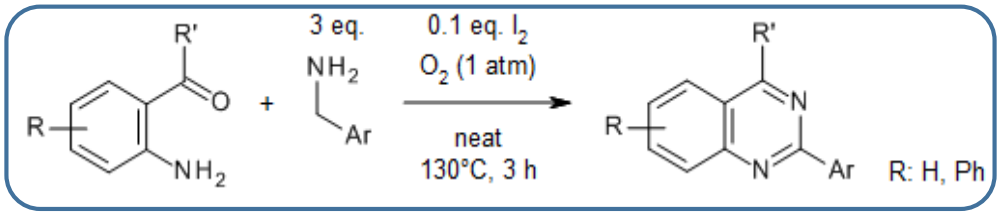

b. It is possible to easily synthesise diversely substituted quinazolines and 3,4-dihydroquinazolines in excellent yields through a tandem reaction of readily available o-aminobenzylamine and aldehydes that is moderately catalysed by o-iodoxybenzoic acid (IBX).

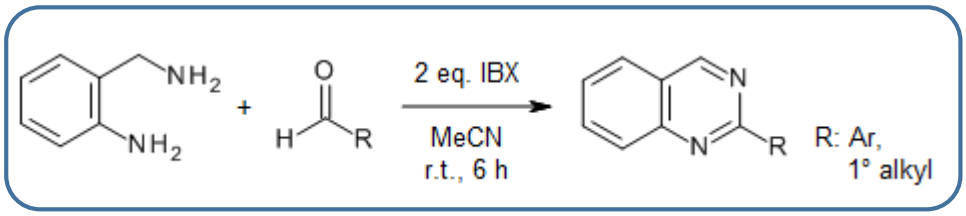

c. Through the activation of C-H/N-H bonds, an atom-economic nickel-catalyzed [4 + 2] annulation of benzylamines and nitriles yields a variety of multi substituted quinazolines. An in-situ created amidine directs the Ni catalyst to activate the C-H bond in ortho.

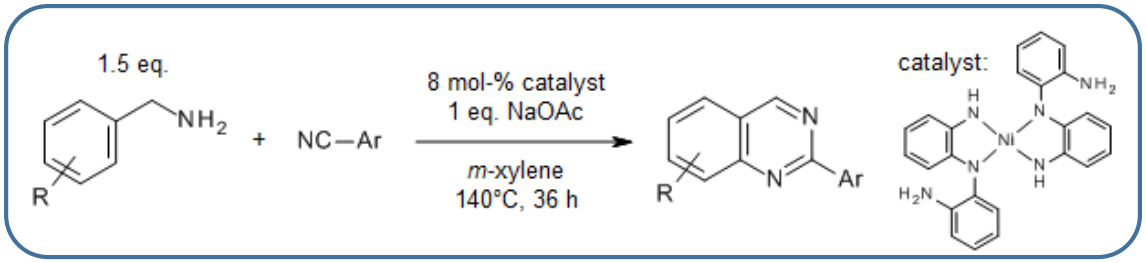

d. 4-arylquinazolines are produced in good yields by a cascade reaction involving triethyl orthocarboxylates, boronic acids, and 2-aminobenzonitriles, which is catalysed by palladium (II). The process starts with C(sp)-C(sp2) coupling and then forms intramolecular C-N bonds.

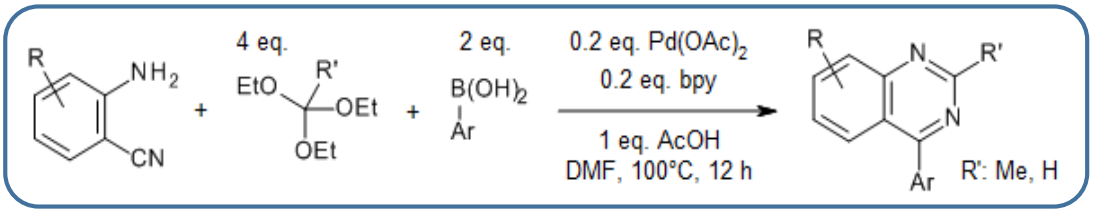

e. Cerium nitrate hexahydrate and ammonium chloride are combined in an effective copper-catalyzed cascade reaction of (2-aminophenyl) methanol's with aldehydes to formed a variety of 2-substituted quinazolines in good yields. The process is flexible and practical, tolerating a range of functional groups, and enables the synthesis of 2-substituted quinazoline derivatives.

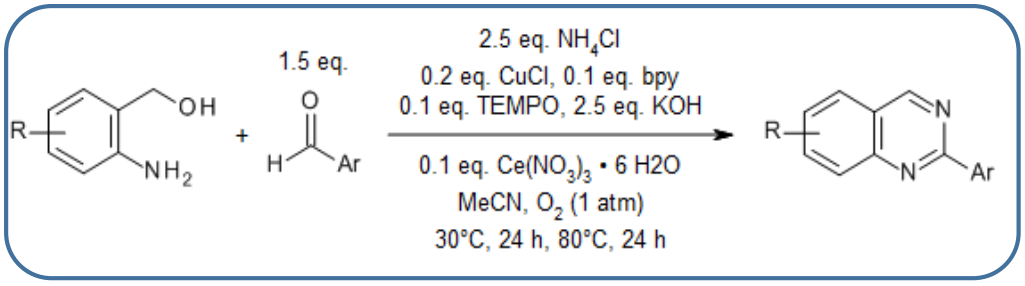

Table.4. FDA approved dug of Heterocyclic moieties

Sr. No.	Marketed drug structure with Name	Manufacture Company name	Cancer types	Target Molecule	FDA approval year
Thiadiazole 1	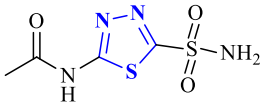 Acetazolamide	Emcure pharma	Renal cell carcinomas	Carbonic anhydrous inhibitor	**2005**
2	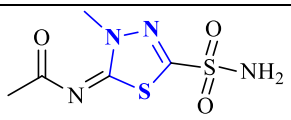 Methazolamine	Remedyrepack inc.	-	-	-
3	 Megazol	Akumentis healthcare ltd	-	-	-
Benzimidazole 4	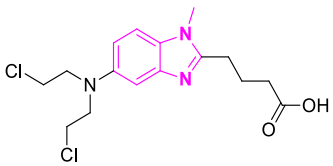 **Bendamustine**	Teva pharmaceutical industries ltd. German product	Chronic lymphocytic leukemia (Cancer of WBC)	β- cell	**2015**

5	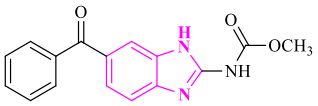 **Mebendazole**	Medix laboratories	Thyroid cancer	Tubulin protein	**2016**
6	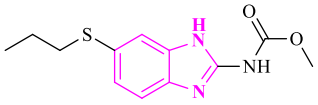 **Albendazole**	Cipla from india. Enaltec labs india. Beijing infoark co ltd from china. Ka malle pharmaceuticals from india	Head and neck squamous cell cancer.	CDK4/6	**1996**
7	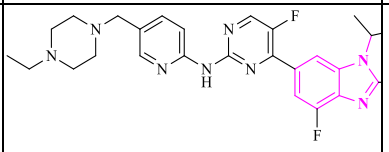 **Abemaciclib**	Eli lilly and company	Breast cancer	HER2	**2015**
8	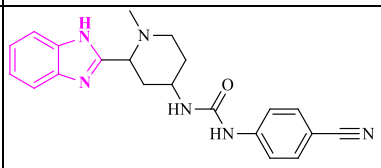 **Glasdegib**	Pfizer oncology	Acute myeloid leukemia	hedgehog receptor inhibitor	**2018**
9	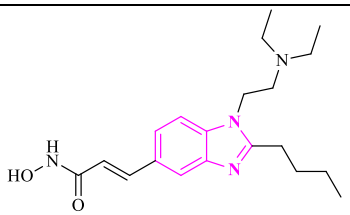 **Pracinostat**	Mei pharma, inc.	Tumors	Histon deacetylase inhibitor	**2013**
10	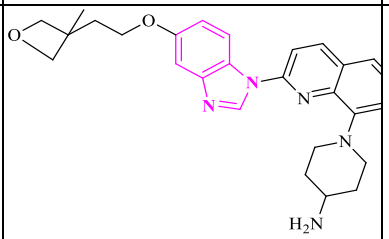 **Crenolanib**	Arog pharmaceuticals,	Acute myeloid Leukemia, Gastrointestinal Stromal Tumor	Type 1 kinase inhibitor	**2017**

11	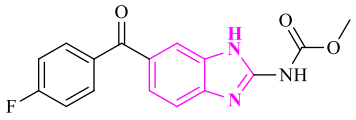 **Flubendazole**	Janssen pharmaceutica n.v.	Breast cancer, prostate cancer, colorectal cancer, lung cancer.	P53	**1952**
12	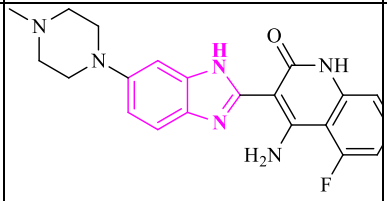 **Dovotinib**	Allerity therapeutics	Renal cell carcinoma, Multiple myeloma	TKI-258	**2021**
Quinazoline 13	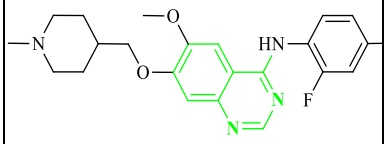 **Vandetanib**	Astrazeneca	Medullary thyroid cancer (MTC)	EGFR, VEGFR	**2011**
14	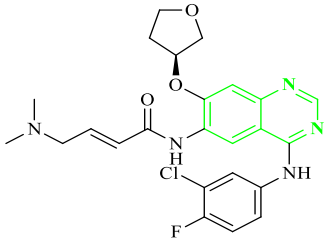 **Afatinib**	Boehringer ingelheim	Non-small cell lung cancer (NSCLC)	EGFR	**2013**
15	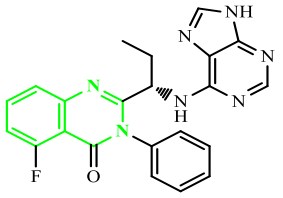 **Idelalisib**	Gilead	Blood cancers	PI3K	**2014**
16	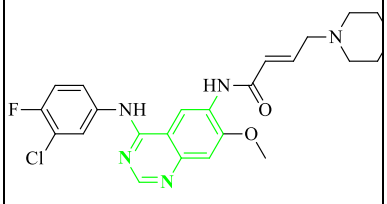 **Dacomitinib**	Pfizer	Non-small cell lung cancer (NSCLC) with EGFR mutation	EGFR, ERBB	**2018**

17	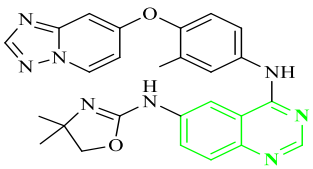 **Tucatinib**	Seattle genetics	Advanced unresectable or metastatic HER-2 positive breast cancer	EGFR, HER2	**2020**
18	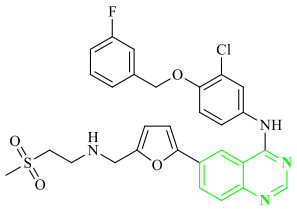 **Lapatinib**	Novartis and gsk	Advanced or metastatic breast cancer	EGFR, ERBB	**2007**
19	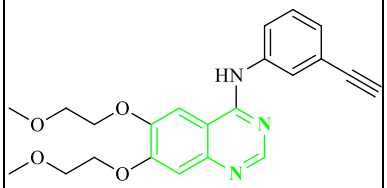 **Erlotinib**	Osi pharms	Non-small cell lung cancer (NSCLC), pancreatic cancer	EGFR	**2004**
20	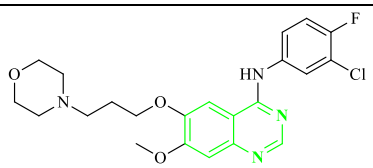 **Gefitinib**	Astrazeneca	Non-small cell lung cancer (NSCLC)	EGFR	**2003**
21	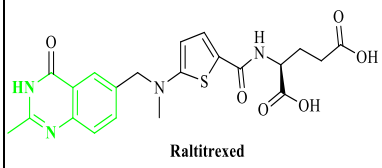 **Raltitrexed**	Astrazeneca	Malignant neoplasm of colon and rectum	TS	**1998**
22	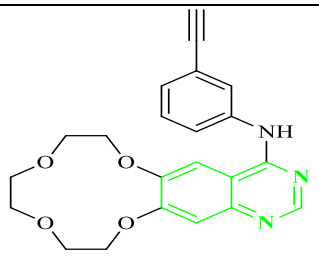 **Icotinib**	Betta pharma	Non-small cell lung cancer (NSCLC)	EGFR-TKI	**2014 (SFDA)**

Pyrimidine 23	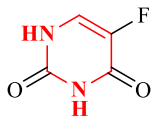 **Fluorouracil**	Biochem pharmaceutical industries ltd, Om biotec (oncomed pharmaceuticals)	Colorectal Cancer, Esophageal Cancer, Pancreatic Cancer, Breast Cancer, Cervical Cancer	HDAC	**1962**
24	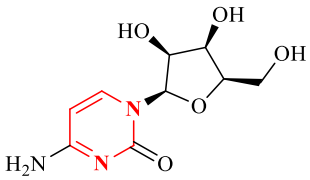 **Cytarabine**	Euticals from italy, Shandong octagon chemicals limited from china, Zhejiang hisun pharma from china.	Acute myeloid and Acute lymphocytic leukemia, non-Hodgkin's lymphoma primary central nervous system lymphoma	*Ara-C*	**1969**
25	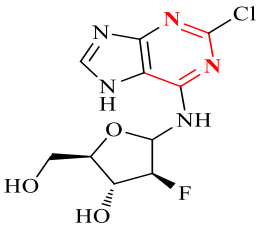 **Clofarabine**	Abon pharms llc, Accord hlthcare, Mylan labs ltd, Gland pharma ltd, Amneal.	Acute lymphoblastic leukemia	T47D	**2004**
26	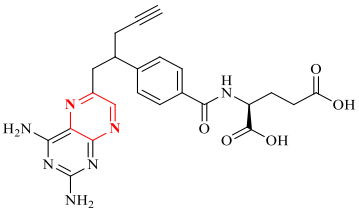 **Pralatrexate**	Allos therapeutics ltd	Treatment of relapsed or refractory peripheral T-cell lymphoma (TCL)	*dihydrofolate reductase (DHFR)*	**2009**

27	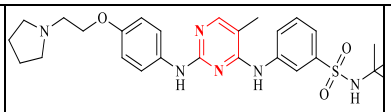 **Fedratinib**	Impact biomedicines	Myelofibrosis	*BRD4 and* JAK2	**2019**
28	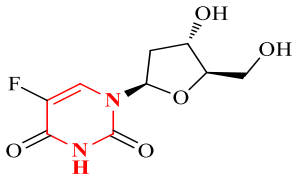 **Floxuridine**	Lgm *pharma*, Zhejiang hisun pharma	Cancer of gastrointestinal (GI) tract (cancer of the stomach or intestines) that has spread to the liver.	-	**1970**

2. Objective

2. OBJECTIVES

The present work entitled **"DESIGN AND SYNTHESIS OF NEW ULK1/2 INHIBITORS AS ANTICANCER AGENTS"** is done at the Department of Pharmaceutical Chemistry, Shree Dhanvantary Pharmacy College, Kim - Surat with the following objectives.

1. To search the novelty of my proposed molecule from chemical databases like Pubchem, Chemspider and Scifinder

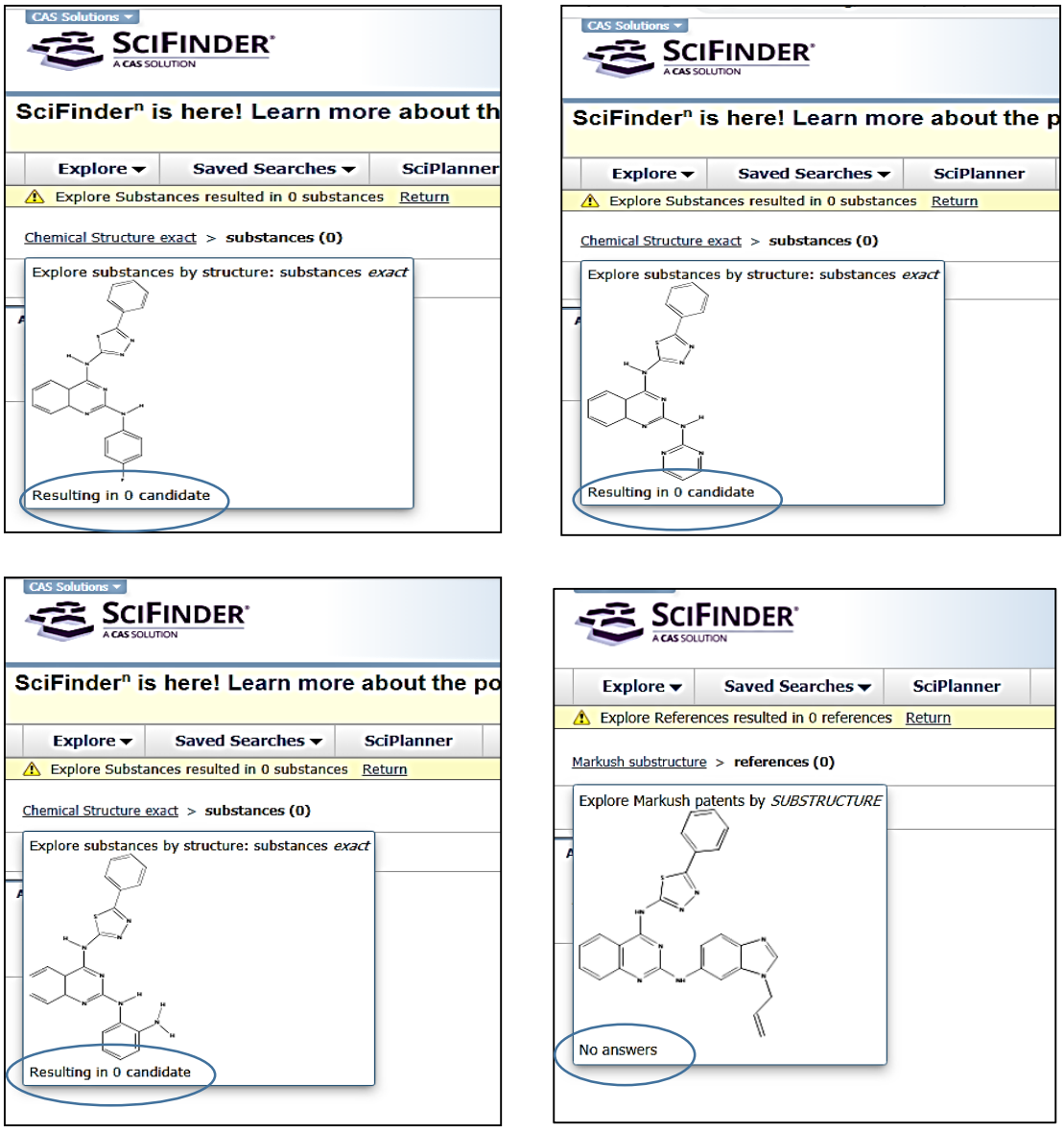

Fig.14. Novelty result of SciFinder

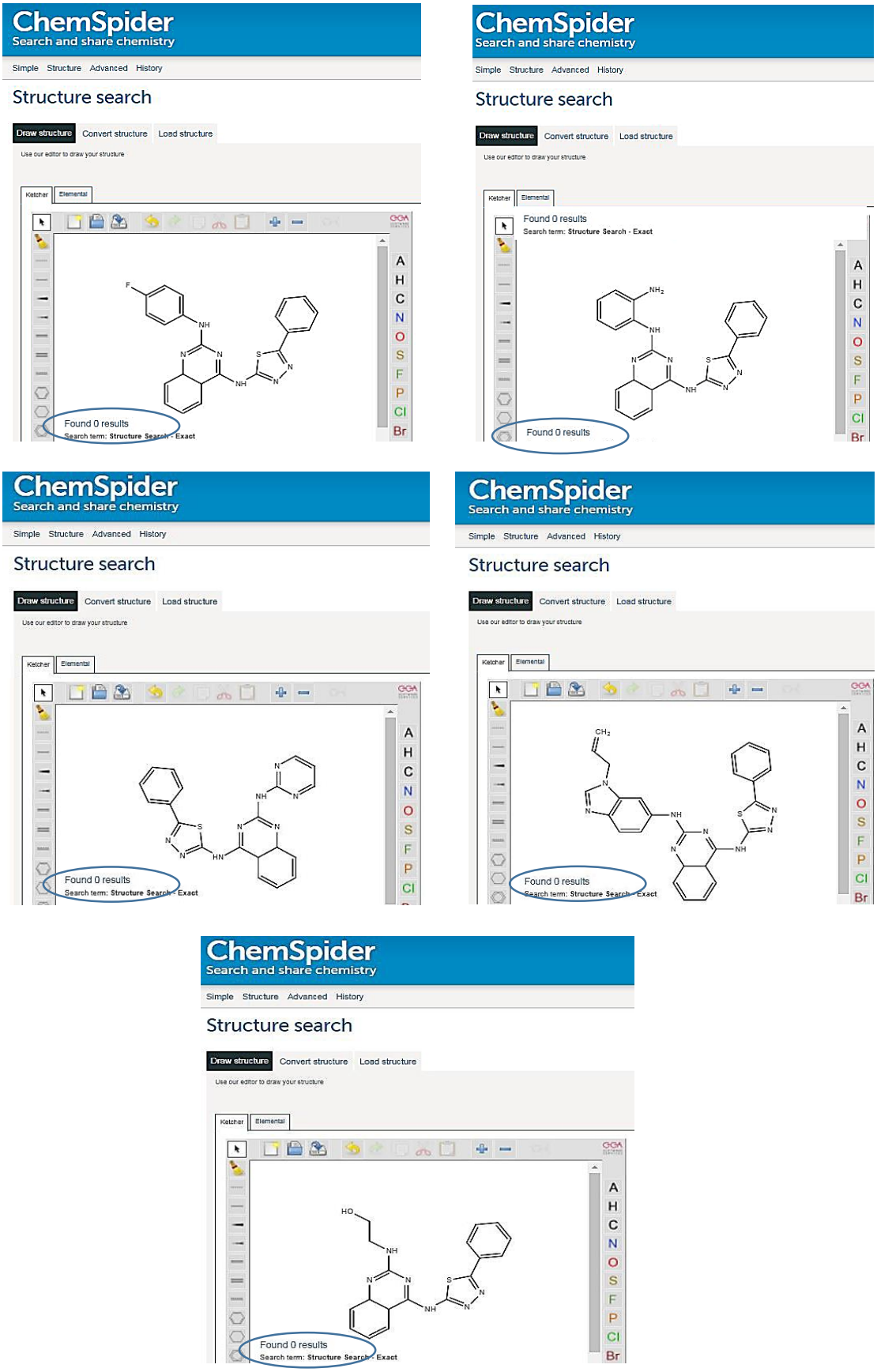

Fig.15. Novelty Result of Chemspider

2. To establish the method of synthesis for the proposed molecule.
3. To perform the *In Silico* assessment of proposed molecule.
4. Synthesize the newly substituted thiadiazole and its derivatives using the appropriate approach.
5. To monitor the progress and purity of molecules by TLC.
6. To purify the molecules by recrystallization using suitable solvents.
7. To characterize the structure of the newly synthesized compounds by physical data (M.P., TLC).
8. To characterize the structure of newly synthesized compounds' spectral data (IR, 1H NMR, and Mass spectroscopy).
9. To evaluate the biological activity of newly synthesized compound by MTT Assay at Gujrat University, Ahmedabad.

3. Review of Literature

3. REVIEW OF LITERATURE

1. Anti-cancerous biological activity of heterocyclic moieties

1.1 Thiadiazole

Guan P et al. discovered that a series of hydroxamic acids derived from 1,3,4-thiadiazole exhibited potent inhibition of HDAC enzymes. Several of these compounds exhibited robust growth inhibition in various tumor cell lines and displayed significant inhibitory activity in HDAC enzyme assays. In a direct comparison with SAHA, where SAHA had an IC50 value of 0.15 µM, compound 1 displayed even greater inhibitory potency with an IC50 value of 0.089 µM. (84).

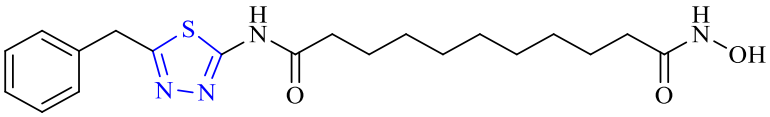

1

Matysiak et al. conducted a study to explore the anti-proliferative properties of various N-substituted 2-amino-5-(2,4-dihydroxyphenyl)-1,3,4-thiadiazole derivatives. They employed substitutions with alkyl, aryl, and morpholinoalkyl groups to modify the compound structures, and their identification was based on analyses of elemental composition, infrared (IR), 1H and 13C nuclear magnetic resonance (NMR), and mass spectrometry (MS) spectra. In vitro cytotoxicity assessments were performed using four human cell lines: SW707 (rectal), HCV29T (bladder), A549 (lung), and T47D (breast). Notably, the phenyl derivatives exhibited weaker anti-proliferative effects compared to the alkyl and morpholinoalkyl derivatives. Among the tested compounds, the most potent chemical was 2-(2,4-dichlorophenylamino)-5-(2,4-dihydroxyphenyl)-1,3,4-thiadiazole, which displayed an ID50 value that was half as low as that of the control compound, cisplatin, when tested on SW707 and T47D cell lines. (85).

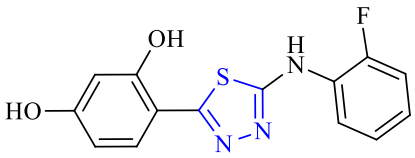

2

Kumar et al. discovered a series of derivatives of 5-(3-indolyl)-2-substituted-1,3,4-thiadiazoles and evaluated their cytotoxicity against six different human cancer cell lines. The most potent compound for preventing cancer cell explosion was identified as indolyl-1,3,4-thiadiazole, specifically compound 3, which featured 5-bromo indolyl and 4-

benzyloxy-3-methoxyphenyl substituents. This compound exhibited remarkable cytotoxicity with an IC50 value of 1.5 mM when tested on the PaCa2 cell line (86).

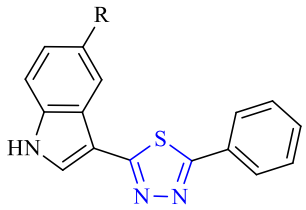

3 **R = H**

Polkam et al. synthesized a series of 2,5-disubstituted 1,3,4-thiadiazole compounds and assessed their antimycobacterial activity against Mycobacterium smegmatis MC-155. Additionally, they evaluated the cytotoxic activity of these compounds against the cancer cell lines HT-29 and MDA-MB-231 using the MTT colorimetric technique. The compounds were well-characterized through various spectral analyses, including 1HNMR, 13CNMR, FT-IR, mass spectrometry, and high-resolution mass spectrometry (HRMS). From the screening results, it was observed that compounds 5g, 7a, and 9 exhibited promising cytotoxic activity against the tested cancer cell lines. Furthermore, they demonstrated good antitubercular activity with MIC values of 65.74 and 40.86, respectively. Among the compounds investigated, compound 4 stood out as a potent antimycobacterial and anticancer agent (87).

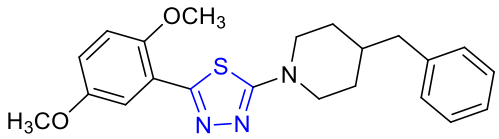

4

Luo et al. identified a novel set of benzisoselenazolone derivatives containing 1,3,4-thiadiazole through the reaction of 2-chloroselenobenzoyl chloride with 2-amino-5-substituted-1,3,4-thiadiazole derivatives. They conducted in vitro assessments of antiproliferative activity in SSMC-7721, MCF-7, and A-549 cells. The results of their study revealed that compounds 5, 6, and 7 exhibited effective antiproliferative activity in multiple tumor cell lines (88).

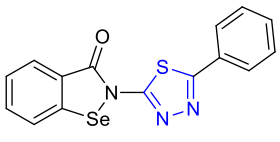

5

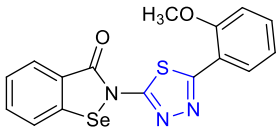

6

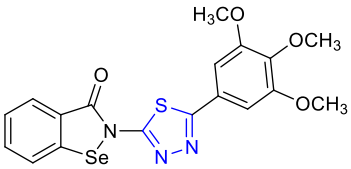

7

Noolvi et al. synthesized a series of novel 2,6-disubstituted imidazo[2,1-b][1,3,4]thiadiazole molecules from 5-substituted-1,3,4-thiadiazol-2-amine. The National Cancer Institute conducted an initial single-dose in vitro primary cytotoxicity assay on these newly synthesized compounds. After meeting the activity requirements in this assay, two compounds, namely compound 8 with identifiers 107166/760239, were selected for further testing against a comprehensive panel of 60 human tumor cell lines. This testing involved a minimum of five concentrations at 10-fold dilutions.

Remarkably, 3-(2-(4-methoxyphenyl)imidazo[2,1-b][1,3,4]thiadiazol-6-yl) aniline, referred to as compound 8, exhibited significant growth inhibition of the Non-Small Cell Lung Cancer HOP-92 cell line (with a GI50 value of 0.114 mM) and the Renal Cancer CAKI-1 cell line (with a GI50 value of 0.743 mM) in vitro (89).

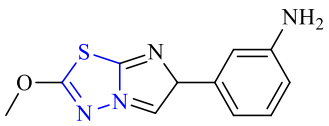

8

Terzioglu et al. synthesized a series of novel 2,6-dimethyl-N-substituted phenylmethylene-imidazo compounds, deriving them from 2,6-dimethylimidazo-[2,1-b][1,3,4]thiadiazole-5-carbohydrazides. They evaluated these newly synthesized compounds using the National Cancer Institute's single-dose in vitro primary cytotoxicity assay, employing the Sulforhodamine B (SRB) protein assay to assess cell stability and growth. Among the compounds tested, 2,6-Dimethyl-N-(2-hydroxyphenylmethylidene)imidazo[2,1-b][1,3,4]thiadiazole-5-carbohydrazide (referred to as compound 9) exhibited the most potent cytotoxicity. When screened in vitro against a panel of 60 human tumor cell lines by the National Cancer Institute, this compound displayed the strongest impact on an ovarian cancer cell line, with a log10 GI50 value of 5.51 (90).

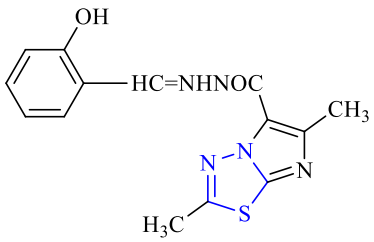

9

Yang et al. synthesized a series of cinnamic acyl 1,3,4-thiadiazole amide derivatives and evaluated their biological activities with a focus on their potential as tubulin polymerization inhibitors and antiproliferation agents. Among these compounds, compound 10 demonstrated the most potent in vitro activity. Specifically, compound 10 exhibited significant growth suppression effects on both the MCF-7 and A549 cell lines, with IC50 values of 0.28 µg/mL and 0.52 µg/mL, respectively. This compound displayed the strongest activity among all the tested compounds in the study (91).

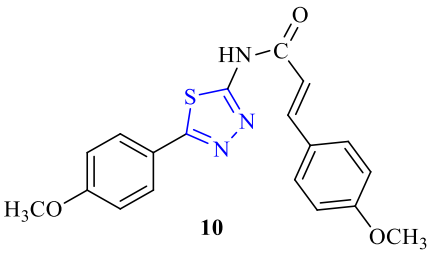

10

1.2 Anti-cancerous activity of Benzimidazole:

Wang et al. conducted the synthesis and evaluation of benzimidazole derivatives for their antitumor efficacy. Among these derivatives, compound 11 exhibited the most potent anti-proliferative activity against MFC cells, with an IC50 value of 3.95 µM. This indicates that compound 11 showed strong inhibitory effects on the growth of MFC cells in the study (92).

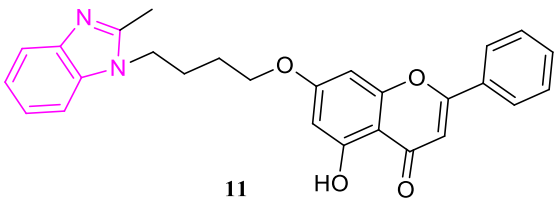

11

Ren et al. designed and synthesized compound 12 as a tubulin inhibitor with potent antiproliferative properties. Notably, compound 12 demonstrated remarkable effectiveness in overcoming paclitaxel resistance in vitro. It displayed nearly equivalent efficacy against both a paclitaxel-resistant cancer cell line (with an IC50 value of 9.7 nM) and the corresponding parental cell line (with an IC50 value of 6.2 nM). This suggests that

compound 12 has the ability to combat drug resistance and inhibit cell proliferation effectively (93).

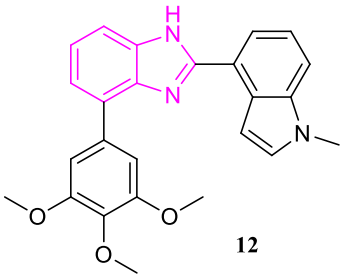

12

Akhtar et al. designed a novel series of benzimidazole-linked pyrazole compounds, and among them, compound 13 exhibited notable activity. Specifically, in the context of lung cancer cell lines, compound 13 demonstrated the most potent activity with an IC50 value of 2.2 µM. Furthermore, it exhibited strong binding to the epidermal growth factor receptor (EGFR) with an IC50 value of 0.97 µM. (94).

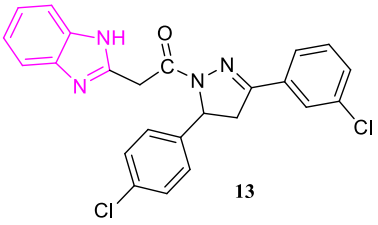

13

Huang et al. synthesized a benzimidazole compound with the intention of using it as an anticancer drug. They evaluated its cytotoxicity against several human carcinoma cell lines, including A-549, BFTC-905, RD, MES-SA, and HELA. Compound 14 demonstrated notable cytotoxic activity with an IC50 value of 2.8 µM.(95).

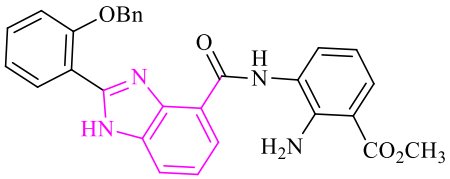

14

Yadav et al. designed and assessed benzimidazole derivatives for their in vitro anticancer activity. Among these derivatives, compound 15 emerged as the most effective one. It demonstrated significant inhibitory effects on several important enzymes: isocitrate lyase, pantothenate synthetase, and chorismite mutase. The inhibition percentages for these enzymes were as follows: 67.56%, 53.45%, 75.3%, and 47.56%, respectively. These

findings suggest that compound 15 may have promising potential as an anticancer agent through its action on these key enzyme (96).

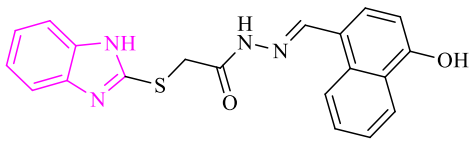

15

Marri et al. conducted research on the in vitro anticancer activity of benzimidazolyl 2-amino-1,3,4-oxadiazole derivatives against various cell lines, including HeLa, MCF7, A549, and HEK293. Among these derivatives, compounds 16a and 16b exhibited notable anticancer activity, with the following IC50 values: HeLa cell line: 6.07 µM and 0.028 µM for compounds 16a and 16b, respectively.

MCF-7 cell line: 5.30 µM and 0.09 µM for compounds 16a and 16b, respectively.

A549 cell line: 7.16 µM and 0.061 µM for compounds 16a and 16b, respectively.

Additionally, these compounds showed good anticancer activity. Moreover, HEK-293 cells were less affected by these compounds.

(97).

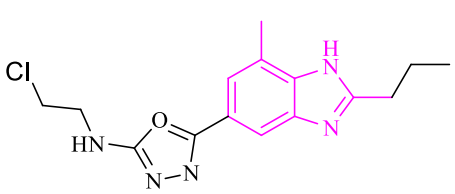

16 a

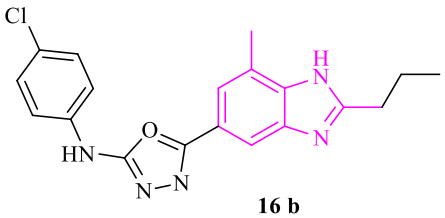

16 b

Woo et al. designed and evaluated a series of derivatives of benzimidazolyl curcumin analogs. Among these derivatives, Compound 17 demonstrated a potent inhibitory effect on the growth of MCF-7 cancer cells in their study, with an IC50 value of 1.9 µM. This suggests that Compound 17 may have significant potential as an anticancer agent targeting MCF-7 cells (98).

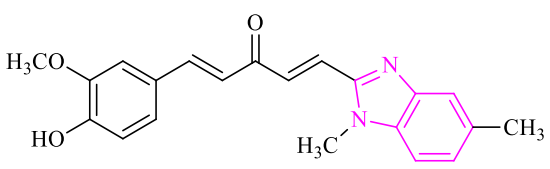

17

Ulviye et al. synthesized a series of new benzimidazole-triazolothiadiazine compounds with the aim of serving as aromatase inhibitors with anticancer properties. Compound 18, among these compounds, exhibited aromatase inhibitory activity, although it was slightly less effective than letrozole, a known aromatase inhibitor. Compound 18 had an IC50 value ranging from 0.032 to 0.042 µM, while letrozole had a more potent aromatase inhibitory activity with an IC50 range of 0.024 to 0.001 µM. This suggests that compound 18 may still have potential as an aromatase inhibitor with anticancer activity, albeit with slightly reduced potency compared to letrozole (99).

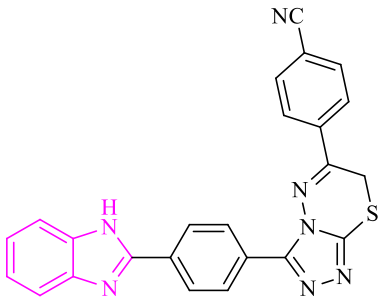

18

Saglik et al. synthesized a new series of benzimidazole compounds and assessed their potential as aromatase inhibitors. Among these compounds, the 4-benzylpiperidine derivative compound 19 displayed strong aromatase inhibitory activity. It had IC50 values of 0.024 µM and 0.001 µM, which were comparable to the reference medication cisplatin with IC50 values of 0.021 µM and 0.001 µM. This indicates that compound 19 is one of the most effective compounds in this series for inhibiting aromatase, particularly in the context of the MCF-7 cell line (100).

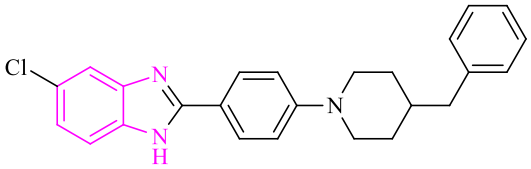

19

Ulviye et al. formulate and assessed novel hydrazone-modified benzimidazole compounds as anticancer drugs. In this **compound 20**, the IC50 for MCF-7 inhibition was 0.0316 M. Due to its stronger anticancer properties and the effect of substituents on cytotoxic activity (101).

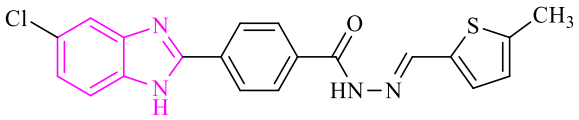

20

Goud et al. designed and synthesized benzimidazole-triazole hybrids with the aim of developing agents that induce apoptosis through the galectin-1 (gal-1) pathway. They then tested these compounds against various human cancer cell lines to assess their potential anticancer properties. Compound 21 stood out as a particularly promising candidate, showing remarkable growth inhibition against lung cancer cells, specifically A-549 and NCI-H460, with IC50 values of 0.63 µM and 0.21 µM, respectively (102).

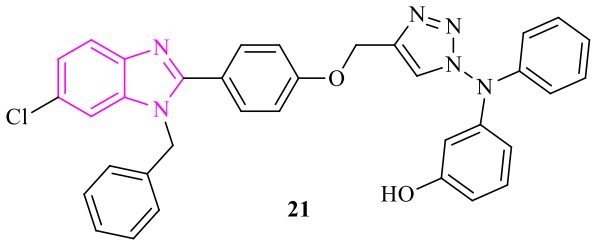

21

Yurttas *et al.* synthesized Novel N- [4-(2-methylthiazol-4-yl) phenyl] acetamide compounds and assessed their anticancer efficacy. **Compounds 22 a and 22 b**, which have benzimidazole and 5-chlorobenzimidazole side groups, respectively, showed significant anticancer activity with IC50 values of 112.7, 18.3 M and 65.2, 5.3 M in a series of anticancer tests that included cytotoxicity, analysis of DNA synthesis, and induction of apoptosis (103).

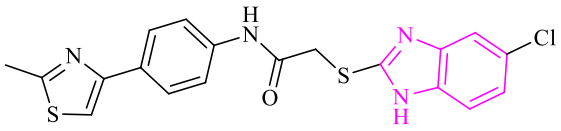

22 a

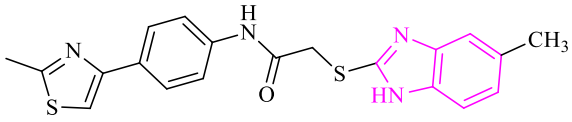

22 b

Harika et al. synthesized a novel series of benzimidazole derivatives and assessed their cytotoxicity against a panel of selected human cancer cell lines, as well as HEK-293 human embryonic kidney cells. Compound 23 stood out in terms of its significant cytotoxic effect against cancer cells, with IC50 values ranging from 9.2 to 166.1 µg/mL. Specifically, compound 23 demonstrated substantial cytotoxic activity against the

following cancer cell lines respectively, MCF-7: IC50 of 17.8 µg/mL, DU145: IC50 of 0.24 µg/mL, H69AR: IC50 of 10.2 µg/mL (104).

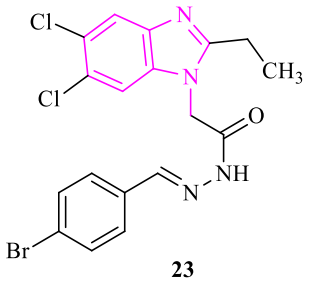

23

1.3 Anti-cancerous activity of Quinazoline:

Abuelizz et al. developed novel quinazoline compounds as potential anticancer agents. They synthesized two unique 2-thioxoquinazolin-4-one compounds by treating 2-amino-5-methylbenzoic acid with butyl isothiocyanate. These compounds were then evaluated in vitro against the HeLa and MDA-MB231 cancer cell lines. Among the tested compounds, compounds 24, 25, and 26 demonstrated promising potential as anticancer agents, with IC50 values as follows: Compound 24: IC50 = 1.85 µM, Compound 25: IC50 = 2.5 µM, Compound 26: IC50 = 2.6 µM (105).

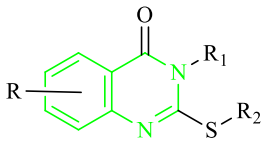

Compound	R	R1	R2
24	Methyl	Benzyl	3-(phthalimido-2-yl)propyl
25	Methoxy	Benzyl	3-(phthalimido-2-yl)propyl
26	Methoxy	Benzyl	Morphilinoethyl

Faraj et al. synthesized and evaluated quinazoline Schiff bases 1 and 2 for their anticancer activities against the MCF7 human breast cancer cell line. Notably, compounds 27 and 28 displayed a significant antiproliferative effect, with IC50 values of 6.246 × 10 (-6) mol/L and 5.910 × 10 (-6) mol/L, respectively, following 72 hours of treatment. These results indicate that compounds 27 and 28 have strong potential as anticancer agents, particularly in the context of breast cancer. (106).

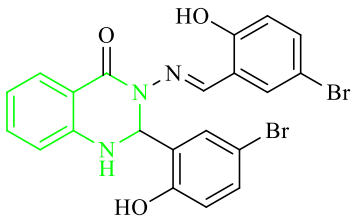

27

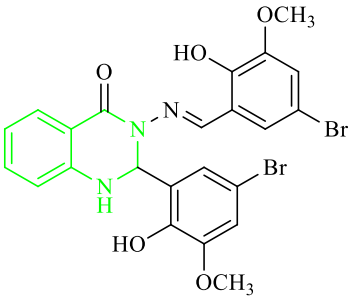

28

Syed et al. developed structurally modified aryl quinazoline-isoxazole derivatives and assessed their potential as anticancer agents against four human cancer cell lines, including MCF-7 (breast cancer), using the MTT assay. Among these derivatives, compounds 29a, 29b, 29c, 29d, and 29j exhibited particularly potent anticancer activities, with the following IC50 values: Compound 29a: IC50 = 1.92 ± 0.85 µM, Compound 29b: IC50 = 1.47 ± 0.51 µM, Compound 29c: IC50 = 0.01 ± 0.008 µM, Compound 29d: IC50 = 2.08 ± 0.77 µM and Compound 29j: IC50 = 0.083 ± 0.001 µM (107).

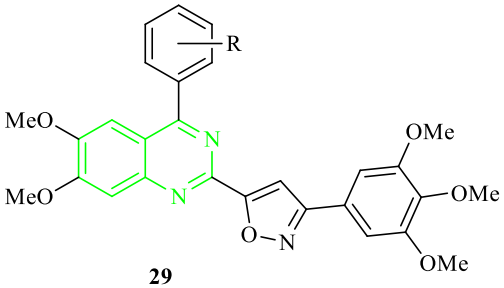

29

Where.,

29a., R = 4-methyl
29b., R = 4-(dimethylamino)
29c., R = 3,4,5-trimethoxy
29d., R = 4-methoxy
29j., R = 2,4,6-trimethoxy

Dhunmati et al. conducted the synthesis and in-vitro anticancer activity testing of quinazoline derivatives on MCF-7 (breast cancer) cell lines using the MTT assay at various concentration levels. Among the nearly 11 synthesized compounds, two compounds, namely 30a and 30b, demonstrated anti-cancer activity. Specifically, compound 30a exhibited an inhibitory action on the breast cancer cell line, resulting in a reduction of cell viability by approximately 51.9% at a concentration of 62.5 µg/mL. Similarly, compound 30b also demonstrated an inhibitory effect on the breast cancer cell line, with a reduction in cell viability of around 50% at a concentration of 62.5 µg/mL (108).

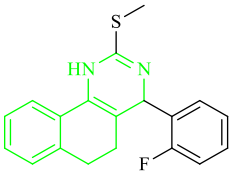

30a

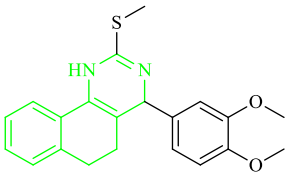

30b

Yong et al. designed isoxazole-moiety-containing quinazoline derivatives for preliminary anticancer efficacy against MCF-7 cell lines utilising the MTT technique. Among them, most compounds showed good to excellent anticancer activity, especially **31a, 31b, 31c** and **31d** exhibited the more potent anticancer activity against MCF-7 cell lines. IC_{50} values of compound **31a** (IC_{50} = **42.82±0.1324µM**), **31b** (IC_{50} = 0.**11±0.0381 µM**), **31c** (IC_{50} = **1.99×10-4±0.0189 µM**), **31d** (IC_{50} **= 5.74±0.00861 µM**) (109).

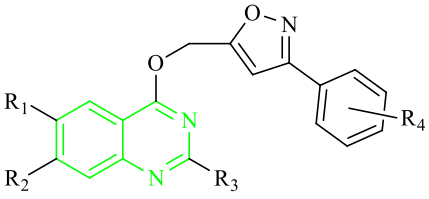

31

Where,

31a: R1 = R2 = H, R3 = Ph, R4 = 2-Cl
31b : R1 = R2 = OCH3, R3 = Cl, R4 = 4-CH3
31c: R1 = R2 = OCH3, R3 = Cl, R4 = 2-Cl
31d: R1 = R2 = OCH3, R3 = Cl, R4 = 2,4-diCl

Madhavi et al. developed and synthesised a series of 10 new chalcone-incorporated quinazoline derivatives. All the synthesized compounds were evaluated for their anticancer activities against four human cancer cell lines HT-29. Among them, four compounds, **32a, 32b, 32c** and **32d** showed more potent anticancer activity than the control drug, Combretastatin – A4, with IC_{50} values of compound **32a** (IC_{50} **= 0.18 µM**), **32b** (IC_{50} = **0.13 µM**), **32c** (IC_{50} = **1.56 µM**), **32d** (IC_{50} **= 2.89 µM**) (110).

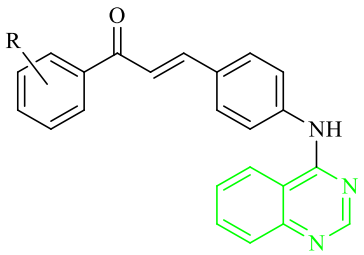

32

Where,

32a; R = 2-fluoro-4-trifluoromethyl
32b; R = 4-trifluoromethy
32c R = 3,4-dimethoxy32d; R= 4-methoxy

Akgun et al. synthesized and tested a series of 6,7-disubstituted-3-2-[4-(substituted) piperazin-1-yl]-2-oxoethyl quinazoline 2,4(1H,3H)-dione derivatives against MCF-7 human cancer cell lines in vitro. Among the compounds evaluated, 3-{2-[4-(4-chlorobenzyl) piperazin-1-yl]-2-oxoethyl} quinazoline-2,4(1H,3H)-dione 33 demonstrated

the highest activity against the MCF-7 cell line, with an IC50 value of 6.8 µM. This suggests that compound 33 has potential as an anticancer agent, particularly against MCF-7 cells. (111)**.**

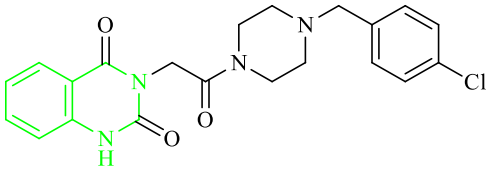

33

Fröhlich et. al., designed five novel quinazoline-artemisinin hybrids synthesized and evaluated for their in vitro anticancer activity against leukemia cells (CCRF-CEM and CEM/ADR5000). Hybrid **34** exhibited an antileukemia effect similar to that of artesunic acid, with EC_{50} values in the low micromolar range, and was 45 times more active toward the multidrug-resistant CEM/ ADR5000 cells (EC_{50} = **0.5 µM**) than the standard drug doxorubicin (112).

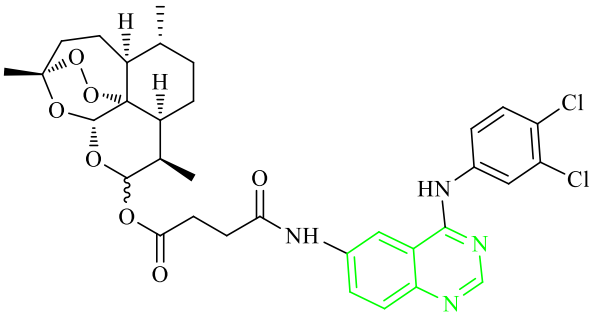

34

Sharma et. al., synthesized novel quinazolinone derivatives through the reaction of N-benzoyl-substituted piperazine-1-carbothioamide with 2-chloromethyl quinazolinone derivatives. These compounds were then evaluated for their anticancer activity against MCF-7 (breast cancer cells) using the MTT method. Among the tested compounds, compound 35 displayed the highest anticancer activity, with an IC50 value of 0.16 ± 0.16 µM. This level of activity was superior to that of the standard anticancer drugs methotrexate (IC50 = 2.20 ± 0.18 µM) and 5-fluorouracil (IC50 = 2.30 ± 0.49 µM). These results suggest that compound 35 has significant potential as an effective anticancer agent, particularly in the context of breast cancer (MCF-7 cells) (113)**.**

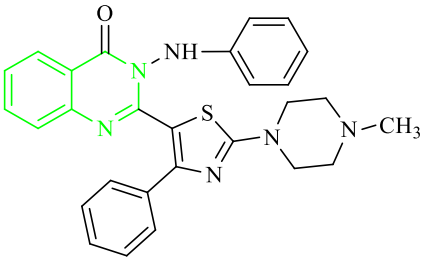

35

1.4 Anti-cancerous activity of Pyrimidine:

Emami et. al., developed and synthesized two novel series of anticancer compounds, namely quinazolinone-pyrimidine and benzyl-pyrimidine hybrids. They assessed the cytotoxic activities of these compounds against three cancer cell lines: HT-29, SW1116, and A549. The results indicated that almost all of the compounds exhibited better antiproliferative activity against colon cancer cell lines (HT-29 and SW1116) compared to the lung cancer cell line A549. Among these compounds, compounds 36 and 37 showed excellent inhibitory activities against the HT-29 cell line, with the following IC50 values: Compound 36: IC50 = 10.67 ± 0.3 μM and Compound 37: IC50 = 27.9 ± 6.5 μM (114).

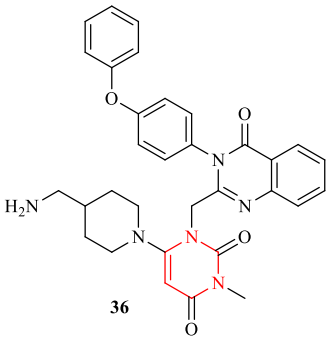

36

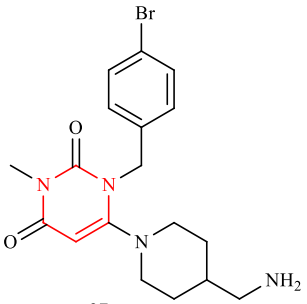

37

Masoud et. al., synthesized three compounds, namely 5-(2-hydroxyphenylide) barbituric acid (L1), 5-(phenyl azo) thiobarbituric acid (L2), and 5-(phenyl azo) barbituric acid (L3), along with their complexes with Os(VIII), Ru(III), Zr(IV), and V(III) ions for potential use as anticancer agents. Among these compounds, 5-(phenyl azo) thiobarbituric acid (L2), referred to as compound 38, exhibited good inhibitory activity against the MCF-7 cancer cell line, with an IC50 value of 22 ± 0.9 μg/mL. This suggests that compound 38 has potential as an anticancer agent, particularly in the context of MCF-7 cells (115).

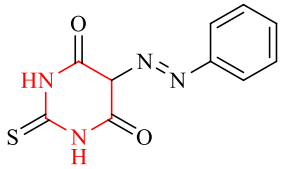

38

Gabera et. al., developed a novel series of 1H-pyrazolo[3,4-d]pyrimidine derivatives and tested their inhibitory properties against the epidermal growth factor receptor (EGFR) for potential use in cancer treatment. Compound 39 was specifically evaluated for its antiproliferative activities against various cancer cell lines, including those bearing wild-type EGFR (EGFRWT) and those with the EGFR T790M mutation (EGFRT790M). Here are the IC50 values for compound 39 against different cancer cell lines: MCF-7 (EGFRWT): IC50 = 0.50 μM, HepG2 (EGFRWT): IC50 = 0.01 μM, A549 (EGFRWT): IC50 = 0.62 μM, H1975 (EGFRT790M): IC50 = 0.04 μM and HCC827 (EGFRT790M): IC50 = 0.12 μM (116).

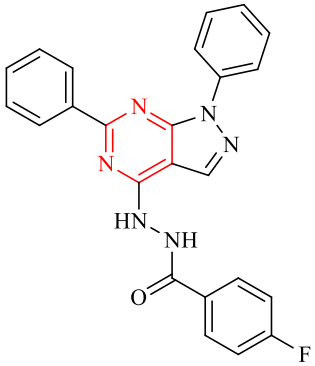

39

Kumar et al. designed and synthesis of novel series of pyrimidine bridged derivatives were examined against breast cancer (MCF-7) and lung cancer (A549) cell lines using MTT assays. From this series, **compounds 40 and 41** were found most potent in the series with **IC_{50}** values of **4.67 μM** & **3.38 μM** and **4.63 μM** & **3.71 μM** against MCF7 and A549 cancer cell lines, respectively (117).

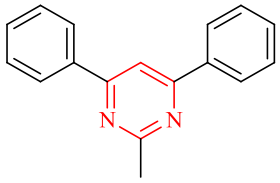

40

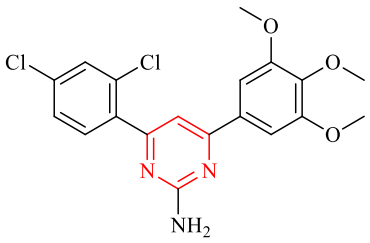

41

Reddy et al. designed and synthesized biscoumarin-pyrimidine conjugates that were tested for anticancer efficacy in vitro. All the compounds especially, **compound 42** exhibited good selectivity profiles by displaying a nontoxic behaviour toward the healthy HEK293 cells and displayed strong binding interactions with a drug carrier protein, HAS. **Compound 42** shows good inhibitory activity against HEK293 cells with **IC_{50}** of **4.85 μM** (118)**.**

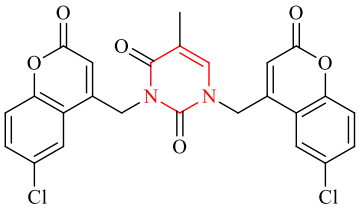

42

El-Metwally et al. designed a novel series of thieno[2,3-d] pyrimidine derivatives that showed **IC_{50}** at **~4–10 µM** against cancerous HepG2 and MCF7 cell lines. In their study, only **compound 43** up-regulated the expression of p53 by ~3–4 folds and reduced the expression of Topo II by ~60%. Also, **43** showed selective cytotoxicity, cell cycle arrest, and induce apoptosis (119).

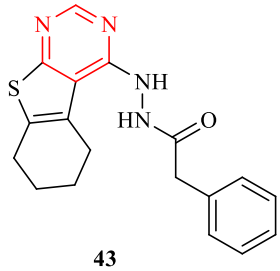

43

Cherukupalli et al. designed and synthesized 4,6-disubstituted pyrazolo [3,4-6 d] pyrimidines as CDK2 inhibitors. SAR confirmed that compounds with thiopentane/thiophenethyl group at C-6 and heteroatom-containing bicyclic moieties (benzofuran) at C-4 exhibited better CDK2 inhibitory activity. Besides, **compound 44** the most potent compound in this series showed antiproliferative activity against K-562 (chronic myelogenous leukemia) and MCF-7 (breast adenocarcinoma) cell lines with **IC_{50}** values of **19.8 µM** and **18.9 µM**, respectively (120).

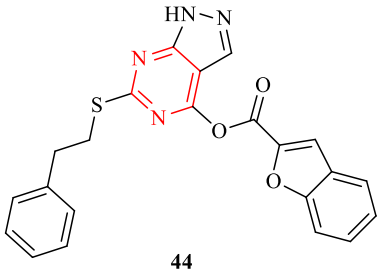

44

Diao et al. designed and synthesized pyrimidine-based benzothiazole derivatives with the aim of developing anticancer agents. Among these compounds, compound 46 displayed remarkable CDK2 inhibitory activity, with an IC50 value of 15.4 nM. This potency was nearly three times better than that of AZD5438, a known CDK inhibitor. (121).

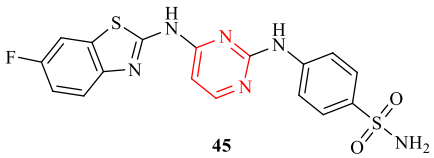

45

Ye et al. designed and synthesized novel 2,4-bismorpholinyl-thieno [3, 2-d] pyrimidine as an antitumor activity. Among them, **compound 46** showed the most potent antitumor activities against HCT116, PC-3, MCF-7, A549 and MDA-MB-231 cell lines with **IC_{50}** values of **3.24 µM, 14.37 µM, 7.39 µM, 7.10 µM,** and **16.85 µM**, respectively. This compound also inhibited the proliferation of A549 cell lines and decreased mitochondrial membrane potential. **Compound 46** as the potent compound was selected for further in vitro anti-PI3Kα and anti-PI3Kβ which demonstrated 92.4% and 62.29% inhibitory activity at 1 µM (122).

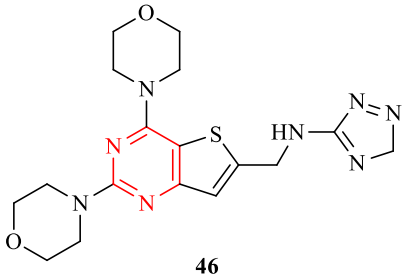

46

M. M. Ghorab et al. synthesized new pyrazole-pyrimidine derivatives and evaluated their in-vitro anticancer activity against the Ehrlich Ascite Carcinoma cell line. Among these derivatives, 5-Benzyl-1-phenyl-1,5-dihydropyrazolo(3,4-d) pyrimidin-4-one, referred to as compound 47, displayed intermediate anticancer activity when compared to doxorubicin, which served as a positive control. Compound 47 exhibited an IC50 value of 90 µg/mL. This suggests that compound 47 has the potential for anticancer activity, although it is not as potent as doxorubicin under the tested conditions. (123).

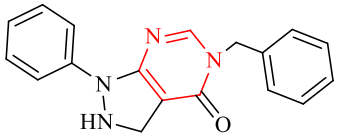

47

ULK ½ inhibitors

ULK100 and ULK101

Martin R. et al. conducted research to identify molecules that could serve as ULK1 and ULK2 inhibitors for non-small cell lung cancer with an oncogenic KRAS mutation. They conducted a search in existing pharmaceutical data to find compounds that exhibited activity against both ULK1 and ULK2 in selectivity screening In their experiments, ULK-100 demonstrated a direct inhibition of ULK1 in vitro with an IC50 of 1.6 nM (95% CI: 1.5–1.8 nM), while ULK-101 had an IC50 of 8.3 nM (95% CI: 7.2–9.6 nM) for ULK1. In comparison, the previously reported ULK1 inhibitor, SBI-0206965, had an IC50 of 38 nM (95% CI: 34–42 nM). Furthermore, ULK2, the mammalian counterpart of yeast ATG1 with a similar role in autophagy as ULK1, was also considered. ULK-100, ULK-101, and SBI-0206965 were tested for their ability to inhibit ULK2 kinase activity in vitro, and all three compounds exhibited nanomolar IC50 values for ULK2. ULK-100 showed the highest potency (ULK2 IC50 2.6 nM), followed by ULK-101 (ULK2 IC50 30 nM), and SBI-0206965 (ULK2 IC50 212 nM) (63).

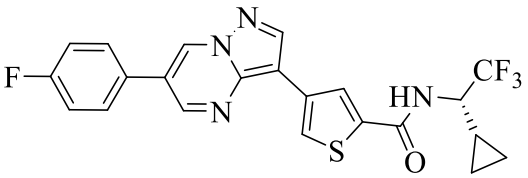

ULK 101
48

SBI-0206965

Egan et al. aimed to identify a selective inhibitor with a pyrimidine scaffold that could suppress ULK1 downstream phosphorylation of VPS34 and Beclin-1, leading to apoptosis in non-small cell lung cancer (NSCLC) cells. This inhibitor destabilized Bcl2 and Bclxl and effectively inhibited autophagy at the initiation point with ULK1, exhibiting an IC50 of 108 nM for ULK1 and 711 nM for ULK2.

The development of the potent ULK1/2 inhibitor, SBI-0206965, involved a target-based reverse pharmacology approach. Analogs were tested using ULK1 in vitro kinase assays, followed by cell-based assays to assess the phosphorylation state of a consensus sequence in VPS34. This process utilized a focal adhesion kinase inhibitor that simultaneously inhibited both FAK and ULK1. The structure-activity relationship (SAR) approach was employed in the development of SBI-0206965, resulting in a compound with nanomolar

IC50 values for both ULK1 and its homolog, ULK2. Cell-based assays confirmed that SBI-0206965 effectively inhibited the phosphorylation of VPS34 and Beclin-1 and reversed the gel mobility shifts of ATG13, indicating a reduction in the phosphorylation of these proteins by ULK1/2.

(126).

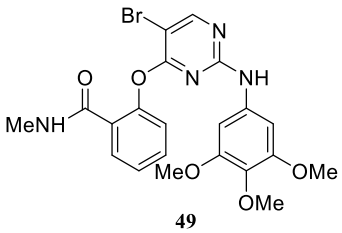

49

SBI-0206965 (ULK1: IC50 of 108 nM; ULK2: IC50 of 711 nM)

MRT67307 and MRT68921

Petherick et al. conducted research in which they explored in vitro inhibitors with a pyrimidine scaffold that also targeted TBK1 and AMPK-related kinases to inhibit ULK1 and ULK2. They discovered two compounds, MRT67307 and MRT68921, which had previously been identified as inhibitors of TANK binding protein 1 (TBK1), a component of the innate immune response system. These compounds showed IC50 values against both ULK1 and ULK2 in the mid to low nanomolar range.

MRT67307 exhibited an IC50 of 45 nM for ULK1 and 38 nM for ULK2, while MRT68921 had an IC50 of 2.9 nM for ULK1 and 1.1 nM for ULK2. When amino acid starvation was induced to activate ULK1, treatment with either MRT67307 or MRT68921 reduced the phosphorylation of serine 318 on ATG13, a site known for ULK1 phosphorylation. Furthermore, these compounds slowed the processing of microtubule-associated protein 1A/1B-light chain (LC3)-I to the lipidated LC3-II phosphatidylethanolamine isoform, which is associated with active autophagy (127).

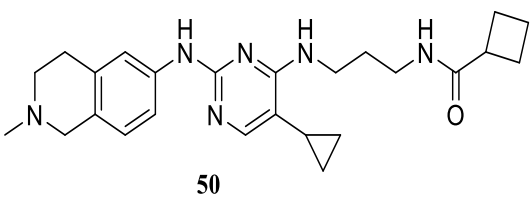

50

MRT67307 (ULK1: IC50 of 45 nM; ULK2: IC50 of 38 nM)

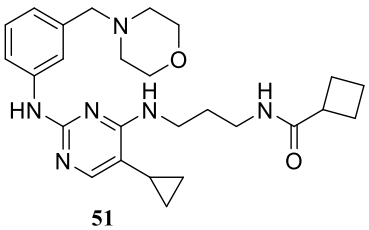

51

MRT68921 (ULK1: IC50 of 2.9 nM; ULK2: IC50 of 1.1 nM)

Compounds 1/3

Lazarus et al. aimed to find structural information on the kinase domain of ULK1. To achieve this, they conducted an in vitro screening process for small molecules that had the capability to stabilize the ULK1 protein. This approach involved identifying compounds that could interact with and enhance the stability of the ULK1 kinase domain, which is crucial for studying its structure and function (130). This process led to the pyrazolyl quinazoline derivative Compound 1(131), which has both ability to stabilizes and inhibits ULK1. Compound 1 is bound in the ATP-binding site of the active conformation of ULK1 in the crystal structure. While equipped with this structural information, chemistry optimization around Compound 1 (ULK1: IC50 of 5.3 nM; ULK2: IC50 of 13 nM; PDPK1: IC50 of 420 nM) did not provide an analog selective enough for ULK1 to merit use in cells (130). Following the original kinase screen, Lazarus et al. explored pyrimidine derivatives (131). The compound BX-795, a phosphoinositide-dependent-kinase-1 (PDPK1) inhibitor, was the stimulation for chemistry focused on improving selectivity for ULK1, which led to the identification of Compound 3 which is inhibitor pyrimidine scaffold crystal structure obtained with ULK1 (ULK1: IC50 of 120 nM; ULK2: IC50 of 360 nM; PDPK1: IC50 of 710 nM) (131). A high-resolution crystal structure of compound 3 was obtained by co-crystallizing it with ULK1. This structure confirmed that compound 3 binds to the ATP-binding site. LC3-I processing was reduced in cells treated with compound 3, suggesting autophagy inhibition. It is the first report of high-resolution crystal structures of ULK1 inhibitors.

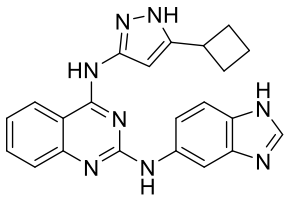

52

Compound 1 (ULK1: IC50 of 5.3 nM; ULK2: IC50 of 13 nM; PDPK1: IC50 of 420 nM)

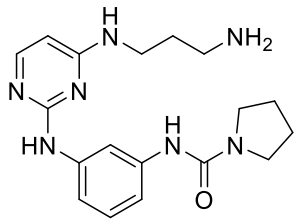

53

Compound 3 (ULK1: IC50 of 120 nM; ULK2: IC50 of 360 nM; PDPK1: IC50 of 710 nM)

SR-17398 and SR-20295:

Using the ULK1 crystal structure from the work of Lazarus et al. (132), Wood et al. developed an indazole-derived inhibitor, which is a mixture of four stereoisomers. They utilized an in-silico screening method to identify inhibitors that prioritize hydrogen-bonding interactions in the hinge region of the ATP-binding pocket. This approach allowed them to design a compound with the desired structural and functional properties to target specific biological molecules. (133). The in vitro phosphorylation of ATG13 was used to test hypothetical hits culminating in the discovery of indazole SR-17398 and founds the IC50 value of 22 mM (134). Analogs were synthesized using molecular modeling, with high potency achieved with SR-20295, a nanomolar-range ULK1 inhibitor with IC50 of 45 nM, In vitro microsome stability half-life of 225 min. When SR-20295 was assessed for drug-like properties, it was found to have few characteristics that would lead to in vivo liabilities (135).

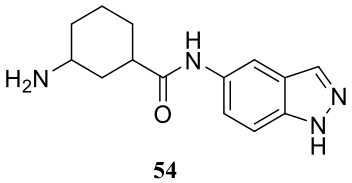

54

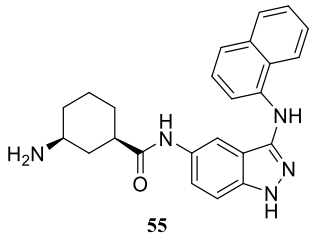

55

SR-17398(ULK1: IC50 of 22 mM) **SR-20295(**ULK1: IC50 of 45 nM, In vitro microsome)

4. *In Silico* Assessment

4. *In Silico* Assesement

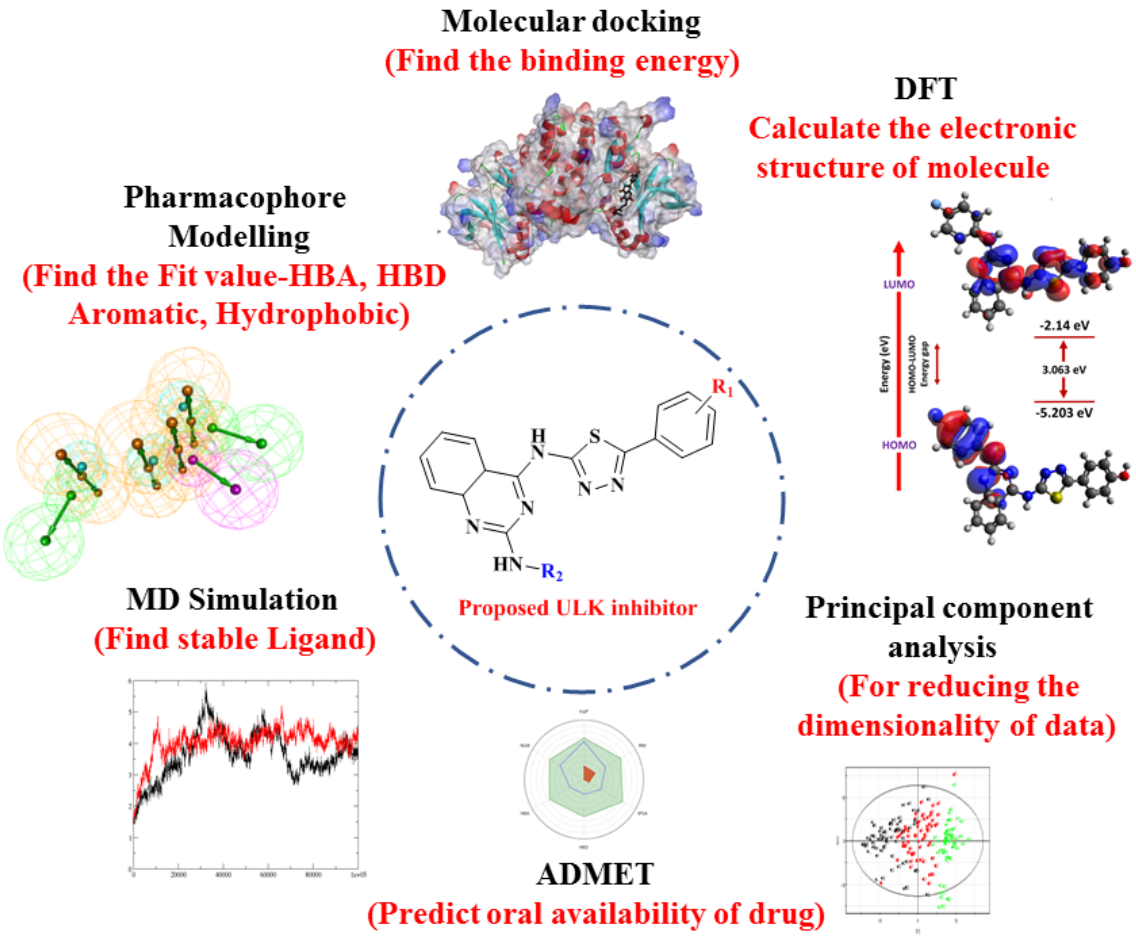

Fig.16. Diagrammatic Representation of methodology

4.1. Drug-likeness and *in-silico* ADMET study

SwissADME and pkCSM were used to assess the drug-likeness and pharmacokinetic characteristics of designed molecules. (136). The degree to which a molecule possesses characteristics linked to effective drugs is referred to as drug likeness. Drug-likeness of compounds was predicted based on various rules, such as LDrug likeness. The concept of drug likeness is used in drug discovery and development to identify and prioritize compounds with a higher likelihood of becoming SwissADME and pkCSM were used to assess the designed molecules' drug-likeness and pharmacokinetic characteristics. g successful drugs(137). The rule of five (Lipinski rules, Ro5) and its extensions have been used to summarize the usefulness of drug ability from a medicinal chemistry perspective. The drug likeness was estimated through the Lipinski, Ghose and Veber rules using Molinspiration software (www. Molinspiration.com) and SWISS ADME software.

Lipinski's rules: The Lipinski`s rules (RO5) states that molecules exhibition good absorption or permeation when they have an **octanol-water partition coefficient (Milog P) < 5, molecular weight (MW) < 500, number hydrogen bond donors (n OHNH) ≤ 5, number hydrogen bond acceptor (n ONH) ≤ 10.**

Ghose's Rules: In extending the work, Ghose et al. established the qualifying ranges for a log P (-0.4 to 5.6), molecular weight (160 to 480), and atom count (20 to 70).

Veber's rules: Molecular flexibility, topological polar surface area (PSA), and hydrogen bond count are crucial factors in determining oral bioavailability, according to Veber's rules for good bioavailability. Veber's state that **rotatable bonds ≤ 10, topological polar surface area (PSA) ≤ 140 Å and total H bond donors and acceptors ≤ 12.**

There are several drug likeness properties that are commonly considered when evaluating a molecule's potential as a drug candidate. These properties include(138):

Lipophilicity: the ability of a molecule to dissolve in lipid or fat-like environments, which is important for drug absorption and distribution.

Molecular weight: smaller molecules tend to have better drug-like properties than larger ones, because they have a higher chance of being effectively absorbed and distributed by the body.

Hydrogen bond donors and acceptors: molecules that can form hydrogen bonds tend to have better drug-like properties, as they can interact more effectively with biological targets.

Toxicity: compounds that are highly toxic or have undesirable side effects are less likely to be successful drugs.

Bioavailability: the ability of a drug to reach the target site in sufficient concentrations to produce a therapeutic effect.

Structural complexity: molecules that are too complex may be difficult to synthesize, purify, and formulate, which can make them less suitable as drug candidates.

Overall, drug likeness properties are used to assess the potential of a molecule to become a successful drug by evaluating its ability to interact effectively with biological targets, be absorbed and distributed effectively in the body, and avoid unwanted side effects or toxicity(139).

LIPINSKI rules

The Lipinski rules, also referred to as the Rule of Five, are a set of recommendations used to assess a molecule's drug-likeness based on its physicochemical

characteristics. The rules were proposed by Christopher Lipinski in 1997 and have become widely used in drug discovery and expansion.

The Lipinski rules state that a compound is likely to have good oral bioavailability and be a successful drug candidate if it satisfies the following criteria(140):

- Molecular weight less than 500 Daltons.
- LogP (octanol-water partition coefficient) less than 5.
- No more than 5 hydrogen bond donors (i.e., the sum of OH and NH groups).
- No more than 10 hydrogen bond acceptors (i.e., the sum of oxygen and nitrogen atoms).

The rationale behind the Lipinski rules is that compounds that meet these criteria are more likely to have favourable pharmacokinetic and pharmacodynamic properties, and be absorbed and distributed effectively in the body (141). However, it's important to note that the Lipinski rules are not absolute and that there are exceptions to these guidelines. The rules are only one of many tools used in drug discovery and development to assess the potential of a molecule to become a successful drug candidate(139).

Application of drug likeness in drug discovery (142–147)

Drug likeness plays a crucial role in drug discovery by guiding the selection and optimization of drug candidates with a higher likelihood of success. By evaluating the drug likeness properties of a molecule, researchers can prioritize compounds that have a higher probability of being absorbed, distributed, metabolized, and excreted effectively in the body, which is important for achieving therapeutic effects.

Drug likeness is used throughout the drug discovery process, from the initial screening of compound libraries to the optimization of lead compounds. In the early stages of drug discovery, researchers use computational and experimental techniques to identify and prioritize molecules with drug-like properties based on their physicochemical and biological properties. This helps to narrow down the number of compounds that are further evaluated and optimized for pharmacological activity.

During the lead optimization stage, researchers use drug likeness properties to guide the selection and modification of lead compounds to improve their drug-like properties. For example, they may modify a lead compound to reduce its molecular weight, increase its lipophilicity, or reduce its toxicity.

Drug likeness is also used to assess the safety and efficacy of potential drug candidates. By evaluating a molecule's drug likeness properties, researchers can predict potential issues

such as toxicity, drug-drug interactions, and adverse effects and optimize the molecule's structure to mitigate these issues.

Overall, drug-likeness plays a critical role in drug discovery by guiding the selection and optimization of drug candidates with a higher likelihood of success and improving the efficiency and effectiveness of the drug discovery process.

4.1.1. Drug-likeness and *in-silico* ADMET prediction

Drug similarity and *in-silico* to identify the drug-like candidates from designed compounds, ADMET studies were carried out. According to the commonly employed techniques for figuring out a compound's drug-like properties, Lipinski's rule of five, Veber's rule, Ghose's rule, Egan's rule, and Muegge's rule, the prediction of the drug-likeness of designed compounds was carried out. All the designed compounds followed Lipinski's rule of five with minimum or zero violation of the rule except 8a does not follow Lipinski's criteria. Therefore, designed compounds are present within an acceptable range of drug-likeness properties with minimum violations in Lipinski's rule of five as shown in **Table 5**.

Table 5. Lipinski's rule of five and Drug-likeness prediction of designed compounds.

Compound	Lipinski's rule of five					Lipinski's violations	Drug likeness				
	MW	mLogP	nHBA	nHBD	MR		Lipinski	Veber	Ghose	Egan	Muegge
12a-I	478.57	3.41	5	2	149.67	0	Yes	Yes	No	Yes	Yes
12a-II	413.5	3.16	4	3	130.38	0	Yes	Yes	No	Yes	Yes
12a-III	400.46	2.07	6	2	121.56	0	Yes	Yes	Yes	Yes	Yes
12a-IV	416.47	4.07	5	2	125.93	0	Yes	Yes	Yes	Yes	Yes
12a-V	366.44	1.94	5	3	110.72	0	Yes	Yes	Yes	Yes	Yes
12b-I	494.57	2.9	6	3	151.69	0	Yes	No	No	No	Yes
12b-II	429.5	2.64	5	4	132.4	0	Yes	No	No	No	Yes
12b-III	416.46	1.97	7	3	123.59	0	Yes	No	Yes	No	Yes
12b-IV	432.47	3.54	6	3	127.95	0	Yes	Yes	Yes	Yes	Yes
12b-V	382.44	1.83	6	4	112.75	0	Yes	No	Yes	No	Yes
12c-I	513.02	3.88	5	2	154.68	1	Yes	Yes	No	Yes	Yes
12c-II	447.94	3.65	4	3	135.39	0	Yes	Yes	No	Yes	Yes
12c-III	434.9	2.97	6	2	126.57	0	Yes	Yes	Yes	Yes	Yes
12c-IV	450.92	4.55	5	2	130.94	1	Yes	Yes	No	Yes	Yes
12c-V	400.89	2.85	5	3	115.73	0	Yes	Yes	Yes	Yes	Yes
12d-I	496.56	3.78	6	2	149.62	0	Yes	Yes	No	Yes	Yes
12d-II	431.49	3.54	5	3	130.33	0	Yes	Yes	No	Yes	Yes
12d-III	418.45	2.86	7	2	121.52	0	Yes	Yes	Yes	Yes	Yes
12d-IV	434.46	4.45	6	2	125.89	1	Yes	Yes	Yes	Yes	Yes
12d-V	384.43	2.73	6	3	110.68	0	Yes	Yes	Yes	Yes	Yes
12e-I	478.57	3.41	5	2	149.67	0	Yes	Yes	No	Yes	Yes
12e-II	427.52	3.38	4	3	135.34	0	Yes	Yes	No	Yes	Yes
12e-III	414.49	2.7	6	2	126.53	0	Yes	Yes	Yes	Yes	Yes

12e-IV	430.5	4.28	5	2	130.9	1	Yes	Yes	No	Yes	Yes
12e-V	380.47	2.58	5	3	115.69	0	Yes	Yes	Yes	Yes	Yes
12f-I	508.6	3.11	6	2	156.16	1	Yes	Yes	No	Yes	Yes
12f-II	427.52	3.38	4	3	135.34	0	Yes	Yes	No	Yes	Yes
12f-III	430.49	2.19	7	2	128.05	0	Yes	Yes	Yes	No	Yes
12f-IV	446.5	3.75	6	2	132.42	0	Yes	Yes	No	Yes	Yes
12f-V	396.47	2.06	6	3	117.22	0	Yes	Yes	Yes	No	Yes
12g-I	557.47	3.98	5	2	157.37	1	Yes	Yes	No	Yes	Yes
12g-II	492.39	3.75	4	3	138.08	0	Yes	Yes	No	Yes	Yes
12g-III	479.36	3.08	6	2	129.26	0	Yes	Yes	Yes	Yes	Yes
12g-IV	495.37	4.66	5	2	133.63	1	Yes	Yes	No	Yes	Yes
12g-V	445.34	2.96	5	3	118.42	0	Yes	Yes	Yes	Yes	Yes
12h-I	523.57	4.08	7	2	158.49	2	No	No	No	No	No
12h-II	458.5	3.53	6	3	139.2	0	Yes	No	No	No	No
12h-III	445.46	2.47	8	2	130.38	1	Yes	No	No	No	No
12h-IV	461.47	4.41	7	2	134.75	1	Yes	No	No	No	Yes
12h-V	411.44	2.31	7	3	119.55	0	Yes	No	Yes	No	No

Pharmacokinetics of designed compounds (Absorption, Distribution, Metabolism, Excretion, and Toxicity) was characterized virtually with the help of pkCSM servers to determine the ADMET profile of designed compounds. The results of ADMET prediction showed that designed compounds showed good ADME properties, as shown in **Table 6**. Some of them tested positively for AMES toxicity, suggesting that they might be mutagenic. *In silico* ADMET profile of the designed compounds was observed with satisfactory results.

Table 6. Predicted *In silico* ADMET properties for designed compounds**.**

Compound	**Absorption**	**Distribution**			**Metabolism**							**Excretion**	**Toxicity**
	Intestinal absorption (human)	**VDss (human)**	**BBB permeability**	**CNS permeability**	**Substrate**		**Inhibitors**					**Total clearance**	**AMES toxicity**
					CYP								
					2D6	**3A4**	**1A2**	**2C19**	**2C9**	**2D6**	**3A4**		
	Numeric (%absorbed)	**Numeric (log L kg^{-1})**	**Numeric (log BB)**	**Numeric (log PS)**	**Categorical (Yes/No)**							**Numeric (log mL min^{-1} kg^{-1})**	**Categorical (Yes/No)**
12a-I	100	0.214	-0.467	-1.969	No	Yes	No	Yes	Yes	No	No	0.178	No
12a-II	92.864	0.57	-0.646	-1.958	No	Yes	No	Yes	Yes	No	No	0.099	Yes
12a-III	97.126	0.846	-1.04	-3.371	No	No	Yes	No	Yes	No	Yes	-0.11	Yes
12a-IV	81.013	0.641	-0.287	-1.824	No	Yes	Yes	Yes	Yes	No	No	-0.105	No
12a-V	82.763	0.872	-0.943	-2.678	No	Yes	No	No	No	No	No	0.094	No
12b-I	100	0.173	-1.035	-2.149	No	Yes	No	Yes	Yes	No	Yes	0.238	No
12b-II	92.916	0.639	-0.842	-2.139	No	Yes	No	Yes	Yes	No	Yes	0.158	Yes
12b-III	86.648	0.75	-1.328	-2.475	No	No	No	No	Yes	No	Yes	-0.06	No
12b-IV	100	0.702	-0.994	-2.005	No	Yes	No	Yes	Yes	No	Yes	-0.045	No
12b-V	75.829	0.985	-1.142	-2.802	No	No	No	No	No	No	No	0.175	No
12c-I	100	0.201	-0.654	-1.856	No	Yes	Yes	Yes	Yes	No	No	0.169	No

12c-II	93.917	0.559	-0.828	-1.845	No	Yes	No	Yes	Yes	No	No	0.09	Yes
12c-III	94.111	0.82	-1.281	-2.171	No	No	No	No	Yes	No	Yes	-0.107	Yes
12c-IV	80.194	0.636	-0.474	-1.712	No	Yes	No	Yes	Yes	No	No	-0.114	No
12c-V	83.292	1.09	-1.128	-2.497	No	No	No	No	No	No	No	0.128	No
12d-I	100	0.162	-0.687	-2.011	No	Yes	No	Yes	Yes	No	Yes	0.179	No
12d-II	99.163	0.378	-0.867	-2	No	Yes	No	Yes	Yes	No	Yes	0.1	Yes
12d-III	93.215	0.745	-1.314	-2.324	No	No	No	No	No	No	Yes	-0.099	No
12d-IV	81.401	0.438	-0.507	-1.867	No	Yes	No	Yes	Yes	No	Yes	-0.104	No
12d-V	82.396	0.992	-1.167	-2.651	No	No	No	No	No	No	No	0.137	No
12e-I	100	0.214	-0.467	-1.969	No	Yes	No	Yes	Yes	No	No	0.178	No
12e-II	93.209	0.582	-0.675	-1.886	No	Yes	No	Yes	Yes	No	No	0.102	Yes
12e-III	93.403	0.856	-1.106	-2.211	No	No	No	No	No	No	Yes	-0.095	Yes
12e-IV	81.652	0.661	-0.299	-1.752	No	Yes	Yes	Yes	Yes	No	No	-0.101	No
12e-V	82.584	1.132	-0.975	-2.538	No	No	No	No	No	No	No	0.141	No
12f-I	100	0.143	-0.714	-2.134	No	Yes	No	Yes	Yes	No	Yes	0.25	No
12f-II	93.209	0.582	-0.675	-1.886	No	Yes	No	Yes	Yes	No	No	0.102	Yes
12f-III	94.675	0.72	-1.341	-2.527	No	No	No	No	No	No	Yes	-0.029	No
12f-IV	82.807	0.433	-0.534	-1.989	No	Yes	No	Yes	Yes	No	Yes	-0.033	No
12f-V	83.856	0.974	-1.163	-2.853	No	No	No	No	No	No	No	0.207	No
12g-I	100	0.201	-0.662	-1.834	No	Yes	Yes	Yes	Yes	No	No	0.15	No
12g-II	93.653	0.561	-0.849	-1.823	No	Yes	No	Yes	Yes	No	No	0.07	Yes
12g-III	93.847	0.829	-1.29	-2.148	No	No	No	No	Yes	No	Yes	-0.127	Yes
12g-IV	80.127	0.638	-0.482	-1.689	No	Yes	No	Yes	Yes	No	No	-0.133	No
12g-V	83.028	1.099	-1.149	-2.474	No	No	No	No	No	No	No	0.109	No
12h-I	99.201	0.379	-0.578	-2.071	No	Yes	No	Yes	Yes	No	Yes	0.051	Yes
12h-II	89.752	1.48	-1.055	-2.061	No	Yes	No	Yes	No	Yes	Yes	-0.02	Yes
12h-III	89.809	0.651	-1.635	-2.499	No	No	No	No	No	No	Yes	-0.289	Yes
12h-IV	97.399	1.178	-0.656	-1.953	No	Yes	No	No	No	Yes	Yes	-0.212	Yes
12h-V	78.989	0.877	-1.186	-2.825	No	Yes	No	No	No	No	No	-0.055	No

4.2. Bioactivity score

A computational tool known as the "bioactivity score" is used in drug discovery and development to forecast the likelihood that a molecule will be active against a particular biological target (148). The bioactivity score is calculated by analyzing the molecular features of the compound and comparing them to known active compounds for the target.

The bioactivity score is typically calculated using machine learning algorithms that analyze a large dataset of known active and inactive compounds for a specific target. The algorithm learns to recognize patterns in the molecular features of active compounds and uses this knowledge to predict the bioactivity of new compounds.

Bioactivity scores can be used to prioritize compounds for further testing and optimization, as well as to identify potential off-target effects and toxicity issues. Researchers can conserve time and resources by concentrating on compounds with the best chance of

success by predicting the bioactivity of compounds early on in the drug discovery process (149).

Bioactivity scores are also useful for virtual screening, where large databases of compounds can be screened for potential activity against a specific target. By using bioactivity scores to filter the database, researchers can quickly identify promising compounds for further testing and development(150).

Overall, bioactivity scores can speed up the process of drug discovery and development and are a useful tool for predicting the activity of compounds against specific biological targets.

By calculating activity scores for GPCR ligands, ion channel modulators, kinase inhibitors, and nuclear receptor ligands, the drugs' bioactivity was also assessed. The parameters were validated using Molinspiration (https://www.molinspiration.com/cgi-bin/properties) 49. The drug-likeness score of each ligand was calculated and compared to the specific activity of each compound with a standard drug(151).

4.2.1 Bioactivity score Prediction

The bioactivity score was calculated for the GPCR ligand, ion channel modulator, kinase inhibitor, nuclear receptor ligand, protease inhibitor, and enzyme inhibitor. An organic molecule is considered to be active if its probability of bioactivity score is greater than 0.00, moderately active if it is between -0.50 and 0.0, and inactive if it is below -0.50. In our study, all the proposed ligands were subjected to the bioactivity score presented in **Table 7**. Comparing the bioactivity score of STD molecule and proposed ligand have similar scores, especially in the case of enzyme inhibition.

Table 7. Bioactivity score of the ligand **(12a(I-V) to 12f(I-V))**

Ligand No.	GPCR ligand	Ion channel modulator	Kinase inhibitor	Nuclear receptor ligand	Protease inhibitor	Enzyme inhibitor
12a-I	-0.09	-0.38	-0.07	-0.40	-0.20	0.03
12a-II	-0.10	-0.46	-0.02	-0.44	-0.11	0.14
12a-III	-0.07	-0.55	-0.02	-0.38	-0.27	0.03
12a-IV	-0.09	-0.47	-0.07	-0.36	-0.16	-0.00
12a-V	0.04	-0.43	-0.00	-0.32	0.01	0.17
12b-I	-0.06	-0.36	-0.04	-.29	-0.19	0.06
12b-II	-0.06	-0.41	0.01	-0.32	-0.10	0.17
12b-III	-0.03	-0.50	0.01	-0.25	-0.25	0.07

12b-IV	**-0.06**	**-0.42**	**-0.04**	**-0.23**	**-0.15**	**0.04**
12b-V	0.07	-0.39	0.03	-0.20	-0.00	0.19
12c-I	-0.09	-0.40	-0.08	-0.40	-0.23	0.00
12c-II	-0.09	-0.45	-0.03	-0.45	-0.14	0.10
12c-III	-0.07	-0.54	-0.04	-0.38	-0.30	0.00
12c-IV	-0.09	-0.46	-0.08	-0.36	-0.19	-0.03
12c-V	-0.04	-0.42	-0.02	-0.32	-0.04	0.13
12d-I	-0.09	-0.40	-0.04	-0.37	-0.22	0.01
12d-II	-0.09	-0.46	0.01	-0.41	-0.13	0.12
12d-III	-0.06	-0.54	0.00	-0.35	-0.28	0.02
12d-IV	**-0.09**	**-0.46**	**-0.07**	**-0.34**	**-0.16**	**0.00**
12d-V	**-0.04**	**-0.43**	**0.02**	**-0.28**	**-0.02**	**0.14**
12e-I	-0.09	-0.38	-0.07	-0.40	-0.20	0.03
12e-II	-0.13	-0.51	-0.06	-0.45	-0.15	0.08
12e-III	-0.10	-0.59	-0.07	-0.39	-0.31	-0.02
12e-IV	-0.12	-0.52	-0.11	-0.37	-0.21	-0.05
12e-V	-0.00	-0.49	-0.05	-0.33	-0.05	0.10
12f-I	-0.12	-0.47	-0.9	-0.38	-0.23	-0.01
12f-II	-0.13	-0.51	-0.06	-0.45	-0.15	0.08
12f-III	-0.10	-0.58	-0.06	-0.37	-0.30	-0.01
12f-IV	-0.13	-0.51	-0.10	-.35	-0.20	-0.04
12f-V	-0.16	-0.45	-0.10	-0.46	-0.28	-0.03
12g-I	-0.17	-0.51	-0.05	-0.52	-0.20	0.07
12g-II	-0.15	-0.59	-0.06	-0.46	-0.36	-0.03
12g-III	-0.17	-0.52	-0.10	-0.43	-0.25	-0.06
12g-IV	-0.05	-0.49	-0.05	-0.41	-0.10	0.09
12g-V	-0.04	-050	-0.04	-0.42	-0.26	0.08
12h-I	-0.19	-0.48	-0.17	-0.43	-0.28	-0.06
12h-II	-0.20	-0.46	-0.13	-0.47	-0.20	0.04
12h-III	-0.19	-0.55	-0.14	-0.43	-0.36	-0.06
12h-IV	0.20	-0.47	-0.18	-0.39	-0.26	-0.08
12h-V	-0.11	-0.44	-0.13	-0.37	-0.13	0.05
STD 1	**0.44**	**0.24**	**0.69**	**-0.09**	**0.60**	**0.33**
STD 2	**0.06**	**0.22**	**0.33**	**-0.26**	**-0.14**	**0.13**
STD 3	**0.27**	**0.07**	**1.06**	**-0.96**	**-0.35**	**0.20**

STD 4	**0.27**	**-0.11**	**0.05**	**-0.08**	**0.03**	**0.10**
STD 5	**0.10**	**-0.01**	**0.60**	**-0.26**	**0.07**	**-0.10**

4.3 Docking Method

Docking is the process of finding the best relationship between two molecules.

- Receptor (typically the protein)
- Ligand (typically the molecule)

The assessment of a potential drug's capability to engage with a specific receptor protein relies on a process called docking. Molecular docking, being a widely used technique in structure-based drug design, excels at forecasting how small molecule ligands will attach themselves to the correct binding site on the target receptor (152–156).

Research on molecular docking focuses on computer modelling of the molecular recognition process (157,158). The primary objective is to attain an ideal arrangement for both the protein and the ligand, along with their mutual alignment, with the purpose of minimizing the overall free energy of the system (159–161).

Different types of Interactions

It is very common to define particle interactions as the result of forces between the molecules the particles contain. Often forces are divided into four categories:

• **Electrostatic forces** - Charges present in the matter are what cause electrostatic forces. The interactions that occur most frequently are dipole-dipole, charge-charge, and charge-charge.

• **Electrodynamics forces**- The van der Waals interaction is likely the most well-known.

• **Steric forces** - Entropy is the root cause of steric forces. For instance, when entropy is constrained, entropy-related forces may work to reduce the system's free energy.

• **Solvent-related forces** - The structural modifications of the solvent are what cause the forces associated with it. When ions, colloids, proteins, etc. are added to the solvent's structure, these structural alterations result. Hydrogen bonds and hydrophobic interactions occur most frequently.

• Common thing to all these forces is the electromagnetic origin.

• Other physical factors - conformational changes in the protein and the ligand are often necessary for a successful docking process.

Molecular docking

Molecular docking can be divided into two separate sections.

1) Search algorithm – An optimal number of configurations with the experimentally determined binding modes should be produced by the algorithm. The following are the various algorithms used for docking analysis(162).

- Molecular dynamics
- Monte Carlo methods
- Genetic algorithms
- Fragment-based methods
- Point complementary methods
- Distance geometry methods
- Systematic searches

2) Scoring Function –These mathematical techniques are used to predict the magnitude of the binding affinity, a non-covalent interaction between two molecules that occurs after docking. In order to predict the strength of additional intermolecular interactions, such as those between proteins, between proteins and DNA, or between proteins and drugs, scoring functions have also been developed. In order to distinguish the experimental binding modes from all other modes discovered by the searching algorithm, these configurations are scored using scoring functions.

• Empirical scoring function of Igemdock

Fitness = vdW + Hbond + Elec

• Binding Energy

ΔG bind = ΔGvdw + ΔGhbond + ΔGelect + ΔGconform + ΔG tor + ΔG sol

Types of Docking

The following are majorly used method for docking-

- **Lock and Key\Rigid Docking –** In rigid docking, both the internal geometry of the receptor and ligand is kept fixed and docking is performed.
- **Induced fit\Flexible Docking -** One of the molecules (typically a smaller one) has its rotations counted. The surface cell occupancy and energy are calculated for each rotation, and the most optimal pose is then chosen.

Major steps in molecular docking:

Step I – Building the Receptor

In this step, the 3D receptor structure that can be downloaded from PDB should be taken into consideration; the currently available structure should then be processed. According to the parameters available, this should involve removing the water molecules from the

cavity, stabilizing the charges, adding the missing residues, creating side chains, etc. The receptor must be in a stable, biologically active state.

Step II – Identification of the Active Site

Once the receptor has been constructed, it's essential to identify the active site. While the receptor might have multiple active sites, the specific one of interest must be selected. In this process, most water molecules and any heteroatoms should be removed

Step III – Ligand Preparation

Ligands can be found in a number of databases, including ZINC and PubChem, or they can be created using the tool Chemsketch. The LIPINSKY'S RULE OF FIVE should be used when choosing a ligand. When a pharmacologically active lead structure is incrementally improved for greater activity and selectivity, as well as for the described drug-like properties, drug development, it is important to follow the rule.

For selection of a ligand according to the **LIPINSKY'S RULE:**

- Not more than 5 –H bond donors.
- Molecular Weight NOT more than 500 Da.
- Log P not over 5.
- NOT more than 10 H bond acceptors.

Step IV- Docking

The ligand is docked onto the receptor at this point, and the interactions are examined. Depending on which ligand is chosen as the best fit, the scoring function will generate a score. For ligand docking studies into the Aromatase protein, the molecular docking tool Auto dock Vina 4.2 of Pyrex Virtual Screening software and Discovery Studio software were used.

The crystal structure of 'Human Autophagy Initiating Kinase ULK1' (RCSB PDB id: 4WNP) was obtained from protein data bank from www.rcsb.org.

4.3.1. Database for molecular modelling

Based on knowledge of various ULK analogues acting as an anticancer agent, we designed some molecules and named **(12a(I-V) to 12f(I-V)),** displayed in Table 1. To design these molecules, the dataset used for molecular docking contains 45 molecules in which 40 proposed molecules **(12a(I-V) to 12f(I-V))** and 05 standard molecules from literature (STD-1 to STD-5). The chemical structure and name of molecules are listed below in Table 1.

To investigate the interaction between the binding pocket of the ULK enzyme and the ligands, protein-ligand docking studies on 40 thiadiazole derivatives were carried out on an HP G62 computer system with an Intel CoreTM i3 Dual CPU, M330 @2.13 GHz, 4

GB of RAM, Auto dock vina 4.2 of Pyrex Virtual Screening software, and Discovery studio software.

4.3.2. Protein preparation

Protein Databank was used to retrieve the 3D structure of the ULK1 bound potent inhibitor with the PDB code 4WNP (PDB) [36–38]. Water molecules and cofactors were taken out of the receptor using the Discovery Studio software before it was saved in the PDB file format. Then, polar hydrogen atoms were introduced to protonate the structure and then saved in PDB format for later use. Protein cleaning and preparation were performed by using BIOVIA Discovery Studio 2021 Visualizer [39]. The CASTp server was employed to evaluate the binding pocket present in the target protein [40]. The PROCHECK server was utilized to evaluate the stereochemical flexibility and quality of the protein structure and they show the Ramachandran plot [41]. The Ramachandran plot can be used to determine the quality of the predicted target protein.

4.3.3. Ligands preparation

Chem Draw ultra 8.0 software (Chemical Structure Drawing Standard; Cambridge Soft Corporation, USA (2003)) was used to create sketches of the compounds used in this study that were ligands that were investigated for their binding activities to the 4WNP receptor. Then, these structures were converted to 3D structures using Chem3D ultra 8.0 software. The energy minimization method Allinger's was used to reduce the energy in constructed 3D structures. Following geometry optimization using semi-empirical quantum mechanics based on AM-1, molecular Mechanics (MM2) force fields are used (Austin Model-1).

Docking of the ligands with the receptor using auto dock version 4.0 of pyrex software. The docking was performed on the enzyme ‘Human Autophagy Initiating Kinase ULK1’ (RCSB PDB id: 4WNP) in the Auto Dock Vina version 12.0 of pyrex software. The receptor and the ligand decoupled following docking with the autodock vina of pyrex, so the complex (ligand-receptor) was built using the Chimera 1.10.2 software. The Discovery studio visualizer was used to view the interactions between the ligand and receptor.

Table 8: Designed structures of ligand used in current study.

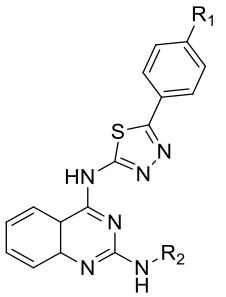

Compound Code	R1	R2	Compound Code	R1	R2
12a-I	H	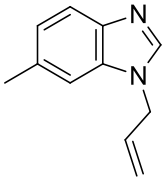	**12e-I**	CH_3	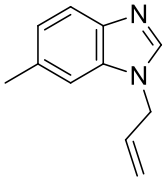
12a-II	H	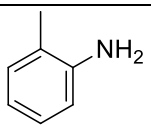	**12e-II**	CH_3	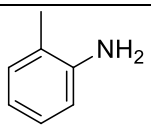
12a-III	H	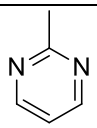	**12e-III**	CH_3	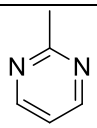
12a-IV	H	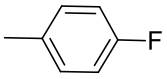	**12e-IV**	CH_3	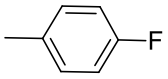
12a-V	H	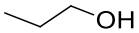	**12e-V**	CH_3	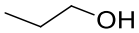
12b-I	OH	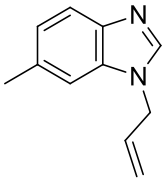	**12f-I**	OCH_3	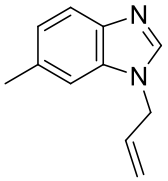
12b-II	OH	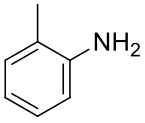	**12f-II**	OCH_3	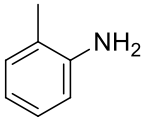
12b-III	OH	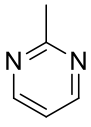	**12f-III**	OCH_3	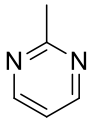
12b-IV	OH	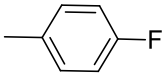	**12f-IV**	OCH_3	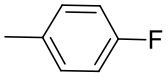

12b-V	OH	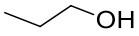	**12f-V**	OCH_3	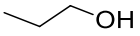
12c-I	Cl	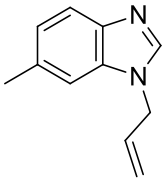	**12g-I**	Br	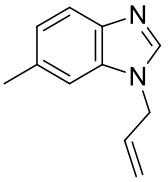
12c-II	Cl	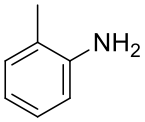	**12g-II**	Br	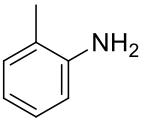
12c-III	Cl	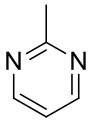	**12g-III**	Br	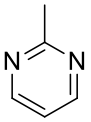
12c-IV	Cl	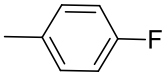	**12g-IV**	Br	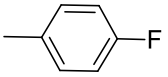
12c-V	Cl	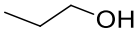	**12g-V**	Br	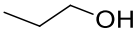
12d-I	F	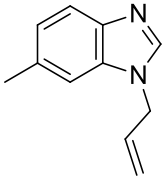	**12h-I**	NO_2	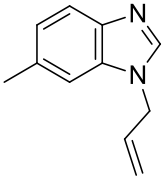
12d-II	F	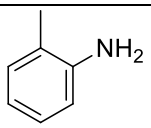	**12h-II**	NO_2	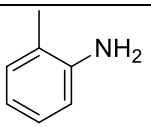
12d-III	F	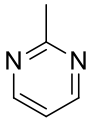	**12h-III**	NO_2	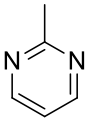
12d-IV	F	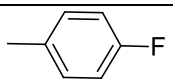	**12h-IV**	NO_2	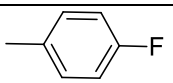
12d-V	F	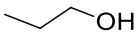	**12h-V**	NO_2	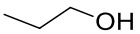
3RJ (PubChem CID: 86346643)					

	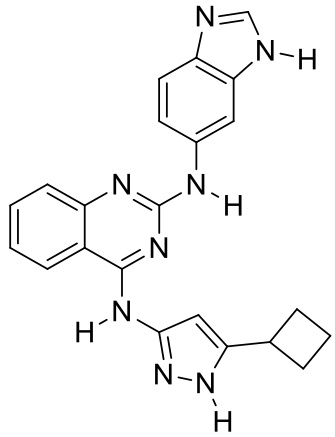

4.3.4 Molecular docking studies

Molecular docking was carried out to confirm the binding sites and interactions that occurred between the designed compounds and ULK1 as the target protein (PDB: 4WNP). Five ligands were selected from previously reported literature, and one naturally bound ligand was used as a standard compound. Molecular docking was performed with the help of the AutoDock Vina package of PyRx 0.8 software. The PDB file format of 4WNP as a macromolecule and the SDF file format of all designed compounds and all standards were imported in the Open Babel plugin PyRx. Further, all compounds were then subjected to energy minimization and converted to PDBQT format using the Open Babel. The grid box for the PDB: 4WNP was selected in the Vina workspace of PyRx to cover the binding site residues, with center X: 126.4941, Y: 40.8135, Z: 1.0241 and dimensions X: 88.3558128357 Å, Y: 52.7755333138 Å, Z: 79.5115510941 Å. The molecular docking procedure was started using the AutoDock Vina plugin of PyRx. The default setting for exhaustiveness was 8. For each compound, nine poses (conformations) were predicted with the displayed target protein. The BIOVIA Discovery Studio Visualizer was used to visualize docking interactions and analyse saved poses.

4.3.5 Molecular docking analysis

A molecular docking study was performed to determine the binding energies and best binding confirmations using designed compounds with ULK1 (PDB: 4WNP). AutoDock Vina package of PyRx 0.8 software was used to carry out the molecular docking study. Ligand library of 46 compounds containing designed compounds, five standard molecules from literature and naturally attached ligand in protein structure were docked against ULK1 (PDB: 4WNP). 3RJ (PubChem CID: 86346643) is a naturally attached ligand in protein structure that was used as one of the standards to compare the docking

results of designed compounds. **Table 9** represents the binding affinity of compounds present in the prepared ligand library against ULK1 (PDB: 4WNP).

The binding affinity of all docked complexes ranged from -8 to -11.3 kcal/mol, respectively. As per molecular docking results, it was observed that 3RJ (PubChem CID: 86346643) showed binding affinity of -10.7 kcal/mol and **12a-IV, 12b-IV, 12c-II, 12c-IV, 12d-IV, 12d-V, 12e-III, 12g-I,** from designed compounds showed the binding affinity equivalent to or more than the binding affinity of 3RJ. It means that designed compounds have a higher binding potential than naturally bound ligand. Five standard molecules selected from the literature were showed binding affinity between -8.9 to -9.3 kcal/mol, which is less than the 3RJ. All the docked molecules were further subjected to determine the interacting residues and type of interaction occurred between all compounds and ULK1 (PDB: 4WNP).

Table 9 represents the hydrophobic interactions, hydrogen bonds, and distance between designed compounds and ULK1. The BIOVIA Discovery Studio Visualizer was used to determine detailed 2D and 3D interactions. 3RJ showed interactions with PHE273, ILE135, HIS130, PHE269, LEU129, SER131, ILE134, HIS130, GLY133, GLY200, LEU172, ASP199, SER174, GLY,133 GLN173, LEU172, GLN173, LYS132, SER174, SER131 amino acid residues of ULK1 (PDB: 4WNP). 2d showed a binding affinity of -11.3 kcal/mol, which is a higher binding affinity as compared to all standard and designed compounds and HIS24, PHE27, LEW59, ILE46, ASN148, PRO149, GLU42, GLY25, TYR94, ALA28, CYS95 are the interacting amino acid residues between **12b-IV** and ULK1 (PDB: 4WNP). Extending to that **12d-IV** and **12-V** also showed a good binding affinity with -11.2 and -11.0 kcal/mol. The first three protein-ligand complexes having good binding affinity were used for further molecular dynamic study over the 100 ns of simulation time. **Figure 5** depicts 2D and 3D visualizations of interactions between top-ranked protein-ligand complexes.

Table 9: Binding energy, hydrophobic interactions, hydrogen and hydrogen bond distance of a ULK and the designed compounds.

Compound ID	Binding Energy (kcal/mol)	Hydrophobic Interactions	Hydrogen Bonds	Hydrogen Bond Distance (Å)
12a-I	-10.3	ASP102, GLY23, LYS140, ILE22, ASP143, ALA164, VAL176,	LYS46, HIS24	2.99 and 3.30

		MET92.		
12a-II	-10.2	LEU145, VAL176, ASP99, GLY23, HIS24, LYS46, ASP146, PHE168	-	-
12a-III	-10.4	LEU59, ALA28, PHE27, GLY167 LYS46, GLN142, LYS46, ASN143, ASP165, CYS95, VAL130, GLU93 LYS46, LEW145	LYS64	3.12
12a-IV	-10.9	PHE168, ALA28, LEW59, LYS46, GLU143, LYS46, ASP165, GLU165, GLN142, LEU145, VAL130.	-	-
12a-V	-9.5	ALA28, PHE168, ASP165, LEU59, GLU160 LYS46, LEU60, MET92, VAL130, ALA44	-	-
12b-I	-10	LEU59, ALA28, PHE27, GLY167 LYS46, GLN142, ASN143, ASP165, CYS95, VAL130, GLU93, LYS46, LEU145	CYS95	2.88
12b-II	-10.4	TYR79, ARG255, LEU246, ALA249, PHE70, GLY151, LEU246, GLU73, GLN142, LYS162, ASN143, ASP165, LYS162, VAL130, GLU93, LEU246, PRO250	SER147, GLU271	2.83, 3.29, 3.13 and 3.18
12b-III	-9.8	GLU73, TYR79, LEU256, LYS256, TYR94, LEW41, ARG160, GLN253, GLY42, ASN96, PRO149	-	-
12b-IV	-11.3	GLY167, PHE27, LEU59, ALA28, LEU60, ASP165, GLY25, ASN143, LYS46, LEU145, LEU145, VAL76, GLU93, ALA44, MET92, VAL30, ALA164, ASP138, SER184, CYS182, GLY183, PHE168	-	-
12b-V	-9.6	GLN253, ARG160, TYR94, SER147, GLU73, ASN148, PRO149, GLU42, GLY271	LYS162, ASN96	3.02 and 3.03

12c-I	-9.1	VAL176, LEU145, GLY98, TYR94, ILE22, VAL130, MET92, ASP165, HIS24, ALA28, LYS46	ASN143	3.17
12c-II	-10.7	LEW59, PHE169, ALA26, LEU60, LYS146, VAL130, ILE22	-	-
12c-III	-9.2	PHE168, GLY25, LYS46, LEW59, ALA28, GLY167, VAL130, ILE22, ALA44	-	-
12c-IV	-10.8	LYS140, GLY183, ASP138, PHE168, LEW59, ALA28, ASP165, LEW60, VAL130, ILE22	-	-
12c-V	-10	LEU59, PHE168, ALA28, ASP165, VAL130, LEW145, ALA164	LYS140, LYS146	2.98 and 3.01
12d-I	-10.5	ILE22, VAL130, LEU145, ASP120, HIS24, LYS146, GLY25, ALA28, ASP165,	ASP99	3.28
12d-II	-9.7	PHE168, ALA28, HIS24, ASP165, LEU145, GLN142, GLY25,	ASN143	3.22
12d-III	-10	PHE168, LEU59, ASP165, HIS24, ALA164, GLU93, LEU145, VAL167.	LYS64, ASN143	3.23 and 2.98
12d-IV	-11	SER184, ASP138, GLY25, ASN143, LYS46, LEU145, ALA44, ALA164, VAL76, VAL30, GLU93, MET92.	-	-
12d-V	-11.2	LYS140, SER184, PHE168, PHE27, ALA28, LEU59, GLY167, ASP165, MET92, ALA44, VAL76, GLU93.	-	-
12e-I	-10.6	GLN142, PHE168, ALA28, PHE27, ASP165, ALA164, LEU59, VAL130, GLU93	LYS46	2.98
12e-II	-10.6	LYS140, PHE27, LEU59, VAL130. ALA164, VAL176, ASP165, LEU145, GLU93	-	-
12e-III	-10.7	GLY25, ASP165, LYS14, GLU142, VAL130, LEU145, ILE22, ALA44,	-	-

		CYS95, VAL130		
12e-IV	-9.7	PHE168, ASP165, LEU59, ALA28, VAL130, ALA164, LEU145, ASP146	LYS140, LYS46	3.20 and 3.25
12e-V	-8.3	PHE27, ALA126, ASP165, LYS140, VAL130, GLY98, ASP99, ILE22. CYS95	ASN143, GLN142, TYR94	3.18, 3.29 and 2.78
12f-I	-9.5	PHE168, ASP165, ALA28, GLY25, GLU142, VAL130, LYS46, ALA44, MET92	-	-
12f-II	-9.2	LEU60, GLY167, LYS46, HIS24, ALA28, ASP165, VAL130, ALA44, TYR94	-	-
12f-III	-9.3	PHE27, LY46, ALA28, GLY25, HIS24, LEU59, ALA44, VAL130	-	-
12f-IV	8.3	LEU59, ALA28, LEU60, ASP165, GLY25, HIS24, LYS46, ILE22	GLU163	2.91
12f-V	-10.3	LYS46, VAL130, GS24, PHE27, GLY183, PHE168, ASP165, LY25, LEU60, HIS24, CYS182	-	-
12g-I	-10.7	ASP138, GLU59, ALA28, VAL13 LYS140, PHE168, ASP165	SER184	3.24
12g-II	-9.6	LEU59, PHE168, LYS46, GLN142, VAL130, ALA28	-	-
12g-III	-10.4	LYS162, ALA28, LEU41, GLN253, ASP40, GLY151, ARG152, PRO276	SER147, GLU142	3.32 and 3.04
12g-IV	-9.7	PHE27, ALA28, ASP146, LEU59, VAL130, ALA164	LYS140, LYS46	2.97 and 3.10
12g-V	-8.9	ALA26, GLN142, PHE27, HIS24, ASN143, GLY25, ASP146, VAL130, LEU145, LYS46	-	-
12h-I	-9.0	LYS46, ALA44, VAL176, GLN93, GLY25, CYS95, ILE22, GLY9	TYR94	2.81
12h-II	-8.9	LEU172, ASP199, PHE268, SER174, HIS130, GLY133, HIS274	ARG127, ASP270	3.25 and 3.06

12h-III	-9.2	ALA26, GLY25, HIS24, PHE168, ASN143, LEU59, LYS46, ALA44, ASP165, MET92, VAL130	-	-
12h-IV	-8.3	ALA28, PHE168, GLN142, LYS140, GLY23, ILE22, ALA44, ASP165, TYR94	ASN143, CYS95	3.17 and 3.16
12h-V	-8.0	GLY25, HIS24, PHE168, ASN143, LEU59, LYS46, ALA44, ASP165, MET92, VAL130		
STD1	-9.3	ALA26, GLY25, HIS24, PHE168, ASN143, LEU59, LYS46, ALA44, ASP165, MET92, VAL130	GLU95, CYS92	2.91 and 2.92
STD2	-8.9	LEU172, ASP199, PHE268, SER174, HIS130, GLY133, HIS274	-	-
STD3	-9.0	PHE168, ASP165, ALA28, GLY25, GLU142, VAL130, LYS46, ALA44, MET92	-	-
STD4	-9.0	LEU172, ASP199, PHE268, SER174, HIS130, GLY133, HIS274	-	-
STD5	-9.0	ASP165, ALA28, GLY25, GLU142, VAL130, LYS46, ALA44, MET92	-	-
3RJ (PubChem CID: 86346643)	-10.7	PHE273, ILE135, HIS130, PHE269, LEU129, SER131, ILE134, HIS130, GLY133, GLY200, LEU172, ASP199, SER174, GLY,133 GLN173, LEU172, GLN173, LYS132, SER174	SER131	2.33

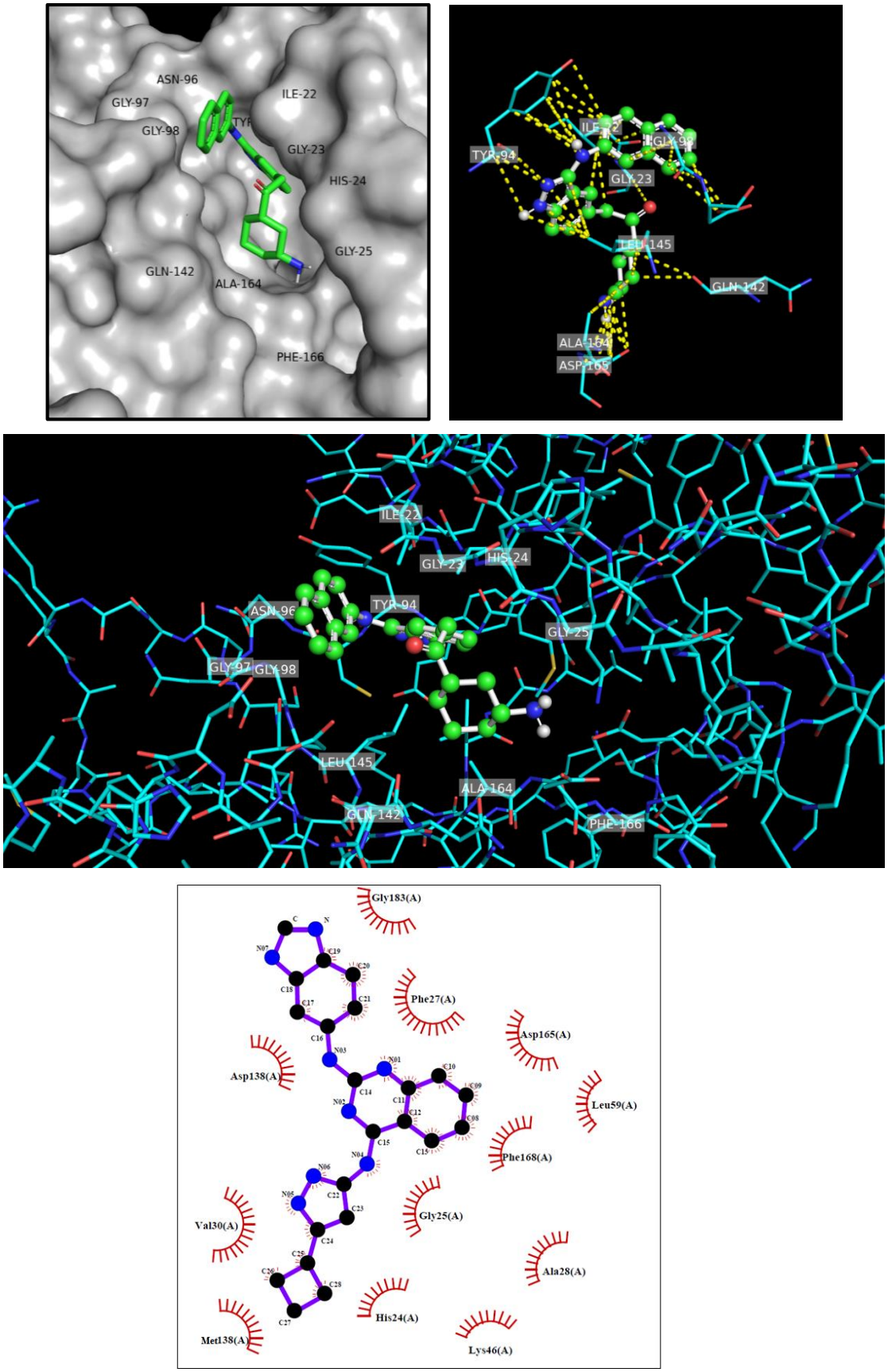

Figure 17. 2D and 3D interactions of protein-ligand complexes having good binding affinity. STD 1 (-9.3 kcal/mol).

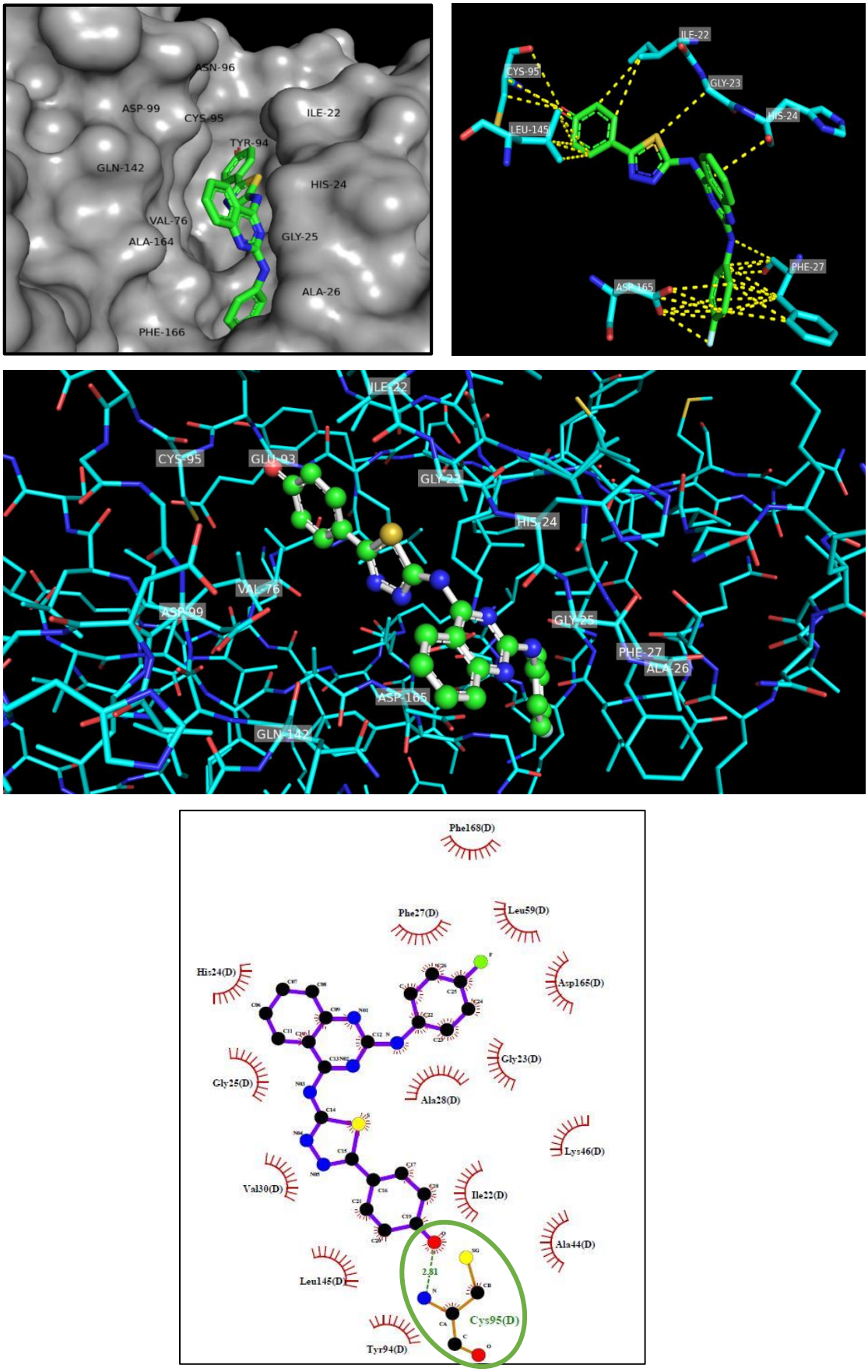

Fig.17.A. 2D and 3D interactions of protein-ligand complexes having good binding affinity. 12b-IV ligand (-11.3 kcal/mol)

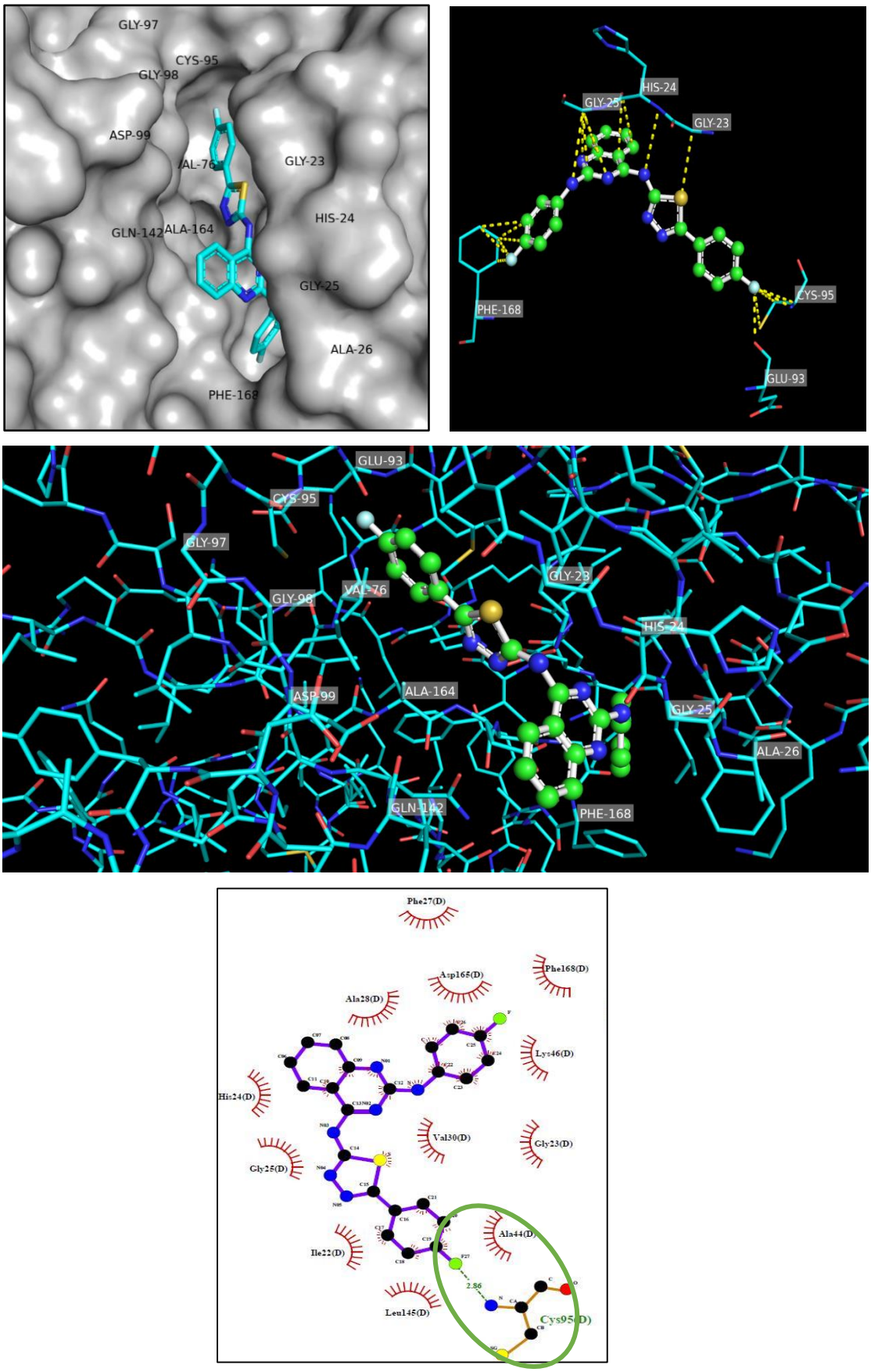

Fig.17.B. 2D and 3D interactions of protein-ligand complexes having good binding affinity. 12d-IV ligand (-11.2 kcal/mol)

4.4. Pharmacophore modelling

Pharmacophore modelling is a computational method used to predict the structural features of molecules that are required to bind to a specific target, such as a protein or a receptor. The main idea behind pharmacophore modelling is to identify the common features of known ligands (molecules that bind to a specific target) and use that information to predict the properties of new ligands (163–166).

A hypothetical three-dimensional representation of the characteristics that a molecule must have in order to bind to a particular target is known as a pharmacophore model. It typically consists of a number of characteristics, such as aromatic rings, hydrophobic regions, hydrogen bond acceptors, and donors (167,168).

4.4.1. The process of pharmacophore modelling involves several steps:

- Selection of a set of known ligands for the target of interest.
- Identification of the structural features that are common among the known ligands.
- Creation of a three-dimensional model that represents the essential features of the known ligands.
- Use of the pharmacophore model to screen a database of compounds for molecules that have similar features.

Pharmacophore modelling is a tool used in drug discovery to find new lead compounds, improve the binding characteristics of already existing drugs, and forecast a compound's potential off-target interactions. It can also be used in the design of new molecules with improved binding properties and reduced toxicity (169).

It's important to note that, like any computational method, the accuracy and reliability of pharmacophore models depend on the quality of the input data and the algorithms used. Therefore, models need to be validated and optimized against experimental data. Here, we ae used ligand-based pharmacophore modelling for the study of current work.

4.4.2. ligand based pharmacophore modelling (170–172)

Ligand-based pharmacophore modelling is a computational method that uses the structures of known ligands (molecules that bind to a specific target) to predict the features that are required for a molecule to bind to the same target. The main idea behind ligand-based pharmacophore modelling is to identify the common features of known ligands and use that information to predict the properties of new ligands.

The process of ligand-based pharmacophore modelling typically involves the following steps:

- Selection of a set of known ligands for the target of interest.
- Alignment of the known ligands to a common reference frame.
- Identification of the structural features that are common among the known ligands, such as hydrogen bond acceptors, hydrogen bond donors, aromatic rings, and hydrophobic regions.
- Creation of a three-dimensional pharmacophore model that represents the essential features of the known ligands.
- Use of the pharmacophore model to screen a database of compounds for molecules that have similar features

Ligand-based pharmacophore modelling is particularly useful for targets for which the three-dimensional structure is not known, but there are some known ligands. It is also useful for predicting the binding properties of new compounds, and for identifying potential off-target interactions.

It's important to note that, like any computational method, the accuracy and reliability of pharmacophore models depend on the quality of the input data and the algorithms used. Therefore, models need to be validated and optimized against experimental data. Also, it's important to have a diverse set of ligands to represent all possible binding modes, in order to have an accurate model(167).

The protein and ligand interaction ecosystem are reflected in the pharmacophore. The biological and functional response that happens when protein and ligand associate is caused by chemical properties like hydrogen bond acceptor, hydrogen bond donor, lipophilic, and aromatic contacts, which are represented by pharmacophore. The designed compounds were subjected to 3D pharmacophore model generation using PharmaGist (https://bioinfo3d.cs.tau.ac.il/PharmaGist/) and determination of pharmacophores was done based on input ligand molecules(173). Pharmacophores of designed compounds were generated in which one of the compounds served as a pivot on which the other subjected compounds were aligned. The user interface of PharmaGist is straightforward to handle 43. Designed compounds were converted to molecules in Sybyl Mol2 format using BIOVIA Discovery Studio and submitted on PharmaGist. After submitting the designed compounds, the pharmacophore detection algorithm started running. The results of PharmaGist were organized in tables by the number of aligned ligands along with their score in descending order. The model having the highest scoring is reported as a pharmacophore. The best pharmacophore was picked based on physicochemical

characteristics and pharmacophore score, and it was downloaded in mol2 format for additional examination.

4.4.3. Pharmacophore analysis

Pharmacophore modelling was done using PharmaGist server to generate the scored sets of pharmacophoric features. All designed compounds aligned together with the pivot molecule. Based on pharmacophoric features scoring highly and the numerous alignments of designed compounds, the best pharmacophore model was chosen. PharmaGist algorithm applies standard weighted properties for each pharmacophore feature. The quantitative characteristics of the best-scored pharmacophore model are shown in **Table 10.** The spatial coordinates for pharmacophore models, obtained from ZincPharmer are shown in **Table 11**. The highest ranked pharmacophore model with a score of 97.500 was selected for spatial feature analysis. A total of 10 features were obtained from which 3 aromatic rings, 3 Hydrogen donors, and 4 Hydrogen acceptors were observed as pharmacophoric features. The most highly rated pharmacophore model's geometric description is shown in **(Figure 18).**

Table 10. Generated pharmacophore models from PharmaGist Tool.

Pharmacophore model	Score of the pharmacophore model	Spatial features	Aromatic ring	Hydrophobic	Hydrogen donor	Hydrogen acceptor
1	97.500	10	3	0	3	4
2	97	11	3	1	3	4
3	90	9	3	0	2	4
4	82.500	9	2	0	3	4
5	82.500	8	3	0	2	3
6	80.777	7	3	0	1	3
7	75	8	2	0	3	3
8	75	8	2	0	2	4
9	75	8	2	0	2	4
10	74.954	9	2	1	3	3

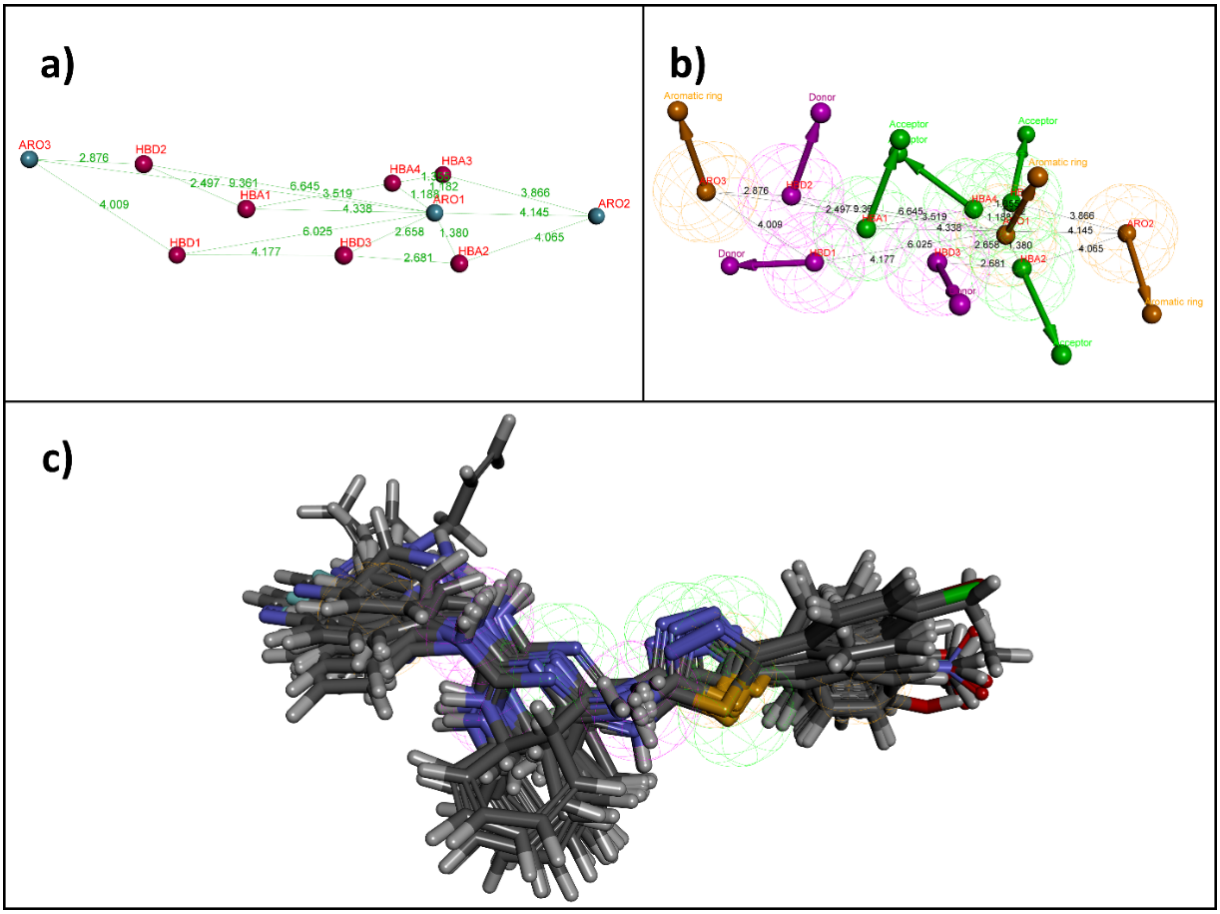

Figure 18. Characteristics of the best pharmacophore model having best score. (a) Geometric distance. (b) Pharmacophoric features. (c) Aligned molecules

Table 11. Pharmacophoric features and spatial coordinates for pharmacophore Models obtained from Pharmagist and ZincPharmer.

Pharmacophoric features	**Spatial coordinates**			
	X	**Y**	**Z**	**Radius**
HBA1	109.68	50.39	19.12	0.50
HBA2	105.57	48.02	16.66	0.50
HBA3	107.25	46.31	17.16	0.50
HBA4	107.69	47.45	17.75	0.50
HBD1	110.68	51.75	18.09	0.50
HBD2	111.09	51.15	20.34	0.50
HBD3	106.98	49.82	18.07	0.50
ARO1	106.68	47.35	17.13	1.10
ARO2	104.59	44.40	15.10	1.10
ARO3	113.56	52.56	20.76	1.10

4.5. Molecular dynamic simulation

Molecular dynamics (MD) simulation is a computational technique that uses classical mechanics to study the motions of atoms and molecules over time. In MD simulations, the behavior of a system is modeled as a collection of particles, and the forces acting on each particle are calculated using physical laws, such as Newton's laws of motion(174–176).

A variety of molecular systems, including proteins, lipids, nucleic acids, and small molecules, can be studied using MD simulations (177). The simulations can predict the behavior of the system under various conditions, such as changes in temperature, pressure, or pH, and they can offer insights into the structure, dynamics, and function of these molecules at the atomic level. (157,158,178–180).

4.5.1. MD simulations typically involve four main steps:

System preparation: In this step, the system's initial configuration is prepared by specifying the initial positions and velocities of the system's particles.

Simulation setup: In this step, the simulation parameters are defined, such as the time step, the force field, and the boundary conditions.

Simulation run: This step involves running the simulation for a predetermined amount of time while updating the particle positions and velocities according to the forces acting on them.

Analysis: In this step, the trajectory data generated by the simulation is analysed to obtain information about the behaviour of the system, such as the structure, dynamics, and energetics of the molecules.

MD simulations can be used to address a wide range of research questions in biology, chemistry, and materials science. For example, MD simulations have been used to study protein folding, drug binding, membrane dynamics, and material properties, among other topics. The technique has become an essential tool in many areas of molecular science and is expected to play an increasingly important role in future research (181-183).

Parameters of md simulation

Molecular dynamics (MD) simulations involve various parameters that are set up at the beginning of the simulation to define the system and simulate its dynamics. Some of the important parameters involved in an MD simulation are:

Force field: A force field defines the interaction potential between particles in the system. It includes parameters such as bond lengths, bond angles, and dihedral angles, which

describe the covalent bonding between atoms, as well as non-bonded interactions such as van der Waals and electrostatic forces.

Initial conditions: The initial conditions of the simulation include the positions, velocities, and sometimes the orientations of the particles in the system. These parameters are usually set randomly or based on experimental data.

Temperature: The temperature of the system is usually set using a thermostat that regulates the kinetic energy of the particles to a specific temperature.

Pressure: The pressure of the system can be set using a barostat that adjusts the volume of the simulation box to maintain a constant pressure.

Time step: The time step is the interval at which the positions and velocities of the particles are updated in the simulation. The time step should be small enough to accurately capture the dynamics of the system but not so small as to make the simulation computationally infeasible.

Boundary conditions: The boundary conditions specify how the system interacts with its environment. For example, periodic boundary conditions can be used to simulate an infinite system by replicating the simulation box in all three dimensions.

Cut-off distance: The cut-off distance is the distance beyond which non-bonded interactions between particles are neglected to reduce the computational cost of the simulation.

Overall, these parameters are critical for defining the behaviour of the system in an MD simulation, and their selection and optimization can have a significant impact on the accuracy and efficiency of the simulation.

Md trajectory

In molecular dynamics (MD) simulations, a trajectory is a time series of atomic positions and velocities that describes the behaviour of the simulated system over time. During an MD simulation, the positions and velocities of the atoms in the system are updated at regular intervals according to the equations of motion. As a result, a trajectory is generated that records the positions and velocities of the atoms at each time step.

To learn more about the system's structure, dynamics, and thermodynamics, the trajectory can be examined. For example, the trajectory can be used to calculate the root-mean-square deviation (RMSD) of the protein structure over time, which provides information about the stability and flexibility of the protein. Similarly, the trajectory can be used to calculate the root-mean-square fluctuation (RMSF) of the protein residues, which indicates the degree of flexibility of each residue.

Trajectory analysis can also be used to calculate thermodynamic properties of the system, such as the potential energy, kinetic energy, and temperature. These properties can be used to calculate free energy changes, which are important for understanding the stability and binding of molecules.

Overall, MD trajectories provide a wealth of information about the behaviour of molecular systems and are an important tool for studying the structure and function of biological macromolecules and other molecular systems.

Root-mean-square deviation (RMSD)

Root-mean-square deviation (RMSD) is a measure of the difference between two structures, such as two protein structures or two conformations of a molecule. RMSD is commonly used in molecular dynamics (MD) simulations and other computational studies to compare the similarity of different conformations of a molecule over time.

To calculate the RMSD, the positions of the corresponding atoms in the two structures are superimposed and the distances between them are calculated. The square of these distances is then averaged over all pairs of corresponding atoms, and the square root of this average is taken to obtain the RMSD value.

RMSD is a measure of the overall deviation between two structures and provides information about the structural similarity or dissimilarity between them. Typically, an RMSD value of less than 2 angstroms indicates a high degree of similarity between the structures, while a value greater than 3-4 angstroms suggests significant structural differences.

In MD simulations, the RMSD can be used to monitor the stability and conformational changes of a protein or other biomolecule over time. By comparing the RMSD of different structures along the simulation trajectory, researchers can identify stable conformations and determine how the structure changes in response to external stimuli or ligand binding.

Overall, RMSD is a useful tool for comparing and analysing the structures of molecules, and it has many applications in structural biology, drug discovery, and materials science.

Application of root-mean-square deviation (RMSD) (184)

In structural biology and computational chemistry, the root-mean-square deviation (RMSD) is a commonly used metric to assess how similar two or more protein or molecular structures are to one another. Some of the common applications of RMSD include:

Conformational analysis: RMSD is often used to compare the structures of different conformations of a protein or other biomolecule, such as the open and closed states of an ion channel. By analyzing the RMSD values between different structures, researchers can identify the most stable and biologically relevant conformations.

Protein-ligand binding: RMSD can be used to assess the quality of protein-ligand docking predictions and to compare the structures of different protein-ligand complexes. For example, researchers can use RMSD to compare the binding modes of a ligand in different protein structures or to evaluate the accuracy of computational predictions of ligand binding affinity.

Drug discovery: RMSD is a key parameter used in drug design and optimization. By comparing the RMSD values of different ligand structures bound to a target protein, researchers can identify promising lead compounds and optimize their structures to improve their binding affinity and selectivity.

Materials science: RMSD is often used to analyze the structural stability and properties of materials, such as crystals or polymers. For example, researchers can use RMSD to compare the structures of different crystal polymorphs or to analyze the structural changes that occur during the formation of a new material.

Root-mean-square fluctuation (RMSF)

Root-mean-square fluctuation (RMSF) is a measure of the variation in the positions of atoms in a molecule over a period of time, usually obtained from molecular dynamics (MD) simulations or NMR experiments. RMSF provides information about the flexibility and dynamics of different parts of a molecule, such as a protein or a nucleic acid.

To calculate RMSF, the average position of each atom in the molecule is determined over the course of the simulation, and the deviation of the atom's position from this average is calculated at each time step. The square of these deviations is then averaged over all time steps and atoms, and the square root of this average is taken to obtain the RMSF value.

RMSF is commonly used in MD simulations to analyze the flexibility and stability of protein structures. By comparing the RMSF values of different residues or regions of the protein, researchers can identify flexible regions, such as loops or hinges, that may play important roles in protein function or interactions with other molecules. RMSF can also be used to evaluate the effects of mutations or ligand binding on protein stability and flexibility.

RMSF is also used in NMR experiments to analyze the dynamic behaviour of proteins and other molecules in solution. By measuring the chemical shifts of atoms in the molecule over time, researchers can obtain information about the fluctuations and motions of different parts of the molecule.

Application of root-mean-square fluctuation (RMSF)

Root-mean-square fluctuation (RMSF) is a versatile measure that has many applications in structural biology and computational chemistry. Some of the common applications of RMSF include:

Protein dynamics: RMSF is often used to analyze the flexibility and dynamics of proteins, which can provide important insights into their function and interactions with other molecules. By comparing the RMSF values of different residues or regions of the protein, researchers can identify flexible regions that may play important roles in protein-protein interactions, allosteric regulation, or ligand binding.

Drug discovery: RMSF is a key parameter used in drug design and optimization. Researchers can find flexible regions that can be targeted to increase the binding affinity and selectivity of the ligand by looking at the RMSF values of a protein-ligand complex.

Protein engineering: RMSF can be used to guide the design of engineered proteins with desired structural and functional properties. By analyzing the RMSF values of different mutations or modifications to the protein, researchers can identify changes that may affect the stability, flexibility, or activity of the protein.

Molecular simulation: RMSF is often used as a quality control measure in molecular dynamics (MD) simulations. By analyzing the RMSF values of different residues or regions of the protein, researchers can assess the stability and convergence of the simulation and identify potential artifacts or errors.

NMR spectroscopy: RMSF is a key parameter used in NMR spectroscopy to analyze the dynamics of proteins and other molecules in solution. By measuring the chemical shifts of atoms in the molecule over time, researchers can obtain information about the fluctuations and motions of different parts of the molecule.

Overall, RMSF is a useful tool for analyzing the dynamics and flexibility of molecules and can provide important insights into their structure, function, and interactions with other molecules

Radius of gyration in md simulation

Radius of gyration (Rg) is a measure of the compactness or size of a molecule, such as a protein or a nucleic acid. In molecular dynamics (MD) simulations, Rg is often used to monitor the conformational changes and stability of the molecule over time.

The root-mean-square distance of the atoms from the molecule's center of mass is known as Rg, and it can be calculated as follows:

Rg = sqrt (1/N * sum[i=1 to N]((ri - rcg)^2))

where N is the number of atoms in the molecule, ri is the position vector of the i-th atom, and rcg is the position vector of the centre of mass of the molecule.

In MD simulations, Rg can be calculated for each frame of the trajectory and used to monitor changes in the size and shape of the molecule over time. For example, an increase in Rg may indicate that the molecule is unfolding or becoming more extended, while a decrease in Rg may indicate that the molecule is becoming more compact or folded.

Rg is also commonly used in combination with other structural measures, such as root-mean-square deviation (RMSD) or root-mean-square fluctuation (RMSF), to analyze the conformational changes and stability of proteins and other biomolecules. By comparing Rg values between different simulations or between different parts of the molecule, researchers can gain insights into the structural and dynamic properties of the molecule and its interactions with other molecules.

Application of Radius of gyration

Radius of gyration (Rg) has numerous applications in molecular biology and computational chemistry. Some of the common applications of Rg include:

Protein folding and stability: Rg is a key parameter used to monitor the folding and stability of proteins. By analyzing the changes in Rg during molecular dynamics simulations or experiments, researchers can gain insights into the kinetics and thermodynamics of protein folding, as well as the stability of protein structures under different conditions.

Protein-protein interactions: Rg can be used to analyze protein-protein interactions and complex formation. By comparing the Rg values of the individual proteins to the Rg value of the complex, researchers can assess the degree of conformational change and flexibility upon complex formation, as well as the contribution of different regions of the proteins to the interaction.

Drug design: Rg is a key parameter used in drug design and optimization. By analyzing the changes in Rg upon binding of a ligand to a protein, researchers can identify potential binding sites and optimize ligand binding affinity and selectivity.

Quality control in molecular dynamics simulations: Rg is often used as a quality control measure in molecular dynamics simulations. By monitoring the Rg values over the course of the simulation, researchers can assess the stability and convergence of the simulation and identify potential errors or artifacts.

Structural biology: Proteins, nucleic acids, and macromolecular complexes are just a few examples of the biomolecules whose size and shape can be determined using the tool Rg. By comparing the Rg values of different structures or complexes, researchers can gain insights into the structural and dynamic properties of these molecules and their interactions with other molecules.

Overall, Rg is a versatile and powerful tool for analyzing the size, shape, and stability of biomolecules and can provide important insights into their structure, function, and interactions.

Hydrogen bonding in md simulation

In biological systems, hydrogen bonding is a vital interaction that is important for both protein structure and function. Different techniques can be used to examine the presence and strength of hydrogen bonds in molecular dynamics (MD) simulations.

One common method for analyzing hydrogen bonds in MD simulations is to use a distance and angle criteria. The distance criteria typically involve measuring the distance between the donor and acceptor atoms, while the angle criteria involve measuring the angle between the donor-hydrogen and acceptor atoms. A hydrogen bond is typically defined as a donor-acceptor distance of less than 3.5 Å and a donor-hydrogen-acceptor angle of greater than 135°.

Another method for analyzing hydrogen bonds in MD simulations is to use a hydrogen bond occupancy analysis. This involves calculating the percentage of time that a hydrogen bond is present between two atoms during the simulation. This can provide insight into the strength and stability of the hydrogen bond over time.

Hydrogen bonding analysis can be particularly useful in MD simulations of proteins, where hydrogen bonds play a critical role in stabilizing protein structure and function. By analyzing the hydrogen bonding patterns and occupancy, researchers can gain insights into the stability and dynamics of protein structure, as well as the role of hydrogen bonding in protein-ligand interactions.

In addition to protein simulations, hydrogen bonding analysis can also be used in simulations of other biological molecules, such as nucleic acids and carbohydrates, as well as in simulations of synthetic molecules and materials. Overall, hydrogen bonding analysis is an important tool for understanding the molecular interactions and dynamics in biological and chemical systems, and it can provide valuable insights into the structure and function of complex molecules.

Molecular dynamics (MD) simulations are one of the crucial tools for structure-based drug design 54. The movement of atoms in a protein or ligand over a time on the basis of physics governing interatomic interactions were predicted using MD simulations 55,56. Docked protein-ligand complexes having good binding affinity were subjected to MD. The main aim of performing MD simulation was to determine the binding stability, conformation and interaction modes occurring between the docked protein-ligand complexes 57. WebGRO and CABS-flex ver. 2.0 were used to perform the MD simulation, and GlycoBioChemPRODRG2 was used to make ligand topology files. The GROMOS96 43a1 force field was chosen for the MD simulation. The protein-ligand complex was immersed in a solvent using the Simple Point Charge (SPC) water model within a triclinic box. All the parameters for energy minimization were set as default. To perform MD simulation, temperature was set constant at 300 K with a pressure of 1.0 bar and the entire simulation was neutralized and performed in the presence of 0.15 M NaCl. Each complex was allowed a simulation time of 100 ns from equilibration using NVT/NPT after energy minimization 63. All other parameters were set to default. The MD trajectory of complexes were further analyzed using RMSD (Root Mean Square Deviation), RMSF (Root Mean Square Fluctuation), RG (Radius of gyration) and HBs (Hydrogen bonds) of complexes.

4.5.2. Molecular dynamic simulation analysis

As per the molecular docking results, **12b-IV, 12d-IV,** and **12d-V** were identified as hit molecules, showing good binding affinity with the targeted protein structure. The protein-ligand complex systems of targeted protein (PDB: 4WNP) and **12d-IV** were further subjected to molecular dynamic (MD) simulation studies to investigate the conformational stability of the complex. MD simulation was performed using WebGro to determine the time-dependent motions, behavior, and configurational changes between subjected protein-ligand complexes over 100 ns. CABS-flex ver. 2.0 was used to determine the root mean square fluctuation (RMSF) of complex systems. Root mean square deviation (RMSD), root mean square fluctuation (RMSF), the radius of gyration (Rg), hydrogen bonds (HBs), and principal component analysis were used to analyze MD trajectory data (PCA).

The RMSD values were calculated for all frames present in the MD simulation trajectory of each simulated protein-ligand complex. The average change of atom displacement for the **4WNP-12d-IV** complex system over 100 ns MD simulation was estimated using RMSD and the structural stability of the complex system was also investigated. These RMSD profiles of the **4WNP-12d-IV** complex help to determine the behavior of the backbone and heavy atoms of the protein. The lower deviations in RMSD values represent the more stable nature of protein and protein-ligand complex. Hence, the stability of subjected **4WNP-12d-IV** complex was analyzed with the help of RMSD values. And the calculations were done to obtain the equilibrium time of the simulated complexes. Through the results of the RMSD analysis, it is observed that the simulated complex has minimum deviations in the RMSD. **Figure 7a** represents the RMSD plot for the **4WNP-12d-IV** complex. The RMSD values for **4WNP-12d-IV** ranged between 0.4 nm to 0.6 nm, respectively According to the RMSD plot for **4WNP-12d-IV**, the complex was stable over 100 ns with a minimum deviation.

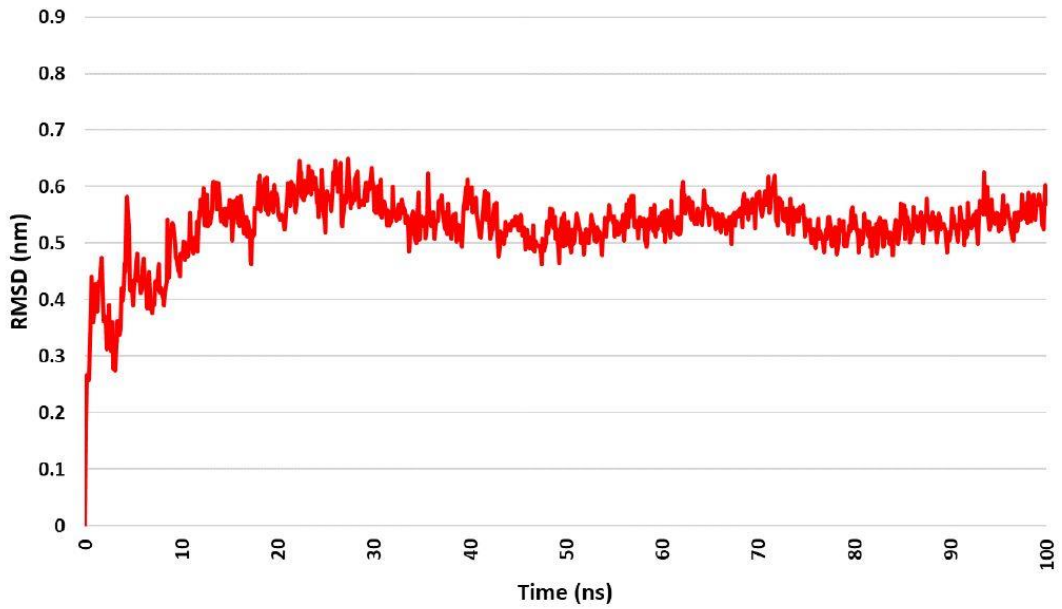

Fig.19. RMSD

The RMSF profile was determined for the protein and protein-ligand complexes (**Figure 7b**). It measures the movement of each residue around the average position along the trajectory, revealing the flexibility of a specific protein region during the MD simulation. **Figure 7b** represents the RMSF of the **4WNP-12d-IV** complex. It was observed that ALA37 (RMSF value: 0.29 nm), ALA36 (RMSF value: 0.4 nm), HIS39 (RMSF value: 0.38 nm), ASP40 (RMSF value: 0.24 nm), ALA150 (RMSF value: 0.29

nm), GLU151 (RMSF value: 0.26 nm), ARG152 (RMSF value: 0.24 nm), ARG153 (RMSF value: 0.25 nm), ALA154 (RMSF value: 0.27 nm), SER174 (RMSF value: 0.31 nm), ASN175 (RMSF value: 0.47 nm), MET176 (RMSF value: 0.33 nm), ALA179 (RMSF value: 0.41 nm) amino acid residues of **4WNP-12d-IV** showed fluctuations in which ASN175, ALA36, ALA179 displayed high fluctuations. However, the RMSF values are lower than the observed RMSD values and remained in the acceptable region, confirming the stability of particular amino acid residues.

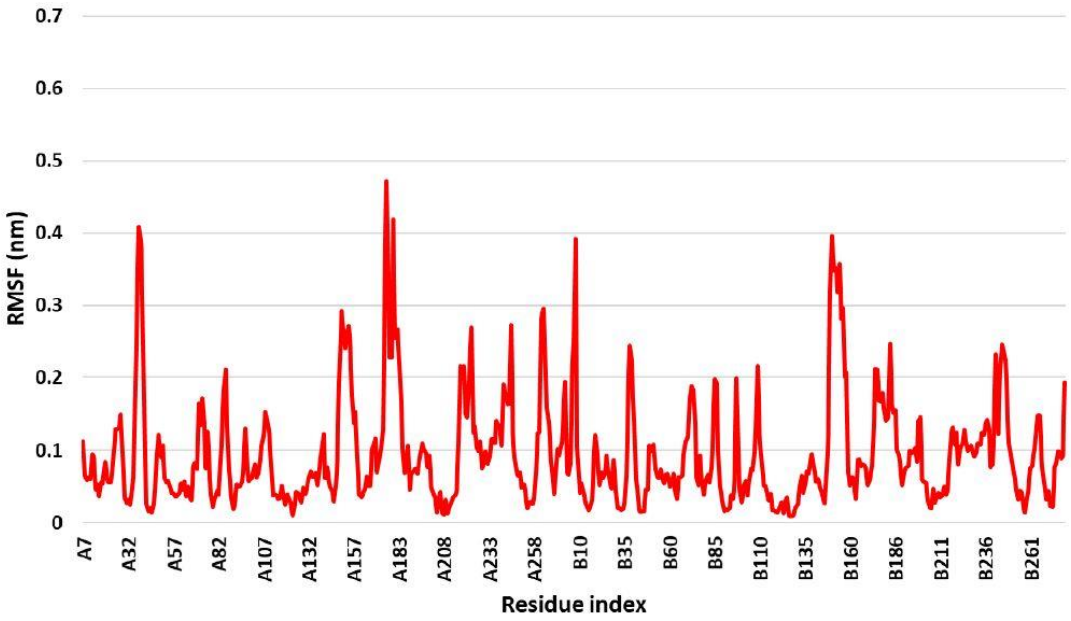

Fig.20. RMSF

*R*g trajectory of MD simulation was computed to assess the overall stability of protein structure during MD simulation. It was also used to determine the compactness of protein due to the presence or absence of ligands over 100 ns. A higher *R*g value of the protein-ligand complex reflects the less compactness in the complex. If the *R*g displays a value that is largely constant during the MD simulation. Otherwise, it would be viewed as an unfolded structure and can be called a stable folded structure. *R*g values for **4WNP-12d-IV** were studied over 100 ns at 300 K. In terms of MD trajectory analysis, the *R*g values for the **4WNP-12d-IV** ranged between 2.6 to 2.7 nm indicating no significant changes after 10 ns. It indicates that protein in presence of 4d, did not show any conformational changes. According to the results of computed *R*g, the simulated complex showed conformational stability with minimum fluctuation in the *R*g values **(Figure 7c)**.

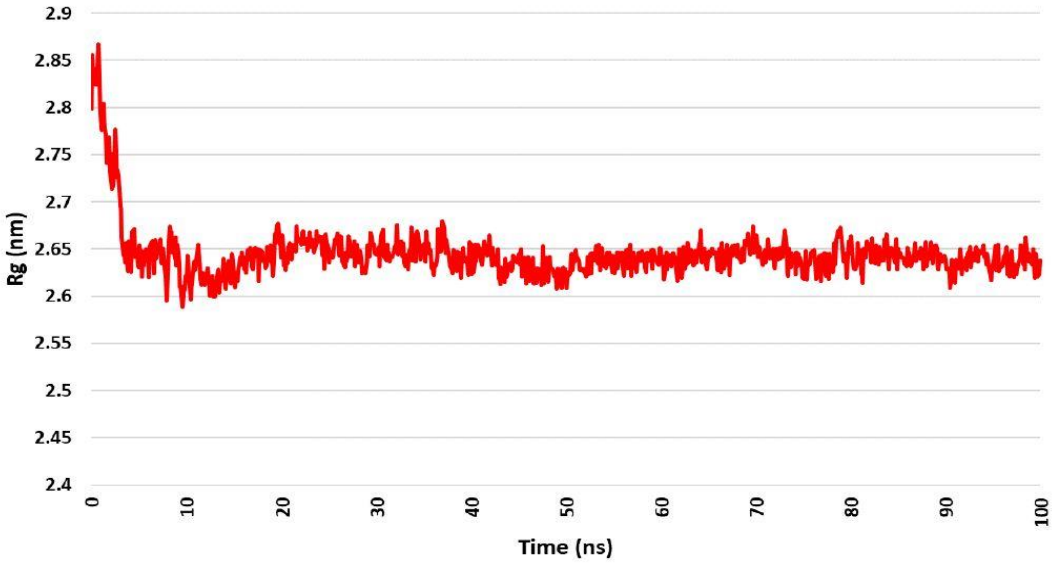

Fig.21. ROG

The protein-ligand complex is significantly stabilized by hydrogen bonds (HBs), which are very important. Additionally, HBs are in charge of drug specificity, metabolization, and body adsorption. The simulated complex's overall confirmation is maintained by HBs. Therefore, MD trajectories were also analyzed to examine the time evaluation of the number of HBs between protein-ligand complexes formed during the 100 ns simulation. The number of HBs present in the 4WNP-4d, complex system with consistent over the 100 ns MD simulation at 300 K **(Figure 7d)**. No significant changes were observed in the hydrogen bond interactions between the **4WNP-12d-IV** complex and a maximum of six hydrogen bonds were observed in the initial phase of MD simulation.

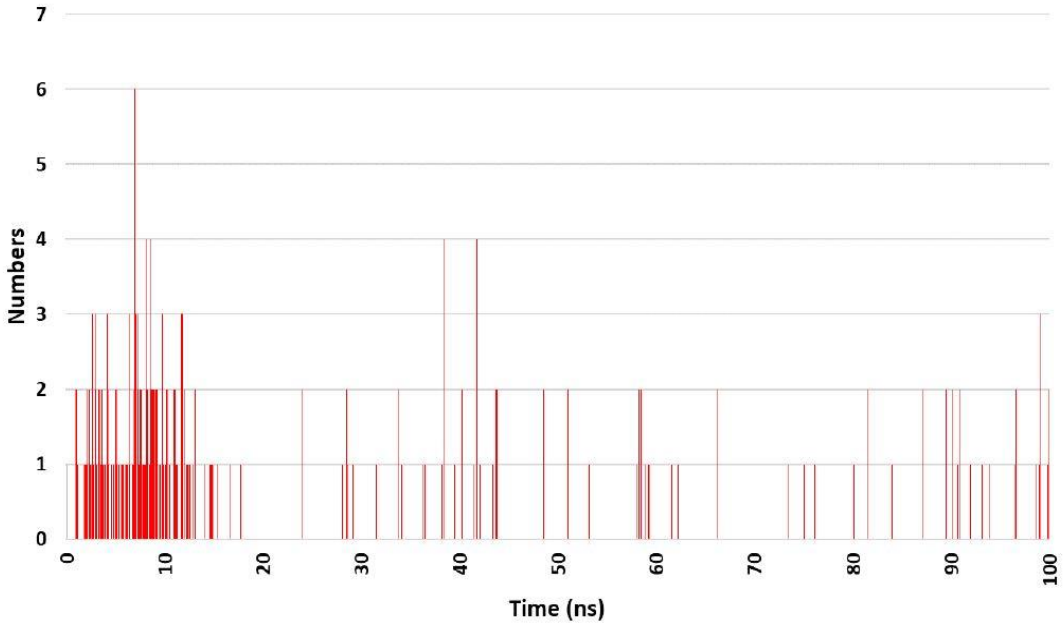

Fig.22. H-Bond

Moreover, the comparison of active sites of 4WNP and 12d-IV at different time points (0, 25, 50, 75, and 100 ns) of MD trajectory period was done to check the dynamic behaviour of the **4WNP-12d-IV** complex system during the 100 ns simulation time and the snapshots of complex at 25, 50, 75, and 100 ns are represented in blow **Figure 21.**

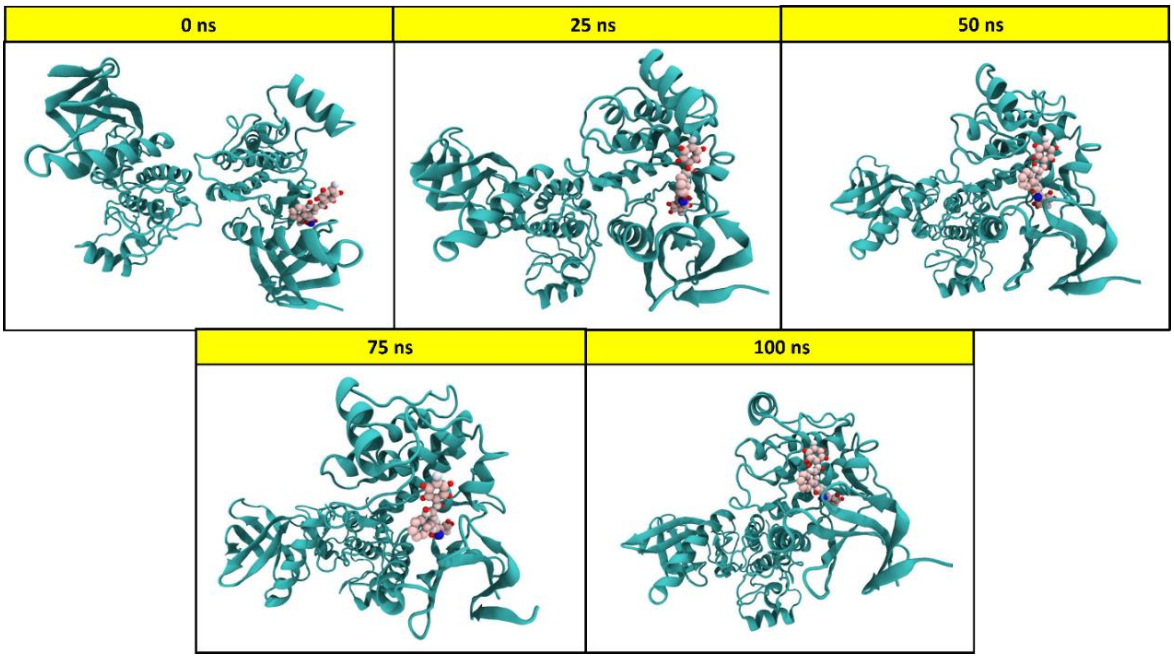

Figure 23. Dynamic changes in the active site of ULK1 at 0, 25, 50, 75, and 100 ns simulation time point with compound (**12d-IV**).

4.6. PCA (Principal Component Analysis)

PCA, or Principal Component Analysis, is a statistical technique used for data analysis and dimensionality reduction. By transforming the data into a lower-dimensional space, it is primarily used to find patterns and relationships in datasets. (185).

In PCA, the original variables of a dataset are transformed into a new set of variables called principal components (186–188). These principal components are linear combinations of the original variables and are created in such a way that they capture the maximum amount of variation present in the data (189). The first principal component accounts for the largest amount of variance, followed by the second, and so on. Each subsequent principal component is orthogonal (uncorrelated) to the previous ones (190–192).

PCA's main goal is to reduce the dataset's dimensionality while retaining as much information as possible. The effects of multicollinearity can be mitigated by reducing the number of variables, which also makes the data easier to visualise and interpret.

4.6.1. The Primary Objectives of PCA are as follows:

Dimensionality Reduction: PCA aims to reduce the number of variables or features in a dataset. This is particularly useful when dealing with high-dimensional data, where the original variables may be redundant or contain noise. PCA streamlines the analysis and visualisation process by choosing a subset of principal components that captures the most significant variation in the data. (193).

Data Compression: PCA enables the compression of data by representing it using a smaller number of principal components. This can be valuable for storage, computational efficiency, or when dealing with large datasets. The compressed data retains the most important patterns and trends while discarding less relevant details.

Variable Selection: PCA helps identify the variables that contribute most to the variation in the dataset. By examining the loadings (coefficients) associated with each variable in the principal components, one can determine the relative importance of variables. This information can guide feature selection and focus further analysis on the most influential variables.

Data Visualization: PCA facilitates the visualization of complex data in a reduced-dimensional space. Finding patterns, clusters, or outliers is made simpler by plotting the data points according to their values along the principal components. Visualization aids in exploratory data analysis and provides insights into the underlying structure of the data.

Data Pre-processing: PCA can be used as a pre-processing step to decorrelate variables or remove multicollinearity. By transforming the data into uncorrelated principal components, PCA can improve the performance of subsequent analysis techniques, such as regression or classification models.

PCA is widely used in various fields, including data science, machine learning, image processing, genetics, and social sciences, to name a few. It provides valuable insights into the underlying structure of data, identifies dominant patterns, and facilitates feature selection for subsequent analyses.

Procedure of PCA analysis

The procedure for conducting a PCA analysis typically involves the following steps:

1. **Data Preparation:** Start by preparing your dataset. Ensure that your data is in a numerical format and free of missing values. If necessary, handle any missing values or outliers using appropriate techniques such as imputation or removal.
2. **Standardization:** If your variables are measured on different scales, it is often recommended to standardize the data. To do this, divide each variable's standard deviation

by its mean before subtracting it. Through standardisation, the PCA analysis is protected from being dominated by variables with larger scales.

3. **Covariance or Correlation Matrix Calculation:** Calculate the covariance matrix if your data represents quantitative variables, or the correlation matrix if your data is standardized or represents qualitative variables. The covariance matrix measures the relationships between variables, while the correlation matrix measures the linear relationships. The matrix will be square, with dimensions equal to the number of variables in your dataset.
4. **Eigenvector-Eigenvalue Decomposition:** Perform an eigenvector-eigenvalue decomposition of the covariance or correlation matrix. This step calculates the eigenvectors and eigenvalues. The principal components are represented by the eigenvectors, and the variance explained by each principal component is shown by the eigenvalues. The eigenvectors are typically normalized to have unit length.
5. **Selection of Principal Components:** The eigenvalues should be sorted descending. The variance explained by each principal component is shown by the eigenvalues. Decide how many principal components to retain based on the explained variance threshold you want to achieve. This can be determined by examining the cumulative explained variance or using techniques like scree plots or eigenvalue thresholds.
6. **Projection:** Project the original data onto the selected principal components. In order to do this, you must multiply the initial data matrix by the matrix of the chosen eigenvectors. The resulting projected data represents the transformed variables along the principal components.
7. **Analysis and Interpretation:** Analyze and interpret the transformed data. This includes examining the contribution of variables to each principal component, exploring the relationships between variables and observations in the reduced-dimensional space, and visualizing the data using scatter plots, biplots, or other techniques.
8. **Reconstruction (Optional):** If desired, you can reconstruct the data from the projected principal components to obtain an approximation of the original data. This reconstruction can be useful for validating the effectiveness of the PCA analysis or for further analyses.

4.6.2. What is the indication of black, red and blue color in PCA Analysis?

The indication or meaning of specific colors in PCA analysis can vary depending on the context, software, or specific choices made during visualization. Without further information about the specific PCA analysis or the software being used, it is difficult to

provide a definitive answer regarding the indication of black, red, and blue colors in the PCA result. However, here are some general interpretations that can be associated with these colors in certain contexts:

Black: In some cases, black color may be used to represent a neutral or reference category. It could indicate that the data points or variables belonging to this category have no specific grouping or distinction compared to other categories.

Red: Red color is often used to represent one category or group, typically highlighting a specific characteristic or condition. It could indicate the presence of a specific group or cluster within the data that exhibits distinct behavior or properties compared to other groups.

Blue: Blue color can be used to represent another category or group, contrasting with the red category. It might indicate the presence of a different group or cluster within the data, which may have its own unique characteristics or properties.

Please note that the color indications can vary depending on the specific context and choices made during visualization. It is important to refer to the legend or color key provided in the PCA plot or consult the documentation of the software or analysis method used to understand the precise meaning of the colors used in your specific PCA result.

Eagan value in PCA Analysis

In PCA (Principal Component Analysis), eigenvalues play a crucial role. The variance explained by each principal component is measured by eigenvalues. They are obtained by breaking down the dataset's covariance or correlation matrix into its eigenvectors and eigenvalues.

The eigenvalues associated with the principal components are typically sorted in descending order. The largest eigenvalue corresponds to the first principal component, which captures the most significant amount of variance in the data. The second eigenvalue corresponds to the second principal component, and so on. Eigenvalues indicate the relative importance of each principal component in explaining the variability present in the original dataset.

Eigenvalues are useful for determining how many principal components to retain in a PCA analysis. By examining the magnitude of the eigenvalues and the cumulative explained variance, one can decide the number of principal components needed to capture a satisfactory amount of information. Retaining principal components with larger eigenvalues ensures that the most important patterns and variations in the data are preserved.

Eigenvector in PCA analysis

In Principal Component Analysis (PCA), eigenvectors play a fundamental role in transforming and representing the data. The covariance or correlation matrix of the dataset is decomposed into eigenvectors and eigenvalues to produce eigenvectors.

In the context of PCA, eigenvectors represent the principal components of the data. Each eigenvector corresponds to a principal component, and collectively they capture the major patterns or directions of variation present in the data.

Typically, the eigenvectors are arranged in descending order according to the corresponding eigenvalues. The eigenvector associated with the largest eigenvalue corresponds to the first principal component, which explains the most significant amount of variance in the data.

Each eigenvector represents a direction or axis in the feature space of the original variables. The magnitude of the elements within an eigenvector indicates the weight or contribution of each variable to that principal component. Eigenvectors are typically normalized to have unit length, meaning that their squared elements sum up to 1.

The eigenvectors provide information about the relationships and correlations between the original variables. By projecting the data onto the eigenvectors, the transformed data represents the original variables along the principal components. This transformation allows for dimensionality reduction and facilitates the exploration and interpretation of the data in a reduced-dimensional space.

The eigenvectors and eigenvalues obtained from the eigenvector-eigenvalue decomposition of the covariance or correlation matrix are critical for interpreting and analyzing the results of PCA. They help identify the most significant principal components, determine the amount of variance explained by each component, and understand the relationships between variables in the dataset.

The main aim of Principal Component Analysis (PCA) is to reduce the dimensionality of a dataset while retaining as much information as possible.

4.6.3. PCA Analysis

Principal component analysis (PCA) of 4WNP-4d was performed using obtained MD trajectory. By as much as possible reducing the dimensionality, a PCA aids in the determination of the variability in the subjected MD trajectories. The collective motions with conformational flexibility of the simulated **4WNP-12d-IV** complex at 300K were studied using the PCA tool of the Bio3D package. Dominant motions of the 4WNP-4d complex were extracted and compared for the first three eigenvectors of 4WNP-4d. The

colors from blue to white to red of captured variance by eigenvectors represented the time of sampling of the simulated complex. Obtained PCA results for 4WNP-4d complex system showed the PCA variability of 28% in terms of the internal motions of MD trajectory while the PC2 statistics represented the minimal variability with 12.21%, and PC3 indicated 10.44% signifying the binding stability between 4WNP and 12d-IV with good Eigen scores and the computed atomic motion variabilities of 4WNP-12d-IV is represented in **Figure 6a-b**.

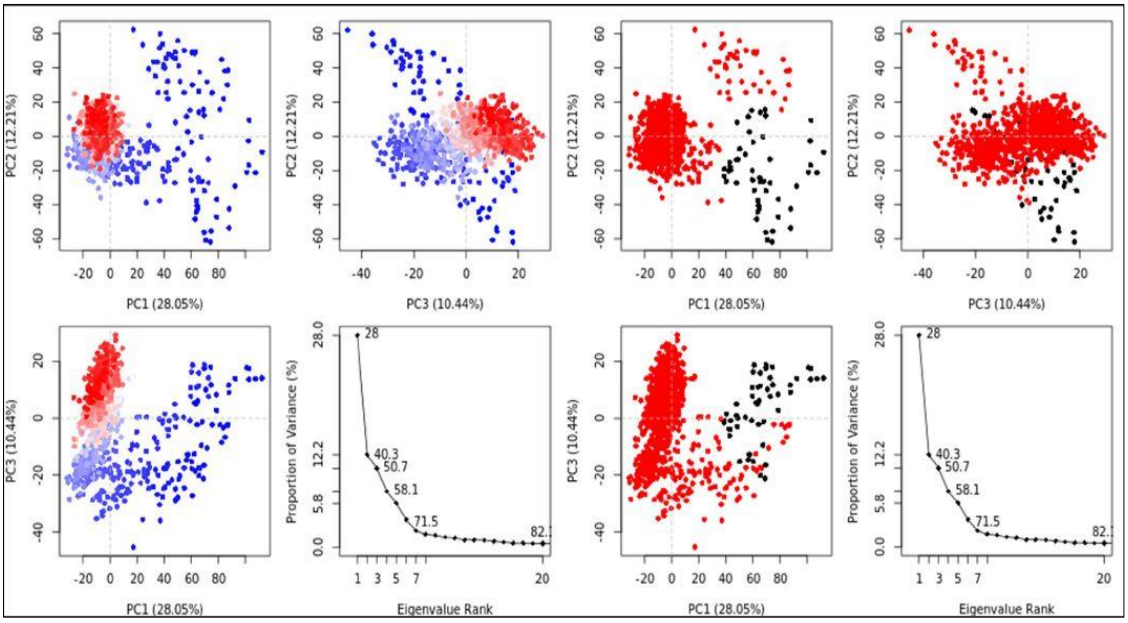

Fig.24. PCA analysis

4.7. DFT (Density Functional Theory)

A computational technique used to investigate the electronic structure of atoms, molecules, and solids is called density functional theory (DFT). It is based on the idea of electron density, which is the likelihood that an electron will be found at a specific location in space. (194–198).

DFT aims to calculate the total energy of a system by considering the electron density instead of the wave function of individual electrons, which makes it more computationally efficient than traditional quantum mechanical methods. The electron density is described by a mathematical function called the density functional, which depends on the positions of the electrons in the system (197–199).

As it enables the prediction of a wide range of properties, including the geometry of molecules and crystals, the electronic structure of materials, and the thermodynamic stability of compounds, DFT has grown in importance in the fields of materials science,

chemistry, and physics. Additionally, it has been utilised to research catalysis, chemical reactions, and the characteristics of surfaces and interfaces (200,201).

4.7.1. Principal of DFT

The basic principle of DFT is to express the total energy of a system in terms of the electron density, rather than the wave function of each individual electron. The Hohenberg-Kohn theorem, which states that an electron density-dependent relationship exists between a system's ground-state energy and its energy, enables this.

In practical terms, The Kohn-Sham equations, a set of equations that describe the behaviour of a hypothetical system of non-interacting electrons with an effective potential that is a function of the electron density, must be solved in order to perform DFT. The Kohn-Sham equations are similar to the Schrödinger equation, but they are easier to solve because the effective potential is simpler than the actual potential that electrons experience in a real system.

The solution of the Kohn-Sham equations yields the electron density and the corresponding total energy of the system. The accuracy of the calculated properties depends on the choice of the density functional, which is a functional that describes the relationship between the electron density and the energy of the system. Different density functionals have different levels of accuracy and are suitable for different types of systems and properties.

In summary, the principal of DFT is to describe the behaviour of a system in terms of its electron density, using the Kohn-Sham equations to solve for the electron density and total energy, and choosing an appropriate density functional to describe the relationship between the electron density and the energy of the system.

What is HOMO and LUMO Concept in DFT

Highest Occupied Molecular Orbital (HOMO) and Lowest Unoccupied Molecular Orbital (LUMO) are key terms used in DFT to describe the electronic structure and characteristics of molecules and solids.

The HOMO is the highest energy level of the occupied molecular orbitals in a system, meaning that it is the energy level that contains the highest energy electron. The HOMO determines the chemical reactivity of a molecule, since it is involved in chemical reactions and bonding. It is also related to the ionization potential of a molecule, which is the energy required to remove an electron from the HOMO.

The LUMO, on the other hand, is the lowest energy level of the unoccupied molecular orbitals in a system, meaning that it is the energy level that would be filled by the next

electron if one were added to the system. The LUMO determines the ability of a molecule to accept electrons and is therefore related to the electron affinity of a molecule, which is the energy released when an electron is added to the LUMO.

The energy difference between the HOMO and LUMO is known as the HOMO-LUMO gap or the band gap, and it is an important parameter that determines the electronic and optical properties of a system. For example, while molecules with large HOMO-LUMO gaps are more likely to be insulators, small HOMO-LUMO gaps are more likely to absorb light and have good electrical conductivity.

4.7.2. Parameters involved in DFT

DFT involves several key parameters that are used to describe the electronic structure and properties of materials. These include:

The electron density: The electron density is the fundamental variable in DFT and is used to describe the distribution of electrons in a system. It is typically represented as a continuous function of position and can be used to calculate many properties of the system, such as the total energy, electrostatic potential, and charge density.

Exchange-correlation functional: The effects of electron-electron interactions that are not taken into account by the Kohn-Sham equations are described by the exchange-correlation functional, a mathematical function. It is a key parameter in DFT, as it determines the accuracy and reliability of the DFT calculations. There are many different exchange-correlation functional available, each with different strengths and weaknesses, and the choice of functional depends on the system being studied and the properties of interest.

Basis set: The basis set is a set of functions used to represent the wave functions of the electrons in the system. It is used to approximate the solution to the Kohn-Sham equations and is a key factor in determining the accuracy of the DFT calculations. The system being studied and the properties of interest also influence the basis set choice.

Integration grid: The integration grid is used to discretize the electron density and other quantities in the system, allowing them to be efficiently computed numerically. The size and spacing of the integration grid can affect the accuracy and efficiency of the DFT calculations.

Cut-off energy: The cut-off energy is a parameter that determines the maximum kinetic energy of the electrons that are included in the DFT calculations. Electrons with higher kinetic energies are neglected, which can affect the accuracy of the calculations.

4.7.3. How to calculate energy in DFT?

In DFT, the total energy of a system can be calculated by integrating the electron density multiplied by the effective potential over all space. The effective potential includes both the external potential due to the nuclei and any additional potential arising from the exchange-correlation functional.

Mathematically, the total energy E can be expressed as:

E = T + Vext + Vh + Exc + Vxc

where T is the kinetic energy of the electrons, Vext is the external potential due to the nuclei, Vh is the Hartree potential due to the electron-electron interactions, Exc is the exchange-correlation energy arising from the exchange-correlation functional, and Vxc is the exchange-correlation potential.

The kinetic energy T is calculated using the Kohn-Sham orbitals, which are obtained by solving the Kohn-Sham equations. The Hartree potential Vh arises from the electron-electron interactions and is calculated from the electron density using the Poisson equation. The exchange-correlation energy Exc and potential Vxc are calculated using the exchange-correlation functional, which is typically chosen based on the system being studied and the properties of interest.

Once the various contributions to the total energy have been calculated, they are added together to obtain the final total energy of the system.

The choice of the basis set, exchange-correlation functional, and other variables, as well as the quality of the approximations used in the calculation, all affect how accurate the DFT energy calculations are. Therefore, it is essential to carefully choose these parameters and validate the results against experimental data and other methods to ensure the accuracy and reliability of the DFT calculations.

4.7.4. Steps involved in DFT

Depending on the specific method and software being used, the size and complexity of the system being studied, as well as other factors, the number of steps needed for a DFT calculation can change. However, in general, a DFT calculation typically involves the following main steps:

Input preparation: This step involves preparing the input files for the DFT software, which typically include the molecular geometry, basis set, exchange-correlation functional, and other parameters.

Geometry optimization: In this step, the DFT software optimizes the molecular geometry to find the lowest-energy configuration of the system. In order to achieve this, the system's

atoms' positions must be modified repeatedly until the forces acting on each atom are reduced to a minimum.

Electronic structure calculation: Once the optimized geometry is obtained, the DFT software calculates the electronic structure of the system, including the Kohn-Sham orbitals, electron density, and total energy. Numerical techniques like density functional theory (DFT), Hartree-Fock (HF) theory, or post-Hartree-Fock methods are frequently used for this.

Property calculation: After the electronic structure has been calculated, the DFT software can be used to compute various properties of the system, such as the molecular orbitals, dipole moment, polarizability, and vibrational frequencies.

Analysis and interpretation: Finally, the results of the DFT calculations can be analyzed and interpreted to gain insights into the electronic structure and properties of the system being studied. This may involve visualizing the electron density or molecular orbitals, comparing the calculated properties to experimental data or other theoretical methods, or using the results to design new materials or optimize existing ones.

4.7.5. DFT study analysis

The density functional theory (DFT), a widely used theoretical chemistry method was used for the electronic structure of synthesized compounds. DFT calculation helped to theoretically compute the frontier molecular orbital (FMO) and chemical reactivity descriptors for the synthesized compounds. The energies of the lowest unoccupied molecular orbital (LUMO) and the highest occupied molecular orbital (HOMO) of the synthesised compounds were calculated. These values offer insights into the compounds' capabilities to donate or accept electrons. Furthermore, HOMO-LUMO energy gap was calculated because it has important implications to understand the chemical and physical properties of a molecule, including its reactivity, stability, and electronic properties. Moreover, it plays a critical role in determining the ability of a molecule to undergo chemical reactions, particularly those involved in enzymatic reactions and cellular processes. In general, a smaller HOMO-LUMO energy gap specifies the highly reactive compound, as electrons can be excited more easily from the HOMO to the LUMO, leading to increased chemical reactivity. While a higher HOMO-LUMO energy gap denotes a more stable compound that is less likely to undergo chemical reactions. The calculated HOMO-LUMO energy gap of the synthesized compounds indicated that compound 7g showed the highest energy gap compared to others. The order of high to low chemical reactivity of synthesized compounds based on the HOMO-LUMO energy gap is **12c-II>**

12a-III> 12g-IV> 12d-IV> 12a-IV> 12e-IV> 12b-IV> 12a-III> 12b-I> and 12b-III, respectively. DFT study also helped to estimate the ionization potential (IP) and electron affinity (EA). The IP and EA are the energies required to remove or add an electron to a neutral molecule, respectively. Compound The electronegativity (χ) of the synthesized compounds was measured to estimate the ability of an atom to attract electrons in a chemical bond and the parameter can be calculated using the HOMO and LUMO energies and the ionization potential and electron affinity. Similarly, other reactivity descriptors including global hardness (η), chemical potential (μ), and electrophilicity (ω) were studied. The calculated FMO and chemical reactivity descriptors for synthesized compounds are represented in **Fig.23.** And **Table 12.** The DFT study helped to understand the electronic structure and molecular behavior of the synthesized compounds.

The Density Functional Theory (DFT) method was used to calculate the synthesized compounds' global chemical reactivity descriptors and the frontier molecular orbitals (FMO). Chemical reactivity descriptors, including dipole moment (DM), ionization potential (IP), electron affinity (EA), global hardness (η), chemical potential (μ), electronegativity (χ), and electrophilicity (ω) were calculated according to the previously reported equations of Koopmans' theory. To perform DFT calculation, B3LYP functional with def2-SVP basis set was done on Orca 4.2.1 software. The orca-enhanced version of Avogadro was utilized to prepare input structures and interpret the output files.

Table 12. Calculated frontier molecular orbital energies and reactivity descriptors for synthesized compounds using the DFT method.

Sr. No.	Code	HOMO (eV)	LUMO (eV)	HLG (eV)	DM (Debye)	IP (eV)	EA (eV)	χ (eV)	μ (eV)	η (eV)	ω (eV)
1	**12a-IV**	-5.233	-2.229	3.004	8.1133	5.23	2.229	3.731	-3.73	1.502	4.633
2	**12a-III**	-5.376	-2.181	3.195	5.0704	5.37	2.181	3.778	-3.778	1.597	4.468
3	**12a-II**	-4.988	-2.211	2.777	6.8332	4.98	2.211	3.599	-3.599	1.388	4.665
4	**12b-IV**	-5.203	-2.14	3.063	7.5548	5.20	2.14	3.671	-3.671	1.531	4.4
5	**12b-III**	-5.703	-1.609	4.094	3.3861	5.70	1.609	3.656	-3.65	2.047	3.264
6	**12b-I**	-4.895	-1.656	3.239	3.4951	4.89	1.656	3.275	-3.275	1.619	3.312

7	**12c-II**	-5.033	-2.314	2.719	6.0423	5.03	2.314	3.673	-3.673	1.359	4.963
8	**12d-IV**	-5.264	-2.287	2.977	7.2632	5.26	2.287	3.775	-3.775	1.488	4.788
9	**12g-IV**	-5.279	-2.356	2.923	7.1298	5.27	2.356	3.817	-3.817	1.461	4.985
10	**12e-IV**	-5.21	-2.186	3.024	8.4959	5.21	2.186	3.698	-3.698	1.512	4.522

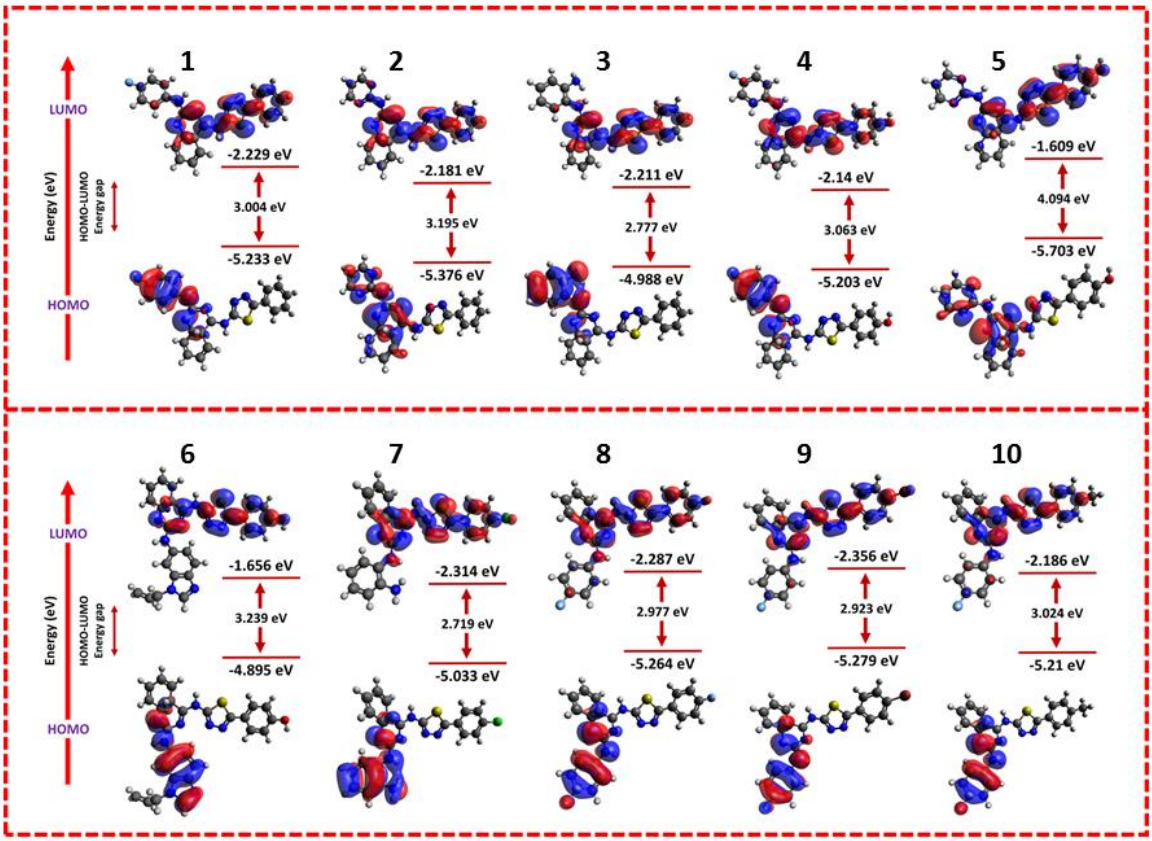

Fig.25. DFT analysis

5. Experimental Method

5. EXPERIMENTAL METHOD

5.1 Materials and Methods

5.1.1. Chemicals for Synthesis

Chemicals which are used for the synthesis of the Thiadiazole derivatives are listed below and from which laboratory it purchased.

Phosphorus Oxychloride - Spectrochem, Thiosemicarbazide - Astron, Triethylamine Loba, N, N -Diisopropylethylamine (DIPEA)- Spectrochem, Stannous dichloride/Tin (II) Chloride ($SnCl_2$)-Loba. All the reagent is from LR-Grade and Solvent From HPLC-Grade.

5.1.2. Instrument used for Synthetic Compounds

The various instruments are used for the synthetic compounds.

The melting points of the synthesized compounds were determined using an open-end capillary on the VEEGO (VMP-PM) melting point apparatus. To assess the purity of the compounds, pre-coated TLC plates and various solvent systems were employed. The TLC plates were examined under UV light at a wavelength of 254 nm and in an iodine chamber.

The FT-IR analysis of the synthesized compounds was carried out using a SIMADZU FT-IR 8400 instrument with KBr pellets provided by the Shree Dhanvantary Pharmaceutical Analysis and Research Centre in KIM.

For Nuclear Magnetic Resonance (NMR) analysis, both 1H-NMR and 13C-NMR were performed using a BRUKER AVANCE-III 400 MHz FT-NMR instrument. DMSO/CDCl3 served as the solvent, with TMS as the internal standard. These NMR experiments were conducted at the Centre of Excellence, NFDD Complex, Department of Chemistry, Saurashtra University in Rajkot, as well as at the NMR Research Centre, Indian Institute of Science in Bangalore.

Mass spectra (GC-MS) of the synthesized compounds were obtained using a SHIMADZU QP-2010 instrument at the Centre of Excellence, NFDD Complex, Department of Chemistry, Saurashtra University, Rajkot.

5.1.3 Reaction Scheme

The Thiadiazole derivatives were synthesized as per schemes.

Scheme-1:

Synthesis of 5-Substituted Phenyl -1,3,4-thiadiazole-2-amine **3a-3h** by using Different aromatic carboxylic acids with thiosemicarbazide (2) in presence of Phosphorus oxychloirde as dehydrating agent and final cyclization using water (84).

Scheme-2:

Urea (460 mmol) was heated until it melted, and then 2-methylaminobenzoic acid (46 mmol) was introduced. The resulting mixture was stirred for 5 hours at 150°C and subsequently cooled to below 100°C. To halt the reaction, 70 mL of water was added. The resulting precipitate was collected and subjected to recrystallization in a mixed solution containing 10 mL of acetone and 100 mL of water, yielding compound 6 in the form of a white powder (202).

Scheme-3:

Quinazoline-2,4(1H,3H)-dione (Benzoylene urea) was refluxed with 10.0 grams (0.061 mole) in the presence of 14.2 grams (0.092 mole) of Phosphorous oxychloride and 7.4 grams (0.061 mole) of N,N-dimethylaniline at a temperature of 108°C. The progress of the reaction was monitored by Thin-Layer Chromatography (TLC) using an eluent mixture of ethyl acetate and hexane in a 7:3 ratio. After the reaction was completed, the reaction mixture was cooled to room temperature and then poured into ice water with stirring. This resulted in the formation of an off-white viscous precipitate. The obtained mixture was basified to a pH of 8.0 using an aqueous 20% w/v solution of potassium carbonate. Once the desired pH was reached, the reaction mixture was extracted with 200.0 mL of dichloromethane. The dichloromethane layer was subjected to a water wash, then dried over sodium sulfate. The final product Compound 7 was obtained by distillation, yielding 5.0 grams of 2,4-dichloroquinazoline (203)**.**

Scheme-4:

DIPEA (0.951ml, 5.3 mmol) was added to a suspension of 2,4 dichloo quinazoline (370 mg, 1.85 mmol) and 5-Phenyl-1,3,4-thiadiazol-2-amino (250mg,0.75mmol) in ethanol (10

ml). The Suspension was stirred at 25 C for 24 hrs. The resulting precipitated was filtered and washed with ethanol to afford **10a-10h** as a white solid (204).

Scheme-5:

A mixture of **10a-10h** (24.3mg, 0.081mmol), and aniline derivatives (55.4mg, 0.416mmol) in ethanol (1.5 ml) was stirred at 120˚ C in a sealed vial for 1.5 h. and the reaction mixture was cooled and purified with suitable solvent, obtained **12I-12-V** (204)**.**

5.2 Experimental Method

Step-1: Synthesis of Substituted 5-phenyl-1,3,4-thiadiazole-2-amine.

(Cyclization reaction)

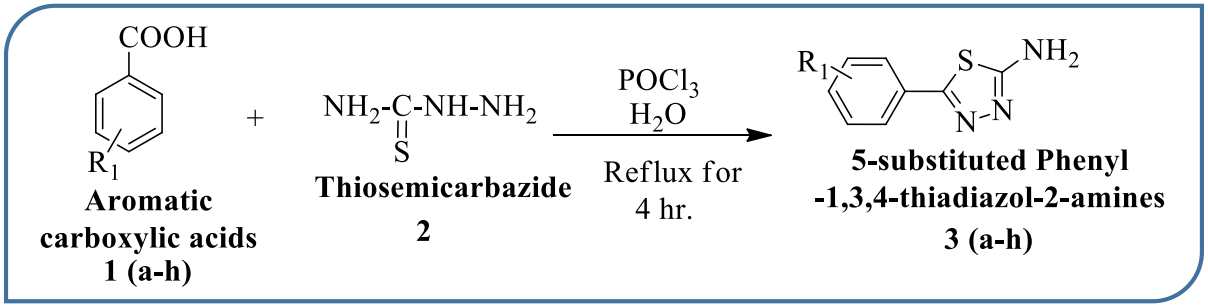

Step-2: Synthesis of Quinazoline-2, 4 (1H, 3H)-dione.

(Condensation and Cyclization reaction)

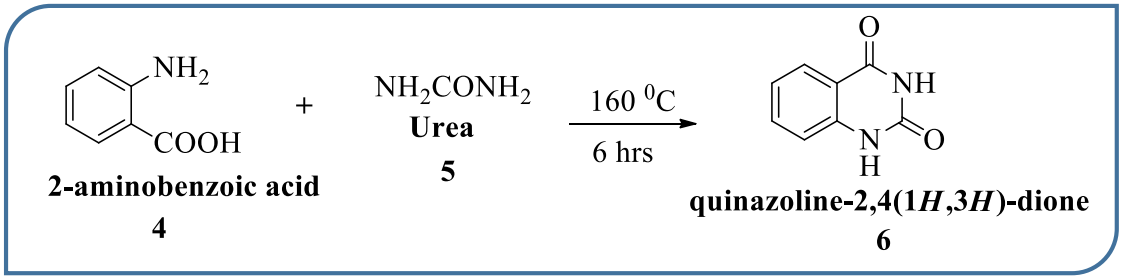

Step-3: Synthesis of 2,4-dichloroquinazoline.

(Chlorination reaction)

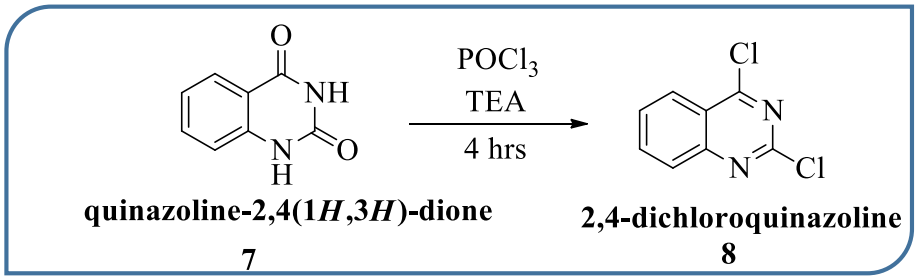

Step-4: Synthesis of N-(2-chloroquinazolin-4-yl)-5-phenyl-1,3,4-thiadiazol-2-amine.

(Substitution reaction)

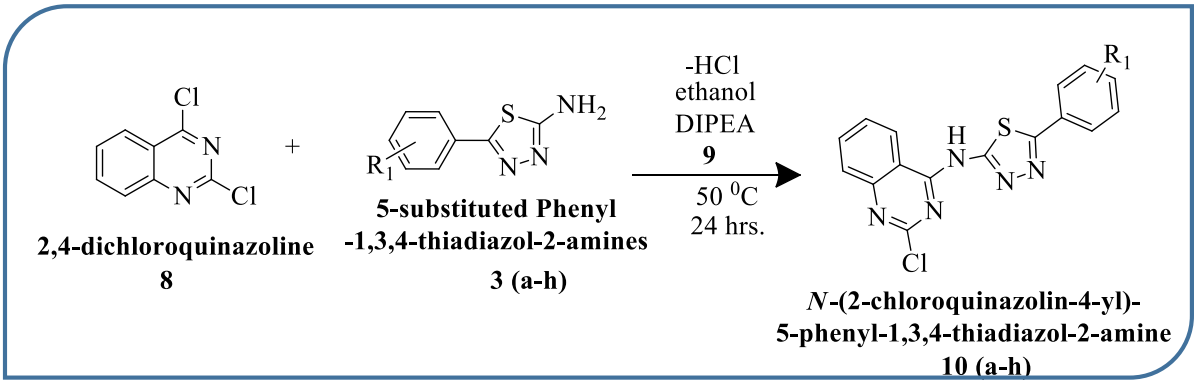

2,4-dichloroquinazoline
8

5-substituted Phenyl
-1,3,4-thiadiazol-2-amines
3 (a-h)

***N*-(2-chloroquinazolin-4-yl)-**
5-phenyl-1,3,4-thiadiazol-2-amine
10 (a-h)

Step-5: Synthesis of N2-(6-methylpyridin-2-yl)-N4-(5-(p-tolyl)-1,3,4-thiadiazol-2-yl) -4a, 8a-dihydroquinazoline-2,4-diamine

(Substitution reaction)

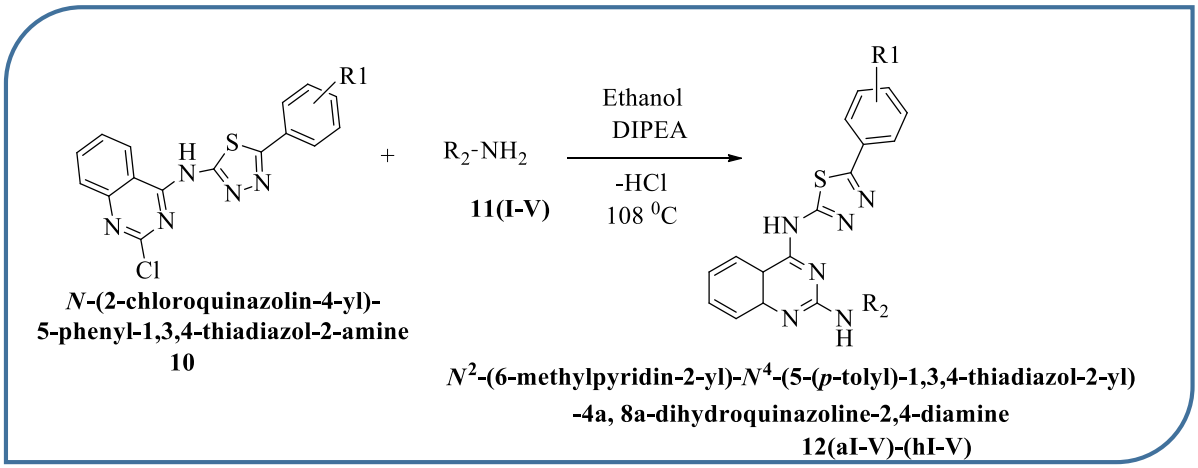

***N*-(2-chloroquinazolin-4-yl)-**
5-phenyl-1,3,4-thiadiazol-2-amine
10

***N*^{2}-(6-methylpyridin-2-yl)-*N*^{4}-(5-(*p*-tolyl)-1,3,4-thiadiazol-2-yl)**
-4a, 8a-dihydroquinazoline-2,4-diamine
12(aI-V)-(hI-V)

POSSIBLE DERIVATIVES OF SCHEME 1

COMPOUND	R	COMPOUND	R
3-a	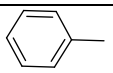	3-e	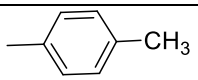
3-b	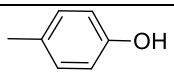	3-f	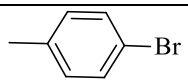
3-c	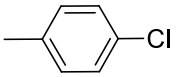	3-g	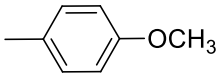
3-d	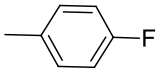	3-h	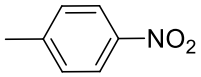

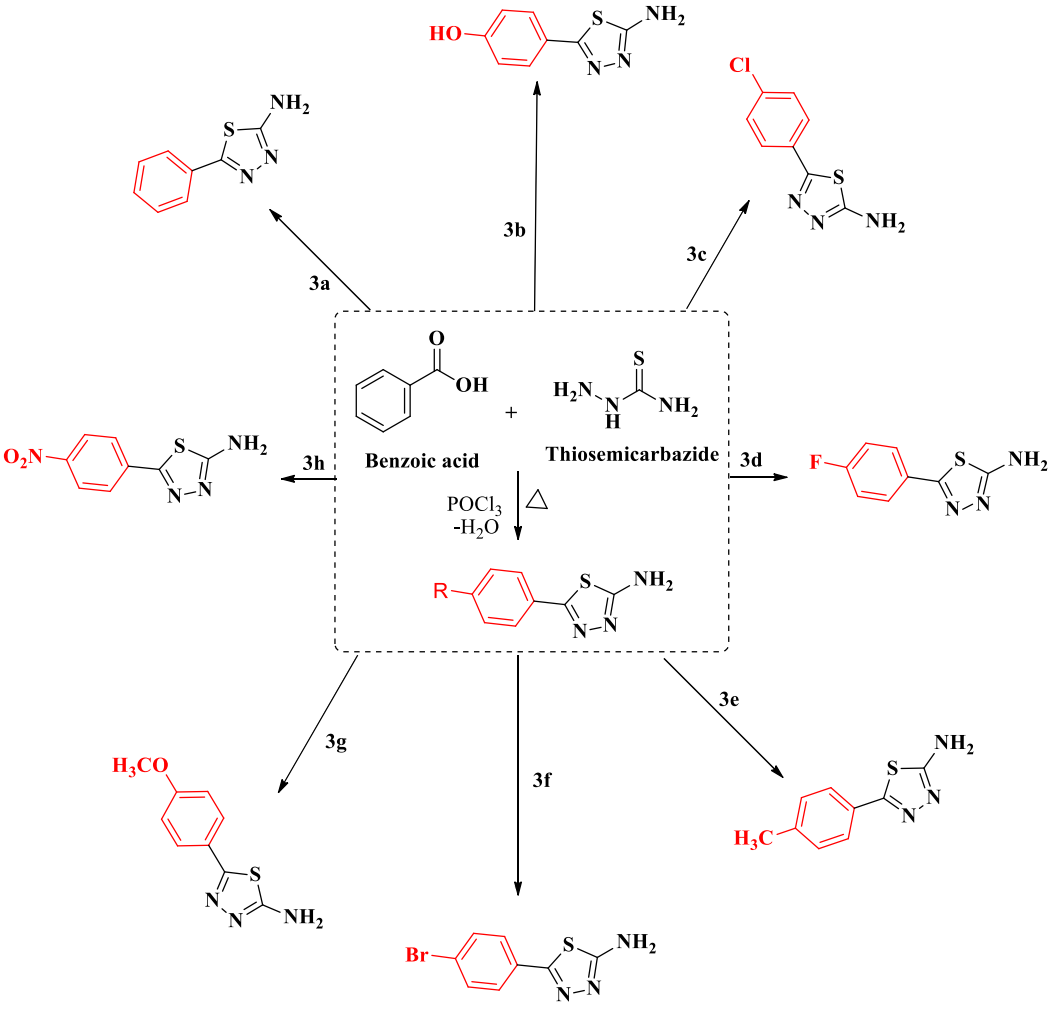

Scheme 1.

POSSIBLE DERIVATIVES OF SCHEME 4

COMPOUND	R	COMPOUND	R
6-a	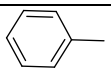	6-e	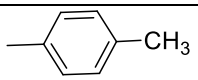
6-b	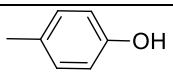	6-f	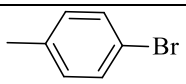
6-c	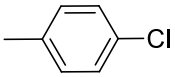	6-g	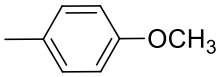
6-d	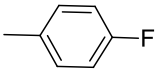	6-h	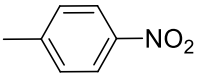

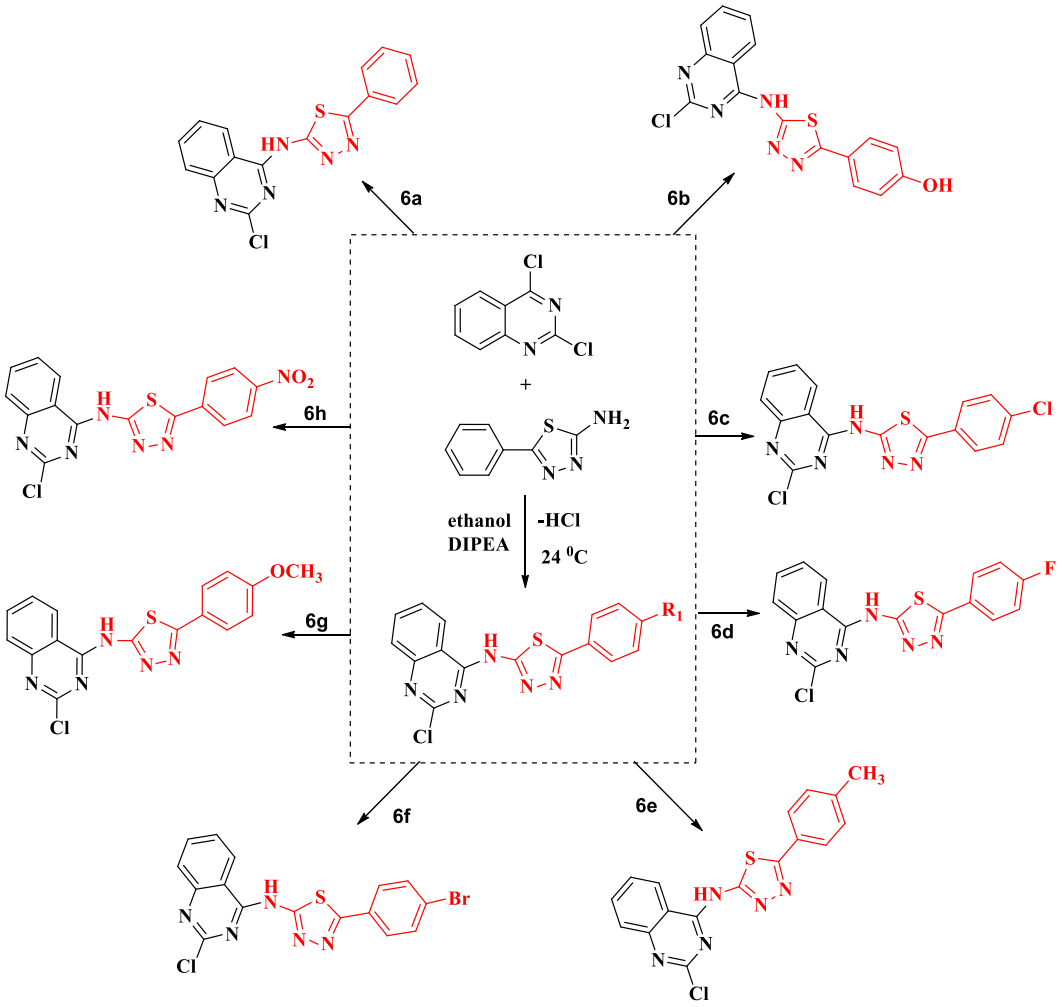

Scheme 4.

POSSIBLE DERIVATIVES OF SCHEME 5

COMPOUND	R_1		R_2	
12	a	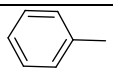	I	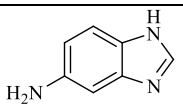
12	b	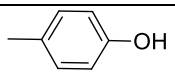	II	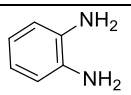
12	c	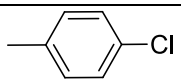	III	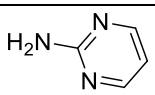
12	d	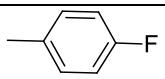	IV	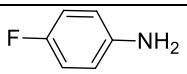
12	e		V	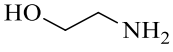
12	f	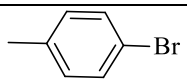	-	
12	g	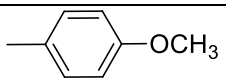		
12	h	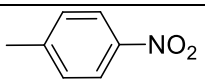		

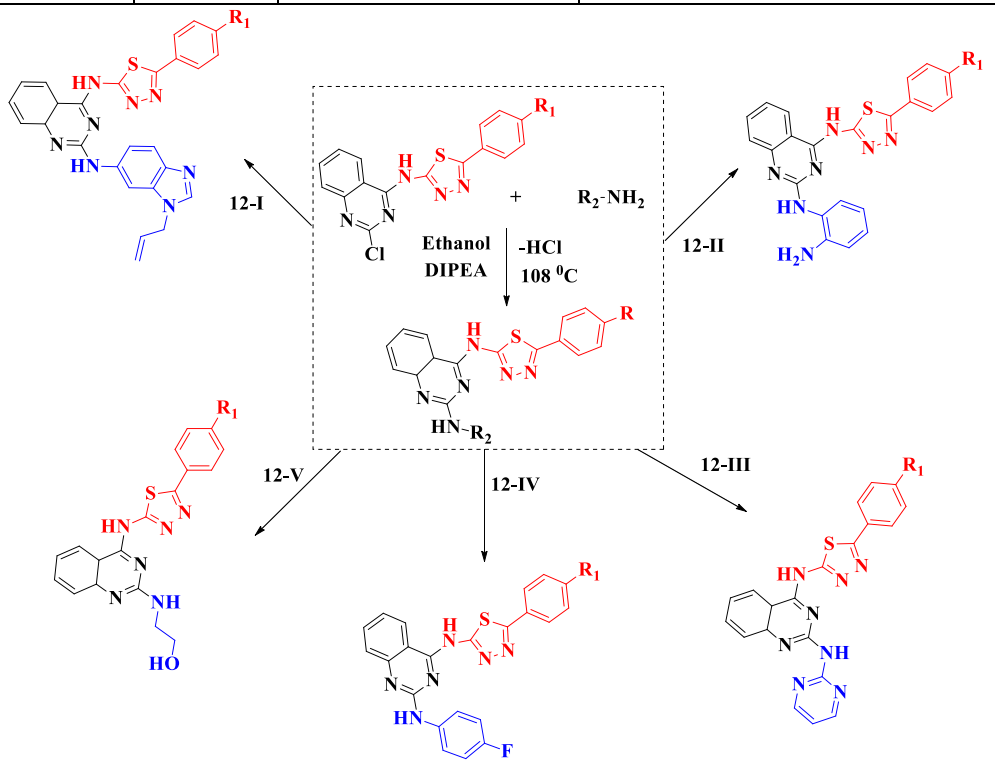

Scheme 5.

PREPARED DERIVATIVES SCHEME 6

COMPOUND	R_1	R_2
12 (a-I)	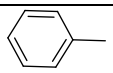	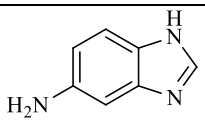
12 (a-II)	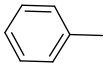	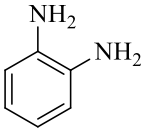
12 (a-III)	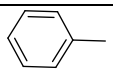	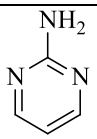
12 (a-IV)	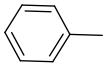	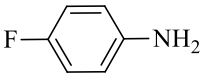
12 (a-V)	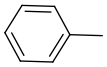	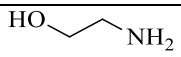
12 (b-I)	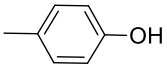	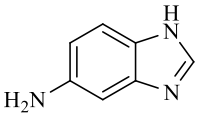
12 (b-III)	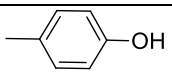	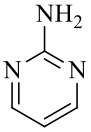
12 (b-IV)	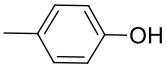	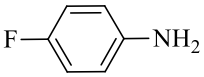
12 (c-II)	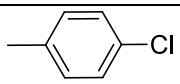	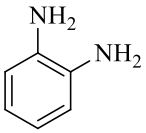
12 (c-IV)	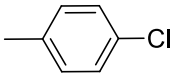	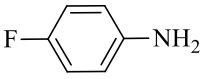
12 (d-II)	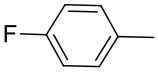	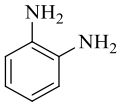
12 (d-IV)	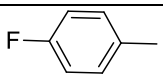	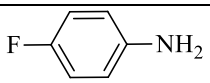
12 (e-IV)	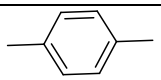	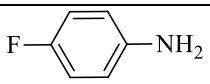

12 (e-V)	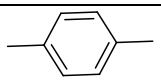	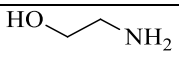
12 (f-IV)	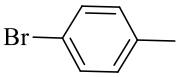	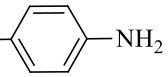
12 (f-V)	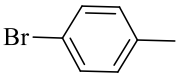	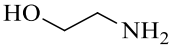

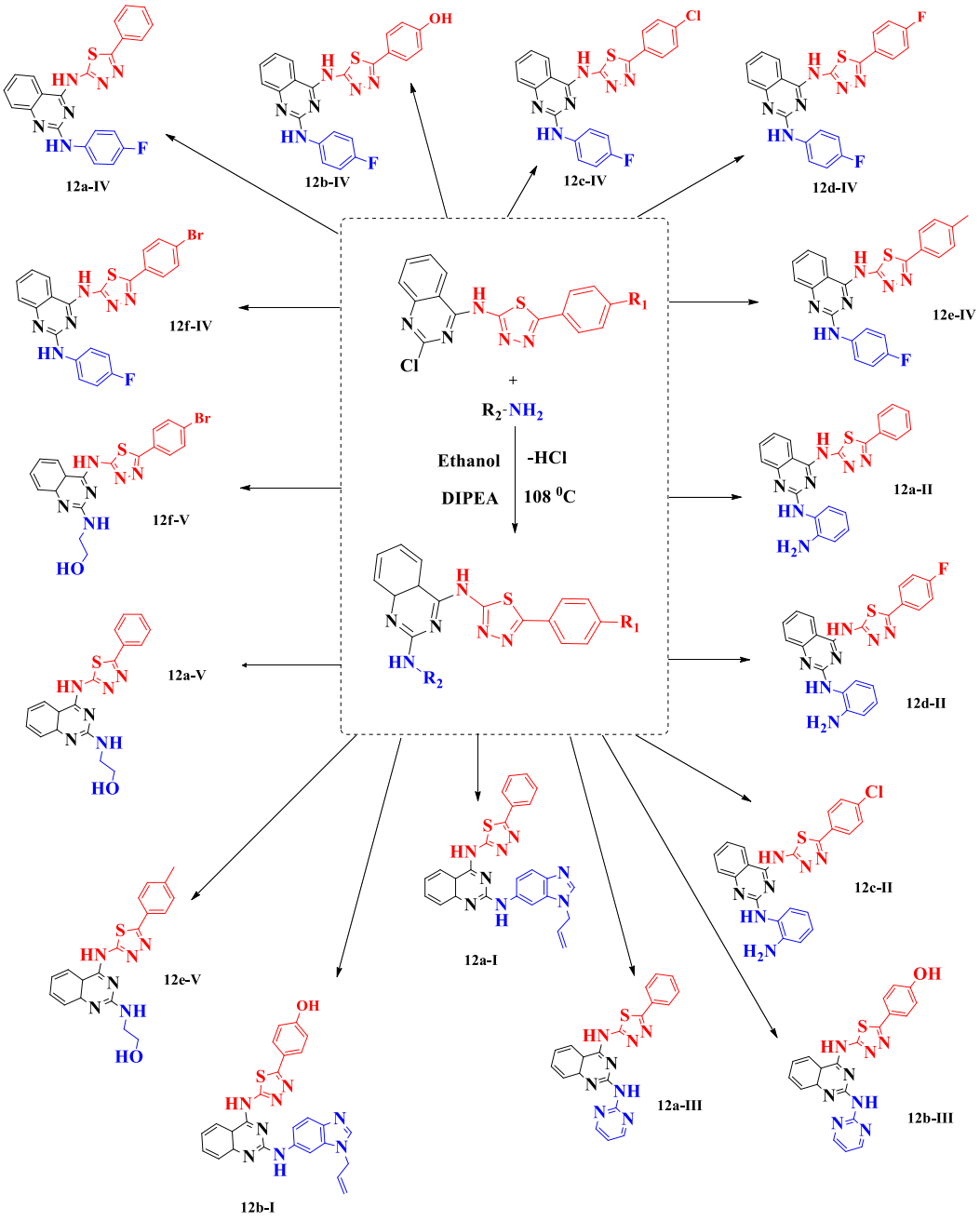

Scheme 6.

5.3 Synthetic Procedure for Individual Compound.

STEP-1

Synthetic Procedure of 2-amino-5-substituted-1,3,4-thiadiazole.

A stirring mixture was prepared, consisting of benzoic acid (0.05 mol), N-amino-thiourea (0.05 mol), and POCl3 (13 ml). This mixture was heated at 75°C for 0.5 hours. After heating, the mixture was allowed to cool to room temperature. At room temperature, 10 ml of water was added to the reaction mixture. The resulting mixture was refluxed for 4 hours. After the reflux, the mixture was allowed to cool. To adjust the pH to 8, 50% NaOH solution was added dropwise to the mixture with stirring. The formed precipitate was filtered. The isolated product was recrystallized from ethanol.

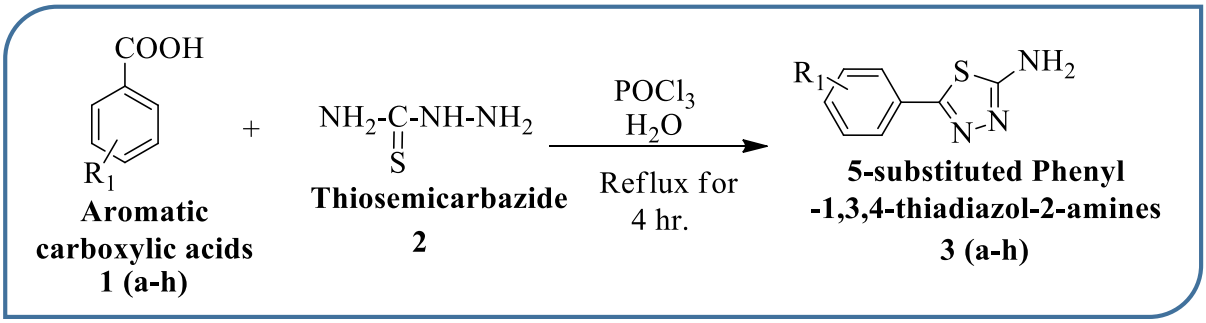

Step-2: Synthesis of Quinazoline-2, 4 (1H, 3H)-dione.

Urea (460 mmol) was heated until it melted. Then, 2-methylaminobenzoic acid (46 mmol) was added to the melted urea. The resulting mixture was stirred for 5 hours at a temperature of 150°C. After the 5-hour stirring, the mixture was cooled to below 100°C. To stop the reaction, 70 mL of water was added. The precipitate that formed was collected. To purify the compound, it was recrystallized in a mixed solution of acetone (10 mL) and water (100 mL). The final product, referred to as compound 1, was obtained as a white powder.

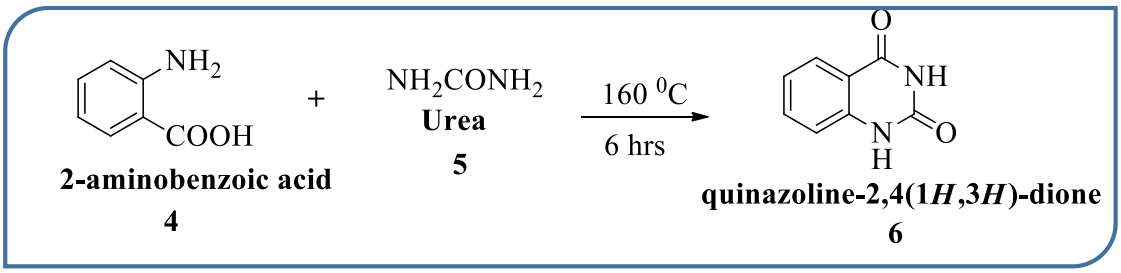

Step-3: Synthesis of 2,4-dichloroquinazoline.

A mixture was prepared by refluxing 10.0g (0.061 mole) of quinazoline-2,4(1H,3H)-dione (Benzoylene urea) in 14.2g (0.092 mole) of Phosphorous oxychloride with 7.4g (0.061 mole) of N,N-dimethylaniline at a temperature of 108°C. The progress of the reaction was monitored using TLC with an eluent consisting of ethyl acetate and hexane in a 7:3 ratio. After the reaction was completed, the reaction mixture was cooled to room temperature. The cooled mixture was poured onto ice water while stirring, resulting in the formation of an off-white viscous precipitate. The resulting mass was then made basic by adding Aqueous 20% w/v of Potassium carbonate until it reached a pH of 8.0. After achieving the desired pH, the reaction mixture was extracted with 200.0 ml of dichloromethane. The dichloromethane layer was washed with water, dried over sodium sulfate, and then distilled to obtain 5.0 g of 2,4-dichloroquinazoline **6a-6h.**

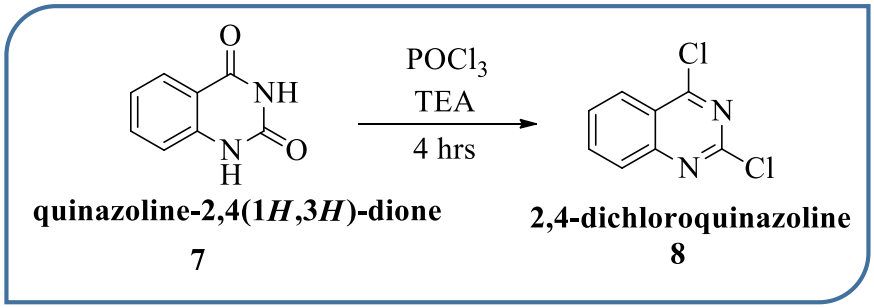

quinazoline-2,4(1*H*,3*H*)-dione
7

2,4-dichloroquinazoline
8

Step-4: Synthesis of N-(2-chloroquinazolin-4-yl)- 5-phenyl-1,3,4-thiadiazol-2-amine

DIPEA (0.951ml, 5.3 mmol) was added to a suspension of 2,4 dichloo quinazoline (370 mg, 1.85 mmol) and 5-Phenyl-1,3,4-thiadiazol-2-amino (250mg,0.75mmol) in ethanol (10 ml). The Suspension was stirred at 25 ºC for 24 hrs. The resulting precipitated was filtered and washed with ethanol to afford **10a-10h** as a white solid.

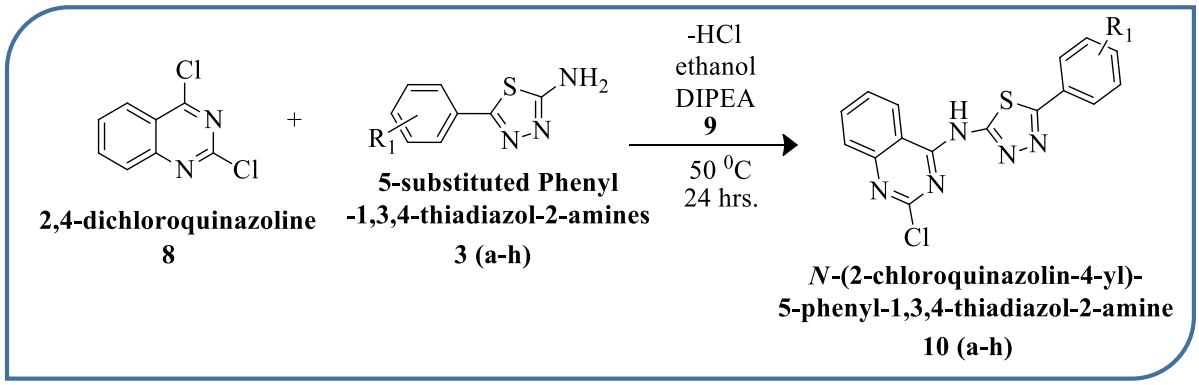

2,4-dichloroquinazoline
8

5-substituted Phenyl
-1,3,4-thiadiazol-2-amines
3 (a-h)

***N*-(2-chloroquinazolin-4-yl)-**
5-phenyl-1,3,4-thiadiazol-2-amine
10 (a-h)

Step-5: Synthesis of N2-(6-methylpyridin-2-yl)-N4-(5-(p-tolyl)-1,3,4-thiadiazol-2-yl) -4a, 8a-dihydroquinazoline-2,4-diamine.

A mixture of **6a-h** (24.3mg, 0.081mmol), and aniline derivatives **12I-12-V** (55.4mg, 0.416mmol) in ethanol (1.5 ml) was stirred at 120˚ C in a sealed vial for 1 h. and the reaction mixture was cooled and purified with suitable solvent.

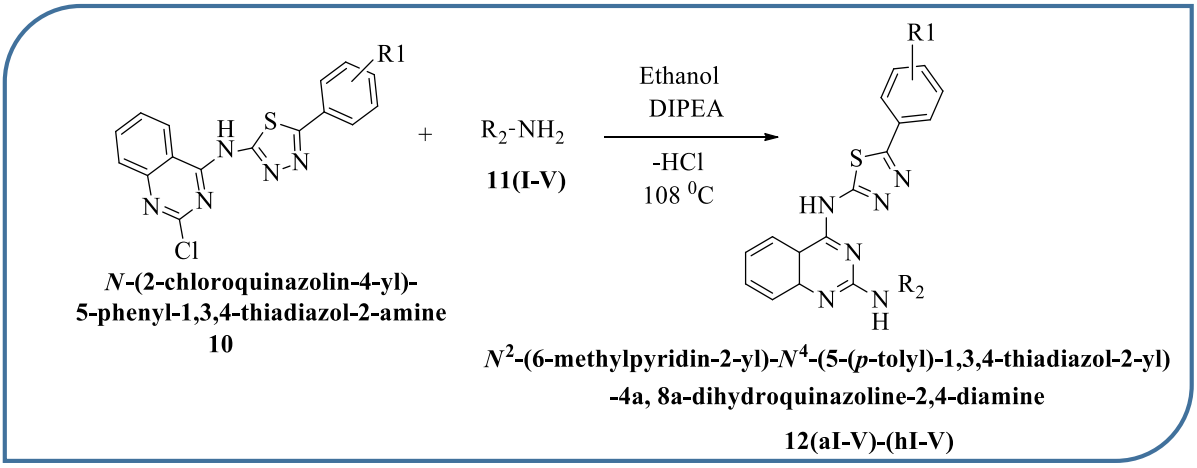

***N*-(2-chloroquinazolin-4-yl)-5-phenyl-1,3,4-thiadiazol-2-amine**
10

N^2-(6-methylpyridin-2-yl)-N^4-(5-(*p*-tolyl)-1,3,4-thiadiazol-2-yl) -4a, 8a-dihydroquinazoline-2,4-diamine
12(aI-V)-(hI-V)

5.4 BIOLOGICAL ACTIVITY

5.4.1 MTT assay

The MTT assay (3-(4,5-dimethylthiazol-2-yl)-2,5-diphenyltetrazolium bromide assay) is a colorimetric assay used to measure the viability of cells in cell culture. The assay is based on the ability of living cells to reduce the yellow MTT dye to a purple formazan product, which can be quantified by measuring the absorbance at a specific wavelength (usually 570 nm). The amount of formazan produced is directly proportional to the number of viable cells in the culture. The assay is commonly used to measure the cytotoxicity of drugs or the effects of other treatments on cell proliferation and survival (205–209).

Principle of MTT assay

The principle of the MTT assay is based on the ability of living cells to reduce the yellow 3-(4,5-dimethythiazol-2-yl)-2,5-diphenyl tetrazolium bromide (MTT) dye to a purple formazan product, which can be quantified by measuring the absorbance at a specific wavelength. The amount of formazan produced is directly proportional to the number of viable cells in the culture.

The MTT dye is a tetrazolium salt that is not toxic to cells. When it enters live cells, it is reduced by the mitochondrial enzymes in the cells to formazan crystals, which are insoluble and remain inside the cells. Dead cells do not have functional mitochondria and cannot reduce the MTT dye to formazan. Therefore, the amount of formazan produced by the cells is proportional to the number of viable cells.

After the cells are treated with the test compound or treatment of interest, the medium is removed and replaced with MTT solution. The cells are then incubated with the MTT solution for a period of time, typically 2-4 hours, to allow the cells to reduce the MTT dye to formazan. Then the medium is removed and replaced with DMSO to dissolve the formazan crystals. The absorbance of the formazan solution is measured at a specific wavelength, usually 570 nm, using a microplate reader. The absorbance values are used to calculate the percentage of viable cells, which is then used to determine the cytotoxicity of the compounds or the effects of the treatments on cell proliferation and survival.

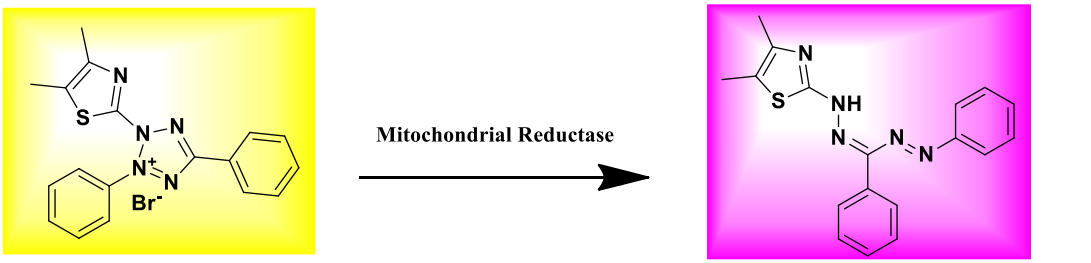

3-(4,5-dimethylthiazol-2-yl)-2,5-diphenyltetrazolium bromide (MTT)

(E/Z)-5-(4,5-dimethylthiazol-2-yl)-1,3,-diphenylformazan (Formazan)

Culture Media:

A cell line A549 procured from the NSCLC was maintained in DMEM medium supplemented with 10% FBS, Penicillin 100 IU/ml, and streptomycin 100 µg/ml. The cell was maintained at 37°C in a humidified atmosphere 95% containing 100 5% CO_2. The cell was dissociated with TPVG solution (0.2% trypsin, 0.02% EDTA, 0.05% glucose in PBS). The viability of the cell was checked and centrifuged. Further 50,000 cells/well seeded in a 96-well plate and incubated for 24 hrs. at 37°C, 5% Co2 incubator.

5.4.3. Procedure:

1. The **A549** cell line was seeded at a density of 104 cells per well in 96-well plates and allowed to adhere for **24 hours** at **37°C** with **5% CO_2**.
2. After a set period, typically 24-72 hours, remove the medium from the wells and add a solution of MTT (usually at a final concentration of 0.5 mg/ml) to each well. Incubate for 2-4 hours at 37°C to allow the cells to reduce the MTT dye to formazan.
3. Remove the MTT solution and add DMSO (dimethyl sulfoxide) to each well to dissolve the formazan crystals. Mix the solution well by shaking the plate.
4. Measure the absorbance of the formazan solution at 570 nm using a microplate reader.
5. Calculate the percentage of viable cells by comparing the absorbance of the test wells to that of the control wells, which should contain only untreated cells. Alternatively, you can use a cell viability reagent that is compatible with the cell line you are using. (210)

6. Result and Discussion

6. RESULT AND DISCUSSION

6.1 Characterization of Compounds.

Physicochemical and Spectral characterization of Compound.

- **Compound 3a**

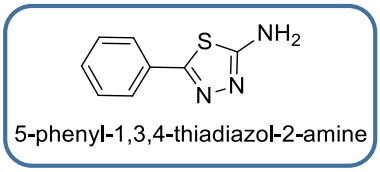

Table 13. Physicochemical data of Compound

Sr No	Observed Parameter	Result
1.	Molecular Formula	$C_8H_7N_3S$
2.	Molecular Weight	177.20
3.	% Yield	85
4.	Melting Point °C	216-219 °C
5.	R_f value Chloroform:Methanol (9:1)	0.6

Table 14. FT-IR spectral data of Compound

Sr No	Standard Frequency (cm^{-1})	Observed Frequency (cm^{-1})	Functional group
1	3500 – 3300 (m)	3281	1° N-H
2	3100 – 3000 (m to w)	3088	C-H
3	1690-1550 (m)	1518	C=N
4	700-600 (m)	690	C-S-C

- **Compound 3b**

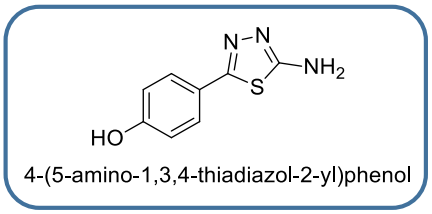

4-(5-amino-1,3,4-thiadiazol-2-yl)phenol

Table 15. Physicochemical data of Compound

Sr No	Observed Parameter	Result
1.	Molecular Formula	$C_8H_7N_3OS$
2.	Molecular Weight	193.23
3.	% Yield	81
4.	Melting Point °C	218-225 °C
5.	R_f value Chloroform:Methanol (9:1)	0.8

Table 16. FT-IR spectral data of Compound

Sr No	Standard Frequency (cm^{-1})	Observed Frequency (cm^{-1})	Functional group
1	3650-3550 (broad, s)	3398	OH
2	3400-3250 (m)	3245	1° N-H
3	3100 – 3000 (m to w)	3011	C-H
4	1690-1550 (m)	1503	C=N
5	700-600 (m)	663	C-S-C

- **Compound 3c**

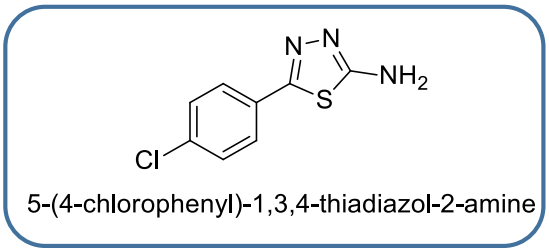

5-(4-chlorophenyl)-1,3,4-thiadiazol-2-amine

Table 17. Physicochemical data of Compound

Sr No	Observed Parameter	Result
1.	Molecular Formula	C_8H6ClN_3S
2.	Molecular Weight	211.05
3.	% Yield	78
4.	Melting Point °C	216-220 °C
5.	R_f value Chloroform:Methanol (9:1)	0.6

Table 18. FT-IR spectral data of Compound

Sr No	Standard Frequency (cm^{-1})	Observed Frequency (cm^{-1})	Functional group
1	3400-3250 (m)	3037	1° N-H
2	3100 – 3000 (m to w)	2806	C-H
3	1690-1550 (m)	1699	C=N
4	850-515 (m)	765	C-Cl
5	700-600 (m)	700	C-S-C

- **Compound 3d**

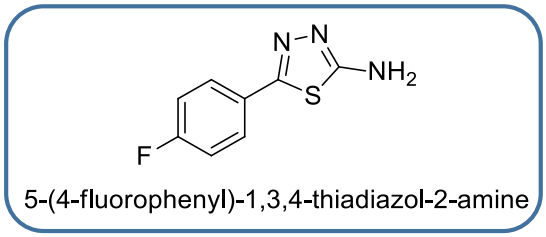

5-(4-fluorophenyl)-1,3,4-thiadiazol-2-amine

Table 19. Physicochemical data of Compound

Sr No	Observed Parameter	Result
1.	Molecular Formula	$C_8H_7FN_3S$
2.	Molecular Weight	195.03
3.	% Yield	85
4.	Melting Point °C	216-221 °C
5.	R_f value Chloroform:Methanol (9:1)	0.7

Table 20. FT-IR spectral data of Compound

Sr No	Standard Frequency (cm^{-1})	Observed Frequency (cm^{-1})	Functional group
1	3400-3250 (m)	3017	1° N-H
2	3100 – 3000 (m to w)	2956	C-H
3	1690-1550 (m)	1669	C=N
4	1000 – 1400	1163	C-F-C
5	700-600 (m)	647	C-S-C

- **Compound 3e**

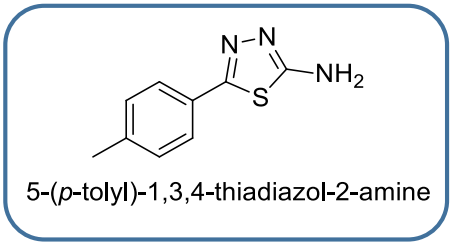

5-(*p*-tolyl)-1,3,4-thiadiazol-2-amine

Table 21. Physicochemical data of Compound

Sr No	Observed Parameter	Result
1.	Molecular Formula	$C_9H_9N_3S$
2.	Molecular Weight	191.05
3.	% Yield	65
4.	Melting Point °C	216-220 °C
5.	R_f value Chloroform:Methanol (9:1)	0.7

Table 22. FT-IR spectral data of Compound

Sr No	Standard Frequency (cm^{-1})	Observed Frequency (cm^{-1})	Functional group
1	3400-3250 (m)	3309	1° N-H
2	3100 – 3000 (m to w)	3122	C-H
3	1690-1550 (m)	1515	C=N
4	1470-1430 (m)	1463	CH_3
5	700-600 (m)	654	C-S-C

- **Compound 3f**

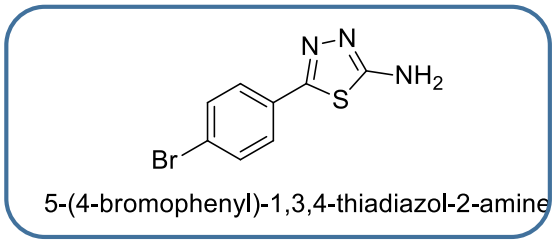

5-(4-bromophenyl)-1,3,4-thiadiazol-2-amine

Table 23. Physicochemical data of Compound

Sr No	Observed Parameter	Result
1.	Molecular Formula	$C_8H_7BrN_3S$
2.	Molecular Weight	254.95
3.	% Yield	80
4.	Melting Point °C	216-220 °C
5.	R_f value Chloroform:Methanol (9:1)	0.8

Table 24. FT-IR spectral data of Compound

Sr No	Standard Frequency (cm^{-1})	Observed Frequency (cm^{-1})	Functional group
1	3400-3250 (m)	3274	1° N-H
2	3100 – 3000 (m to w)	3087	C-H
3	1690-1550 (m)	1515	C=N
4	850-515 (s)	759	C-Br
5	700-600 (m)	690	C-S-C

- **Compound 4**

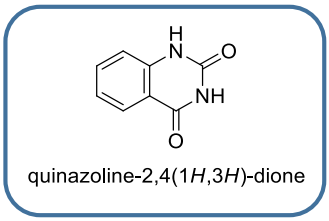

Table 25. Physicochemical data of Compound

Sr No	Observed Parameter	Result
1.	Molecular Formula	$C_8H_6N_2O_2$
2.	Molecular Weight	162.04
3.	% Yield	70
4.	Melting Point °C	277-282 °C
5.	R_f value Chloroform:Methanol (9:1)	0.8

Table 26. FT-IR spectral data of Compound

Sr No	Standard Frequency (cm^{-1})	Observed Frequency (cm^{-1})	Functional group
1	3500-3300 (s)	3508	2° N-H (Amide)
2	3100 – 3000 (m to w)	3113	C-H
3	1690 - 1630 (s)	1676,1612	C=O

- **Compound 5**

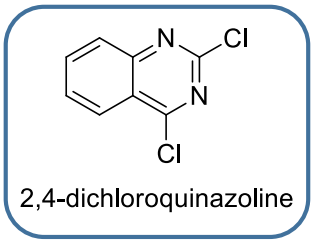

Table 27. Physicochemical data of Compound

Sr No	Observed Parameter	Result
1.	Molecular Formula	$C_8H_4Cl_2N_2$
2.	Molecular Weight	199.98
3.	% Yield	81
4.	Melting Point °C	118-120 °C
5.	R_f value Chloroform:Methanol (9:1)	0.6

Table 28. FT-IR spectral data of Compound

Sr No	Standard Frequency (cm^{-1})	Observed Frequency (cm^{-1})	Functional group
1	3100 – 3000 (m to w)	3142	C-H
2	1690-1550 (m)	1558,1512	C=N
3	850-515 (s)	831,752	C-Cl

- **Compound 6a**

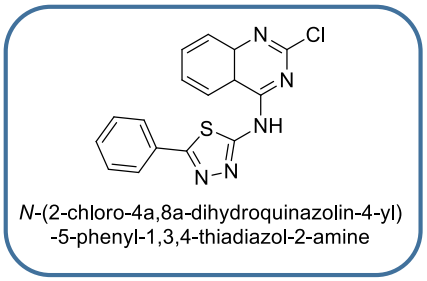

N-(2-chloro-4a,8a-dihydroquinazolin-4-yl)
-5-phenyl-1,3,4-thiadiazol-2-amine

Table 29. Physicochemical data of Compound

Sr No	Observed Parameter	Result
1.	Molecular Formula	$C_{16}H_{12}ClN_5S$
2.	Molecular Weight	341.82
3.	% Yield	75
4.	Melting Point °C	210-215 °C
5.	R_f value Chloroform:Methanol (9:1)	0.7

Table 30. FT-IR spectral data of Compound

Sr No	Standard Frequency (cm^{-1})	Observed Frequency (cm^{-1})	Functional group
1	3300-3000 (s)	3378	2° N-H
2	3100 – 3000 (m to w)	2955	C-H
3	1690-1550 (m)	1518	C=N
4	850-515 (s)	845	C-Cl
5	700-600 (m)	632	C-S-C

Table 31. Mass spectral data of Compound

Compound code	Molecular Weight of Compound	Observed Molecular Weight
6a	341.82	341(M+) 343 (M+2)

- **Compound 6b**

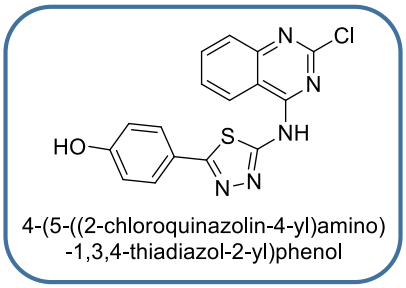

4-(5-((2-chloroquinazolin-4-yl)amino)
-1,3,4-thiadiazol-2-yl)phenol

Table 32. Physicochemical data of Compound

Sr No	Observed Parameter	Result
1.	Molecular Formula	$C_{16}H_{10}ClN_5OS$
2.	Molecular Weight	355.80
3.	% Yield	65
4.	Melting Point °C	213-216 °C
5.	R_f value Chloroform:Methanol (9:1)	0.6

Table 33. FT-IR spectral data of Compound

Sr No	Standard Frequency (cm^{-1})	Observed Frequency (cm^{-1})	Functional group
1	3650-3550 (broad, s)	3649	OH
2	3300-3000 (s)	3280	2° N-H
3	3100 – 3000 (m to w)	3091	C-H
4	1690-1550 (m)	1518	C=N
5	850-515 (s)	760	C-Cl
6	700-600 (m)	690	C-S-C

Table 34. Mass spectral data of Compound

Compound code	Molecular Weight of Compound	Observed Molecular Weight
6b	355.80	355 (M+) 357 (M+2)

- **Compound 6c**

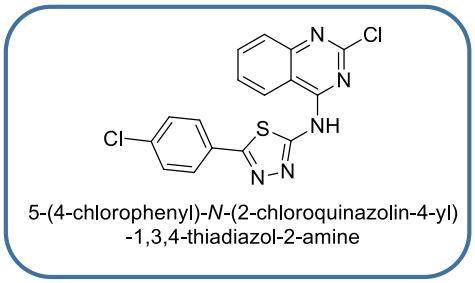

5-(4-chlorophenyl)-*N*-(2-chloroquinazolin-4-yl)
-1,3,4-thiadiazol-2-amine

Table 35. Physicochemical data of Compound

Sr No	Observed Parameter	Result
1.	Molecular Formula	$C_{17}H_9ClN_5S$
2.	Molecular Weight	374.25
3.	% Yield	85
4.	Melting Point °C	216-219 °C
5.	R_f value Chloroform:Methanol (9:1)	0.6

Table 36. FT-IR spectral data of Compound

Sr No	Standard Frequency (cm^{-1})	Observed Frequency (cm^{-1})	Functional group
1	3300-3000 (s)	3387	2° N-H
2	3100 – 3000 (m to w)	2924	C-H
3	1690-1550 (m)	1504	C=N
4	850-515 (s)	833	C-Cl
5	700-600 (m)	630	C-S-C

Table 37. Mass spectral data of Compound

Compound code	Molecular Weight of Compound	Observed Molecular Weight
6c	374.25	374 (M+) 376 (M+2)

- **Compound 6d**

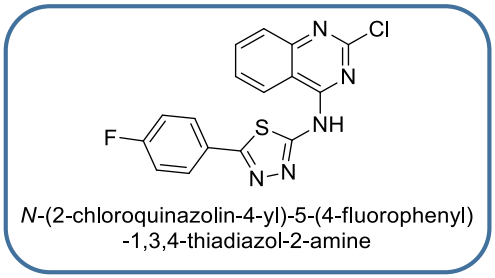

N-(2-chloroquinazolin-4-yl)-5-(4-fluorophenyl) -1,3,4-thiadiazol-2-amine

Table 38. Physicochemical data of Compound

Sr No	Observed Parameter	Result
1.	Molecular Formula	$C_{16}H_9ClFN_5S$
2.	Molecular Weight	357.79
3.	% Yield	60
4.	Melting Point °C	216-220 °C
5.	R_f value Chloroform:Methanol (9:1)	0.6

Table 39. FT-IR spectral data of Compound

Sr No	Standard Frequency (cm^{-1})	Observed Frequency (cm^{-1})	Functional group
1	3300-3000 (s)	3029	2° N-H
2	3100 – 3000 (m to w)	2937	C-H
3	1690-1550 (m)	1556	C=N
4	850-515 (s)	841	C-Cl
5	700-600 (m)	622	C-S-C

Table 40. Mass spectral data of Compound

Compound code	Molecular Weight of Compound	Observed Molecular Weight
6d	357.79	357 (M+) 359 (M+2)

- **Compound 6e**

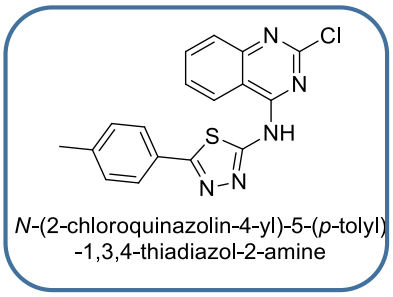

N-(2-chloroquinazolin-4-yl)-5-(*p*-tolyl) -1,3,4-thiadiazol-2-amine

Table 41. Physicochemical data of Compound

Sr No	Observed Parameter	Result
1.	Molecular Formula	$C_{17}H_{12}ClN_5S$
2.	Molecular Weight	352.83
3.	% Yield	62
4.	Melting Point °C	218-222 °C
5.	R_f value Chloroform:Methanol (9:1)	0.6

Table 42. FT-IR spectral data of Compound

Sr No	Standard Frequency (cm^{-1})	Observed Frequency (cm^{-1})	Functional group
1	3400-3250 (m)	3281	2° N-H
2	3100 – 3000 (m to w)	3066	C-H
3	1690-1550 (m)	1636	C=N
4	850-515 (s)	790	C-Cl
5	700-600 (m)	675	C-S-C

Table 43. Mass spectral data of Compound

Compound code	Molecular Weight of Compound	Observed Molecular Weight
6e	352.83	352 (M+) 354 (M+2)

- **Compound 6f**

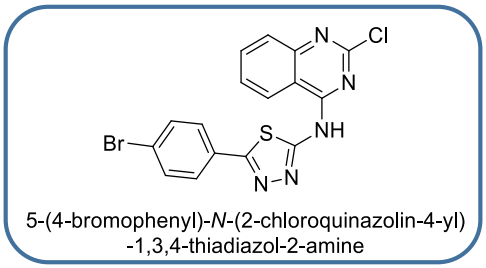

5-(4-bromophenyl)-*N*-(2-chloroquinazolin-4-yl)
-1,3,4-thiadiazol-2-amine

Table 44. Physicochemical data of Compound

Sr No	Observed Parameter	Result
1.	Molecular Formula	$C_{16}H_9ClBrN_5S$
2.	Molecular Weight	416.95
3.	% Yield	68
4.	Melting Point °C	218-223 °C
5.	R_f value Chloroform:Methanol (9:1)	0.6

Table 45. FT-IR spectral data of Compound

Sr. No.	Standard Frequency (cm^{-1})	Observed Frequency (cm^{-1})	Functional group
1	3300-3000 (s)	3319	2° N-H
2	3100 – 3000 (m to w)	3072	C-H
3	1690-1550 (m)	1691	C=N
4	850-515 (s)	769	C-Cl
5	700-600 (m)	649	C-S-C

Table 46. Mass spectral data of Compound

Compound code	Molecular Weight of Compound	Observed Molecular Weight
6f	416.95	416 (M+)

Compound (12a-I)

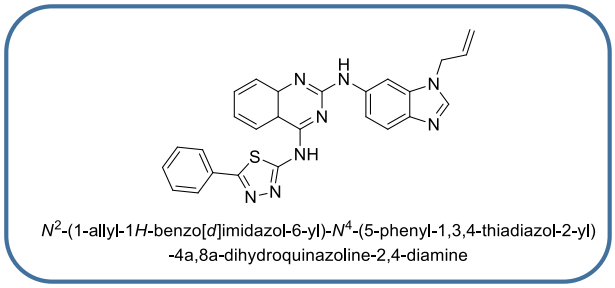

Table 47. Physicochemical data of Compound

Sr No	Observed Parameter	Result
1.	Molecular Formula	$C_{26}H_{22}N_8S$
2.	Molecular Weight	478.57
3.	% Yield	62
4.	Melting Point °C	245-250 °C
5.	R_f value Ethyl acetate: n-Hexane (7:3)	0.6

Table 48. FT-IR spectral data of Compound

Sr No	Standard Frequency (cm^{-1})	Observed Frequency (cm^{-1})	Functional group
1	3300-3000 (s)	3358	2° N-H
2	3100 – 3000 (m to w)	3061	C-H
3	1690-1550 (m)	1612	C=N
4	1440-1350 (m)	1157	CH_2
5	700-600 (m)	675	C-S-C

Table 49. 1H NMR and Mass spectral data of Compound

Compound code	1H NMR (400 MHz, DMSO;δ ppm)	Mass (m/z%)
12a-I	9.7(s, H, NH) 7.08-7.75(m, 4H, Ph-C_2-C_3-C_5-C_6) 6.91(s, 2H, NH_2) 4.11-4.16(m, 4H, CH_2-CH_2)	478 (M+)

Compound (12a-II)

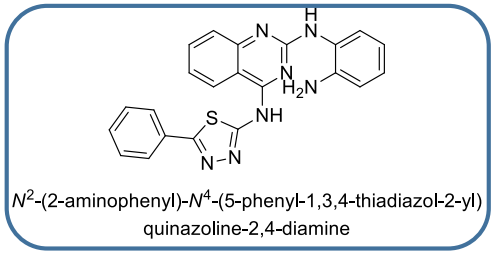

N^2-(2-aminophenyl)-N^4-(5-phenyl-1,3,4-thiadiazol-2-yl) quinazoline-2,4-diamine

Table 50. Physicochemical data of Compound

Sr No	Observed Parameter	Result
1.	Molecular Formula	$C_{22}H_{17}N_7S$
2.	Molecular Weight	411.48
3.	% Yield	62
4.	Melting Point °C	246-251 °C
5.	R_f value Ethyl acetate: n-Hexane (7:3)	0.7

Table 51. FT-IR spectral data of Compound

Sr No	Standard Frequency (cm^{-1})	Observed Frequency (cm^{-1})	Functional group
1	3300-3000 (s)	3290	2° N-H
2	3400-3250 (m)	3032	1° N-H
3	3100 – 3000 (m to w)	2879	C-H
4	1690-1550 (m)	1695	C=N
5	700-600 (m)	694	C-S-C

Table 52. 1H NMR and Mass spectral data of Compound

Compound code	1H NMR (400 MHz, DMSO;δ ppm)	Mass (m/z%)
12a-II	5.11-6.53 (m, 4H, Quinazoline Ar-H), 6.90 (d, 2H, NH_2), 7.30-7.98 (m, 2H, Orthophenylene diamine, Ar-H), 8.00-8.02 (m, 4H, Thiadiazole Ar-H), 11.76 (s, 1H, NH), 11.78 (s, 1H, NH)	413 (M+2)

Compound (12a-III)

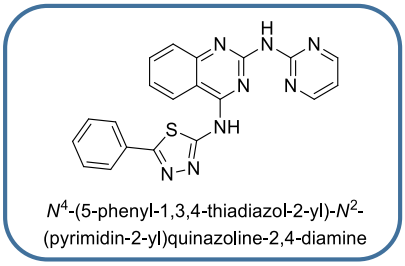

Table 53. Physicochemical data of Compound

Sr No	Observed Parameter	Result
1.	Molecular Formula	$C_{20}H_{14}N_8S$
2.	Molecular Weight	398.44
3.	% Yield	60
4.	Melting Point °C	247-250 °C
5.	R_f value Ethyl acetate: n-Hexane (7:3)	0.8

Table 54. FT-IR spectral data of Compound

Sr No	Standard Frequency (cm^{-1})	Observed Frequency (cm^{-1})	Functional group
1	3300-3000 (s)	3277	2° N-H
2	3100 – 3000 (m to w)	3057	C-H
3	1690-1550 (m)	1546	C=N
4	700-600 (m)	684	C-S-C

Table 55. 1H NMR and Mass spectral data of Compound

Compound code	1H NMR (400 MHz, DMSO;δ ppm)	Mass (m/z%)
12a-III	4.49-5.26 (m, 4H, Quinazoline Ar-H), 6.90-7.98 (m, 4H, Pyrimidine Ar-H), 8.01-8.02 (m, 4H, Thiadiazole Ar-H), 10.93 (s, 1H, NH), 11.06 (s, 1H, NH)	400 (M+2)

- **Compound 12a-IV**

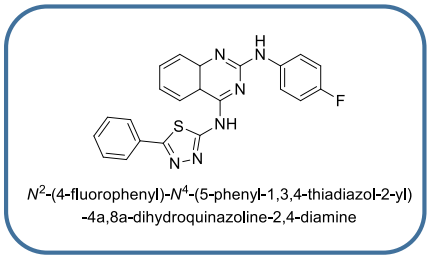

N^2-(4-fluorophenyl)-N^4-(5-phenyl-1,3,4-thiadiazol-2-yl)-4a,8a-dihydroquinazoline-2,4-diamine

Table 56. Physicochemical data of Compound

Sr No	Observed Parameter	Result
1.	Molecular Formula	$C_{22}H_{17}FN_6S$
2.	Molecular Weight	416.12
3.	% Yield	65
4.	Melting Point °C	248-255 °C
5.	R_f value Ethyl acetate: n-Hexane (7:3)	0.6

Table 57. FT-IR spectral data of Compound

Sr No	Standard Frequency (cm^{-1})	Observed Frequency (cm^{-1})	Functional group
1	3300-3000 (s)	3487	2° N-H
2	3100 – 3000 (m to w)	3182	C-H
3	1690-1550 (m)	1583	C=N
4	1000 – 1400	763	C-F
5	700-600 (m)	688	C-S-C

Table 58. 1H NMR and Mass spectral data of Compound

Compound code	1H NMR (400 MHz, DMSO;δ ppm)	Mass (m/z%)
12a-IV	6.90-6.99 (m, 4H, Quinazoline Ar-H), 7.04-7.83 (m, 4H, 4-Floroaniline Ar-H), 8.14-8.16 (m, 4H, Thiadiazole Ar-H), 11.05 (s, 1H, NH), 12.23 (s, 1H, NH)	418 (M+2)

Compound (12a-V)

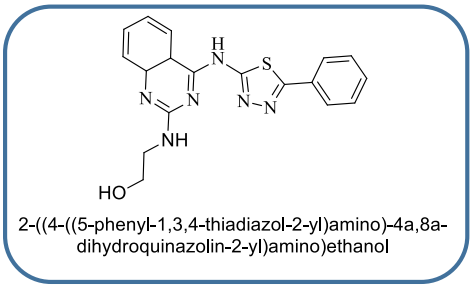

2-((4-((5-phenyl-1,3,4-thiadiazol-2-yl)amino)-4a,8a-dihydroquinazolin-2-yl)amino)ethanol

Table 59. Physicochemical data of Compound

Sr No	Observed Parameter	Result
1.	Molecular Formula	$C_{18}H_{18}N_6OS$
2.	Molecular Weight	366.44
3.	% Yield	64
4.	Melting Point °C	248-256 °C
5.	R_f value Ethyl acetate: n-Hexane (7:3)	0.8

Table 60. FT-IR spectral data of Compound

Sr No	Standard Frequency (cm^{-1})	Observed Frequency (cm^{-1})	Functional group
1	3650-3550 (broad, s)	3252	OH
2	3300-3000 (s)	3123	2° N-H
3	3100 – 3000 (m to w)	3095	C-H
4	1690-1550 (m)	1512	C=N
5	1440-1350 (m)	1322,1401	CH_2-CH_2
6	700-600 (m)	653	C-S-C

Table 61. 1H NMR and Mass spectral data of Compound

Compound code	1H NMR (400 MHz, DMSO;δ ppm)	Mass (m/z%)
12a-V	3.60-4.05 (t, 4H, CH_2- CH_2), 7.40-7.48 (m, 4H, Quinazoline Ar-H),	366 (M+)

	7.98-8.11 (m, 4H, Thiadiazole Ar-H), 11.05 (s, 1H, NH), 11.40 (s, 1H, NH), 12.73 (s, 1H, OH)	

Compound (12b-I)

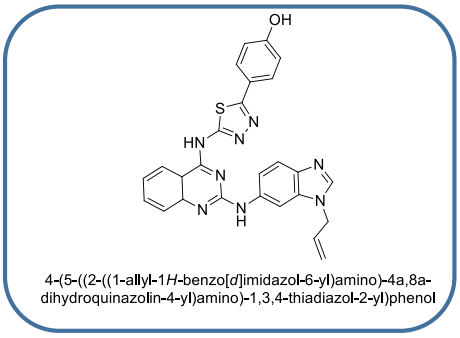

Table 62. Physicochemical data of Compound

Sr No	Observed Parameter	Result
1.	Molecular Formula	$C_{26}H_{22}N_8OS$
2.	Molecular Weight	494.57
3.	% Yield	68
4.	Melting Point °C	250-255 °C
5.	R_f value Ethyl acetate: n-Hexane (7:3)	0.6

Table 63. FT-IR spectral data of Compound

Sr No	Standard Frequency (cm^{-1})	Observed Frequency (cm^{-1})	Functional group
1	3650-3550 (broad, s)	3412	OH
2	3300-3000 (s)	3290	2° N-H
3	3100 – 3000 (m to w)	3163	C-H
4	1690-1550 (m)	1510	C=N
5	850-515(m)	850	C-F
6	700-600 (m)	692	C-S-C

Table 64. 1H NMR and Mass spectral data of Compound

Compound code	1H NMR (400 MHz, DMSO;δ ppm)	Mass (m/z%)
12b-I	3.43-3.93 (3, 3H, CH=CH, H), 4.10-4.92 (m, 2H, methyl), 5.11-5.24 (m, 4H, Quinazoline Ar-H), 5.99-7.61(m, 3H, Benzimidazole Ar-H), 7.62-7.89 (m, 4H, Thiadiazole Ar-H), 11.11 (s, 1H, NH), 11.25 (s, 1H, NH), 12.50 (s, 1H, OH)	430 (M+)

Compound (12b-III)

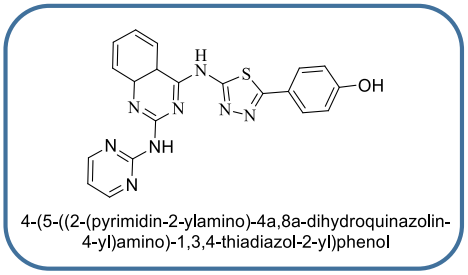

4-(5-((2-(pyrimidin-2-ylamino)-4a,8a-dihydroquinazolin-4-yl)amino)-1,3,4-thiadiazol-2-yl)phenol

Table 65. Physicochemical data of Compound

Sr No	Observed Parameter	Result
1.	Molecular Formula	$C_{20}H_{16}N_8OS$
2.	Molecular Weight	416.46
3.	% Yield	60
4.	Melting Point °C	251-255 °C
5.	R_f value Ethyl acetate: n-Hexane (7:3)	0.7

Table 66. FT-IR spectral data of Compound

Sr No	Standard Frequency (cm^{-1})	Observed Frequency (cm^{-1})	Functional group
1	3650-3550 (broad, s)	3462	OH

2	3300-3000 (s)	3355	2° N-H
3	3100 – 3000 (m to w)	3081	C-H
4	1690-1550 (m)	1612	C=N
5	700-600 (m)	678	C-S-C

Table 67. 1H NMR and Mass spectral data of Compound

Compound code	1H NMR (400 MHz, DMSO;δ ppm)	Mass (m/z%)
12b-III	6.90-6.21 (m, 4H, Quinazoline Ar-H), 7.66-7.60 (m, 4H, Pyrimidine Ar-H), 7.93-7.70 (m, 4H, Thiadiazole Ar-H), 11.00 (s, 1H, NH), 11.39 (s, 1H, NH) 12.39 (s, 1H, OH)	418 (M+2)

Compound (12b-IV)

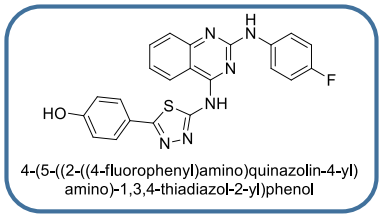

4-(5-((2-((4-fluorophenyl)amino)quinazolin-4-yl) amino)-1,3,4-thiadiazol-2-yl)phenol

Table 68. Physicochemical data of Compound

Sr No	Observed Parameter	Result
1.	Molecular Formula	$C_{22}H_{15}FN_6OS$
2.	Molecular Weight	430.46
3.	% Yield	62
4.	Melting Point °C	252-258 °C
5.	R_f value Ethyl acetate: n-Hexane (7:3)	0.6

Table 69. FT-IR spectral data of Compound

Sr No	Standard Frequency (cm^{-1})	Observed Frequency (cm^{-1})	Functional group
1	3650-3550 (broad, s)	3456	OH
2	3300-3000 (s)	3290	2° N-H
3	3100 – 3000 (m to w)	3146	C-H
4	1690-1550 (m)	1506	C=N
5	850-515 (s)	754	C-F
6	700-600 (m)	700	C-S-C

Table 70. 1H NMR and Mass spectral data of Compound

Compound code	1H NMR (400 MHz, DMSO;δ ppm)	Mass (m/z%)
12b-IV	5.45-5.59 (d, 2H, Quinazoline Ar-H), 6.61-6.67 (d, 2H, Quinazoline Ar-H), 7.91-7.60 (m, 4H, 4-Floroaniline Ar-H), 7.61-8.26 (m, 4H, Thiadiazole Ar-H), 10.90 (s, 1H, NH), 11.45 (s, 1H, NH), 12.0 (s, 1H, OH)	430 (M+)

Compound (12c-II)

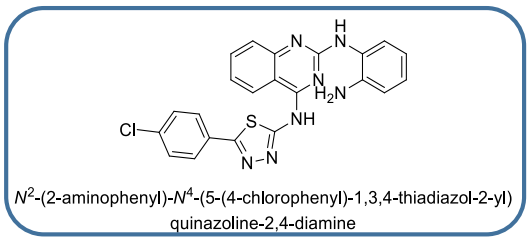

N^2-(2-aminophenyl)-N^4-(5-(4-chlorophenyl)-1,3,4-thiadiazol-2-yl) quinazoline-2,4-diamine

Table 71. Physicochemical data of Compound

Sr No	Observed Parameter	Result
1.	Molecular Formula	$C_{22}H_{16}ClN_7S$
2.	Molecular Weight	445.93

3.	% Yield	60
4.	Melting Point °C	253-260 °C
5.	R_f value Ethyl acetate: n-Hexane (7:3)	0.7

Table 72. FT-IR spectral data of Compound

Sr No	Standard Frequency (cm^{-1})	Observed Frequency (cm^{-1})	Functional group
1	3300-3000 (s)	3290	2° N-H
2	3400-3250 (m)	3031	1° N-H
3	3100 – 3000 (m to w)	2879	C-H
4	1690-1550 (m)	1668	C=N
4	850-515 (s)	877	C-Cl
6	700-600 (m)	684	C-S-C

Table 73. 1H NMR and Mass spectral data of Compound

Compound code	1H NMR (400 MHz, DMSO;δ ppm)	Mass (m/z%)
12c-II	6.19 (d, 2H, NH_2), 6.87-7.32 (m, 4H, Quinazoline Ar-H), 7.34-7.72 (m, 4H, 4-Orthophenylene, Ar-H), 7.78-8.11 (m, 4H, Thiadiazole Ar-H), 11.19 (s, 1H, NH), 11.40 (s, 1H, NH)	445 (M+)

Compound (12c-IV)

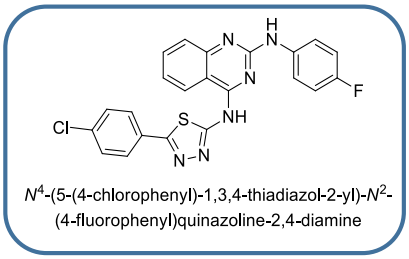

N^4-(5-(4-chlorophenyl)-1,3,4-thiadiazol-2-yl)-N^2-(4-fluorophenyl)quinazoline-2,4-diamine

Table 74. Physicochemical data of Compound

Sr No	Observed Parameter	Result
1.	Molecular Formula	$C_{22}H_{14}ClN_6OS$
2.	Molecular Weight	450.90
3.	% Yield	65
4.	Melting Point °C	255-261 °C
5.	R_f value Ethyl acetate: n Hexane (9:1)	0.6

Table 75. FT-IR spectral data of Compound

Sr No	Standard Frequency (cm^{-1})	Observed Frequency (cm^{-1})	Functional group
1	3300-3000 (s)	3437	2° N-H
2	3100 – 3000 (m to w)	3184	C-H
3	1690-1550 (m)	1591	C=N
4	850-515 (s)	761	C-F
5	850-515 (s)	827	C-Cl
6	700-600 (m)	682	C-S-C

Table 76. 1H NMR and Mass spectral data of Compound

Compound code	1H NMR (400 MHz, DMSO;δ ppm)	Mass (m/z%)
12c-IV	5.11-6.90 (m, 4H, Quinazoline Ar-H), 7.30-7.98 (m, 4H, 4-Floroaniline Ar-H), 8.00-8.02 (m, 4H, Thiadiazole Ar-H), 11.17 (s, 1H, NH), 11.32 (s, 1H, NH)	450 (M+), 452 (M+2)

Compound (12d-II)

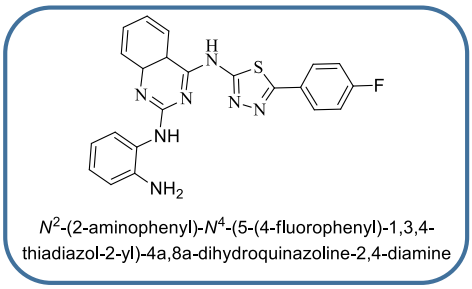

N^2-(2-aminophenyl)-N^4-(5-(4-fluorophenyl)-1,3,4-thiadiazol-2-yl)-4a,8a-dihydroquinazoline-2,4-diamine

Table 77. Physicochemical data of Compound

Sr No	Observed Parameter	Result
1.	Molecular Formula	$C_{22}H_{18}FN_7S$
2.	Molecular Weight	448.90
3.	% Yield	63
4.	Melting Point °C	256-265 °C
5.	R_f value Ethyl acetate: n Hexane (7:3)	0.6

Table 78. FT-IR spectral data of Compound

Sr No	Standard Frequency (cm^{-1})	Observed Frequency (cm^{-1})	Functional group
1	3300-3000 (s)	3454	2° N-H
2	3400-3250 (m)	3267	1° N-H
3	3100 – 3000 (m to w)	2992	C-H
4	1690-1550 (m)	1658	C=N
5	850-515 (s)	752	C-F
6	700-600 (m)	681	C-S-C

Table 79. 1H NMR and Mass spectral data of Compound

Compound code	1H NMR (400 MHz, DMSO;δ ppm)	Mass (m/z%)
12d-II	3.35-4.54 (m, 4H, Quinazoline Ar-H), 6.91 (d, 2H, NH_2), 6.87-7.63 (m, 2H, Orthophenylene diamine, Ar-H), 7.70-7.96 (m, 4H, Thiadiazole Ar-H),	450 (M+)

	10.75 (s, 1H, NH), 11.00 (s, 1H, NH)	

Compound (12d-IV)

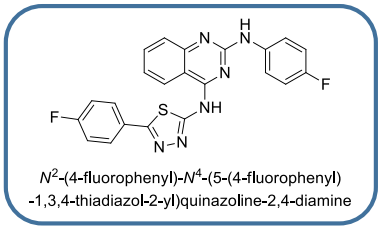

N^2-(4-fluorophenyl)-N^4-(5-(4-fluorophenyl)-1,3,4-thiadiazol-2-yl)quinazoline-2,4-diamine

Table 80. Physicochemical data of Compound

Sr No	Observed Parameter	Result
1.	Molecular Formula	$C_{22}H_{14}F_2N_6S$
2.	Molecular Weight	432.45
3.	% Yield	61
4.	Melting Point °C	258-265 °C
5.	R_f value Ethyl acetate: n-Hexane (7:3)	0.7

Table 81. FT-IR spectral data of Compound

Sr No	Standard Frequency (cm^{-1})	Observed Frequency (cm^{-1})	Functional group
1	3300-3000 (s)	3433	2° N-H
2	3100 – 3000 (m to w)	3190	C-H
3	1690-1550 (m)	1583	C=N
4	850-515 (s)	742	C-F
5	700-600 (m)	678	C-S-C

Table 82. 1H NMR and Mass spectral data of Compound

Compound code	1H NMR (400 MHz, DMSO;δ ppm)	Mass (m/z%)
12d-IV	4.523-4.54 (d, 2H, Quinazoline Ar-H), 5.00-5.25 (m, 2H, Quinazoline Ar-H),	433 (M+)

	7.11-7.23 (d, 4H, 4-Floroaniline Ar-H), 8.13-8.68 (m, 4H, Thiadiazole Ar-H), 11.42 (s, 1H, NH), 11.66 (s, 1H, NH)	

Compound (12g-IV)

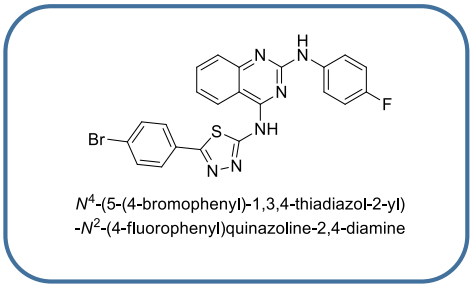

N^4-(5-(4-bromophenyl)-1,3,4-thiadiazol-2-yl)-N^2-(4-fluorophenyl)quinazoline-2,4-diamine

Table 83. Physicochemical data of Compound

Sr No	Observed Parameter	Result
1.	Molecular Formula	$C_{22}H_{14}BrFN_6S$
2.	Molecular Weight	493.35
3.	% Yield	63
4.	Melting Point °C	259-267 °C
5.	R_f value Ethyl acetate: n Hexane (7:3)	0.6

Table 84. FT-IR spectral data of Compound

Sr No	Standard Frequency (cm^{-1})	Observed Frequency (cm^{-1})	Functional group
1	3300-3000 (s)	3437	2° N-H
2	3100 – 3000 (m to w)	3184	C-H
3	1690-1550 (m)	1537	C=N
4	850-515 (s)	833	C-F
5	850-515 (s)	750	C-Br
6	700-600 (m)	636	C-S-C

Table 85. 1H NMR and Mass spectral data of Compound

Compound code	1H NMR (400 MHz, DMSO;δ ppm)	Mass (m/z%)
12g-IV	7.25-7.27 (m, 4H, Quinazoline Ar-H), 7.28-7.35 (m, 4H, 4-Floroaniline Ar-H), 7.36-8.17 (m, 4H, Thiadiazole Ar-H), 11.11 (s, 1H, NH), 11.51 (s, 1H, NH)	495 (M+2)

Compound (12g-V)

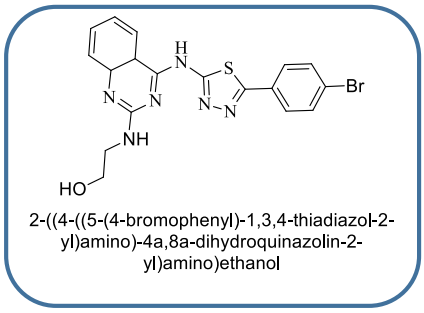

2-((4-((5-(4-bromophenyl)-1,3,4-thiadiazol-2-yl)amino)-4a,8a-dihydroquinazolin-2-yl)amino)ethanol

Table 86. Physicochemical data of Compound

Sr No	Observed Parameter	Result
1.	Molecular Formula	$C_{18}H_{17}BrN_6OS$
2.	Molecular Weight	445.34
3.	% Yield	68
4.	Melting Point °C	260-267 °C
5.	R_f value Ethyl acetate: n Hexane (7:3)	0.6

Table 87. FT-IR spectral data of Compound

Sr No	Standard Frequency (cm^{-1})	Observed Frequency (cm^{-1})	Functional group
1	3650-3550 (broad, s)	3438	OH
2	3300-3000 (s)	3331	2° N-H
3	3100 – 3000 (m to w)	3190	C-H
4	1690-1550 (m)	1575	C=N

5	850-515 (s)	788	C-Br
6	700-600 (m)	681	C-S-C

Table 88. 1H NMR and Mass spectral data of Compound

Compound code	1H NMR (400 MHz, DMSO;δ ppm)	Mass (m/z%)
12g-V	3.35-4.33 (t, 4H, CH_2-CH_2), 7.25-7.32 (m, 4H, Quinazoline Ar-H), 7.34-8.17 (m, 4H, Thiadiazole Ar-H), 11.25 (s, 1H, NH), 11.35 (s, 1H, NH), 12.51 (s, 1H, OH)	445 (M+), 447 (M+2)

Compound (12e-IV)

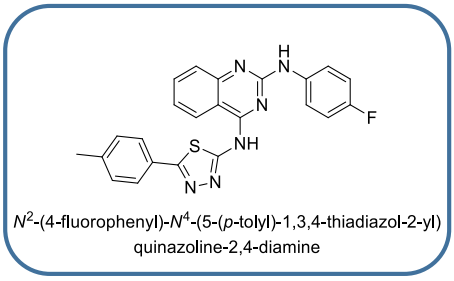

N^2-(4-fluorophenyl)-N^4-(5-(*p*-tolyl)-1,3,4-thiadiazol-2-yl) quinazoline-2,4-diamine

Table 89. Physicochemical data of Compound

Sr No	Observed Parameter	Result
1.	Molecular Formula	$C_{23}H_{17}FN_6S$
2.	Molecular Weight	428.48
3.	% Yield	65
4.	Melting Point °C	260-265 °C
5.	R_f value Ethyl acetate: n-Hexane (7:3)	0.7

Table 90. FT-IR spectral data of Compound

Sr No	Standard Frequency (cm^{-1})	Observed Frequency (cm^{-1})	Functional group
1	3300-3000 (s)	3402	2° N-H
2	3100 – 3000 (m to w)	2987	C-H
3	1690-1550 (m)	1591	C=N
4	1470-1430 (m)	1419	CH_3
5	850-515 (s)	765	C-F
6	700-600 (m)	680	C-S-C

Table 91. 1H NMR and Mass spectral data of Compound

Compound code	1H NMR (400 MHz, DMSO;δ ppm)	Mass (m/z%)
12e-IV	3.34 (m, 3H, methyl), 6.64-6.70 (m, 4H, Quinazoline Ar-H), 6.91-7.44 (m, 4H, 4-Floroaniline Ar-H), 7.57-7.84 (m, 4H, Thiadiazole Ar-H), 11.36 (s, 1H, NH), 11.47 (s, 1H, NH)	428 (M+)

Compound (12e-V)

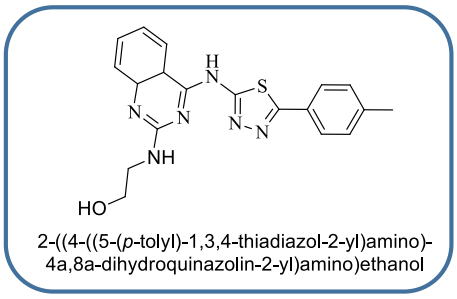

2-((4-((5-(*p*-tolyl)-1,3,4-thiadiazol-2-yl)amino)-4a,8a-dihydroquinazolin-2-yl)amino)ethanol

Table 92. Physicochemical data of Compound

Sr No	Observed Parameter	Result
1.	Molecular Formula	$C_{19}H_{20}N_6OS$
2.	Molecular Weight	380.47

3.	% Yield	63
4.	Melting Point °C	260-267 °C
5.	R_f value Ethyl acetate: n Hexane (7:3)	0.6

Table 93. FT-IR spectral data of Compound

Sr No	Standard Frequency (cm^{-1})	Observed Frequency (cm^{-1})	Functional group
1	3650-3550 (broad, s)	3546	OH
2	3300-3000 (s)	3446	2° N-H
3	3100 – 3000 (m to w)	2914	C-H
4	1690-1550 (m)	1540	C=N
	1470-1430 (m)	1464	CH_3-CH_3
5	700-600 (m)	680	C-S-C

Table 94. 1H NMR and Mass spectral data of Compound

Compound code	1H NMR (400 MHz, DMSO;δ ppm)	Mass (m/z%)
12e-V	3.60-4.05 (t, 4H, CH_2-CH_2), 7.46-7.52 (m, 4H, Quinazoline, Ar-H), 7.71-7.94 (m, 4H, Thiadiazole Ar-H), 11.33 (s, 1H, NH), 11.60 (s, 1H, NH), 12.71 (s, 1H, OH)	428 (M+)

6.2 Biological Activity

6.2.2 Results of In-Vitro Anticancer Screening

Anticancer Activity:

Among the synthesized compounds, compound **12(a-II), 12(a-III), 12(a-IV), 12(b-I), 12(b-III), 12(b-IV), 12(c-II), 12(d-IV), 12(f-IV)** and **12(e-IV)** were tested for in-vitro 96 well MTT assay on A549 cell line (NSCLC) with Cisplatin as positive control at Gujarat University, Ahmedabad. Result of the compound has been obtained. Compound have shown good anticancer activity.

Table.95: Biological activity of synthesized compound

Compound	Code	A-549		
		Conc. (µM)	% Survival	IC50 (µM)
1	12(d-IV)	1000	19.9086758	20.61
		100	31.87214612	
		10	70.68493151	
		1	85.47945205	
		0.1	95.89041096	
		0.01	104.3835616	
2	12 (f-IV)	1000	20.3652968	22.01
		100	30.1369863	
		10	70.86757991	
		1	82.00913242	
		0.1	94.24657534	
		0.01	95.89041096	
3	12(b-III)	1000	21.73515982	74.09
		100	39.36073059	
		10	63.92694064	
		1	81.00456621	
		0.1	89.13242009	
		0.01	102.4657534	
4	12(a-IV)	1000	20.3652968	68.02
		100	37.44292237	
		10	69.5890411	
		1	76.52968037	
		0.1	88.94977169	
		0.01	95.70776256	
5	12(b-IV)	1000	22.00913242	12.2
		100	31.41552511	
		10	62.46575342	
		1	91.05022831	
		0.1	93.51598174	

		0.01	101.2785388	
6	**12(b-III)**	1000	26.48401826	74.88
		100	52.69406393	
		10	86.02739726	
		1	94.61187215	
		0.1	95.70776256	
		0.01	104.0182648	
7	**12(c-II)**	1000	21.55251142	**16.35**
		100	33.60730594	
		10	67.03196347	
		1	79.45205479	
		0.1	97.53424658	
		0.01	107.2146119	
8	**12(b-I)**	1000	18.08219178	**20.76**
		100	29.9543379	
		10	73.88127854	
		1	91.96347032	
		0.1	100.8219178	
		0.01	104.56621	
9	**12(a-III)**	1000	21.73515982	208.06
		100	52.42009132	
		10	64.65753425	
		1	77.26027397	
		0.1	91.87214612	
		0.01	105.2054795	
10	**12(A-II)**	1000	28.49315068	**32.04**
		100	38.90410959	
		10	73.05936073	
		1	76.89497717	
		0.1	88.21917808	
		0.01	95.15981735	
Cisplatin		1000	27.91000011	**33.81**
		100	38.90410959	
		10	73.05936073	
		1	76.89497717	
		0.1	88.21917808	
		0.01	95.15981735	

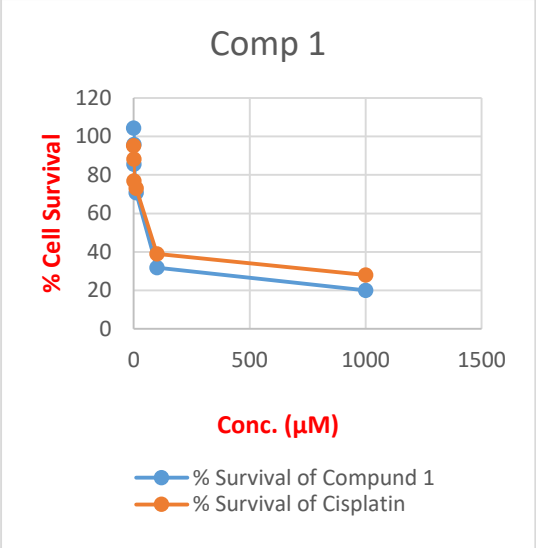
Comp 1
% Cell Survival
120
100
80
60
40
20
0
0
500
1000
1500
Conc. (µM)
% Survival of Compund 1
% Survival of Cisplatin

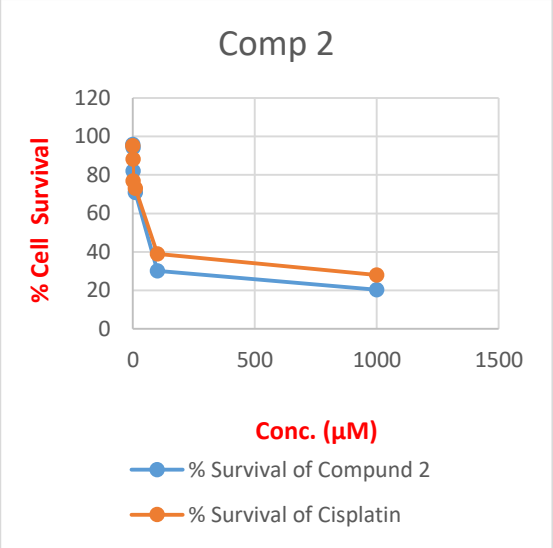
Comp 2
% Cell Survival
120
100
80
60
40
20
0
0
500
1000
1500
Conc. (µM)
% Survival of Compund 2
% Survival of Cisplatin

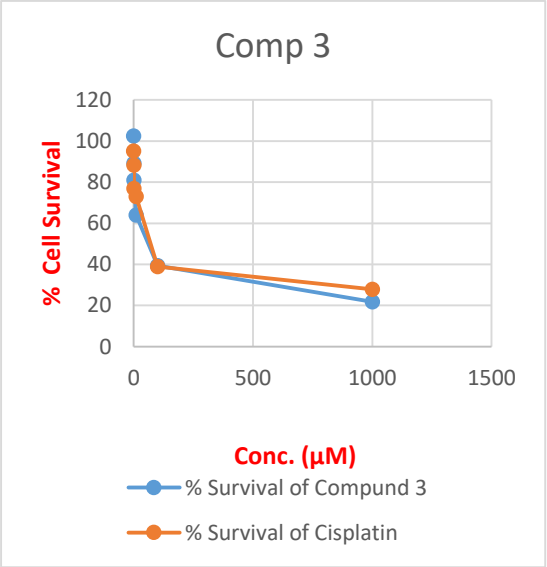
Comp 3
% Cell Survival
120
100
80
60
40
20
0
0
500
1000
1500
Conc. (µM)
% Survival of Compund 3
% Survival of Cisplatin

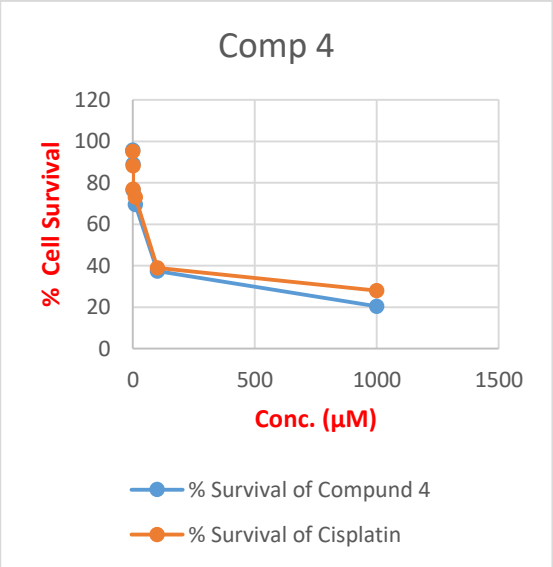
Comp 4
% Cell Survival
120
100
80
60
40
20
0
0
500
1000
1500
Conc. (µM)
% Survival of Compund 4
% Survival of Cisplatin

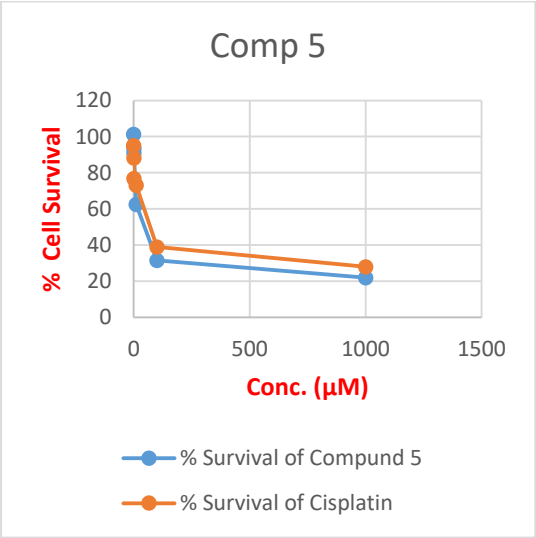
Comp 5
% Cell Survival
120
100
80
60
40
20
0
0
500
1000
1500
Conc. (µM)
% Survival of Compund 5
% Survival of Cisplatin

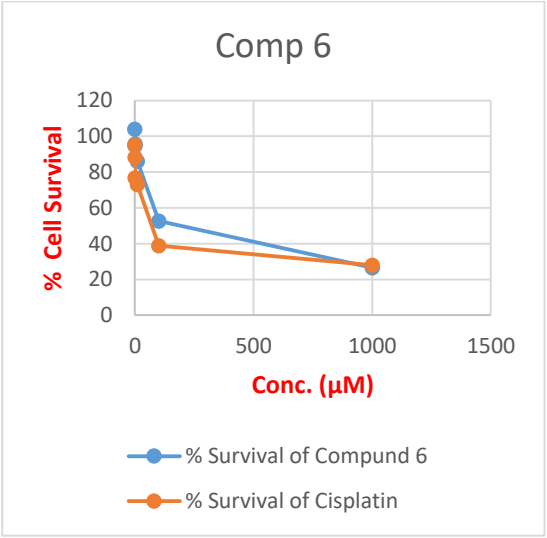
Comp 6
% Cell Survival
120
100
80
60
40
20
0
0
500
1000
1500
Conc. (µM)
% Survival of Compund 6
% Survival of Cisplatin

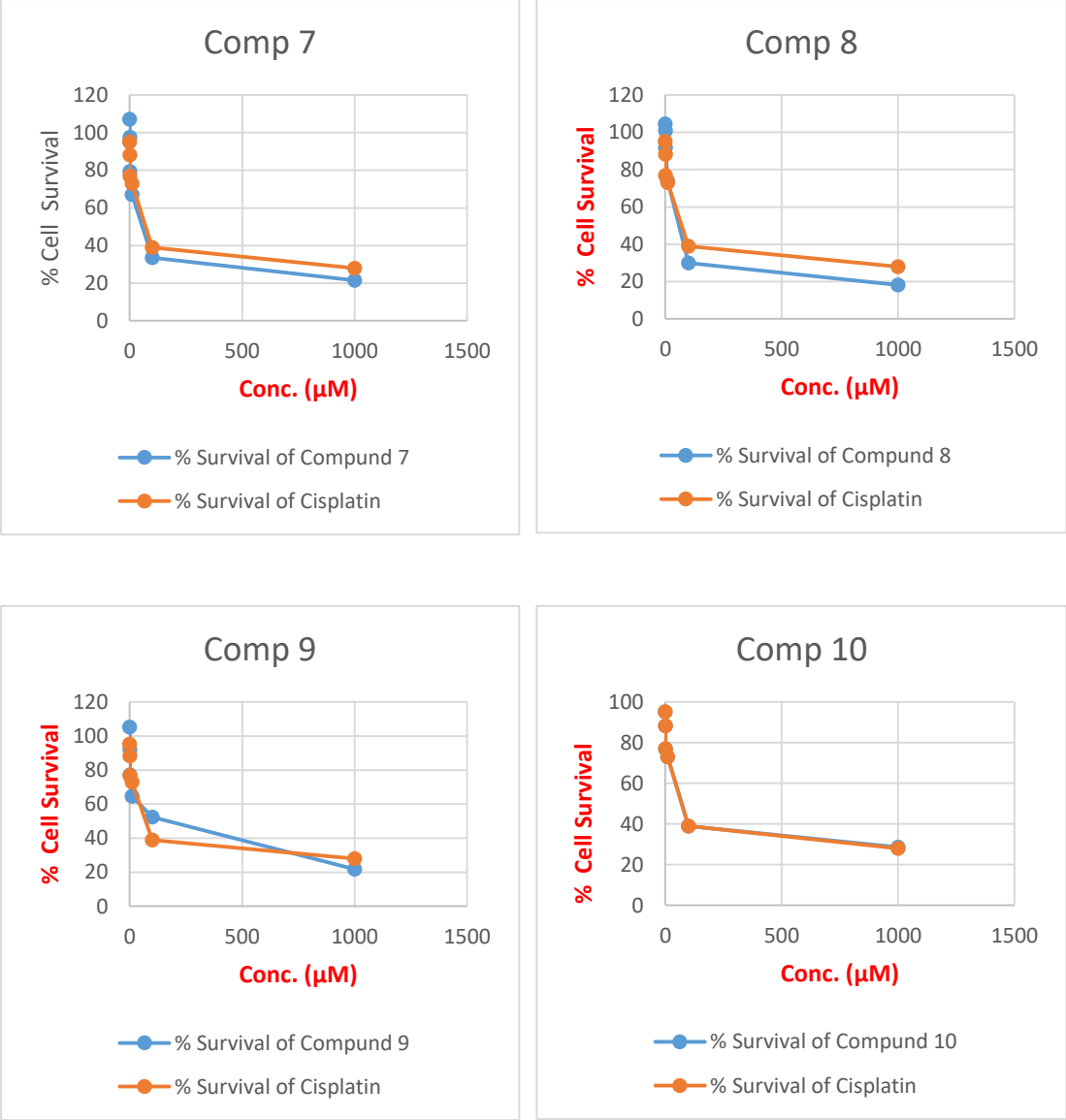

Fig.27 Graph of Biological activity

6.3 DISCUSSION

- We have synthesized a series of 6 derivatives of 1,3,4-Thiadiazole **(3a-f)**. Synthesis was carried out according to the reaction shown in reaction Schemes. 1,3,4-Thiadiazole was prepared using various aromatic carboxylic acids and thiosemicarbazide as starting material. It was confirmed by IR spectra, which showed the presence of amino group stretching at 3281 ($-NH_2$) and 1626 (C=N) stretching cm^{-1}
- The various 1,3,4-thiadiazole with 2,4-dichloroquinazoline derivatives **(6a-f)** were prepared by condensing the 1,3,4-thiadiazole **(3a-f)** and 2,4-dichloro quinazoline. 1,3,4-thiadiazole with 2,4-dichloroquinazoline derivatives were

confirmed by the characteristic IR absorption peak at 815-550 (C-Cl) group, 3281 ($-NH_2$), 3300 (-NH) cm^{-1}.

- Finally synthesized the proposed compounds having Quinazoline moiety are connected by 1,3,4-thiadiazole moiety at R_1, 2-amino benzimidazole, 2-amino pyrimidine and, different aniline derivatives such as (para fluoro aniline, orthophenylene diamine and ethanolamine) at R_2 **(12a(I-V) to 12f(I-V)).** The reaction was monitored by Thin-layer chromatography using suitable mobile phases such as chloroform and methanol (9:1) and n-hexane and ethyl acetate (7:3). The R_f values were compared and found that they were different from each other. The melting point of the derivatives was determined.
- The synthesized compound **12(a-II), 12(a-III), 12(a-IV), 12(b-I), 12(b-III), 12(b-IV), 12(c-II), 12(d-IV), 12(f-IV)** and **12(e-IV)** were evaluated for their *in-vitro* anticancer activity at **Gujarat University, Ahmedabad** by **MTT** assay. And showed encouraging anticancer activity.
- Compounds **12(b-IV), 12(c-II), 12(b-I), 12(d-IV), 12(f-IV),** and **12(a-II)** showed maximum inhibition IC_{50} values respectively (12.2 µM, 16.35 µM, 20.61 µM, 20.76 µM, 22.01 µM, and 32.04 µM) against **Non-small-cell Lung Cancer (A549)** cell line concerning cisplatin as a standard drug.
- We observed that the compound have a halogen atom and polar functional group gave good biological activity. Compounds **12(b-IV), 12(c-II), 12(b-I), 12(d-IV), 12(f-IV),** and **12(a-II)** contain halogen atoms (F, Cl, Br) and OH group, which have good binding activity as well as good biological activity. Among that fluorine atoms are commonly used in drug design to increase the potency and selectivity of a compound. The small size and high electronegativity of fluorine can enhance the binding affinity of a compound to its target receptor by increasing the strength and specificity of intermolecular interactions. Additionally, the addition of fluorine atoms to a drug can improve its pharmacokinetic properties by enhancing its metabolic stability and reducing its clearance rate. Chlorine atoms are often used in drug design to improve the lipophilicity of a compound, which can enhance its penetration through biological membranes and increase its bioavailability. Chlorine atoms can also increase the metabolic stability of a compound by reducing its susceptibility to enzymatic degradation in the liver. However, the addition of chlorine atoms to a drug can also increase its toxicity and potential

for off-target effects. Hydroxyl (OH) groups are polar functional groups that can affect the solubility and polarity of a compound. The presence of OH groups can increase the water solubility of a drug and enhance its ability to dissolve in biological fluids, which can improve its pharmacokinetic properties. OH groups can also affect the biological activity of a compound by forming hydrogen bonds with the target receptor and altering its conformation or orientation. However, the presence of OH groups can also increase the susceptibility of a compound to metabolic degradation and reduce its stability.

- In summary, the effects of halogen atoms on the biological activity of a drug depend on the specific functional group and its position within the molecule. Chlorine and fluorine atoms can enhance the lipophilicity, potency, and selectivity of a compound, while OH groups can affect its solubility, stability, and binding affinity.

7. Conclusion

7. CONCLUSION

- In the present study, we synthesized thiadiazole derivatives by using the conventional method with good yield and then it was confirmed by spectral data.
- The yield of the synthesized compounds was found to be in the range of 35%-80%.
- The synthesized compound **12(a-II), 12(a-III), 12(a-IV), 12(b-I), 12(b-III), 12(b-IV), 12(c-II), 12(d-IV), 12(f-IV)** and **12(e-IV)** were evaluated for their *in-vitro* anticancer activity at **Gujarat University, Ahmedabad** by **MTT** assay. And showed encouraging anticancer activity.
- Compounds **12(b-IV), 12(c-II), 12(b-I), 12(d-IV), 12(f-IV),** and **12(a-II)** showed maximum inhibition IC_{50} values respectively (12.2 µM, 16.35 µM, 20.61 µM, 20.76 µM, 22.01 µM, and 32.04 µM) against **Non-small-cell Lung Cancer (A549)** cell line concerning **Cisplatin** as a standard drug.
- All the Synthesized compounds were characterized by the Physical and Spectral data. The IR, MASS, and ^{1}H NMR of the re-presented compounds were analysed and studied in the section of spectral studies in the Appendix.
- So finally, we can conclude that the synthesized compounds showed better anticancer activity. These findings can help in the future while designing new chemical entities as anticancer agents.

8. References

REFERENCES

1. Siegel RL, Miller KD, Jemal A. Cancer statistics, 2020. CA Cancer J Clin. 2020;70(1):7–30.
2. Koo MM, Swann R, McPhail S, Abel GA, Elliss-Brookes L, Rubin GP, et al. Presenting symptoms of cancer and stage at diagnosis: evidence from a cross-sectional, population-based study. Lancet Oncol [Internet]. 2020;21(1):73–9. Available from: http://dx.doi.org/10.1016/S1470-2045(19)30595-9
3. Siddiqui MJA, Jafri A, Khan RR. JIPBS Review article Role of environment in development of cancer. 2017;(October 2016).
4. Key TJ, Bradbury KE, Perez-Cornago A, Sinha R, Tsilidis KK, Tsugane S. Diet, nutrition, and cancer risk: What do we know and what is the way forward? BMJ [Internet]. 2020;368(March):1–9. Available from: http://dx.doi.org/doi:10.1136/bmj.m511
5. Key TJA. Hormones and cancer in humans. Mutat Res - Fundam Mol Mech Mutagen. 1995;333(1–2):59–67.
6. Sauter ER. Cancer prevention and treatment using combination therapy with natural compounds. Expert Rev Clin Pharmacol [Internet]. 2020;13(3):265–85. Available from: https://doi.org/10.1080/17512433.2020.1738218
7. Jabo B, Lin AC, Aljehani MA, Ji L, Morgan JW, Selleck MJ, et al. Impact of Breast Reconstruction on Time to Definitive Surgical Treatment, Adjuvant Therapy, and Breast Cancer Outcomes. Ann Surg Oncol [Internet]. 2018;25(10):3096–105. Available from: https://doi.org/10.1245/s10434-018-6663-7
8. Dickens E, Ahmed S. Principles of cancer treatment by chemotherapy. Surg (United Kingdom) [Internet]. 2018;36(3):134–8. Available from: https://doi.org/10.1016/j.mpsur.2017.12.002
9. Hayat MA. Overview of autophagy. Vol. 12, Autophagy: Cancer, Other Pathologies, Inflammation, Immunity, Infection, and Aging Volume 12. 2017. 1–122 p.
10. Piacentini M, Kroemer G. Dying to survive - Apoptosis, necroptosis, autophagy as the supreme experiments of nature. Int J Dev Biol. 2015;59(1–3):5–9.
11. Kroemer G, Mariño G, Levine B. Autophagy and the Integrated Stress

Response. Mol Cell. 2010;40(2):280–93.

12. Kocaturk NM, Akkoc Y, Kig C, Bayraktar O, Gozuacik D, Kutlu O. Autophagy as a molecular target for cancer treatment. Eur J Pharm Sci [Internet]. 2019;134(September 2018):116–37. Available from: https://doi.org/10.1016/j.ejps.2019.04.011
13. Cao Y, Luo Y, Zou J, Ouyang J, Cai Z, Zeng X, et al. Autophagy and its role in gastric cancer. Clin Chim Acta [Internet]. 2019;489(September 2018):10–20. Available from: https://doi.org/10.1016/j.cca.2018.11.028
14. Zachari M, Ganley IG. The mammalian ULK1 complex and autophagy initiation. Essays Biochem. 2017;61(6):585–96.
15. Chen Y, Klionsky DJ. The regulation of autophagy - Unanswered questions. J Cell Sci. 2011;124(2):161–70.
16. An H, Harper JW. Systematic analysis of ribophagy in human cells reveals bystander flux during selective autophagy. Nat Cell Biol [Internet]. 2018;20(2):135–43. Available from: http://dx.doi.org/10.1038/s41556-017-0007-x
17. Feng Y, Backues SK, Baba M, Heo JM, Harper JW, Klionsky DJ. Phosphorylation of Atg9 regulates movement to the phagophore assembly site and the rate of autophagosome formation. Autophagy [Internet]. 2016;12(4):648–58. Available from: http://dx.doi.org/10.1080/15548627.2016.1157237
18. Papinski D, Kraft C. Atg1 kinase organizes autophagosome formation by phosphorylating Atg9. Autophagy. 2014;10(7):1338–40.
19. Pattingre S, Tassa A, Qu X, Garuti R, Xiao HL, Mizushima N, et al. Bcl-2 antiapoptotic proteins inhibit Beclin 1-dependent autophagy. Cell. 2005;122(6):927–39.
20. Mercer TJ, Gubas A, Tooze SA. A molecular perspective of mammalian autophagosome biogenesis. J Biol Chem. 2018;293(15):5386–95.
21. Park JM, Jung CH, Seo M, Otto NM, Grunwald D, Kim KH, et al. The ULK1 complex mediates MTORC1 signaling to the autophagy initiation machinery via binding and phosphorylating ATG14. Autophagy [Internet]. 2016;12(3):547–64. Available from: http://dx.doi.org/10.1080/15548627.2016.1140293
22. Wirth M, Joachim J, Tooze SA. Autophagosome formation-The role of ULK1

and Beclin1-PI3KC3 complexes in setting the stage. Semin Cancer Biol [Internet]. 2013;23(5):301–9. Available from: http://dx.doi.org/10.1016/j.semcancer.2013.05.007

23. Tsuboyama K, Koyama-honda I, Sakamaki Y, Koike M, Morishita H. The ATG conjugation systems are important for degradation of the inner autophagosomal membrane. 2016;6136:1–10.
24. Klionsky DJ, Schulman BA. Dynamic regulation of macroautophagy by distinctive ubiquitin-like proteins. Nat Publ Gr. 2014;21(4):336–45.
25. Limpert AS, Lambert LJ, Bakas NA, Bata N, Brun SN, Shaw RJ, et al. Autophagy in Cancer: Regulation by Small Molecules. Trends Pharmacol Sci [Internet]. 2018;39(12):1021–32. Available from: https://doi.org/10.1016/j.tips.2018.10.004
26. Colasanti T, Vomero M, Barbati C, Finucci A, Conti F, Alessandri C, et al. Autophagy and Autoimmunity [Internet]. Mosaic of Autoimmunity. Elsevier Inc.; 2019. 143–153 p. Available from: https://doi.org/10.1016/B978-0-12-814307-0.00016-5
27. Kriegenburg F, Ungermann C, Reggiori F. Coordination of Autophagosome–Lysosome Fusion by Atg8 Family Members. Curr Biol [Internet]. 2018;28(8):R512–8. Available from: https://doi.org/10.1016/j.cub.2018.02.034
28. Jäger S, Bucci C, Tanida I, Ueno T, Kominami E, Saftig P, et al. Role for Rab7 in maturation of late autophagic vacuoles. J Cell Sci. 2004;117(20):4837–48.
29. Panda PK, Mukhopadhyay S, Das DN, Sinha N, Naik PP, Bhutia SK. Mechanism of autophagic regulation in carcinogenesis and cancer therapeutics. Semin Cell Dev Biol [Internet]. 2015;39:43–55. Available from: http://dx.doi.org/10.1016/j.semcdb.2015.02.013
30. Levine B, Kroemer G. Autophagy in the Pathogenesis of Disease. Cell. 2008;132(1):27–42.
31. Liang XH, Jackson S, Seaman M, Brown K, Kempkes B, Hibshoosh H, et al. Beclin 1. Sci Exch. 2008;1(19):460–460.
32. Wen L, Chen XZ, Yang K, Chen ZX, Zhang B, Chen JP, et al. Prognostic Value of Cancer Stem Cell Marker CD133 Expression in Gastric Cancer: A Systematic Review. PLoS One. 2013;8(3).
33. Galluzzi L, Pietrocola F, Bravo-San Pedro JM, Amaravadi RK, Baehrecke EH, Cecconi F, et al. Autophagy in malignant transformation and cancer

progression. EMBO J. 2015;34(7):856–80.

34. Wong PM, Puente C, Ganley IG, Jiang X. The ULK1 complex sensing nutrient signals for autophagy activation. Autophagy. 2013;9(2):124–37.
35. Das CK, Banerjee I, Mandal M. Pro-survival autophagy: An emerging candidate of tumor progression through maintaining hallmarks of cancer. Semin Cancer Biol [Internet]. 2019;(July):1–16. Available from: https://doi.org/10.1016/j.semcancer.2019.08.020
36. Lee EJ, Tournier C. The requirement of uncoordinated 51-like kinase 1 (ULK1) and ULK2 in the regulation of autophagy. Autophagy. 2011;7(7):689–95.
37. Ahlberg J, Glaumann H. Uptake-Microautophagy-and degradation of exogenous proteins by isolated rat liver lysosomes. Effects of pH, ATP, and inhibitors of proteolysis. Exp Mol Pathol. 1985;42(1):78–88.
38. Egan D, Kim J, Shaw RJ, Guan K, Egan D, Kim J, et al. a n d e s i o s c i e n c e o n o t d i s t r i b u t e. 2011;8627.
39. Young ARJ, Narita M, Ferreira M, Kirschner K, Sadaie M, Darot JFJ, et al. Autophagy mediates the mitotic senescence transition. Genes Dev. 2009;23(7):798–803.
40. Chan EY. MTORC1 phosphorylates the ULK1-mAtg13-FIP200 autophagy regulatory complex. Sci Signal. 2009;2(84):13–6.
41. Sophie Mokas JRM, Cristina Garreau M-J, Fournier ´e, Robert F, Arya P, Kaufman RJ, et al. Uncoupling Stress Granule Assembly and Translation Initiation Inhibition. Mol Biol Cell. 2009;20:2673–83.
42. Ronan B, Flamand O, Vescovi L, Dureuil C, Durand L, Fassy F, et al. A highly potent and selective Vps34 inhibitor alters vesicle trafficking and autophagy. Nat Chem Biol. 2014;10(12):1013–9.
43. Dowdle WE, Nyfeler B, Nagel J, Elling RA, Liu S, Triantafellow E, et al. Selective VPS34 inhibitor blocks autophagy and uncovers a role for NCOA4 in ferritin degradation and iron homeostasis in vivo. Nat Cell Biol. 2014;16(11):1069–79.
44. Yu L, Alva A, Su H, Dutt P, Freundt E, Welsh S, et al. Science 2004 Paez. 2004;304(June):1–3.
45. Noda NN, Fujioka Y. Atg1 family kinases in autophagy initiation. Cell Mol Life Sci. 2015;72(16):3083–96.

46. Ganley IG, Lam DH, Wang J, Ding X, Chen S, Jiang X. ULK1·ATG13·FIP200 complex mediates mTOR signaling and is essential for autophagy. J Biol Chem. 2009;284(18):12297–305.
47. Yamada Y, Suzuki NN, Hanada T, Ichimura Y, Kumeta H, Fujioka Y, et al. The crystal structure of Atg3, an autophagy-related ubiquitin carrier protein (E2) enzyme that mediates Atg8 lipidation. J Biol Chem. 2007;282(11):8036–43.
48. Jiang H, Cheng D, Liu W, Peng J, Feng J. Protein kinase C inhibits autophagy and phosphorylates LC3. Biochem Biophys Res Commun [Internet]. 2010;395(4):471–6. Available from: http://dx.doi.org/10.1016/j.bbrc.2010.04.030
49. Jaber N, Dou Z, Chen JS, Catanzaro J, Jiang YP, Ballou LM, et al. Class III PI3K Vps34 plays an essential role in autophagy and in heart and liver function. Proc Natl Acad Sci U S A. 2012;109(6):2003–8.
50. Duran A, Amanchy R, Linares JF, Joshi J, Abu-Baker S, Porollo A, et al. P62 Is a Key Regulator of Nutrient Sensing in the mTORC1 Pathway. Mol Cell [Internet]. 2011;44(1):134–46. Available from: http://dx.doi.org/10.1016/j.molcel.2011.06.038
51. Moscat J, Diaz-Meco MT. p62 at the Crossroads of Autophagy, Apoptosis, and Cancer. Cell. 2009;137(6):1001–4.
52. Chandrasekar T, Evans CP. Autophagy and urothelial carcinoma of the bladder: A review. Investig Clin Urol. 2016;57:S89–97.
53. Cianfanelli V, Fuoco C, Lorente M, Salazar M, Quondamatteo F, Gherardini PF, et al. AMBRA1 links autophagy to cell proliferation and tumorigenesis by promoting c-Myc dephosphorylation and degradation. Nat Cell Biol. 2015;17(1):20–30.
54. Chano T, Ikegawa S, Saito-Ohara F, Inazawa J, Mabuchi A, Saeki Y, et al. Isolation, characterization and mapping of the mouse and human RB1CC1 genes. Gene. 2002;291(1–2):29–34.
55. Liang C, Lee JS, Inn KS, Gack MU, Li Q, Roberts EA, et al. Beclin1-binding UVRAG targets the class C Vps complex to coordinate autophagosome maturation and endocytic trafficking. Nat Cell Biol. 2008;10(7):776–87.
56. Ahn CH, Jeong EG, Lee JW, Kim MS, Kim SH, Kim SS, et al. Expression of beclin-1, an autophagy-related protein, in gastric and colorectal cancers.

Apmis. 2007;115(12):1344–9.

57. Mariño G, Salvador-Montoliu N, Fueyo A, Knecht E, Mizushima N, López-Otín C. Retractions: Tissue-specific autophagy alterations and increased tumorigenesis in mice deficient in Atg4C/autophagin-3 (Journal of Biological Chemistry (2007) 282 (18573–18583) DOI: 10.1074/jbc.W118.007329). J Biol Chem. 2019;294(4):1435.
58. Takamura A, Komatsu M, Hara T, Sakamoto A, Kishi C, Waguri S, et al. Autophagy-deficient mice develop multiple liver tumors. Genes Dev. 2011;25(8):795–800.
59. Review I. Immune activation and inflammation in HIV-1 infection : 2008;(December 2008):231–41.
60. Kashuba VI, Gizatullin RZ, Protopopov AI, Allikmets R, Korolev S, Li J, et al. NotI linking/jumping clones of human chromosome 3: Mapping of the TFRC, RAB7 and HAUSP genes to regions rearranged in leukemia and deleted in solid tumors. FEBS Lett. 1997;419(2–3):181–5.
61. Xu P, Das M, Reilly J, Davis RJ. JNK regulates FoxO-dependent autophagy in neurons. Genes Dev. 2011;25(4):310–22.
62. Pike LRG, Singleton DC, Buffa F, Abramczyk O, Phadwal K, Li JL, et al. Transcriptional up-regulation of ULK1 by ATF4 contributes to cancer cell survival. Biochem J. 2013;449(2):389–400.
63. Martin KR, Celano SL, Solitro AR, Gunaydin H, Scott M, O'Hagan RC, et al. A Potent and Selective ULK1 Inhibitor Suppresses Autophagy and Sensitizes Cancer Cells to Nutrient Stress. iScience [Internet]. 2018;8:74–84. Available from: https://doi.org/10.1016/j.isci.2018.09.012
64. Lin MG, Hurley JH. Structure and function of the ULK1 complex in autophagy. Curr Opin Cell Biol [Internet]. 2016;39:61–8. Available from: http://dx.doi.org/10.1016/j.ceb.2016.02.010
65. Chen Y, He J, Tian M, Zhang SY, Guo MR, Kasimu R, et al. UNC51-like kinase 1, autophagic regulator and cancer therapeutic target. Cell Prolif. 2014;47(6):494–505.
66. Wang C, Wang H, Zhang D, Luo W, Liu R, Xu D, et al. Phosphorylation of ULK1 affects autophagosome fusion and links chaperone-mediated autophagy to macroautophagy. Nat Commun [Internet]. 2018;9(1). Available from: http://dx.doi.org/10.1038/s41467-018-05449-1

67. Mizushima N. The role of the Atg1/ULK1 complex in autophagy regulation. Curr Opin Cell Biol [Internet]. 2010;22(2):132–9. Available from: http://dx.doi.org/10.1016/j.ceb.2009.12.004
68. Liu L, Yan L, Liao N, Wu WQ, Shi JL. A review of ULK1-mediated autophagy in drug resistance of cancer. Cancers (Basel). 2020;12(2):1–23.
69. Alers S, Löffler AS, Wesselborg S, Stork B. The incredible ULKs. Cell Commun Signal. 2012;10:1–15.
70. Chan EY. Regulation and function of uncoordinated-51 like kinase proteins. Antioxidants Redox Signal. 2012;17(5):775–85.
71. Russell RC, Yuan HX, Guan KL. Autophagy regulation by nutrient signaling. Cell Res [Internet]. 2014;24(1):42–57. Available from: http://dx.doi.org/10.1038/cr.2013.166
72. Lee EJ, Tournier C. The requirement of uncoordinated 51-like kinase 1 (ULK1) and ULK2 in the regulation of autophagy. Autophagy. 2011;7(7):689–95.
73. Kundu M, Lindsten T, Yang CY, Wu J, Zhao F, Zhang J, et al. Ulk1 plays a critical role in the autophagic clearance of mitochondria and ribosomes during reticulocyte maturation. Blood. 2008;112(4):1493–502.
74. Zhang L, Ouyang L, Guo Y, Zhang J, Liu B. UNC-51-like Kinase 1: From an Autophagic Initiator to Multifunctional Drug Target. J Med Chem. 2018;61(15):6491–500.
75. Chan EYW, Longatti A, McKnight NC, Tooze SA. Kinase-Inactivated ULK Proteins Inhibit Autophagy via Their Conserved C-Terminal Domains Using an Atg13-Independent Mechanism. Mol Cell Biol. 2009;29(1):157–71.
76. Mao T, Liang O. ULK1 Can Suppress or Promote Tumor Growth Under Different Conditions [Internet]. 11th ed. Vol. 11, Autophagy: Cancer, Other Pathologies, Inflammation, Immunity, Infection, and Aging. Elsevier Inc.; 2017. 245–257 p. Available from: http://dx.doi.org/10.1016/B978-0-12-805420-8.00012-3
77. Badadani M. Autophagy Mechanism, Regulation, Functions, and Disorders. ISRN Cell Biol. 2012;2012(2):1–11.
78. Chan EY, Tooze SA. Evolution of Atg1 function and regulation. Autophagy. 2009;5(6):758–65.
79. Löffler AS, Alers S, Dieterle AM, Keppeler H, Franz-Wachtel M, Kundu M, et

al. Ulk1-mediated phosphorylation of AMPK constitutes a negative regulatory feedback loop. Autophagy. 2011;7(7):696–706.

80. Kang R, Zeh HJ, Lotze MT, Tang D. The Beclin 1 network regulates autophagy and apoptosis. Cell Death Differ [Internet]. 2011;18(4):571–80. Available from: http://dx.doi.org/10.1038/cdd.2010.191
81. Colecchia D, Dapporto F, Tronnolone S, Salvini L, Chiariello M. MAPK15 is part of the ULK complex and controls its activity to regulate early phases of the autophagic process. J Biol Chem. 2018;293(41):15962–76.
82. Chan EYW, Kir S, Tooze SA. siRNA screening of the kinome identifies ULK1 as a multidomain modulator of autophagy. J Biol Chem. 2007;282(35):25464–74.
83. Romeo-Guitart D, Leiva-Rodriguez T, Forés J, Casas C. Improved motor nerve regeneration by SIRT1/Hif1a-mediated autophagy. Cells. 2019;8(11).
84. Guan P, Sun F, Hou X, Wang F, Yi F, Xu W, et al. Design, synthesis and preliminary bioactivity studies of 1,3,4-thiadiazole hydroxamic acid derivatives as novel histone deacetylase inhibitors. Bioorganic Med Chem [Internet]. 2012;20(12):3865–72. Available from: http://dx.doi.org/10.1016/j.bmc.2012.04.032
85. Matysiak J, Opolski A. Synthesis and antiproliferative activity of N-substituted 2-amino-5-(2,4-dihydroxyphenyl)-1,3,4-thiadiazoles. Bioorganic Med Chem. 2006;14(13):4483–9.
86. Kumar D, Maruthi Kumar N, Chang KH, Shah K. Synthesis and anticancer activity of 5-(3-indolyl)-1,3,4-thiadiazoles. Eur J Med Chem [Internet]. 2010;45(10):4664–8. Available from: http://dx.doi.org/10.1016/j.ejmech.2010.07.023
87. Polkam N, Rayam P, Anireddy JS, Yennam S, Anantaraju HS, Dharmarajan S, et al. Synthesis, in vitro anticancer and antimycobacterial evaluation of new 5-(2,5-dimethoxyphenyl)-1,3,4-thiadiazole-2-amino derivatives. Bioorganic Med Chem Lett [Internet]. 2015;25(7):1398–402. Available from: http://dx.doi.org/10.1016/j.bmcl.2015.02.052
88. Luo Z, Chen B, He S, Shi Y, Liu Y, Li C. Synthesis and antitumor-evaluation of 1,3,4-thiadiazole-containing benzisoselenazolone derivatives. Bioorganic Med Chem Lett [Internet]. 2012;22(9):3191–3. Available from: http://dx.doi.org/10.1016/j.bmcl.2012.03.043

89. Noolvi MN, Patel HM, Kamboj S, Kaur A, Mann V. 2,6-Disubstituted imidazo[2,1-b][1,3,4]thiadiazoles: Search for anticancer agents. Eur J Med Chem [Internet]. 2012;56:56–69. Available from: http://dx.doi.org/10.1016/j.ejmech.2012.08.012
90. Terzioglu N, Gürsoy A. Synthesis and anticancer evaluation of some new hydrazone derivatives of 2,6-dimethylimidazo[2,1-b][1,3,4]thiadiazole-5-carbohydrazide. Eur J Med Chem. 2003;38(7–8):781–6.
91. Yang XH, Wen Q, Zhao TT, Sun J, Li X, Xing M, et al. Synthesis, biological evaluation, and molecular docking studies of cinnamic acyl 1,3,4-thiadiazole amide derivatives as novel antitubulin agents. Bioorganic Med Chem. 2012;20(3):1181–7.
92. Wang Z, Deng X, Xiong S, Xiong R, Liu J, Zou L, et al. Design, synthesis and biological evaluation of chrysin benzimidazole derivatives as potential anticancer agents. Nat Prod Res [Internet]. 2018;32(24):2900–9. Available from: http://doi.org/10.1080/14786419.2017.1389940
93. Ren Y, Wang Y, Li G, Zhang Z, Ma L, Cheng B, et al. Discovery of Novel Benzimidazole and Indazole Analogues as Tubulin Polymerization Inhibitors with Potent Anticancer Activities. J Med Chem. 2021;64(8):4498–515.
94. Akhtar MJ, Khan AA, Ali Z, Dewangan RP, Rafi M, Hassan MQ, et al. Synthesis of stable benzimidazole derivatives bearing pyrazole as anticancer and EGFR receptor inhibitors. Bioorg Chem [Internet]. 2018;78:158–69. Available from: https://doi.org/10.1016/j.bioorg.2018.03.002
95. Huang ST, Hsei IJ, Chen C. Synthesis and anticancer evaluation of bis(benzimidazoles), bis(benzoxazoles), and benzothiazoles. Bioorganic Med Chem. 2006;14(17):6106–19.
96. Yadav S, Narasimhan B, Lim SM, Ramasamy K, Vasudevan M, Shah SAA, et al. Synthesis and evaluation of antimicrobial, antitubercular and anticancer activities of benzimidazole derivatives. Egypt J Basic Appl Sci [Internet]. 2018;5(1):100–9. Available from: https://doi.org/10.1016/j.ejbas.2017.11.001
97. Katikireddy R, Marri S, Kakkerla R, Murali Krishna MPS, Gandamalla D, Reddy YN. Synthesis, Anticancer Activity and Molecular Docking Studies of Hybrid Benzimidazole-1,3,4-Oxadiazol-2-N-Alkyl/Aryl Amines. Polycycl Aromat Compd [Internet]. 2021;0(0):1–15. Available from: https://doi.org/10.1080/10406638.2021.1959352

98. Woo HB, Eom YW, Park KS, Ham J, Ahn CM, Lee S. Synthesis of substituted benzimidazolyl curcumin mimics and their anticancer activity. Bioorganic Med Chem Lett [Internet]. 2012;22(2):933–6. Available from: http://dx.doi.org/10.1016/j.bmcl.2011.12.074
99. Osmaniye D. New Benzimidazole- Triazolothiadiazine Derivatives. 2020;
100. Sağlık BN, Şen AM, Evren AE, Çevik UA, Osmaniye D, Çavuşoğlu BK, et al. Synthesis, investigation of biological effects and in silico studies of new benzimidazole derivatives as aromatase inhibitors. Zeitschrift fur Naturforsch - Sect C J Biosci. 2020;75(910):353–62.
101. Synthesis and evaluation of new benzimidazole derivatives with hydrazone moiety as anticancer agents Hidrazon yapısı içeren yeni benzimidazol türevlerinin sentezi ve antikanser ajan olarak değerlendirilmesi. 2018;3–10.
102. Sridhar Goud N, Pooladanda V, Muni Chandra K, Lakshmi Soukya PS, Alvala R, Kumar P, et al. Novel benzimidazole-triazole hybrids as apoptosis inducing agents in lung cancer: Design, synthesis, 18F-radiolabeling & galectin-1 inhibition studies. Bioorg Chem [Internet]. 2020;102:104125. Available from: https://doi.org/10.1016/j.bioorg.2020.104125
103. Yurttaş L, Özkay Y, Akalin-Çiftçi G, Ulusoylar-Yildirim Ş. Synthesis and anticancer activity evaluation of N-[4-(2-methylthiazol-4-yl) phenyl]acetamide derivatives containing (benz)azole moiety. J Enzyme Inhib Med Chem. 2014;29(2):175–84.
104. Atmaca H, İlhan S, Batır MB, Pulat ÇÇ, Güner A, Bektaş H. Novel benzimidazole derivatives: Synthesis, in vitro cytotoxicity, apoptosis and cell cycle studies. Chem Biol Interact. 2020;327.
105. Abuelizz HA, Marzouk M, Ghabbour H, Al-Salahi R. Synthesis and anticancer activity of new quinazoline derivatives. Saudi Pharm J [Internet]. 2017;25(7):1047–54. Available from: https://doi.org/10.1016/j.jsps.2017.04.022
106. Faraj FL, Zahedifard M, Paydar M, Looi CY, Majid NA, Ali HM, et al. Synthesis, characterization, and anticancer activity of new quinazoline derivatives against MCF-7 cells. Sci World J. 2014;2014.
107. Syed T, Asiri YI, Shaheen S, Gangarapu K. Design, synthesis and anticancer evaluation of structurally modified substituted aryl-quinazoline derivatives as anticancer agents. Synth Commun [Internet]. 2021;51(18):2782–95. Available

from: https://doi.org/10.1080/00397911.2021.1941113

108. Wasfy AAF, Mohmed NA, Salman AA. Synthesis and anti-cancer properties of novel quinazoline derivatives. Int J Res Pharm Chem. 2015;5(1):34–40.
109. Yong J-P, Lu C-Z, Wu X. Potential Anticancer Agents. I. Synthesis of Isoxazole Moiety Containing Quinazoline Derivatives and Preliminarily in vitro Anticancer Activity. Anticancer Agents Med Chem. 2014;15(1):131–6.
110. Madhavi S, Sreenivasulu R, Yazala JP, Raju RR. Synthesis of chalcone incorporated quinazoline derivatives as anticancer agents. Saudi Pharm J [Internet]. 2017;25(2):275–9. Available from: http://dx.doi.org/10.1016/j.jsps.2016.06.005
111. Akgun H, Us Yilmaz D, Cetin Atalay R, Gozen D. A Series of 2,4(1H,3H)-Quinazolinedione Derivatives: Synthesis and Biological Evaluation as Potential Anticancer Agents. Lett Drug Des Discov. 2015;13(1):64–76.
112. Fröhlich T, Reiter C, Ibrahim MM, Beutel J, Hutterer C, Zeitträger I, et al. Synthesis of Novel Hybrids of Quinazoline and Artemisinin with High Activities against Plasmodium falciparum, Human Cytomegalovirus, and Leukemia Cells. ACS Omega. 2017;2(6):2422–31.
113. Sharma RN, Ravani R. Synthesis and screening of 2-(2-(4-substituted piperazine-1-yl)-5- phenylthiazol-4-yl)-3-aryl quinazolinone derivatives as anticancer agents. Med Chem Res. 2013;22(6):2788–94.
114. Emami L, Faghih Z, Sakhteman A, Rezaei Z, Faghih Z, Salehi F, et al. Design, synthesis, molecular simulation, and biological activities of novel quinazolinone-pyrimidine hybrid derivatives as dipeptidyl peptidase-4 inhibitors and anticancer agents. New J Chem. 2020;44(45):19515–31.
115. Masoud MS, Sweyllam AM, Ahmed MM. Synthesis, characterization, coordination chemistry and biological activity of some pyrimidine complexes. J Mol Struct [Internet]. 2020;1219:128612. Available from: https://doi.org/10.1016/j.molstruc.2020.128612
116. Gaber AA, Bayoumi AH, El-morsy AM, Sherbiny FF, Mehany ABM, Eissa IH. Design, synthesis and anticancer evaluation of 1H-pyrazolo[3,4-d]pyrimidine derivatives as potent EGFR WT and EGFR T790M inhibitors and apoptosis inducers. Bioorg Chem [Internet]. 2018;80(March):375–95. Available from: https://doi.org/10.1016/j.bioorg.2018.06.017
117. Kumar B, Sharma P, Gupta VP, Khullar M, Singh S, Dogra N, et al. Synthesis

and biological evaluation of pyrimidine bridged combretastatin derivatives as potential anticancer agents and mechanistic studies. Bioorg Chem [Internet]. 2018;78:130–40. Available from: https://doi.org/10.1016/j.bioorg.2018.02.027

118. Reddy DS, Kongot M, Singh V, Siddiquee MA, Patel R, Singhal NK, et al. Biscoumarin–pyrimidine conjugates as potent anticancer agents and binding mechanism of hit candidate with human serum albumin. Arch Pharm (Weinheim). 2021;354(1):1–15.
119. El-Metwally SA, Khalil AK, El-Sayed WM. Design, molecular modeling and anticancer evaluation of thieno[2,3-d]pyrimidine derivatives as inhibitors of topoisomerase II. Bioorg Chem [Internet]. 2020;94:103492. Available from: https://doi.org/10.1016/j.bioorg.2019.103492
120. Cherukupalli S, Chandrasekaran B, Aleti RR, Sayyad N, Hampannavar GA, Merugu SR, et al. Synthesis of 4,6-disubstituted pyrazolo[3,4-d]pyrimidine analogues: Cyclin-dependent kinase 2 (CDK2) inhibition, molecular docking and anticancer evaluation. J Mol Struct [Internet]. 2019;1176:538–51. Available from: https://doi.org/10.1016/j.molstruc.2018.08.104
121. Diao PC, Lin WY, Jian XE, Li YH, You WW, Zhao PL. Discovery of novel pyrimidine-based benzothiazole derivatives as potent cyclin-dependent kinase 2 inhibitors with anticancer activity. Eur J Med Chem [Internet]. 2019;179:196–207. Available from: https://doi.org/10.1016/j.ejmech.2019.06.055
122. Ye T, Han Y, Wang R, Yan P, Chen S, Hou Y, et al. Design, synthesis and biological evaluation of novel 2,4-bismorpholinothieno[3,2-d]pyrimidine and 2-morpholinothieno[3,2-d]pyrimidinone derivatives as potent antitumor agents. Bioorg Chem [Internet]. 2020;99(March):103796. Available from: https://doi.org/10.1016/j.bioorg.2020.103796
123. Ghorab MM, Ragab FA, Alqasoumi SI, Alafeefy AM, Aboulmagd SA. Synthesis of some new pyrazolo[3,4-d]pyrimidine derivatives of expected anticancer and radioprotective activity. Eur J Med Chem [Internet]. 2010;45(1):171–8. Available from: http://dx.doi.org/10.1016/j.ejmech.2009.09.039
124. El-Sayed NS, El-Bendary ER, El-Ashry SM, El-Kerdawy MM. Synthesis and antitumor activity of new sulfonamide derivatives of thiadiazolo[3,2-a]pyrimidines. Eur J Med Chem [Internet]. 2011;46(9):3714–20. Available

from: http://dx.doi.org/10.1016/j.ejmech.2011.05.037

125. Egan DF, Chun MGH, Vamos M, Zou H, Rong J, Miller CJ, et al. Small Molecule Inhibition of the Autophagy Kinase ULK1 and Identification of ULK1 Substrates. Mol Cell [Internet]. 2015;59(2):285–97. Available from: http://dx.doi.org/10.1016/j.molcel.2015.05.031
126. Tang F, Hu P, Yang Z, Xue C, Gong J, Sun S, et al. SBI0206965, a novel inhibitor of Ulk1, suppresses non-small cell lung cancer cell growth by modulating both autophagy and apoptosis pathways. Oncol Rep. 2017;37(6):3449–58.
127. Petherick KJ, Conway OJL, Mpamhanga C, Osborne SA, Kamal A, Saxty B, et al. Pharmacological inhibition of ULK1 kinase blocks mammalian target of rapamycin (mTOR)-dependent autophagy. J Biol Chem. 2015;290(18):11376–83.
128. Mitophagy A, Joo JH, Dorsey FC, Joshi A, Hennessy-walters KM, Rose KL, et al. Article Hsp90-Cdc37 Chaperone Complex Regulates. Mol Cell [Internet]. 2010;43(4):572–85. Available from: http://dx.doi.org/10.1016/j.molcel.2011.06.018
129. Tanida I, Ueno T, Kominami E. LC3 and Autophagy. 445(2):77–88.
130. Lazarus MB, Novotny CJ, Shokat KM. Structure of the human autophagy initiating kinase ULK1 in complex with potent inhibitors. ACS Chem Biol. 2015;10(1):257–61.
131. Lazarus MB, Shokat KM. Discovery and structure of a new inhibitor scaffold of the autophagy initiating kinase ULK1. Bioorganic Med Chem [Internet]. 2015;23(17):5483–8. Available from: http://dx.doi.org/10.1016/j.bmc.2015.07.034
132. Lazarus MB, Novotny CJ, Shokat KM. Structure of the human autophagy initiating kinase ULK1 in complex with potent inhibitors. ACS Chem Biol. 2015;10(1):257–61.
133. Wood SD, Grant W, Adrados I, Choi JY, Alburger JM, Duckett DR, et al. In Silico HTS and Structure Based Optimization of Indazole-Derived ULK1 Inhibitors. ACS Med Chem Lett. 2017;8(12):1258–63.
134. Rosenberg LH, Lafitte M, Grant W, Chen W, Cleveland JL, Duckett DR. Development of an HTS-Compatible Assay for the Discovery of Ulk1 Inhibitors. 2015;

135. Wood SD, Grant W, Adrados I, Choi JY, Alburger JM, Duckett DR, et al. In Silico High-Throughput Screening To Identify Novel Indazole-Derived ULK1 Inhibitors. 2(pg 5):1–26.
136. Wang Y, Xing J, Xu Y, Zhou N, Peng J, Xiong Z, et al. In silico ADME / T modelling for rational drug design. 2015;1308.
137. Article R. Computational Approaches for Drug Design and Discovery : An Overview. (i):99–105.
138. Vrbanac J, Slauter R. Chapter 3 - ADME in Drug Discovery [Internet]. Second Edi. A Comprehensive Guide to Toxicology in Nonclinical Drug Development. Elsevier Inc.; 2017. 39–67 p. Available from: http://dx.doi.org/10.1016/B978-0-12-803620-4.00003-7
139. Brogi S, Ramalho TC, Kuca K, Medina-franco JL. Editorial : In silico Methods for Drug Design and Discovery. 2020;8(August):1–5.
140. Chen X, Li H, Tian L, Li Q, Luo J, Zhang Y. Analysis of the Physicochemical Properties of Acaricides Based on Lipinski's Rule of Five. J Comput Biol. 2020;27(9):1397–406.
141. Eddershaw PJ, Beresford AP, Bayliss MK. REVIEWS ADME / PK as part of a rational approach to drug discovery. 2000;5(9):409–14.
142. Cardoso WB, Mendanha SA. Molecular dynamics simulation of docking structures of SARS-CoV-2 main protease and HIV protease inhibitors. J Mol Struct [Internet]. 2021;1225:129143. Available from: https://doi.org/10.1016/j.molstruc.2020.129143
143. Abd N, Salam E, El S. Virtual Screening , Drug Likeness , Bioavailability and Docking Studies of Small Molecules of Heterocyclic. World J Pharm Pharm Sci. 2017;6(3):1145–60.
144. Peng W, Liu YJ, Zhao CB, Huang XS, Wu N, Hu MB, et al. In silico assessment of drug-like properties of alkaloids from Areca catechu L nut. Trop J Pharm Res. 2015;14(4):635–9.
145. Maziasz T, Kadambi VJ, Silverman L, Fedyk E, Alden CL. Predictive toxicology approaches for small molecule oncology drugs. Toxicol Pathol. 2010;38(1):148–64.
146. Zuegg J, A. Cooper M. Drug-Likeness and Increased Hydrophobicity of Commercially Available Compound Libraries for Drug Screening. Curr Top Med Chem. 2012;12(14):1500–13.

147. Lipinski CA, Lombardo F, Dominy BW, Feeney PJ. Experimental and computational approaches to estimate solubility and permeability in drug discovery and development settings. Adv Drug Deliv Rev [Internet]. 2012;64(SUPPL.):4–17. Available from: http://dx.doi.org/10.1016/j.addr.2012.09.019
148. Martin YC. A bioavailability score. J Med Chem. 2005;48(9):3164–70.
149. Rajan AP, Jayachandra S, Lulu S, Manju SL. Insilco screening and molecular docking to identify a novel inhibitor for aldose reductase. J Pharm Sci Res. 2017;9(7):1169–72.
150. Sidat PS, Shah J V, Shah FB, Ganie AH. Drug Design & Discovery In Silico Assessment of Drug like Properties of Some Thiadiazole and Oxadiazole Derivatives as HDAC Inhibitors. 2022;9(2):1–12.
151. Veber DF, Johnson SR, Cheng HY, Smith BR, Ward KW, Kopple KD. Molecular properties that influence the oral bioavailability of drug candidates. J Med Chem. 2002;45(12):2615–23.
152. Gschwend DA, Good AC, Kuntz ID. Molecular Docking Towards Drug Discovery. 1996;9(October 1995):175–86.
153. Shoichet BK, McGovern SL, Wei B, Irwin JJ. Lead discovery using molecular docking. Curr Opin Chem Biol. 2002;6(4):439–46.
154. Tovchigrechko A, Wells CA, Vakser IA. Docking of protein models. Protein Sci. 2002;11(8):1888–96.
155. Boysen N, Fliedner M. Cross dock scheduling: Classification, literature review and research agenda. Omega [Internet]. 2010;38(6):413–22. Available from: http://dx.doi.org/10.1016/j.omega.2009.10.008
156. Krovat E, Steindl T, Langer T. Recent Advances in Docking and Scoring. Curr Comput Aided-Drug Des. 2006;1(1):93–102.
157. Bliznyuk AA, Gready JE. Combining Docking and Molecular Dynamic Simulations in Drug Design. 2006;26(5).
158. Borhani DW, Shaw DE. The future of molecular dynamics simulations in drug discovery. 2012;15–26.
159. Bhagat RT, Butle SR, Khobragade DS, Wankhede SB, Prasad CC, Mahure DS, et al. Molecular Docking in Drug Discovery. 2021;33:46–58.
160. Eweas AF, Maghrabi IA, Namarneh AI. Advances in molecular modeling and docking as a tool for modern drug discovery Advances in molecular modeling

and docking as a tool for modern drug discovery. 2015;(February).

161. Ferreira LG, Santos RN, Oliva G, Andricopulo AD. Molecular Docking and Structure-Based Drug Design Strategies. 2015. 13384–13421 p.
162. Brooijmans N, Kuntz ID. Molecular recognition and docking algorithms. Annu Rev Biophys Biomol Struct. 2003;32:335–73.
163. Muhammed MT, Aki-Yalcin E. Pharmacophore modeling in drug discovery: Methodology and current status. J Turkish Chem Soc Sect A Chem. 2021;8(3):749–62.
164. Schaller D, Šribar D, Noonan T, Deng L, Nguyen TN, Pach S, et al. Next generation 3D pharmacophore modeling. Wiley Interdiscip Rev Comput Mol Sci. 2020;10(4):1–20.
165. De Vivo M, Cavalli A. Recent advances in dynamic docking for drug discovery. Wiley Interdiscip Rev Comput Mol Sci. 2017;7(6):1–10.
166. Guner O, Clement O, Kurogi Y. Pharmacophore Modeling and Three Dimensional Database Searching for Drug Design Using Catalyst: Recent Advances. Curr Med Chem. 2012;11(22):2991–3005.
167. Guner OF. The impact of pharmacophore modeling in drug design The impact of pharmacophore modeling in drug design Osman F Güner. 2015;(February).
168. Kaserer T, Beck KR, Akram M, Odermatt A, Schuster D, Willett P. Pharmacophore models and pharmacophore-based virtual screening: Concepts and applications exemplified on hydroxysteroid dehydrogenases. Molecules. 2015;20(12):22799–832.
169. Dixon SL, Smondyrev AM, Rao SN. PHASE : A Novel Approach to Pharmacophore Modeling and 3D Database Searching. 2006;370–2.
170. Pal S, Kumar V, Kundu B, Bhattacharya D, Preethy N. Ligand-based Pharmacophore Modeling , Virtual Screening and Molecular Docking Studies for Discovery of Potential Topoisomerase I Inhibitors. Comput Struct Biotechnol J [Internet]. 2019;17:291–310. Available from: https://doi.org/10.1016/j.csbj.2019.02.006
171. Kandakatla N, Ramakrishnan G. Ligand Based Pharmacophore Modeling and Virtual Screening Studies to Design Novel HDAC2 Inhibitors. 2014;2014.
172. Vuorinen A, Engeli R, Meyer A, Bachmann F, Griesser UJ, Schuster D, et al. Ligand-Based Pharmacophore Modeling and Virtual Screening for the Discovery of Novel 17 β -Hydroxysteroid Dehydrogenase 2 Inhibitors. 2014;

173. Schneidman-duhovny D, Dror O, Inbar Y, Nussinov R, Wolfson HJ. PharmaGist : a webserver for ligand-based pharmacophore detection. 2008;36(April):223–8.
174. Kazemi S, Güntert P. Molecular Dynamics Simulation Tutorial. 2018;(Sommersemester):1–22.
175. Tran Q, Nguyen Q, Vo N, Mai TT, Tran T, Tran T, et al. modeling to discover novel interleukin 6 inhibitors : An in silico screening , molecular dynamics simulations and binding free energy calculations. 2022;1–21. Available from: http://dx.doi.org/10.1371/journal.pone.0266632
176. Durrant JD, Mccammon JA. Molecular dynamics simulations and drug discovery. 2011;
177. Fujiwara K, Yajima K, Arai N, Yasuoka K. Prediction of transport property via machine learning molecular movements arXiv : 2203 . 03103v1 [physics . chem-ph] 7 Mar 2022. 2020;1–24.
178. Caflisch A. ScienceDirect Protein structure-based drug design : from docking to molecular dynamics Pawe ł Sled z and Amedeo Caflisch.
179. Venkataramana CHS, Ramya Sravani KM, Swetha Singh S, Madhavan V. In-silico ADME and toxcity studies of some novel indole derivatives. J Appl Pharm Sci. 2011;1(10):159–62.
180. Negi JS, Bisht AS, Sharma DK. Chemistry and activity of quinazoline moiety : A systematic review study. 2020;7(2):61–5.
181. Kaboli PJ. Molecular Dynamics (MD) Simulations , step by step protocol. 2018;(February).
182. Chitongo R, Obasa AE, Mikasi SG, Id BJ, Id RC. Molecular dynamic simulations to investigate the structural impact of known drug resistance mutations on HIV-1C Integrase- Dolutegravir binding. 2020;1–15. Available from: http://dx.doi.org/10.1371/journal.pone.0223464
183. Sangande F, Julianti E, Tjahjono DH. Ligand-Based Pharmacophore Modeling , Molecular Docking , and Molecular Dynamic Studies of Dual Tyrosine Kinase Inhibitor of EGFR. 2020;
184. Linus O, Wiley J, Jin Y, Johannissen LO, Hay S. Predicting new protein conformations from molecular dynamics simulation conformational landscapes and machine learning article Predicting new protein conformations from molecular dynamics simulation conformational landscapes and machine

learning. 2022;

185. Anwar MA, Choi S. Structure-activity relationship in tlr4 mutations: Atomistic molecular dynamics simulations and residue interaction network analysis. Sci Rep. 2017;7(March):1–14.
186. Ramsey JM, Cooper JD, Penninx BWJH, Bahn S. Variation in serum biomarkers with sex and female hormonal status: Implications for clinical tests. Sci Rep [Internet]. 2016;6(June). Available from: http://dx.doi.org/10.1038/srep26947
187. Wolf A, Kirschner KN. Principal component and clustering analysis on molecular dynamics data of the ribosomal L11·23S subdomain. J Mol Model. 2013;19(2):539–49.
188. Sittel F, Jain A, Stock G. Principal component analysis of molecular dynamics: On the use of Cartesian vs. internal coordinates. Vol. 141, Journal of Chemical Physics. 2014.
189. Haider S, Parkinson GN, Neidle S. Molecular dynamics and principal components analysis of human telomeric quadruplex multimers. Biophys J. 2008;95(1):296–311.
190. Kitao A. Principal Component Analysis and Related Methods for Investigating the Dynamics of Biological Macromolecules. J. 2022;5(2):298–317.
191. Rueda M, Ferrer-Costa C, Meyer T, Pérez A, Camps J, Hospital A, et al. A consensus view of protein dynamics. Proc Natl Acad Sci U S A. 2007;104(3):796–801.
192. Essential Dynamics of Proteins 407645.pdf.
193. Salmas RE, Yurtsever M, Durdagi S. Investigation of inhibition mechanism of chemokine receptor CCR5 by micro-second molecular dynamics simulations. Vol. 5, Scientific Reports. 2015.
194. Tariq K, Shaheen I, Shaheen R, Khalil A. Role of DFT in Drug Design : A Mini Review Drug Designing : Open Access. (1):9–12.
195. Tandon H, Chakraborty T, Suhag V. A Brief Review on Importance of DFT In Drug Design. Res Med Eng Sci. 2019;7(4):791–5.
196. Mazurek AH, Szeleszczuk Ł, Pisklak DM. Periodic DFT calculations—Review of applications in the pharmaceutical sciences. Pharmaceutics. 2020;12(5).
197. Bai Y, Srikanth N, Chua CK, Zhou K. Density Functional Theory Study of M n+1 AX n Phases: A Review. Crit Rev Solid State Mater Sci [Internet].

2019;44(1):56–107. Available from: https://doi.org/10.1080/10408436.2017.1370577

198. de Proft F, Geerlings P. Conceptual and Computational DFT in the Study of Aromaticity. Chem. Rev.; (Review); 2001; 101(5); 1451-1464. Chem Rev. 2001;101(5):1451.
199. Tandon H, Chakraborty T, Suhag V. A Brief Review on Importance of DFT In Drug Design. 2019;791–5.
200. Pereira C, João D, Teixeira B, Laura R, Marco O, Pablo B, et al. In silico studies of - M pro and - PL pro from SARS - CoV - 2 and a new class of cephalosporin drugs containing 1 , 2 , 4 - thiadiazole. 2022;2205–20.
201. Gholivand K, Mohammadpanah F, Pooyan M, Roohzadeh R. Evaluating anti-coronavirus activity of some phosphoramides and their influencing inhibitory factors using molecular docking, DFT, QSAR, and NCI-RDG studies. J Mol Struct [Internet]. 2022;1248:131481. Available from: https://doi.org/10.1016/j.molstruc.2021.131481
202. Ji Q, Yang D, Wang X, Chen C, Deng Q, Ge Z, et al. Design, synthesis and evaluation of novel quinazoline-2,4-dione derivatives as chitin synthase inhibitors and antifungal agents. Bioorganic Med Chem [Internet]. 2014;22(13):3405–13. Available from: http://dx.doi.org/10.1016/j.bmc.2014.04.042
203. Bhat KS. Innovare Academic Sciences SYNTHESIS , CHARACTERIZATION AND ANTICONVULSANT ACTIVITY OF SUBSTITUTED 4-. Int J Pharm Pharm Sci. 2014;6(5):3–7.
204. Sharma A, Luxami V, Paul K. Synthesis, single crystal and antitumor activities of benzimidazole- quinazoline hybrids. Bioorganic Med Chem Lett [Internet]. 2013;23(11):3288–94. Available from: http://dx.doi.org/10.1016/j.bmcl.2013.03.107
205. Rai Y, Pathak R, Kumari N, Sah DK, Pandey S, Kalra N, et al. Mitochondrial biogenesis and metabolic hyperactivation limits the application of MTT assay in the estimation of radiation induced growth inhibition. Sci Rep [Internet]. 2018;8(1):1–15. Available from: http://dx.doi.org/10.1038/s41598-018-19930-w
206. Benov L. Effect of growth media on the MTT colorimetric assay in bacteria.

PLoS One. 2019;14(8):1–15.

207. Buranaamnuay K. The MTT assay application to measure the viability of spermatozoa: A variety of the assay protocols. Open Vet J. 2021;11(2):251–69.
208. Van Meerloo J, Kaspers GJL, Cloos J. Cell sensitivity assays: The MTT assay. Methods Mol Biol. 2011;731(March):237–45.
209. Bahuguna A, Khan I, Bajpai VK, Kang SC. MTT assay to evaluate the cytotoxic potential of a drug. Bangladesh J Pharmacol. 2017;12(2):115–8.
210. Kamiloglu S, Sari G, Ozdal T, Capanoglu E. Guidelines for cell viability assays. Food Front. 2020;1(3):332–49.

9. Appendixes

- **APPENDIX-A SPECTRA OF COMPOUNDS**

Compound 3 (a-h)

IR Spectrum of Compound (3a)

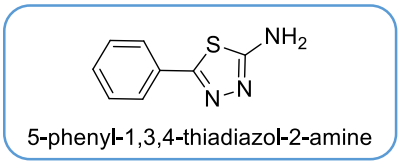

5-phenyl-1,3,4-thiadiazol-2-amine

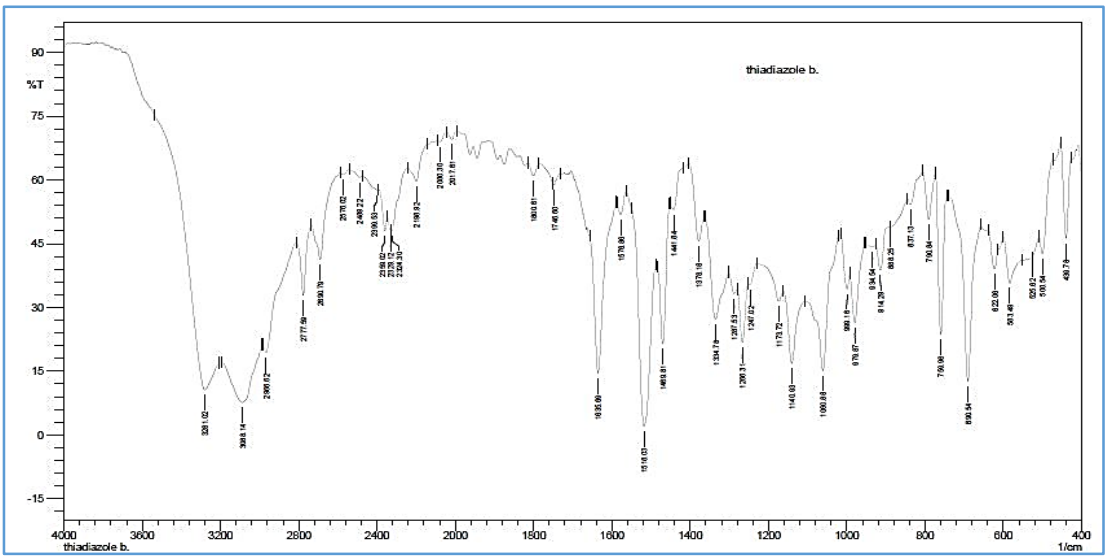

IR Spectrum of Compound (3b)

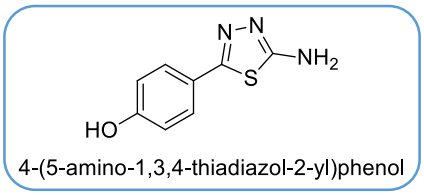

4-(5-amino-1,3,4-thiadiazol-2-yl)phenol

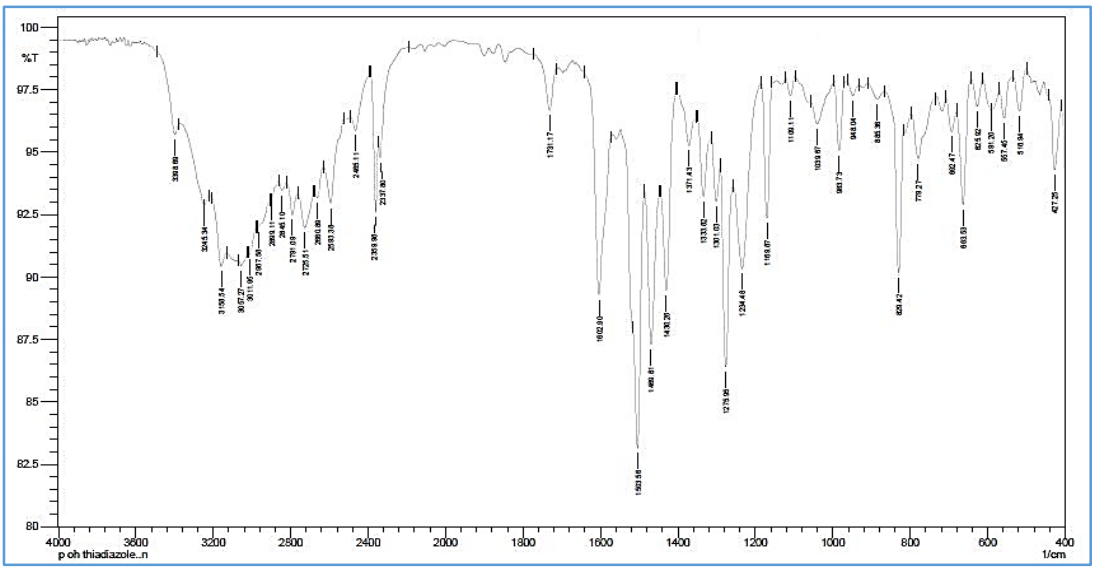

IR Spectrum of Compound (3c)

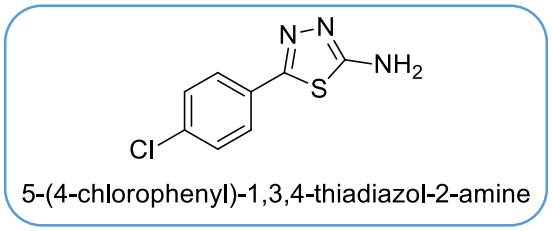

5-(4-chlorophenyl)-1,3,4-thiadiazol-2-amine

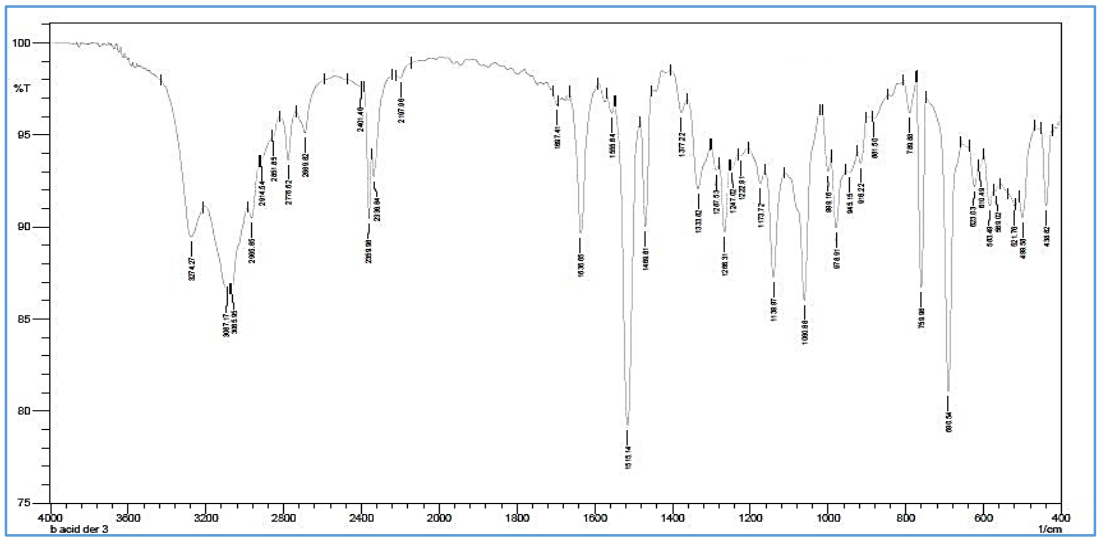

IR Spectrum of Compound (3d)

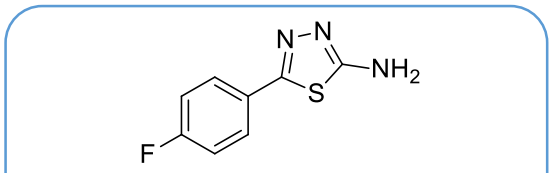

5-(4-fluorophenyl)-1,3,4-thiadiazol-2-amine

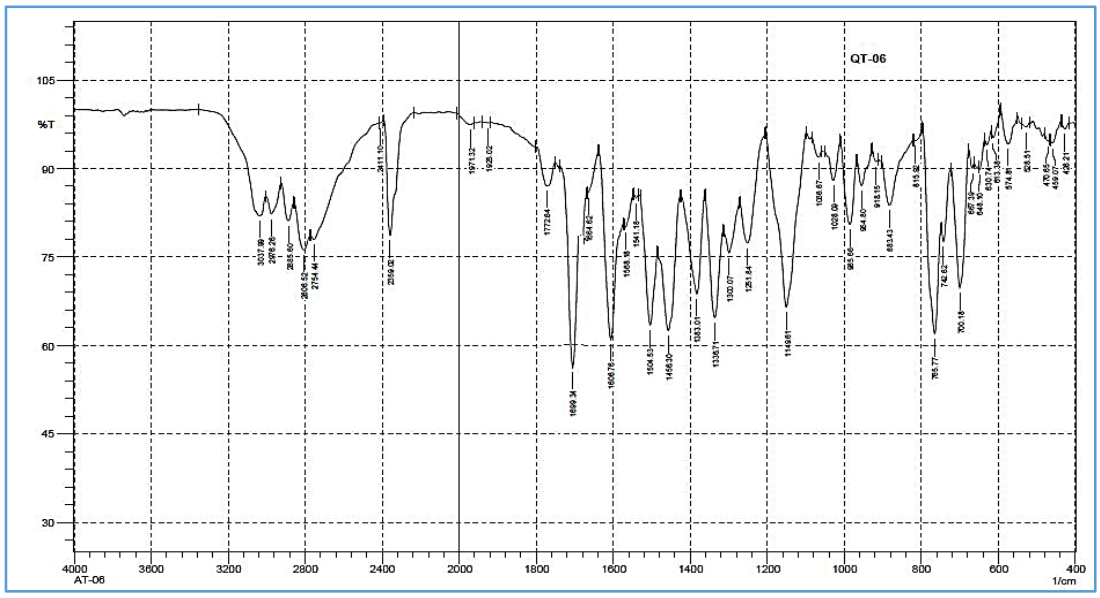

IR Spectrum of Compound (3e)

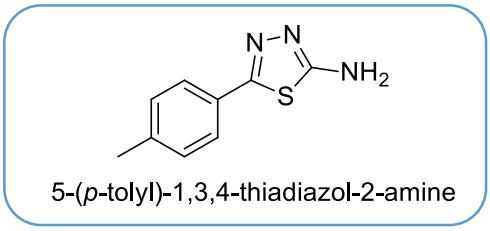

5-(*p*-tolyl)-1,3,4-thiadiazol-2-amine

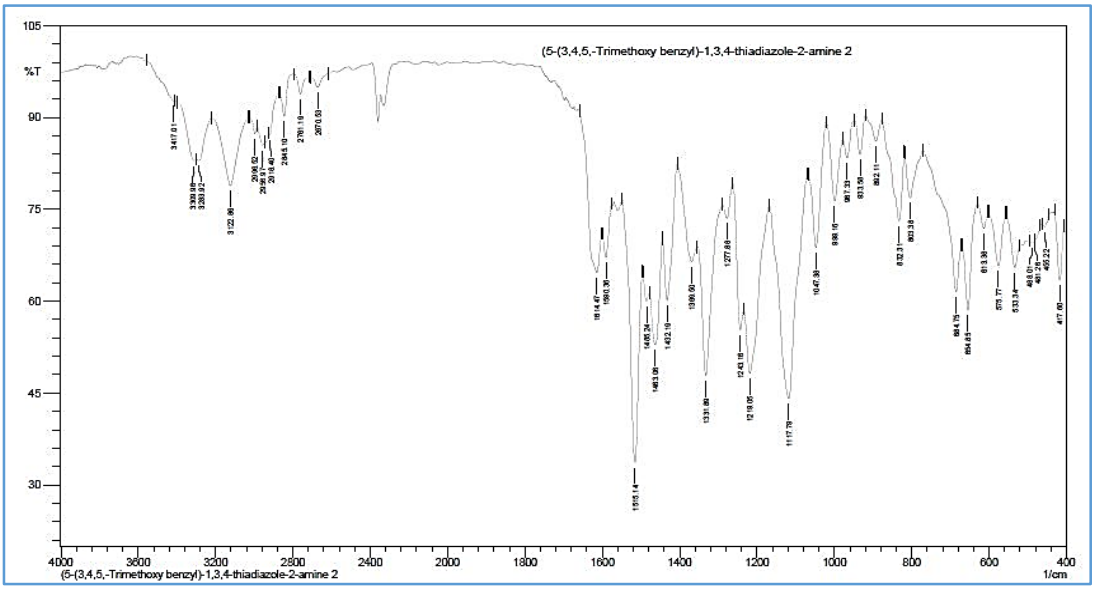

IR Spectrum of Compound (3g)

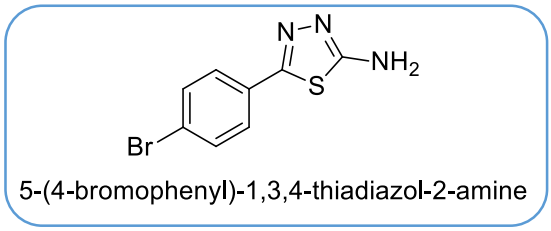

5-(4-bromophenyl)-1,3,4-thiadiazol-2-amine

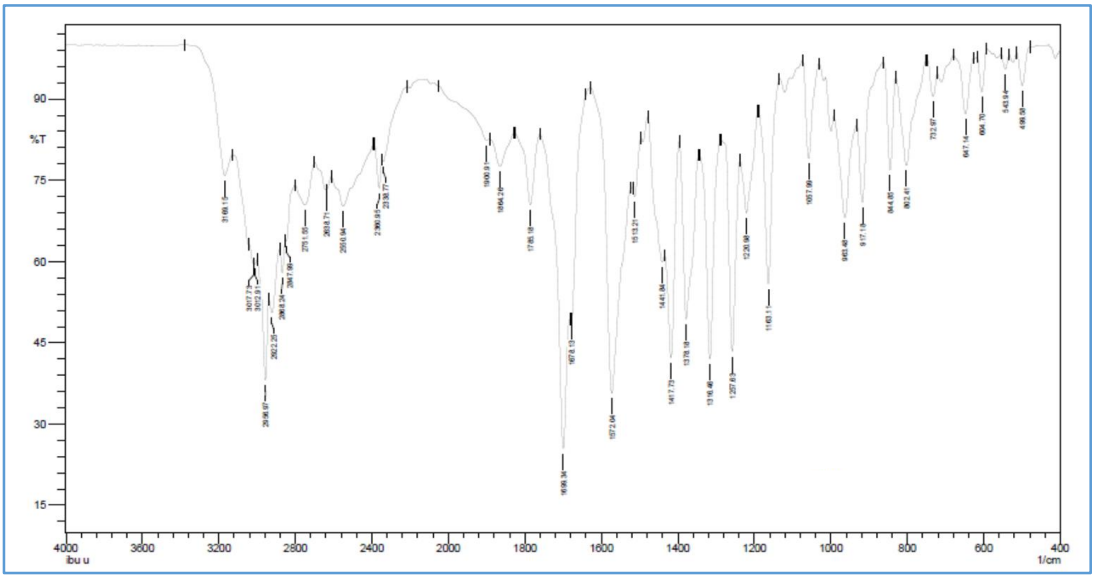

Compound 4

IR Spectrum of Compound (4)

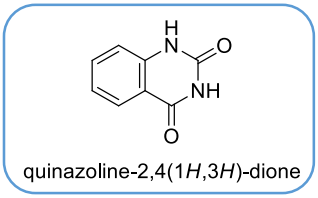

quinazoline-2,4(1*H*,3*H*)-dione

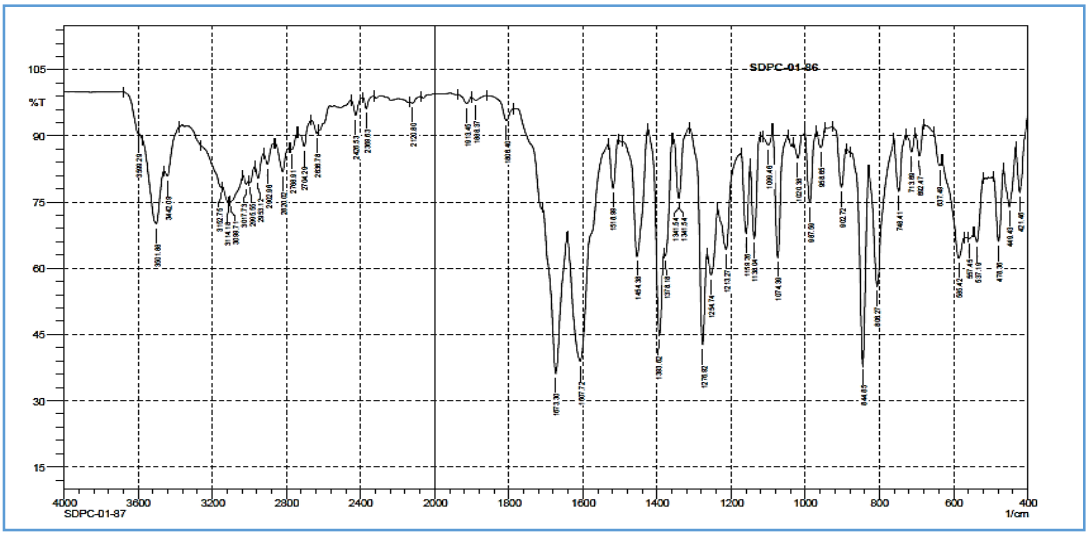

Compound 5

IR Spectrum of Compound (5)

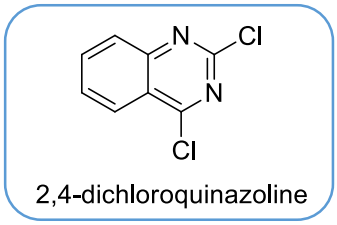

2,4-dichloroquinazoline

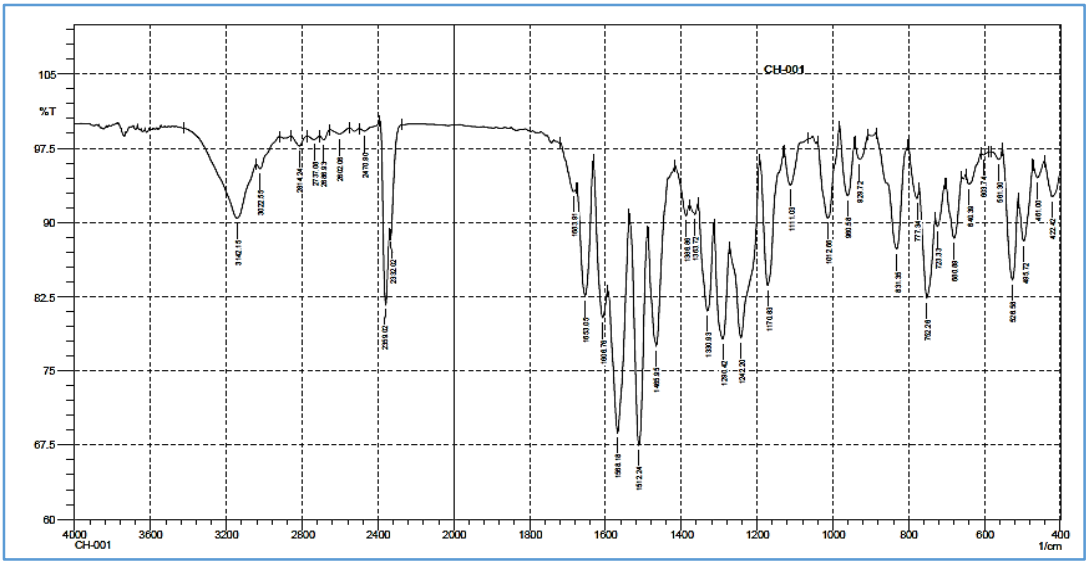

Compound 6 (a-h)

IR Spectrum of Compound (6a)

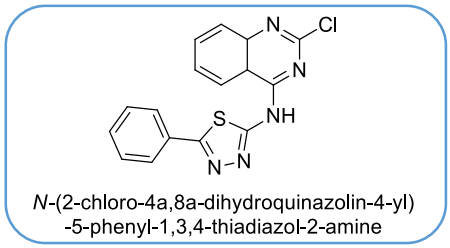

N-(2-chloro-4a,8a-dihydroquinazolin-4-yl)
-5-phenyl-1,3,4-thiadiazol-2-amine

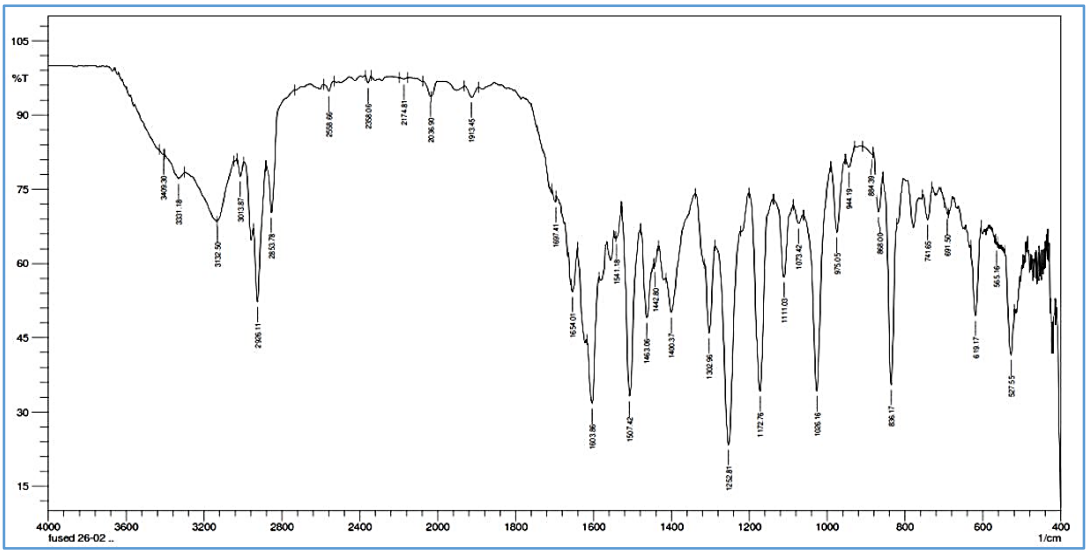

MASS Spectrum of Compound (6a)

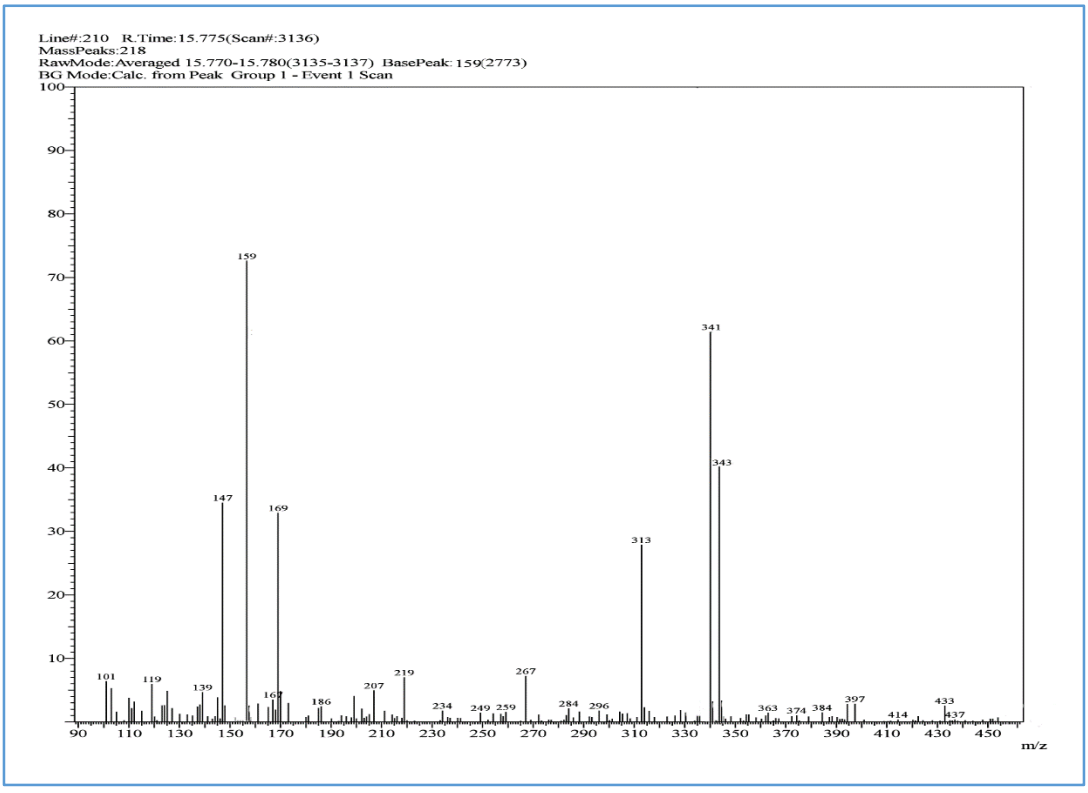

IR Spectrum of Compound (6b)

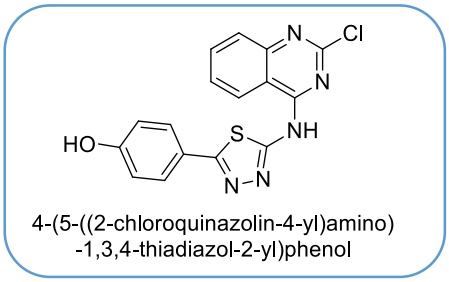

4-(5-((2-chloroquinazolin-4-yl)amino)
-1,3,4-thiadiazol-2-yl)phenol

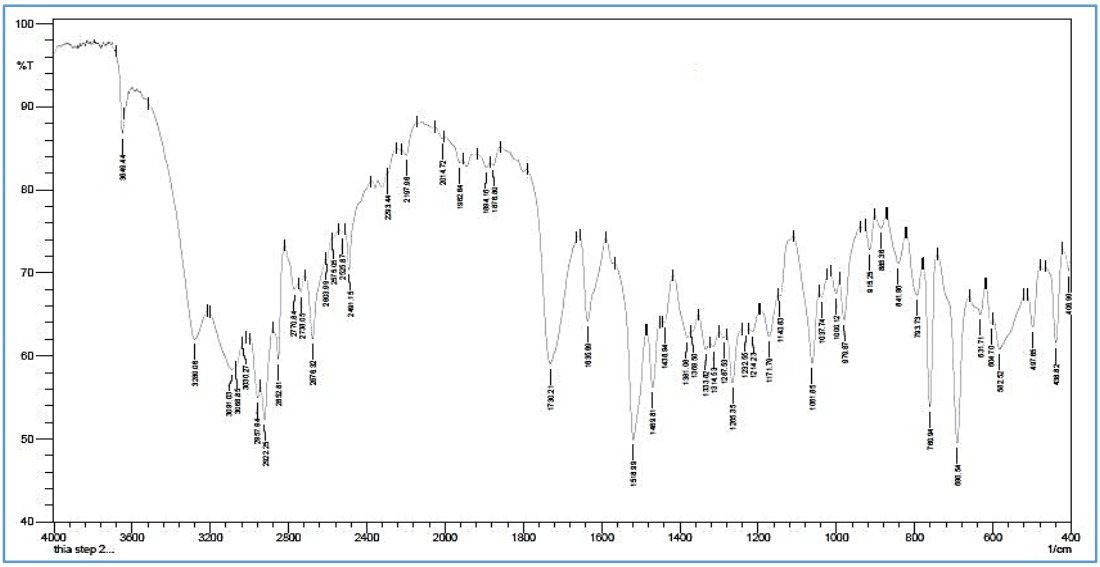

MASS Spectrum of Compound (6b)

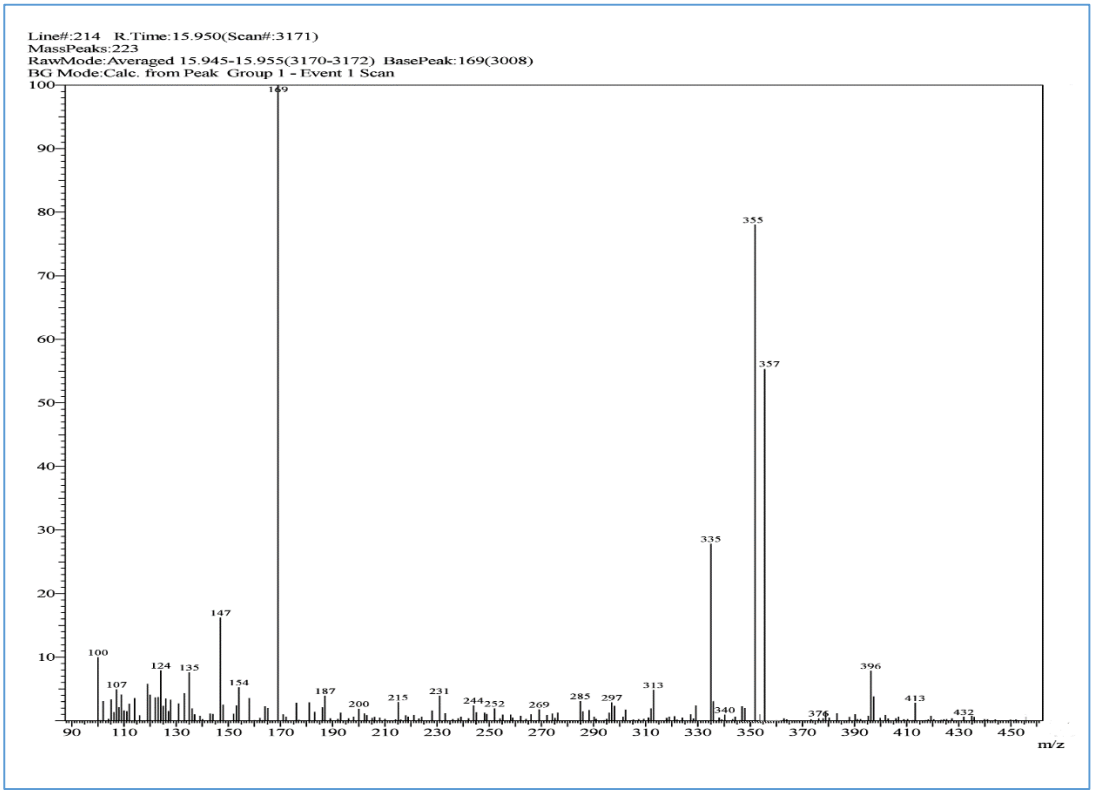

IR Spectrum of Compound (6c)

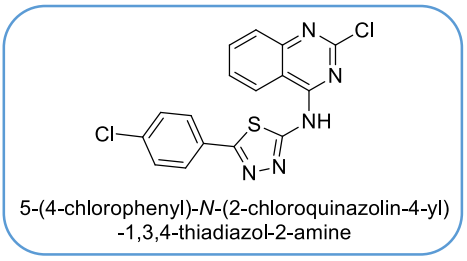

5-(4-chlorophenyl)-*N*-(2-chloroquinazolin-4-yl)
-1,3,4-thiadiazol-2-amine

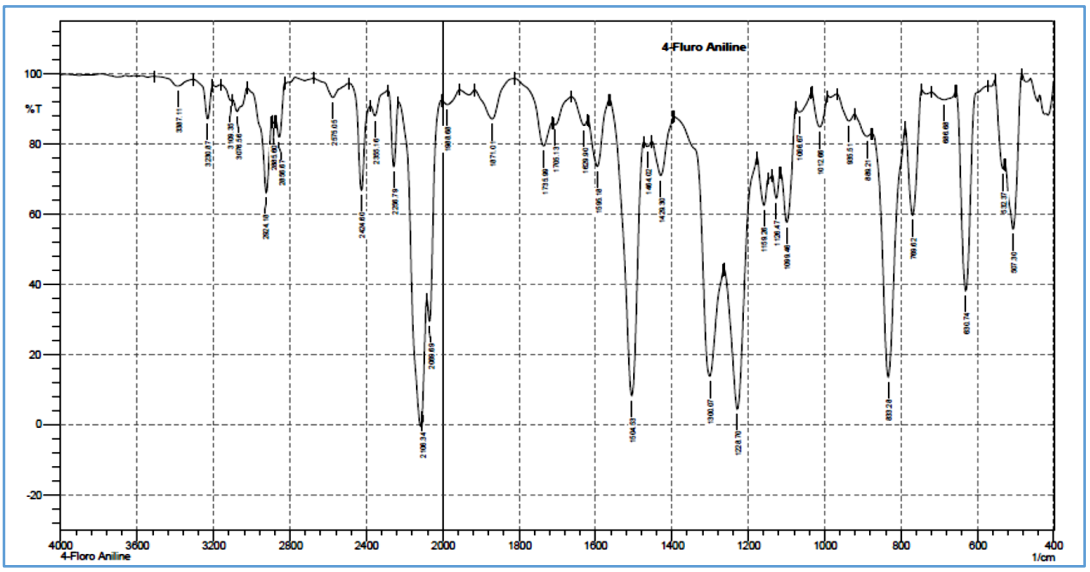

MASS Spectrum of Compound (6c)

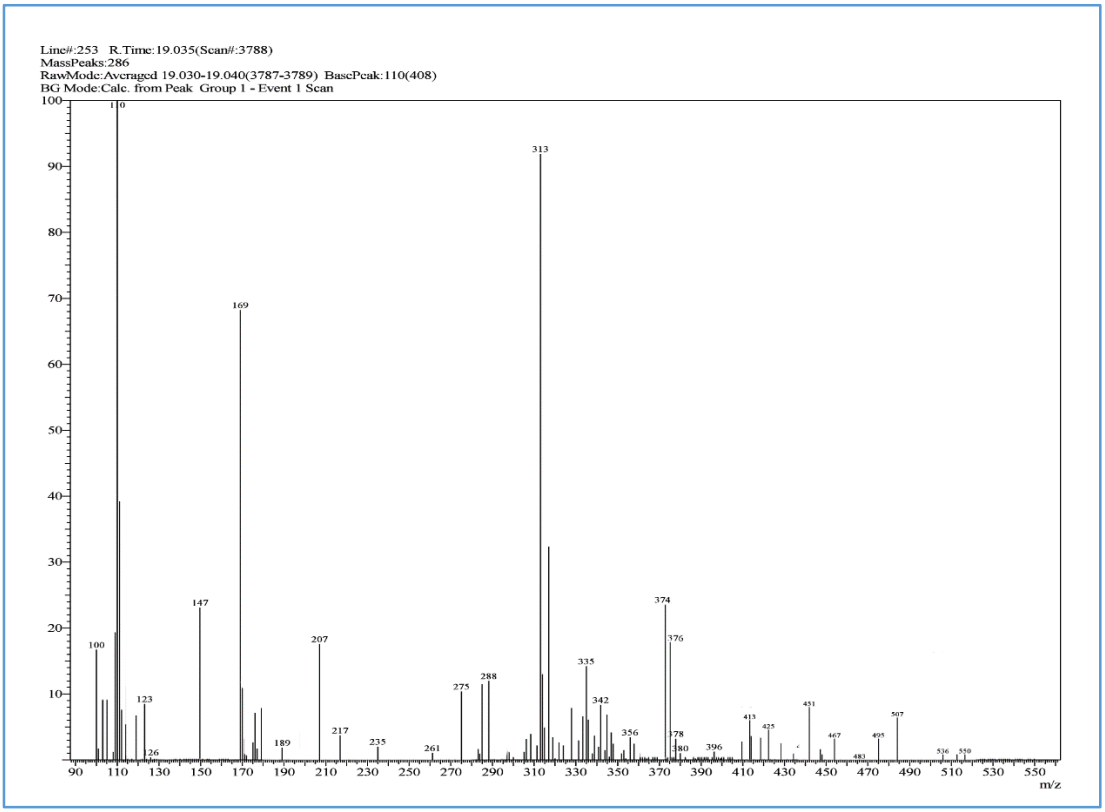

IR Spectrum of Compound (6d)

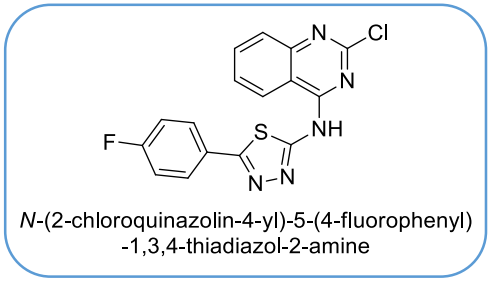

N-(2-chloroquinazolin-4-yl)-5-(4-fluorophenyl)
-1,3,4-thiadiazol-2-amine

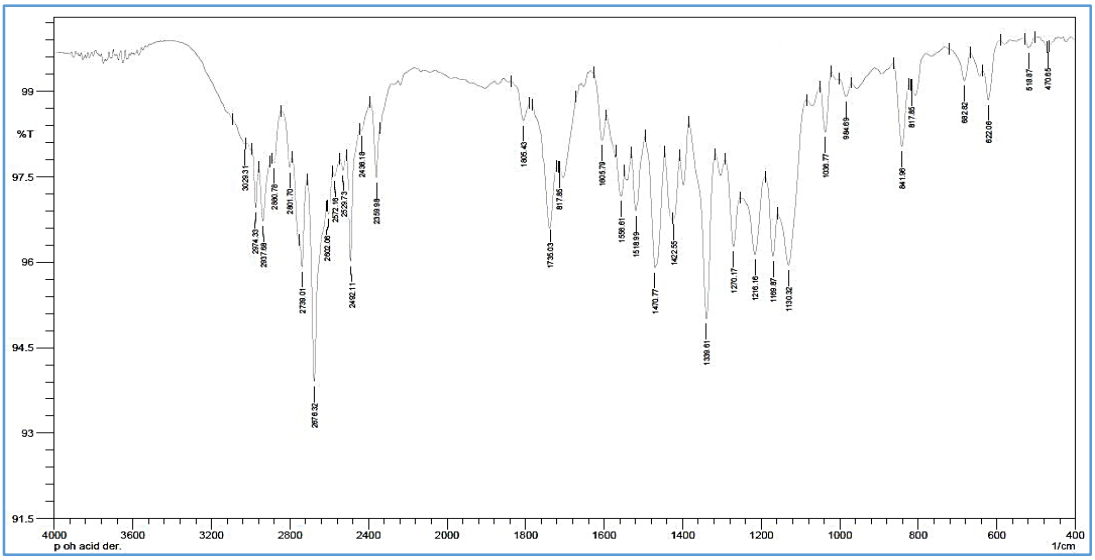

MASS Spectrum of Compound (6d)

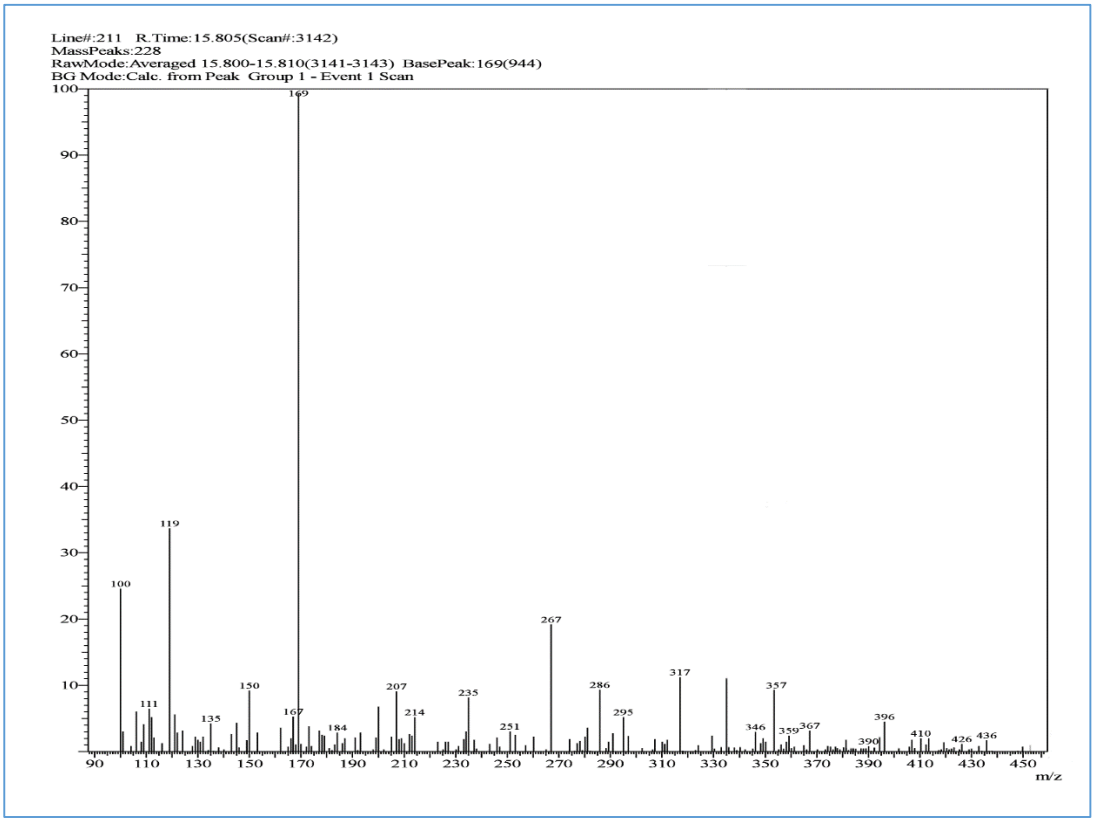

IR Spectrum of Compound (6e)

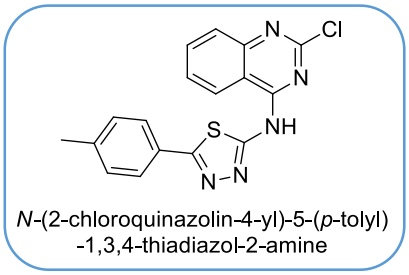

N-(2-chloroquinazolin-4-yl)-5-(*p*-tolyl)
-1,3,4-thiadiazol-2-amine

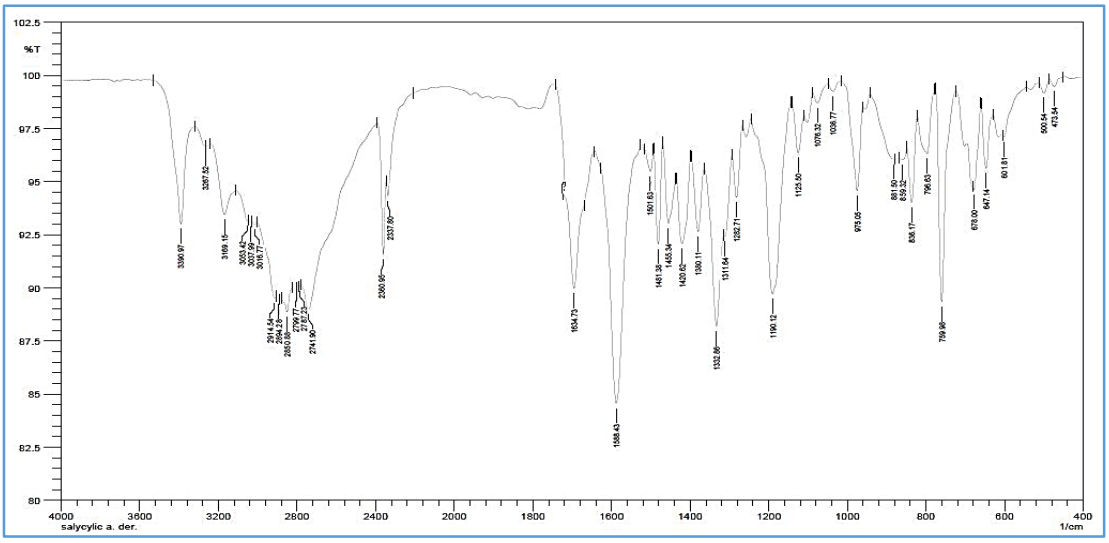

MASS Spectrum of Compound (6e)

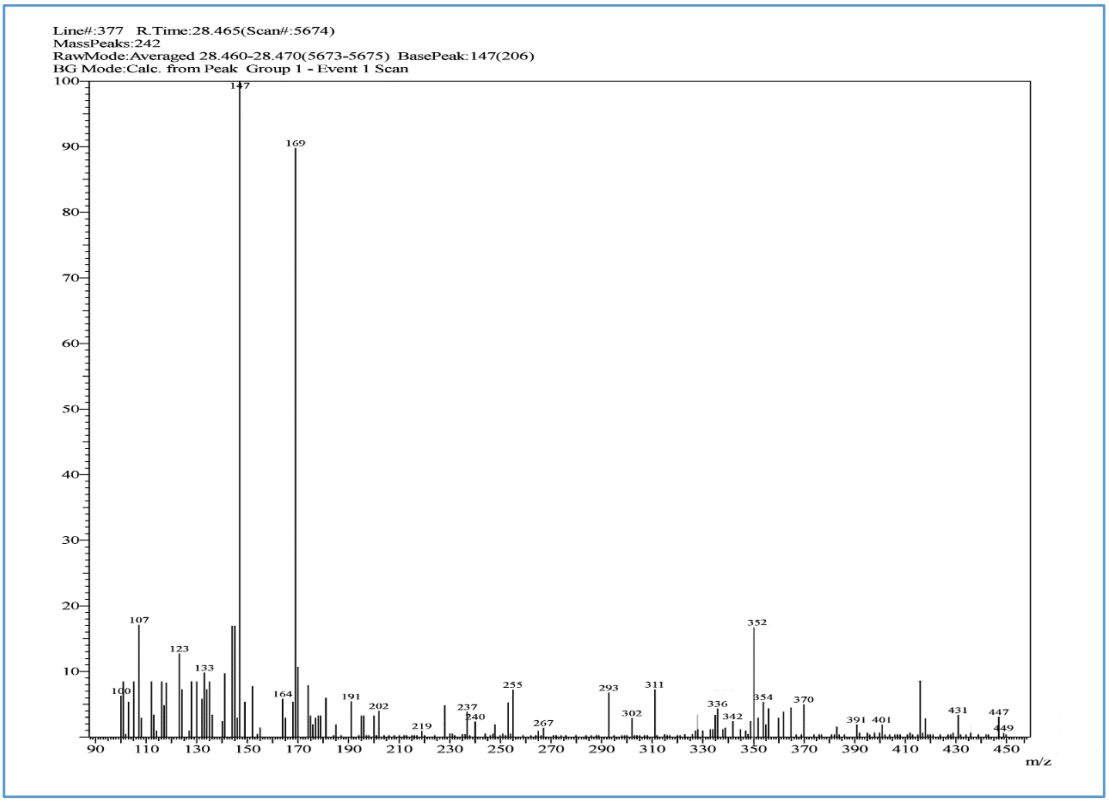

IR Spectrum of Compound (6g)

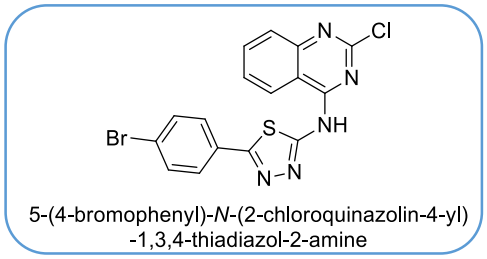

5-(4-bromophenyl)-*N*-(2-chloroquinazolin-4-yl)
-1,3,4-thiadiazol-2-amine

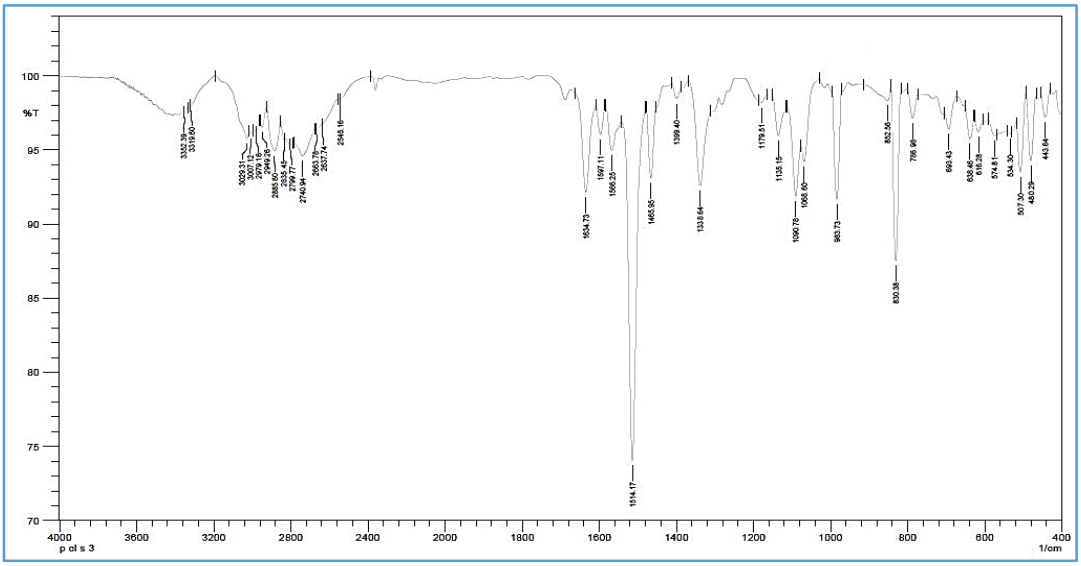

MASS Spectrum of Compound (6g)

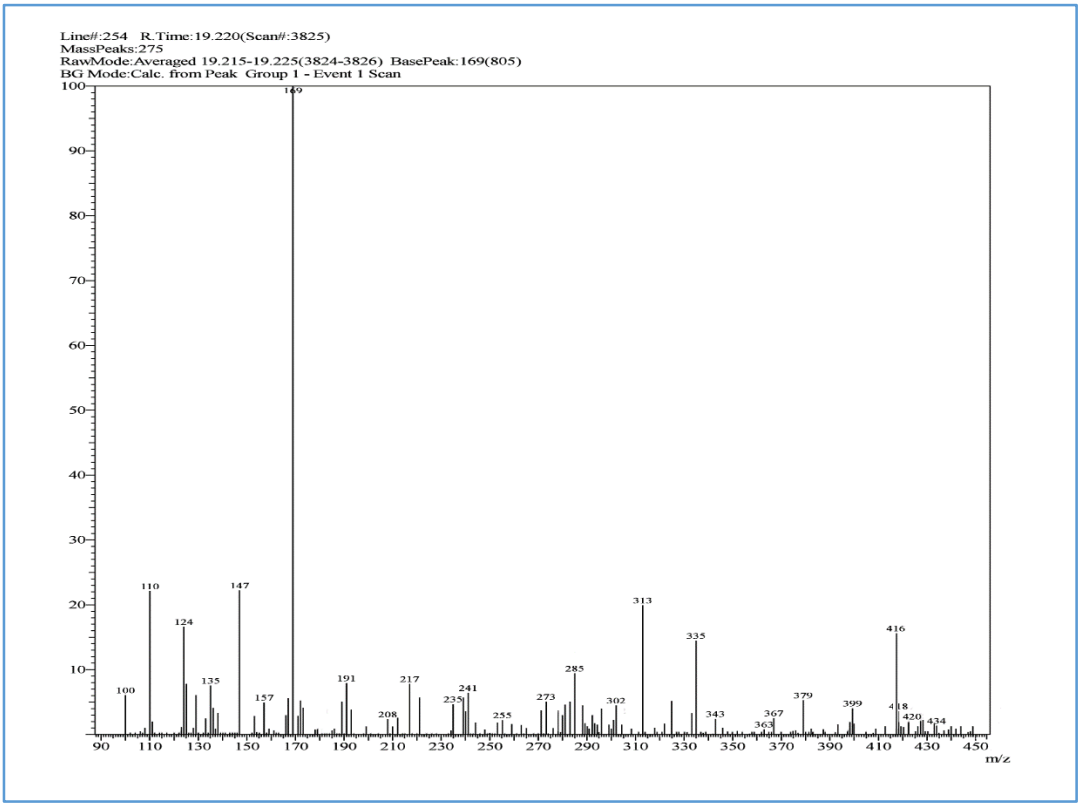

Compound 12(aI-V)-(hI-V)

IR Spectrum of Compound (12a-I)

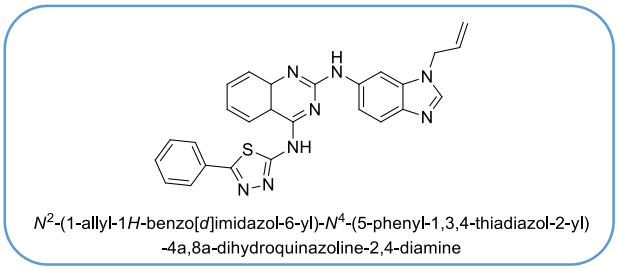

N^2-(1-allyl-1*H*-benzo[*d*]imidazol-6-yl)-N^4-(5-phenyl-1,3,4-thiadiazol-2-yl)
-4a,8a-dihydroquinazoline-2,4-diamine

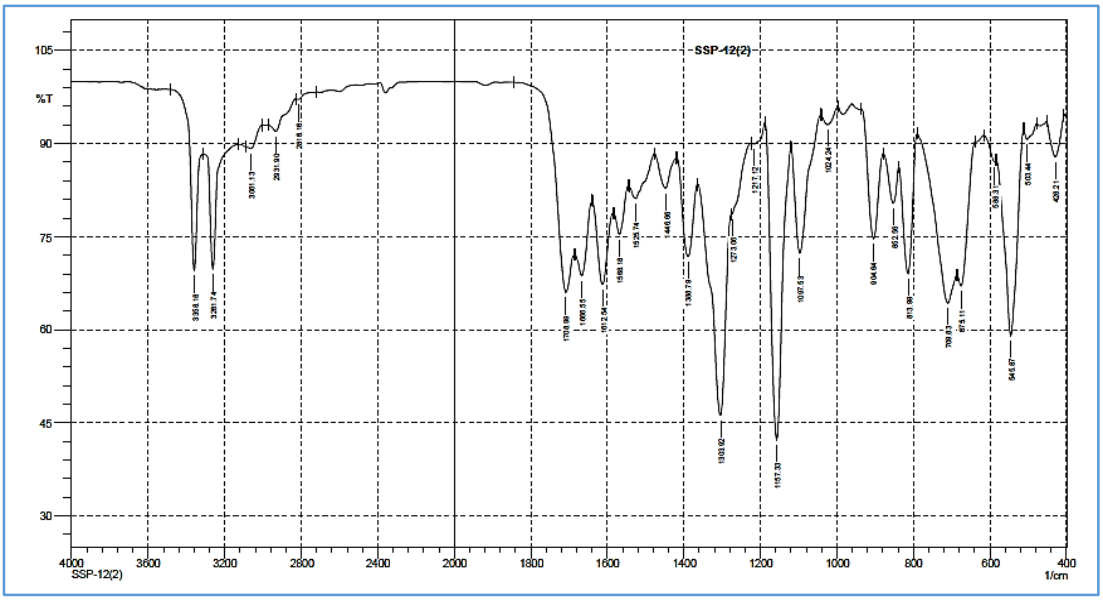

NMR Spectrum of Compound (12a-I)

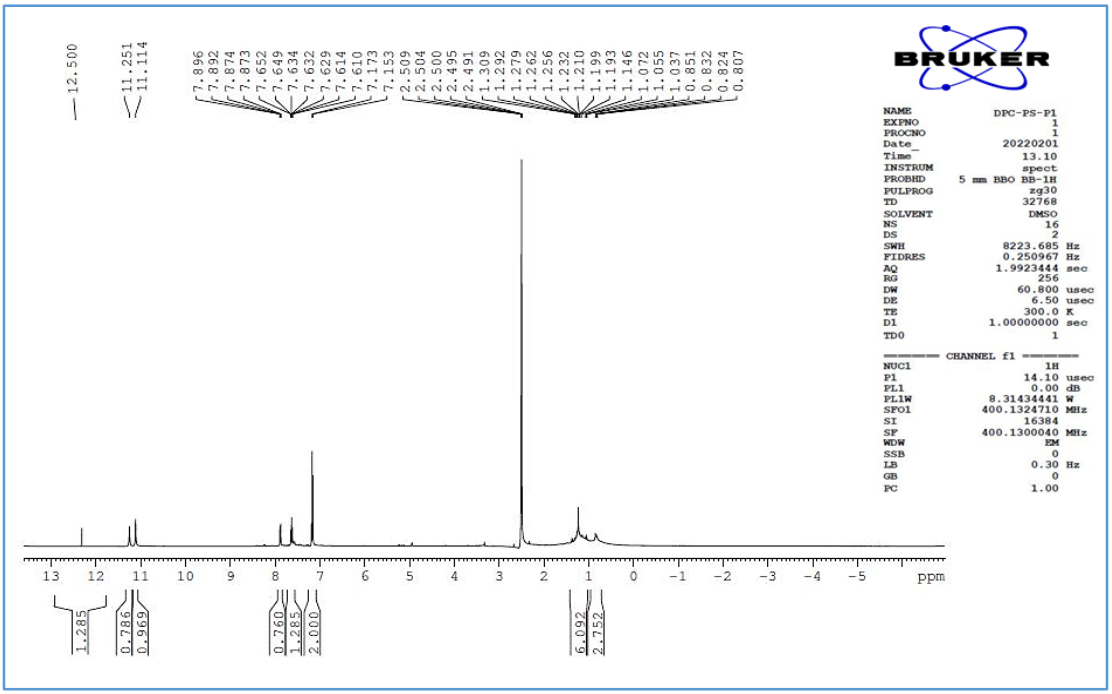

MASS Spectrum of Compound (12a-I)

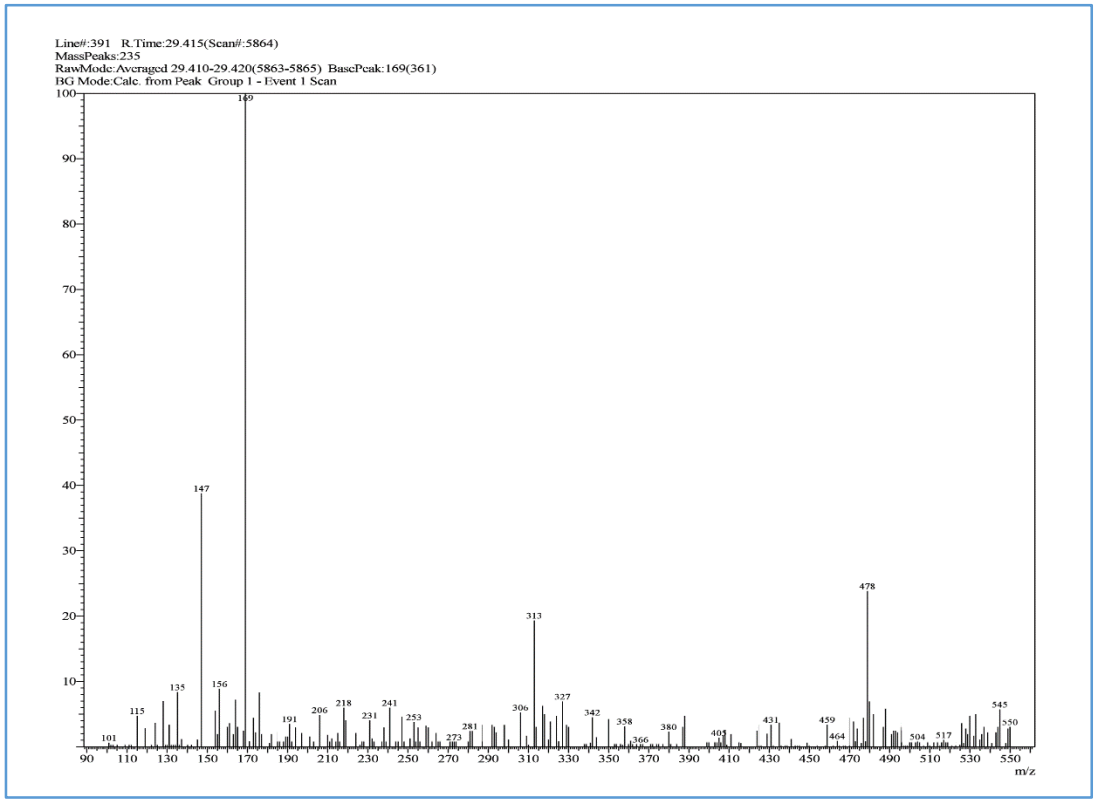

IR Spectrum of Compound (12a-II)

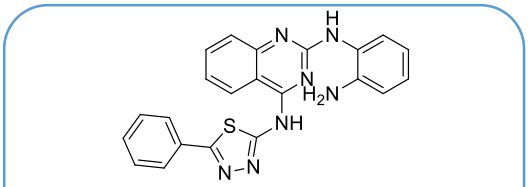

N^2-(2-aminophenyl)-N^4-(5-phenyl-1,3,4-thiadiazol-2-yl) quinazoline-2,4-diamine

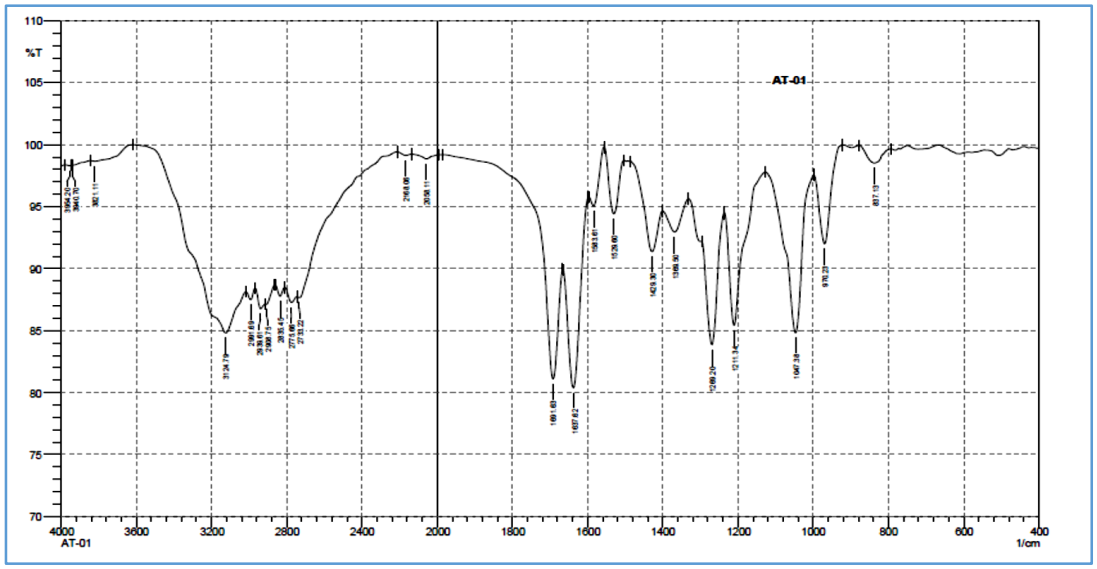

NMR Spectrum of Compound (12a-II)

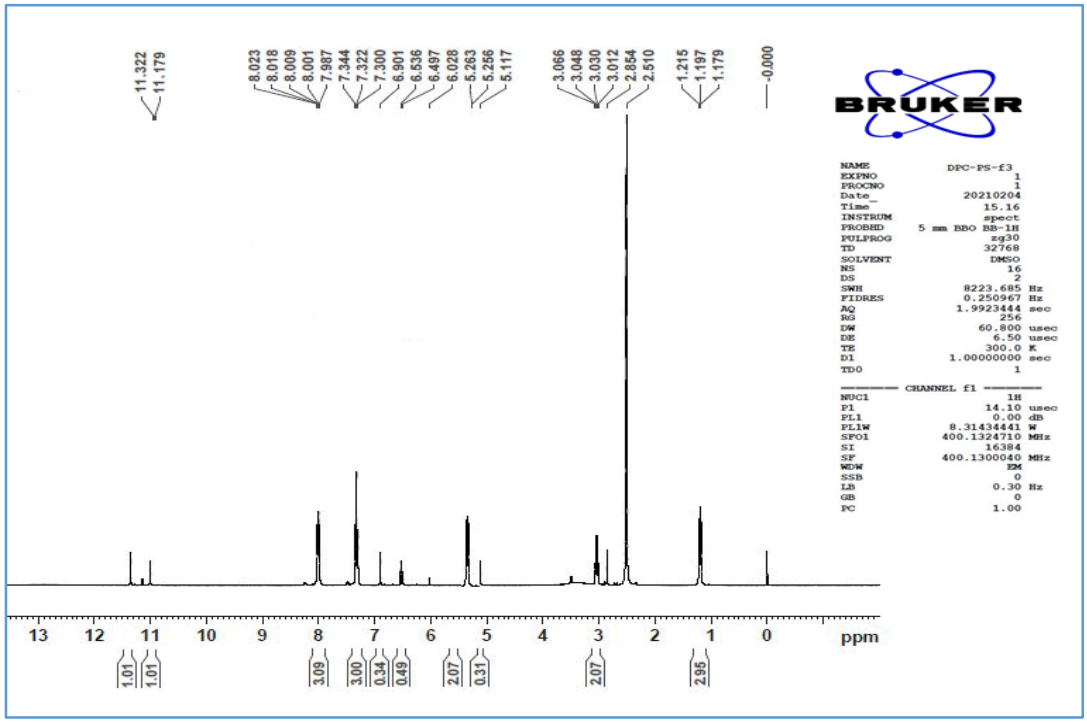

MASS Spectrum of Compound (12a-II)

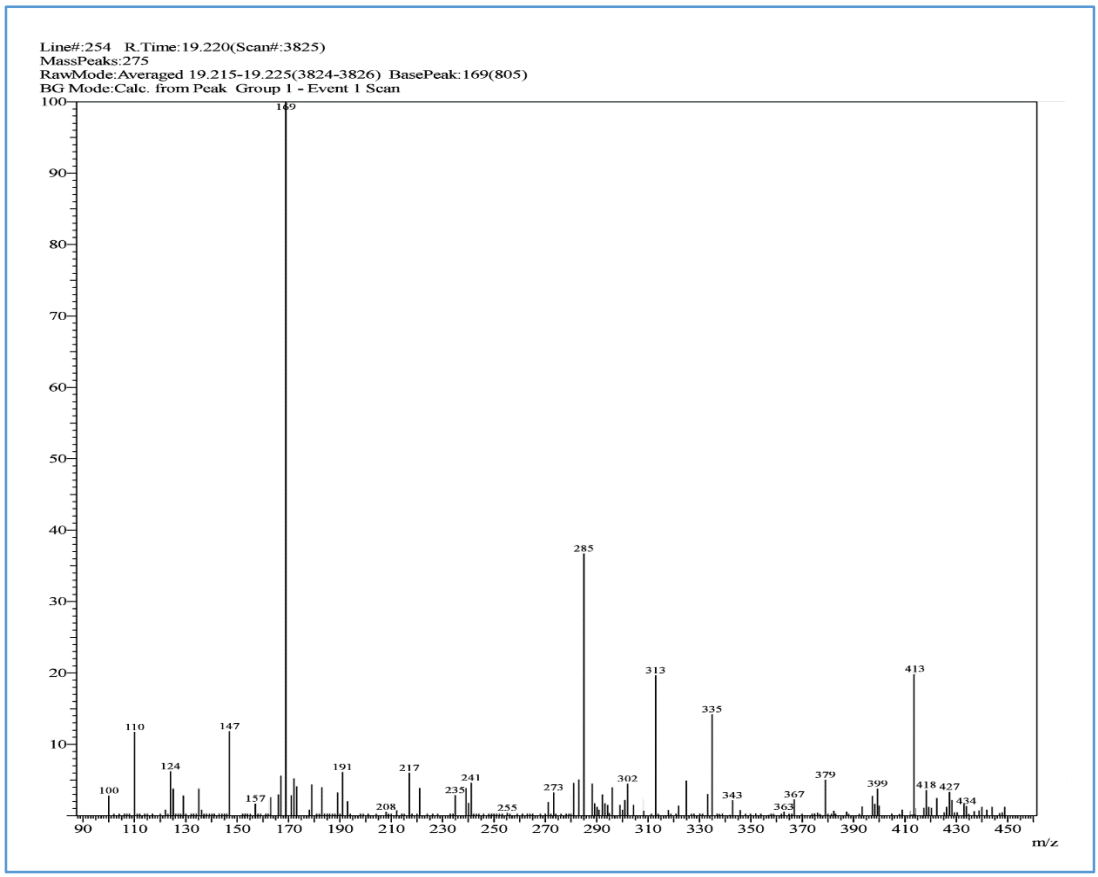

IR Spectrum of Compound (12a-III)

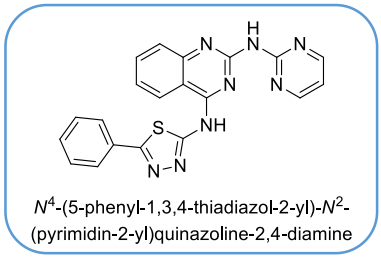

N^4-(5-phenyl-1,3,4-thiadiazol-2-yl)-N^2-(pyrimidin-2-yl)quinazoline-2,4-diamine

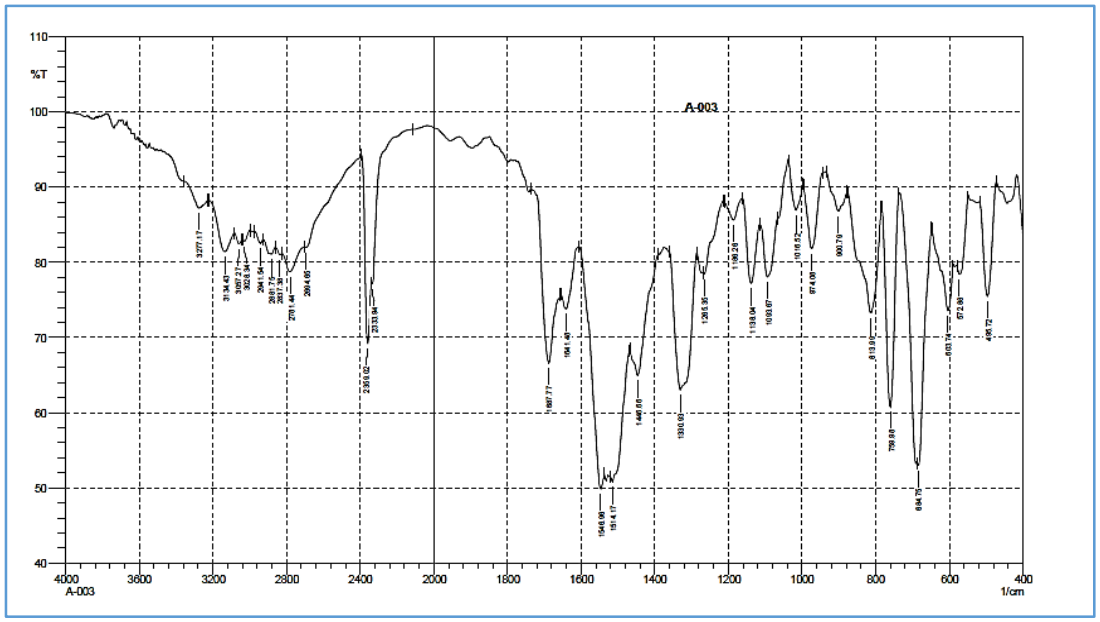

NMR Spectrum of Compound (12a-III)

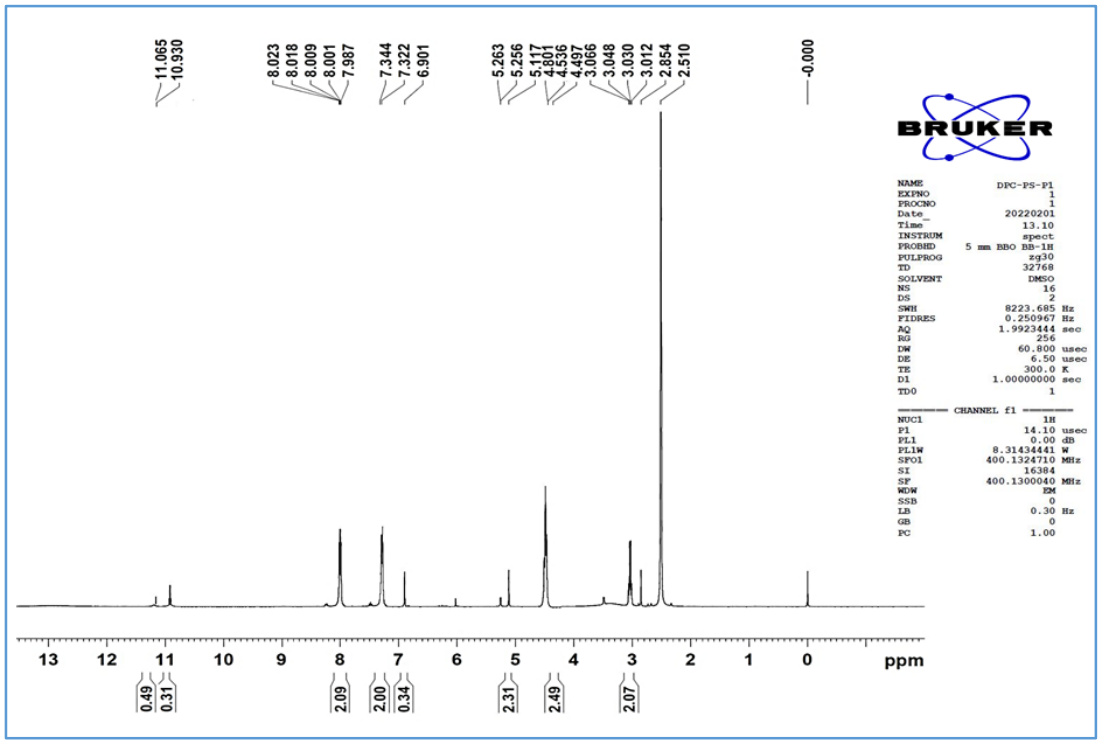

MASS Spectrum of Compound (12a-III)

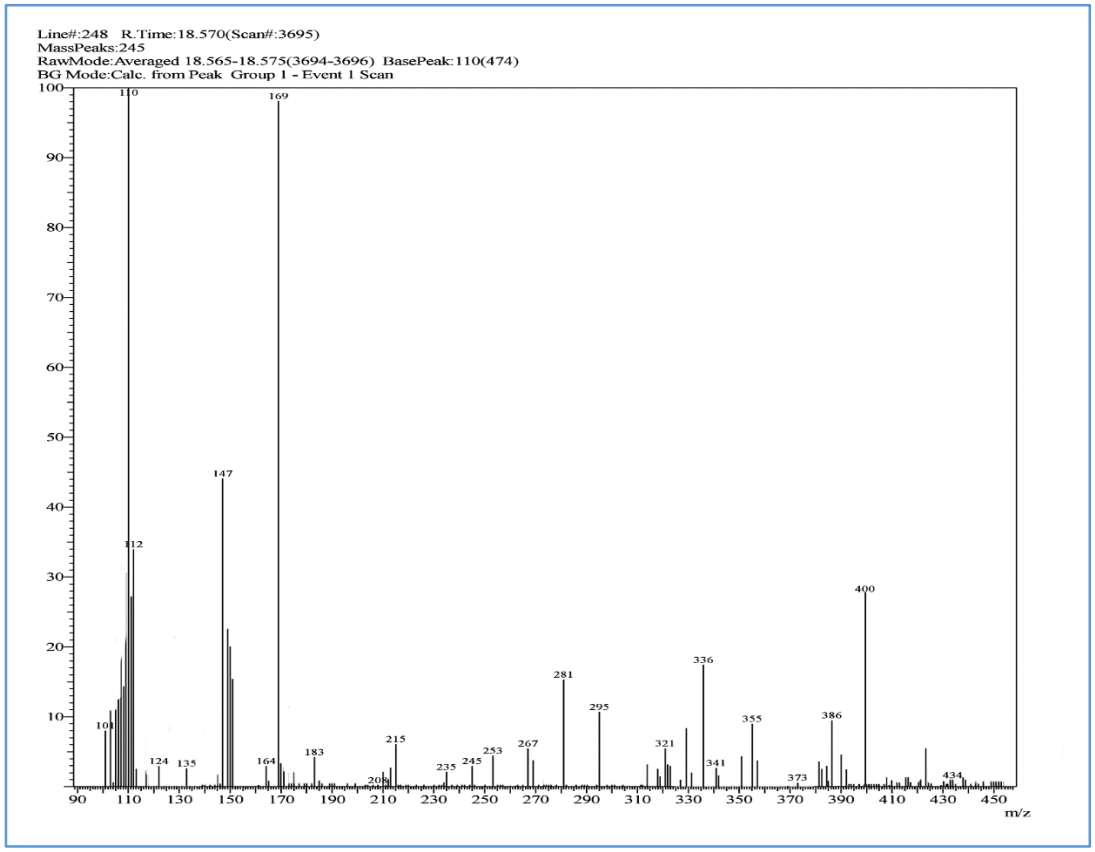

IR Spectrum of Compound (12a-IV)

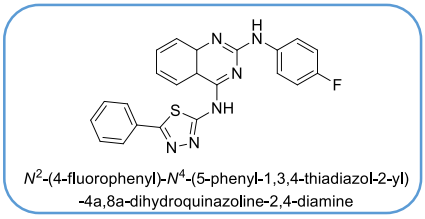

N^2-(4-fluorophenyl)-N^4-(5-phenyl-1,3,4-thiadiazol-2-yl)
-4a,8a-dihydroquinazoline-2,4-diamine

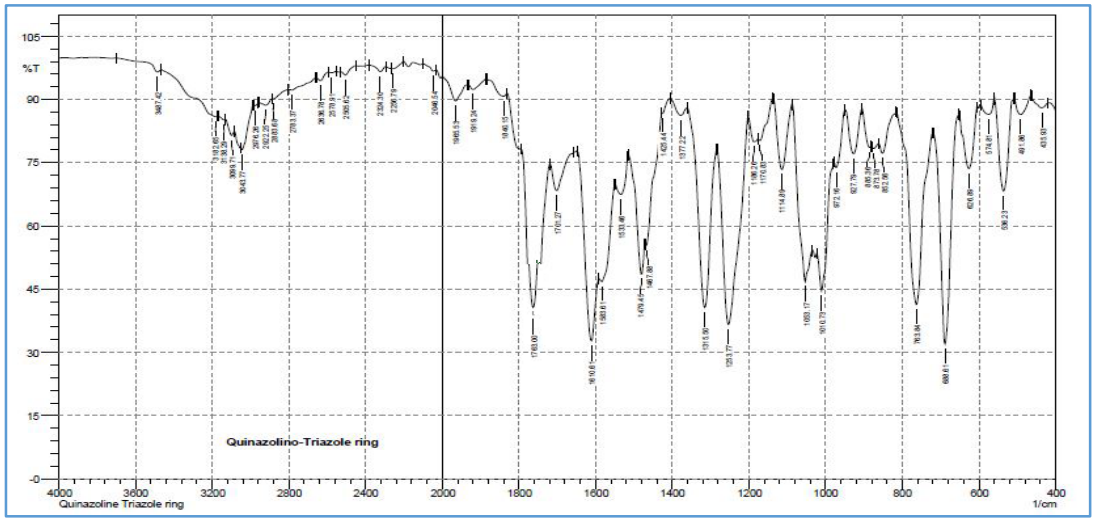

NMR Spectrum of Compound (12a-IV)

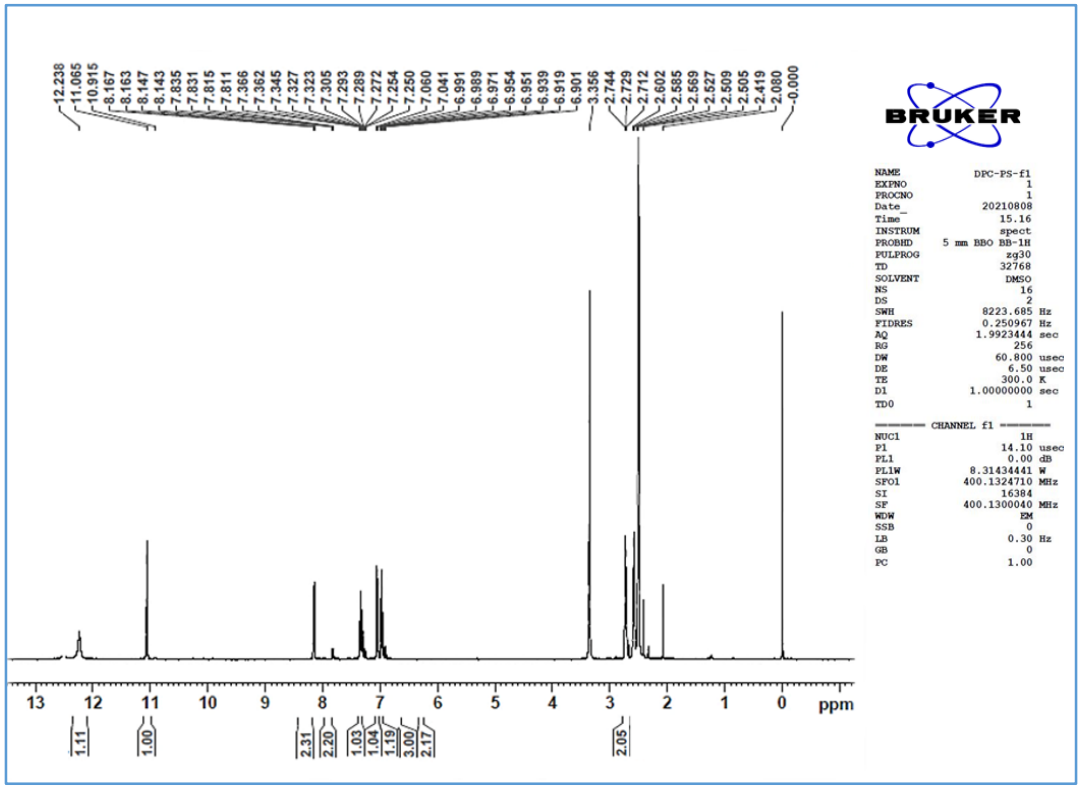

MASS Spectrum of Compound (12a-IV)

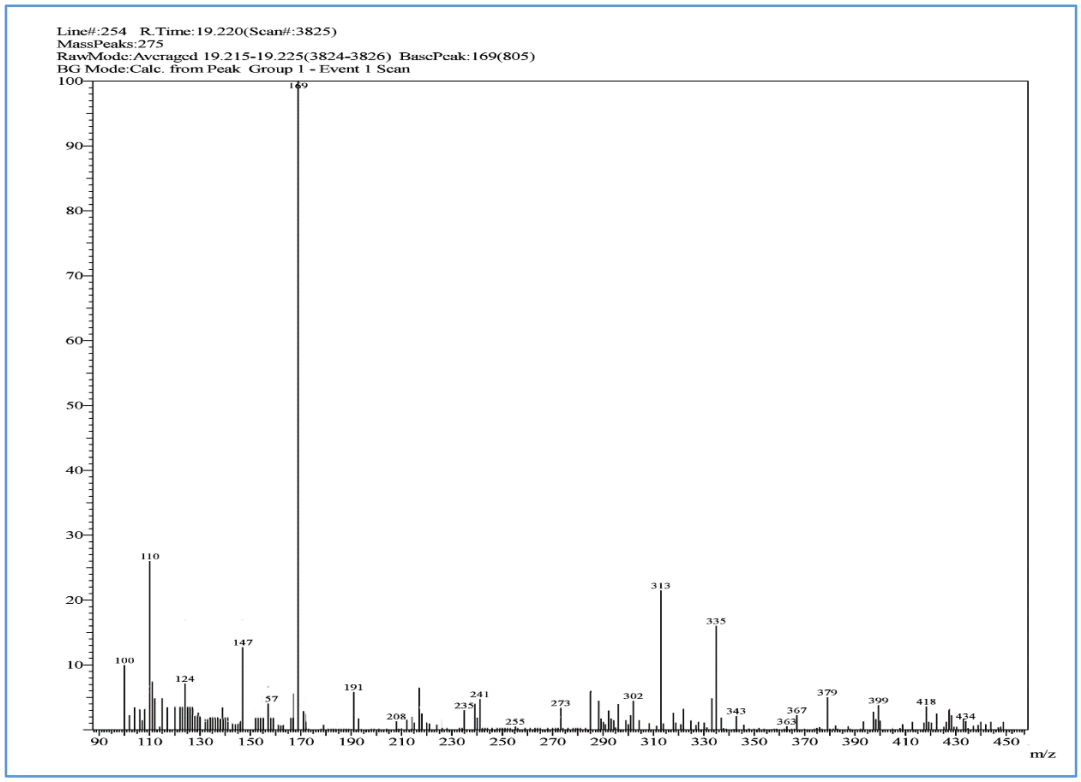

IR Spectrum of Compound (12a-V)

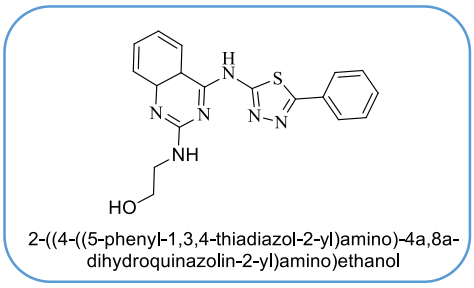

2-((4-((5-phenyl-1,3,4-thiadiazol-2-yl)amino)-4a,8a-dihydroquinazolin-2-yl)amino)ethanol

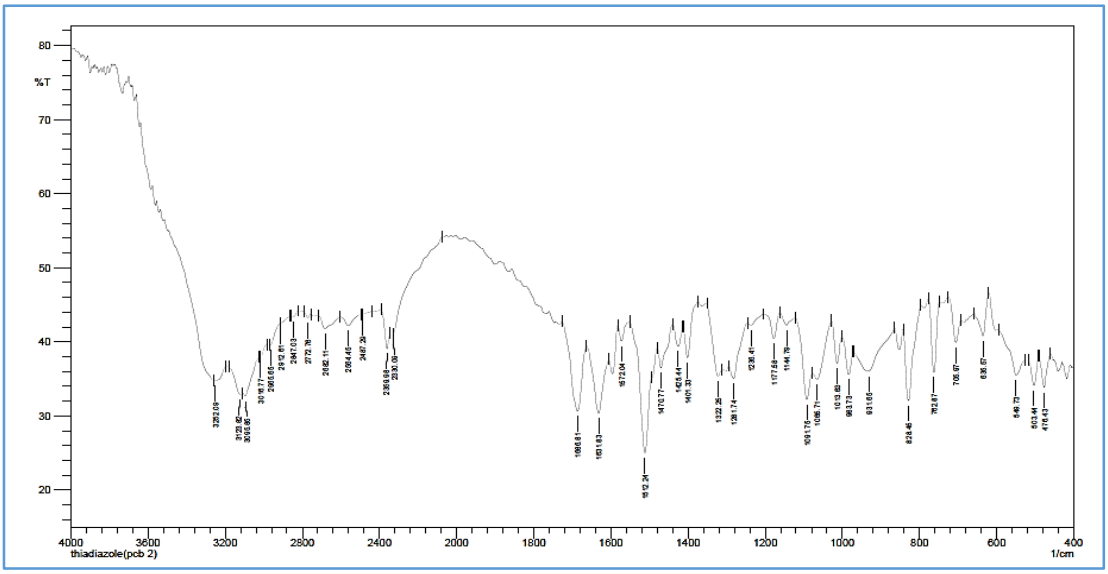

NMR Spectrum of Compound (12a-V)

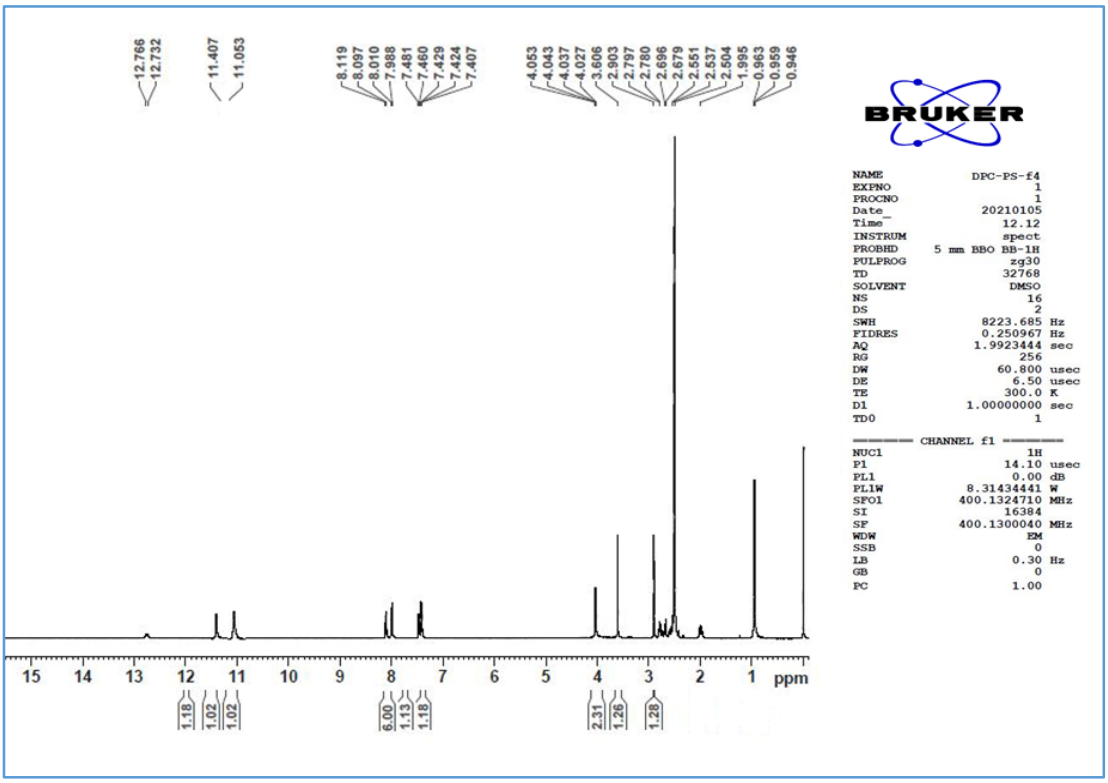

MASS Spectrum of Compound (12a-V)

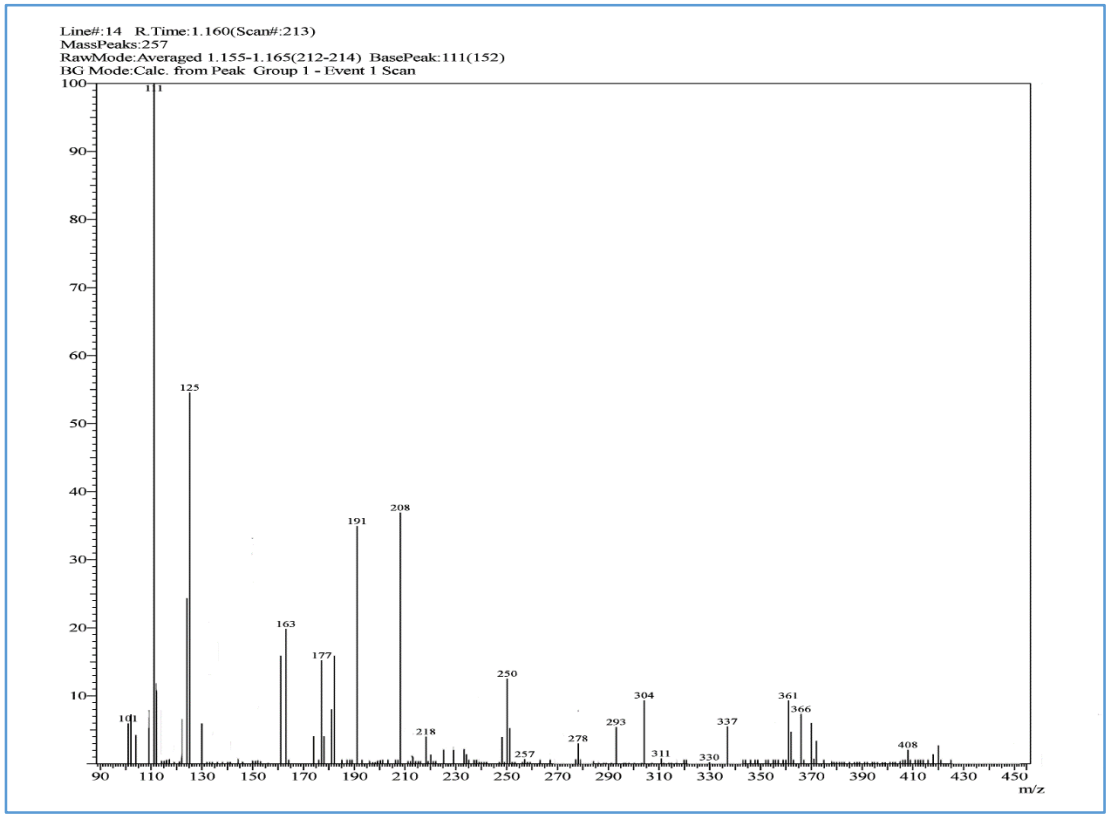

IR Spectrum of Compound (12b-I)

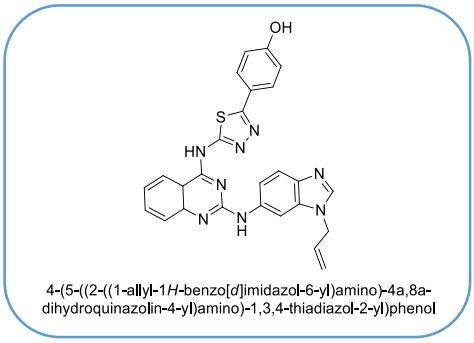

4-(5-((2-((1-allyl-1*H*-benzo[*d*]imidazol-6-yl)amino)-4a,8a-dihydroquinazolin-4-yl)amino)-1,3,4-thiadiazol-2-yl)phenol

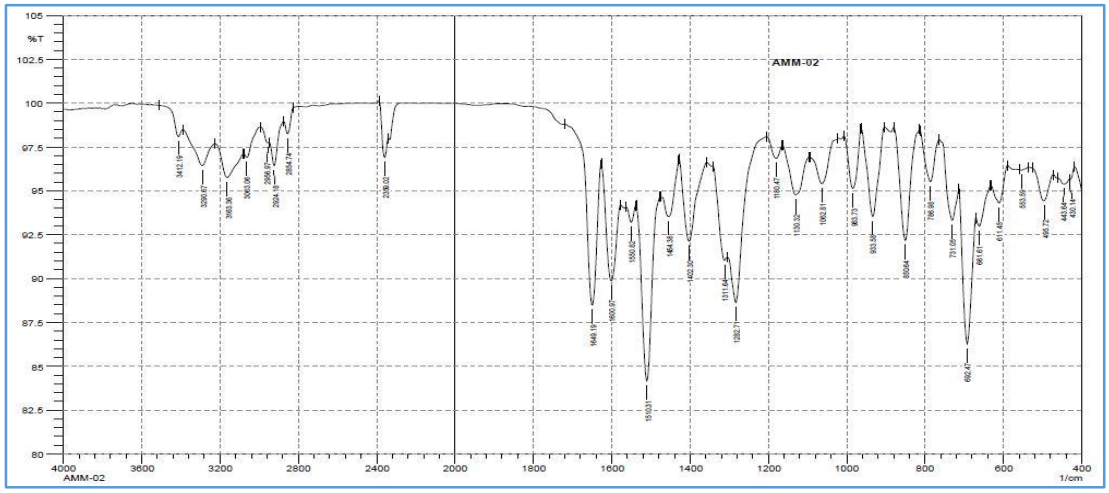

NMR Spectrum of Compound (12b-I)

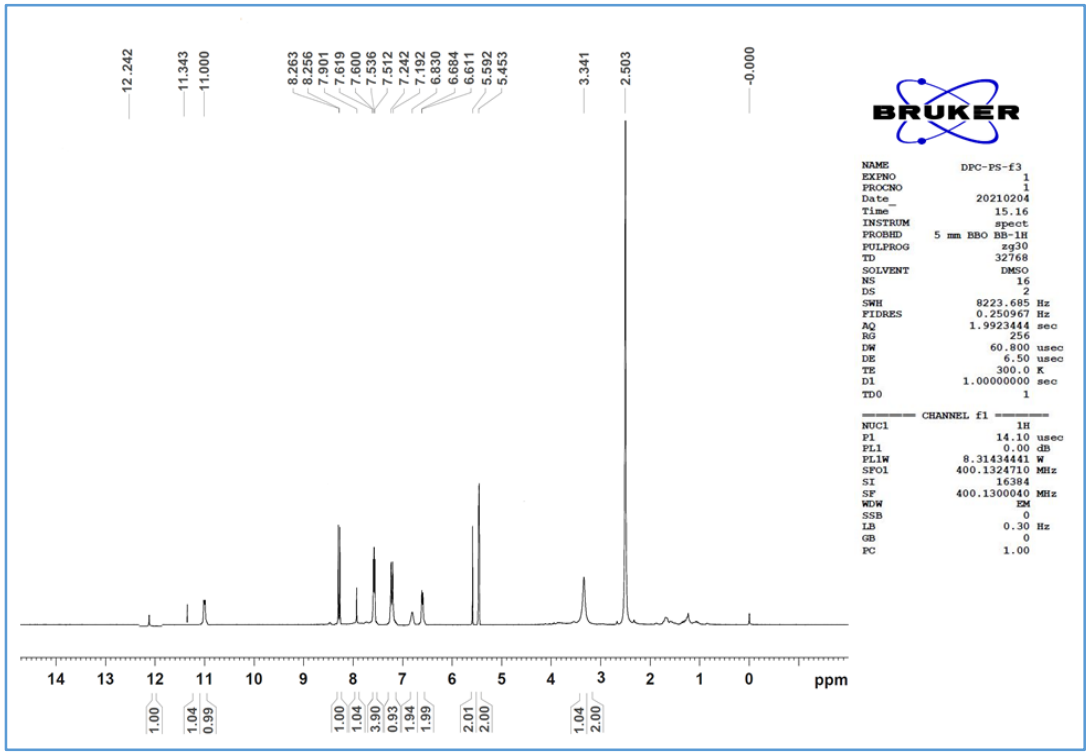

MASS Spectrum of Compound (12b-I)

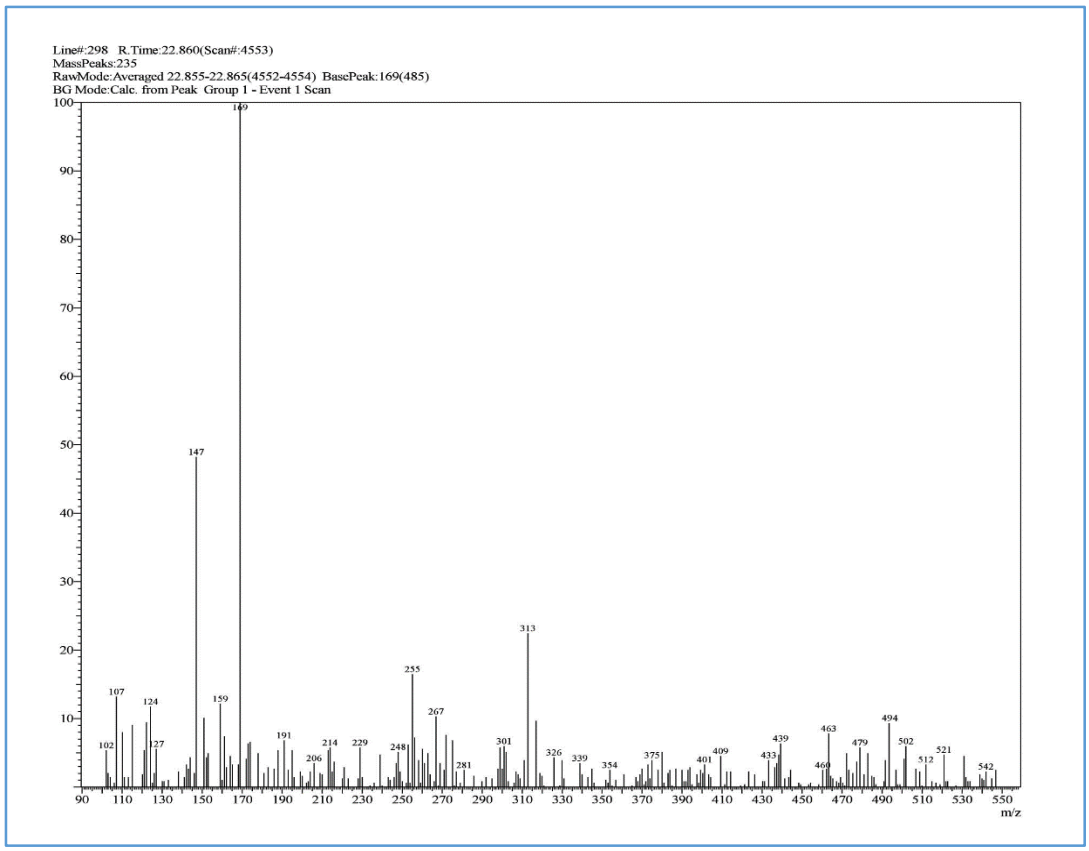

IR Spectrum of Compound (12b-III)

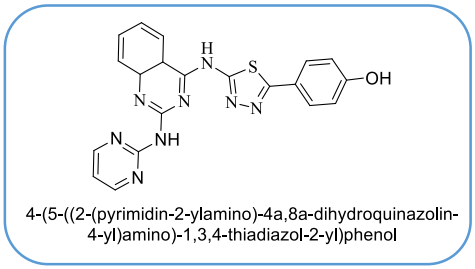

4-(5-((2-(pyrimidin-2-ylamino)-4a,8a-dihydroquinazolin-4-yl)amino)-1,3,4-thiadiazol-2-yl)phenol

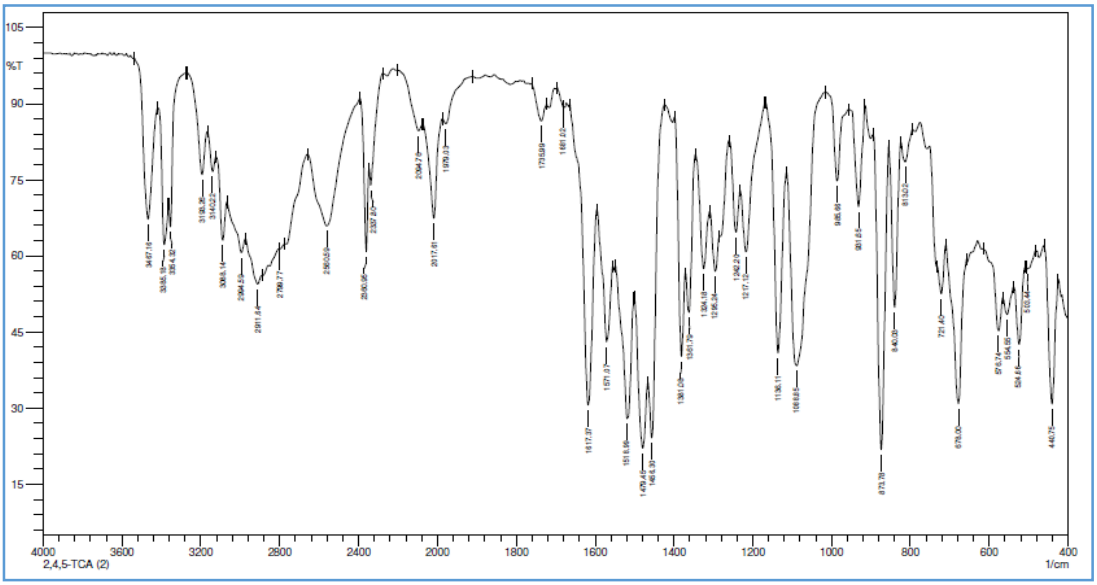

NMR Spectrum of Compound (12b-III)

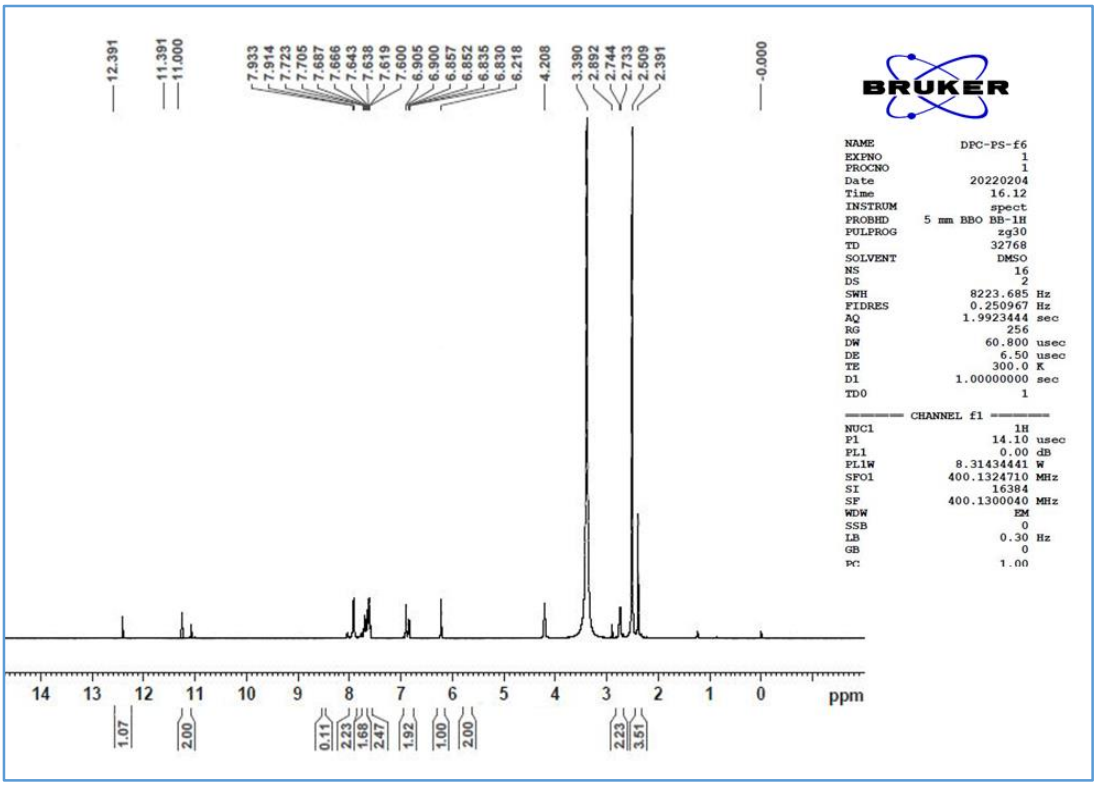

MASS Spectrum of Compound (12b-III)

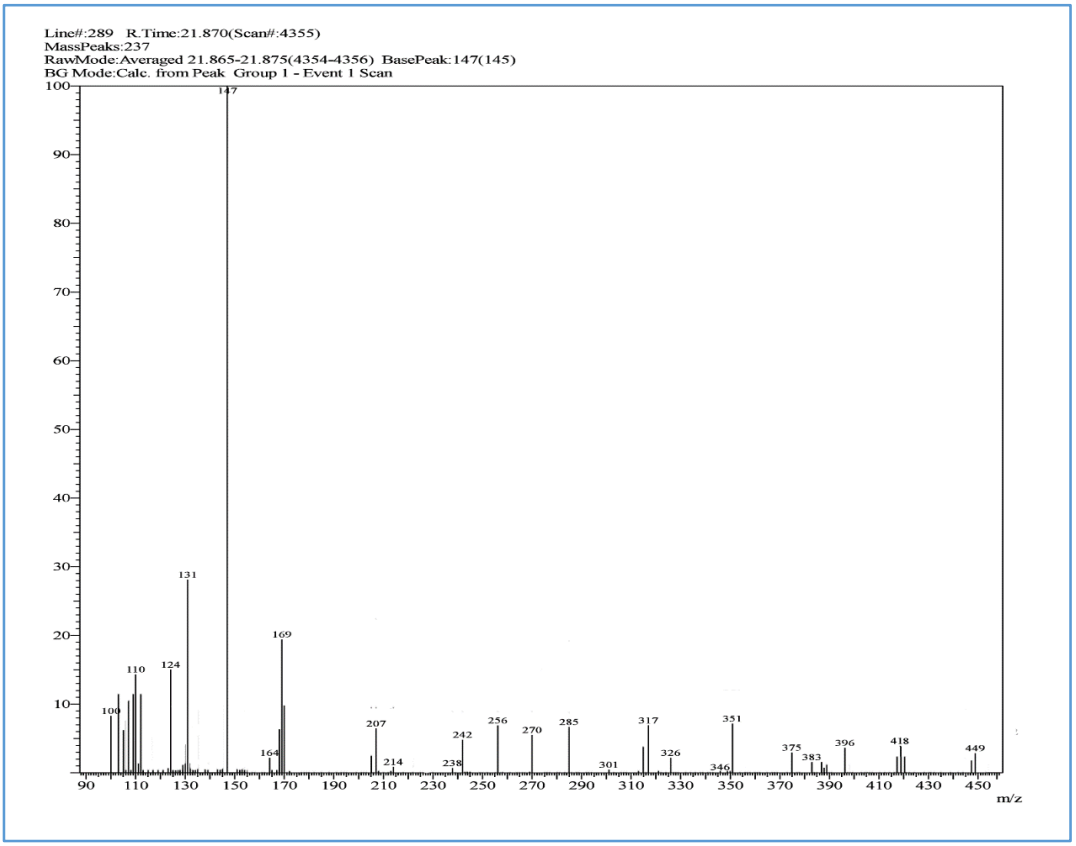

IR Spectrum of Compound (12b-IV)

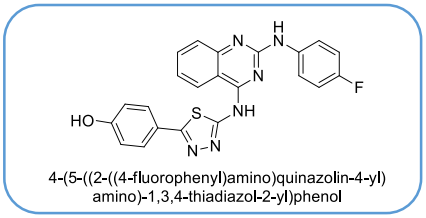

4-(5-((2-((4-fluorophenyl)amino)quinazolin-4-yl) amino)-1,3,4-thiadiazol-2-yl)phenol

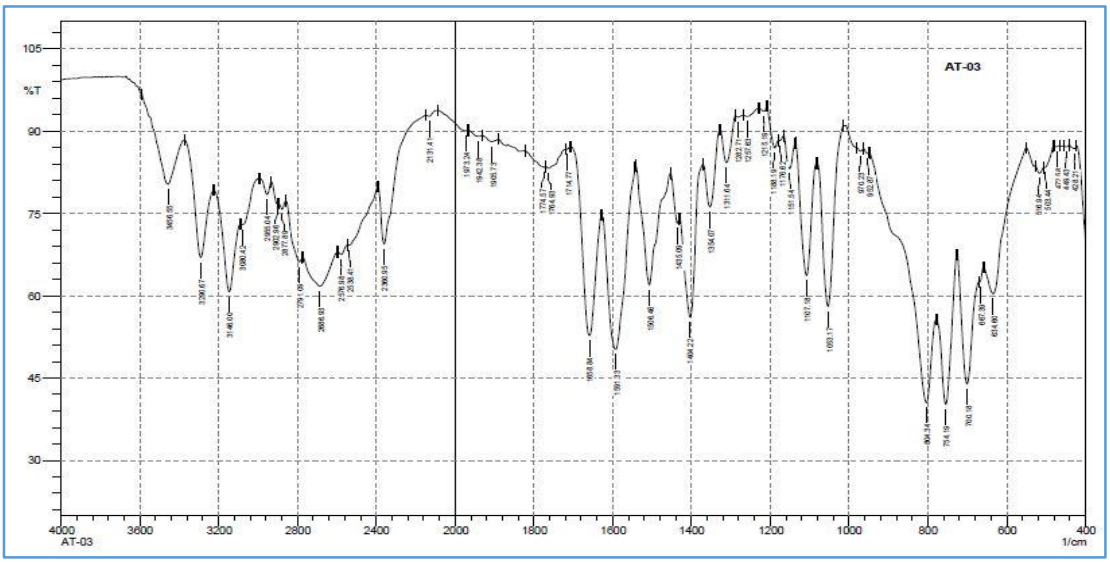

NMR Spectrum of Compound (12b-IV)

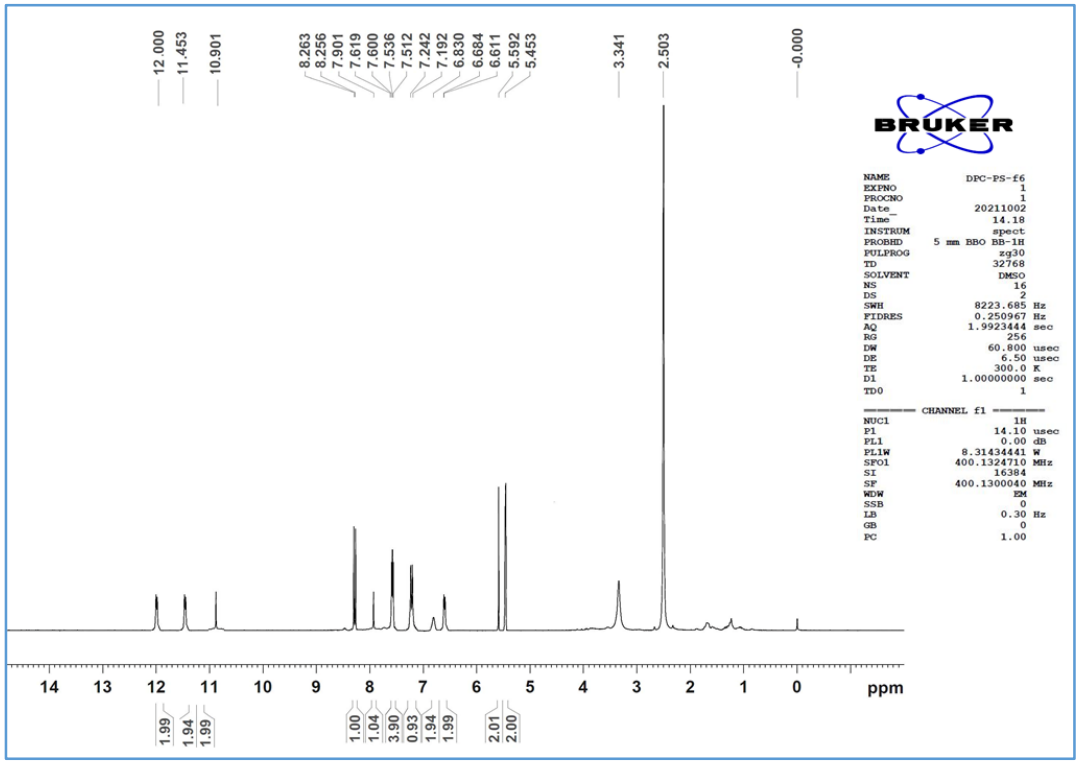

MASS Spectrum of Compound (12b-IV)

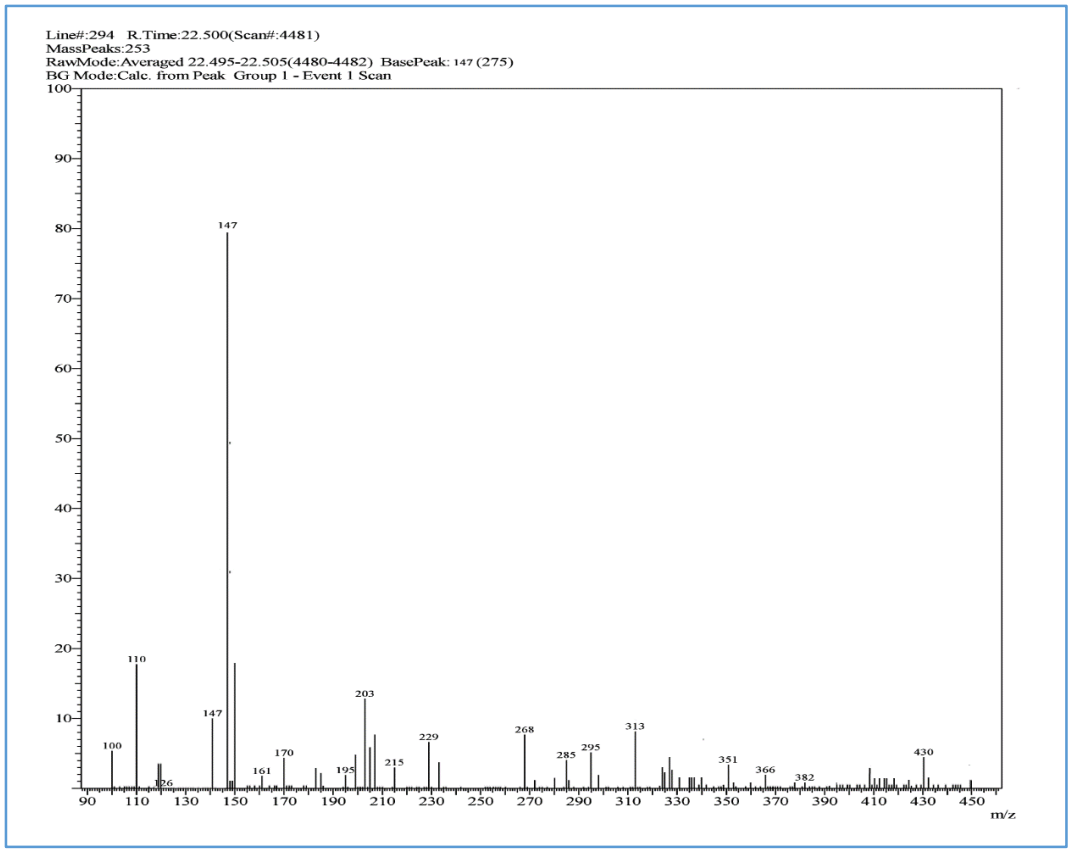

IR Spectrum of Compound (12c-II)

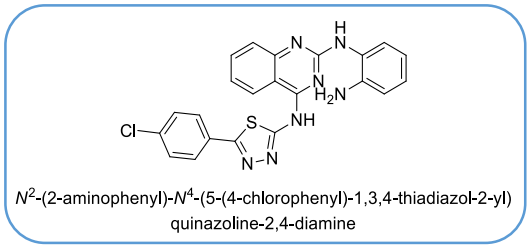

N^2-(2-aminophenyl)-N^4-(5-(4-chlorophenyl)-1,3,4-thiadiazol-2-yl) quinazoline-2,4-diamine

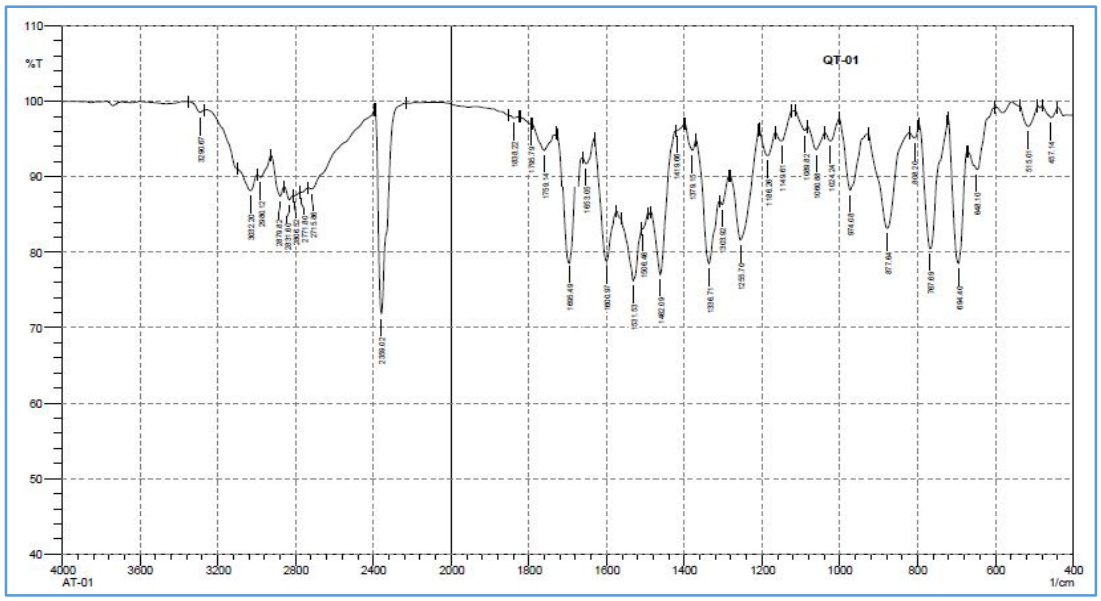

NMR Spectrum of Compound (12c-II)

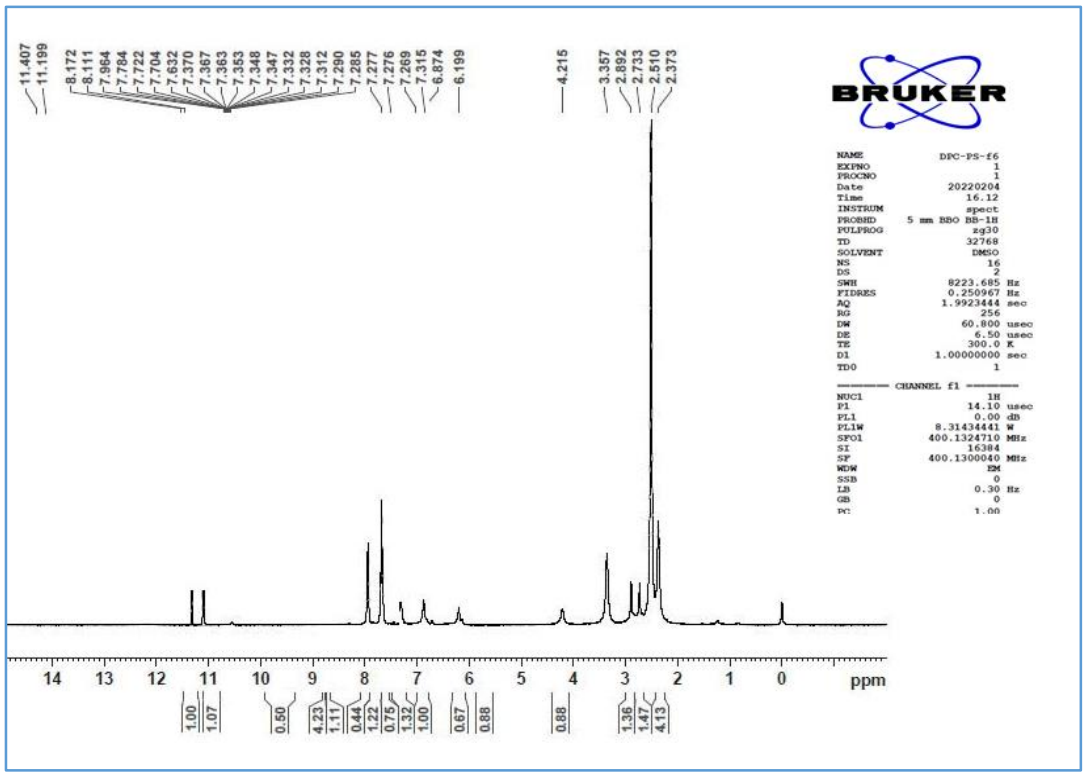

MASS Spectrum of Compound (12c-II)

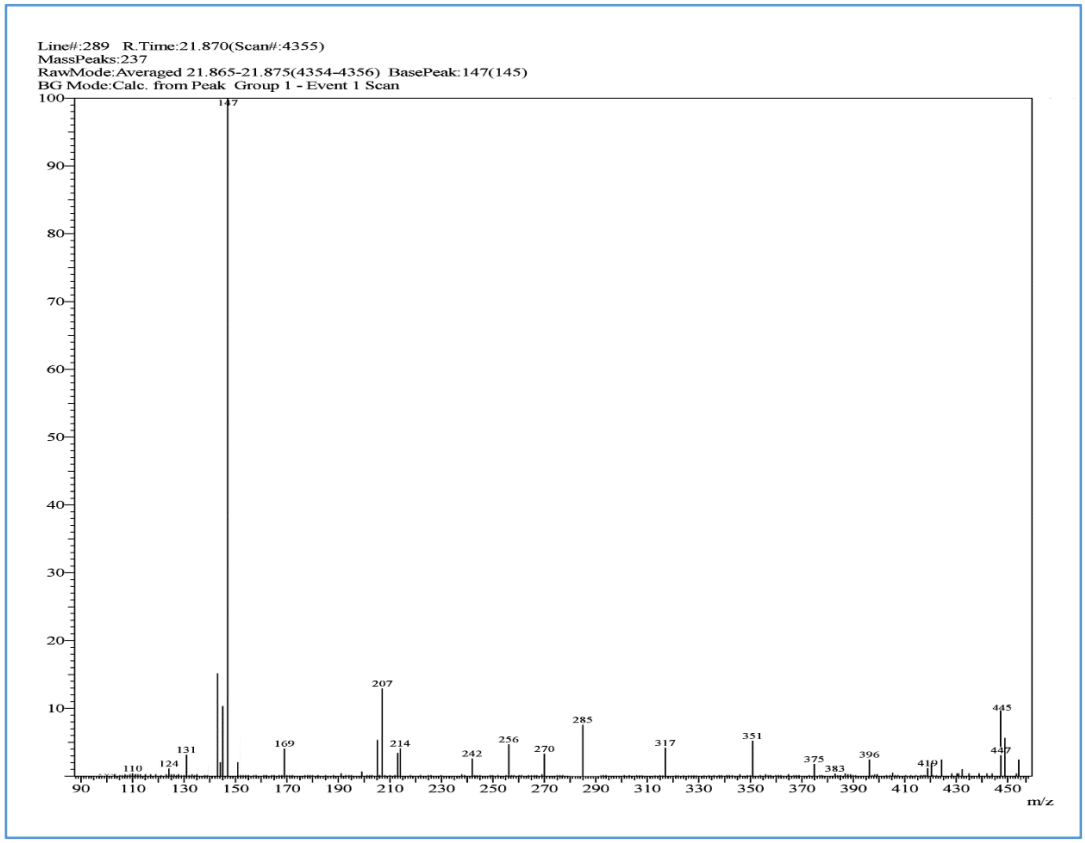

IR Spectrum of Compound (12c-IV)

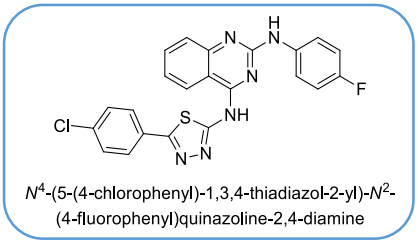

N^4-(5-(4-chlorophenyl)-1,3,4-thiadiazol-2-yl)-N^2-(4-fluorophenyl)quinazoline-2,4-diamine

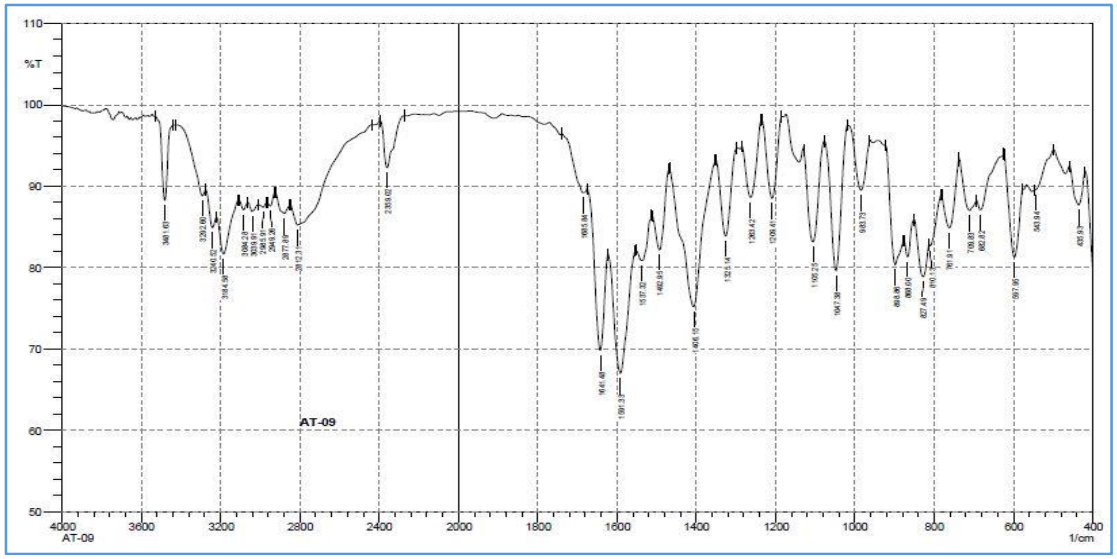

NMR Spectrum of Compound (12c-IV)

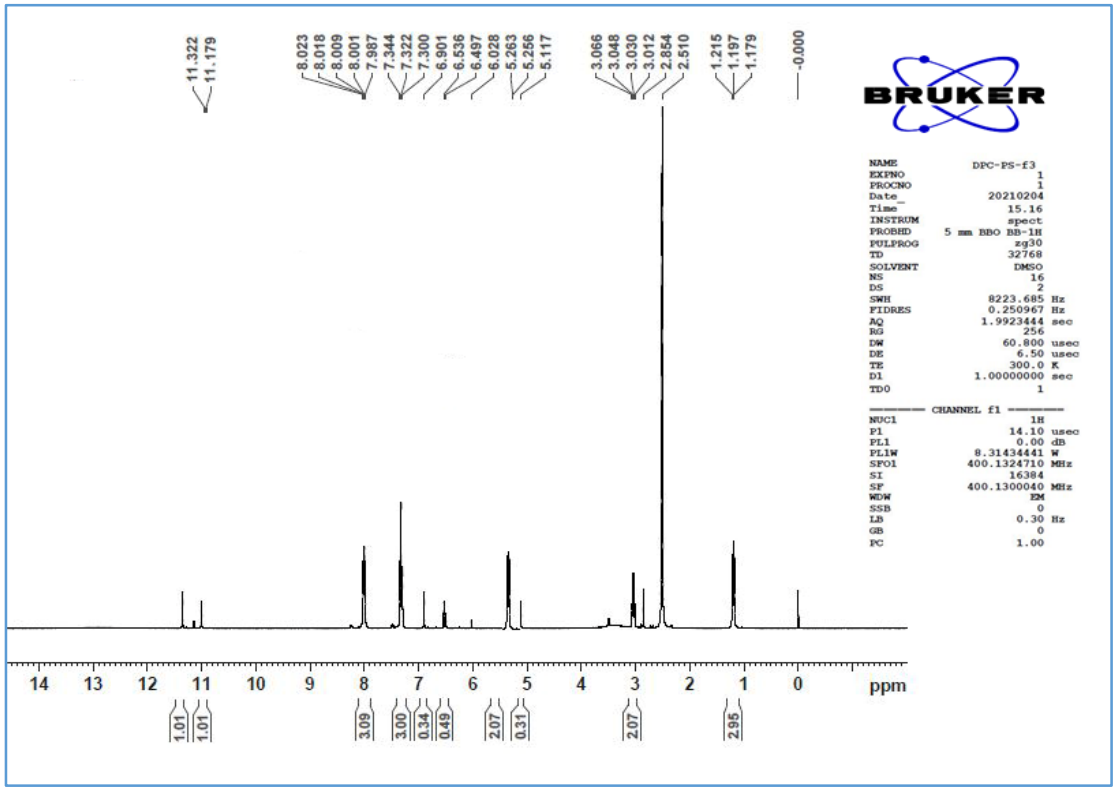

MASS Spectrum of Compound (12c-IV)

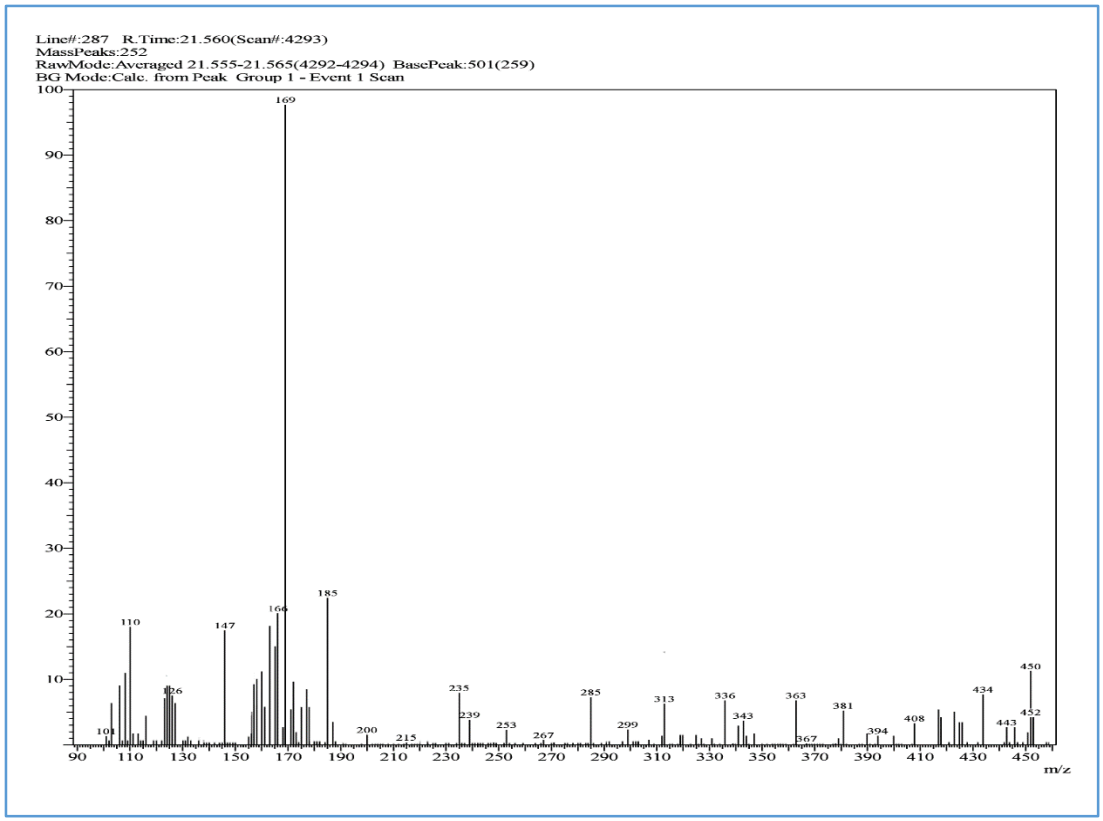

IR Spectrum of Compound (12d-II)

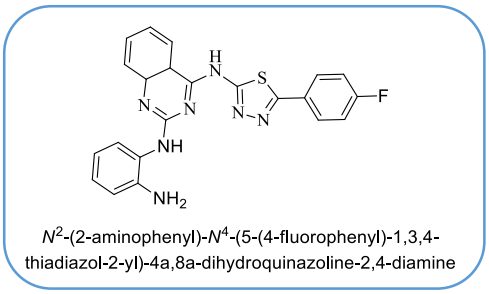

N^2-(2-aminophenyl)-N^4-(5-(4-fluorophenyl)-1,3,4-thiadiazol-2-yl)-4a,8a-dihydroquinazoline-2,4-diamine

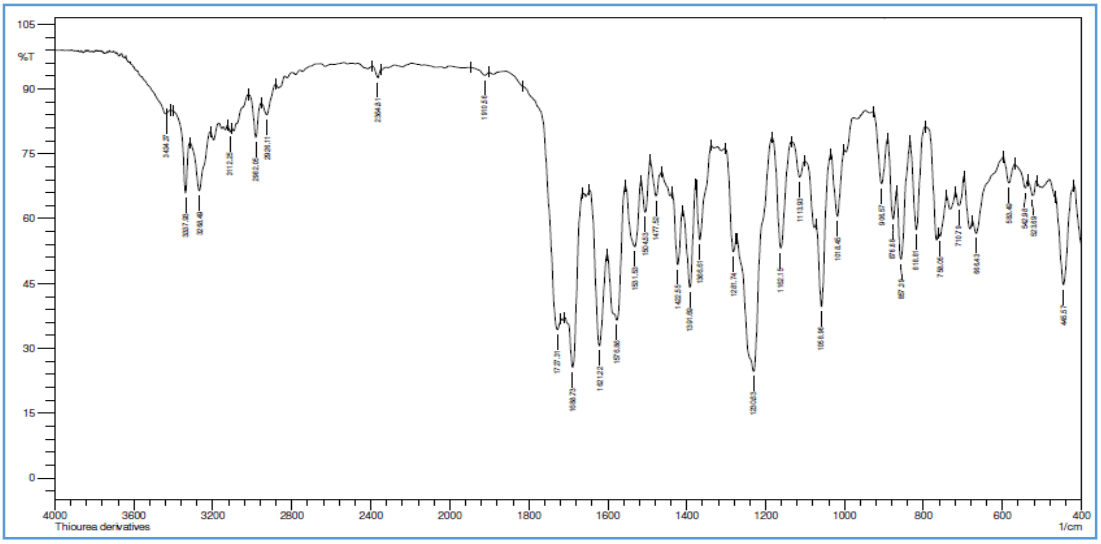

NMR Spectrum of Compound (12d-II)

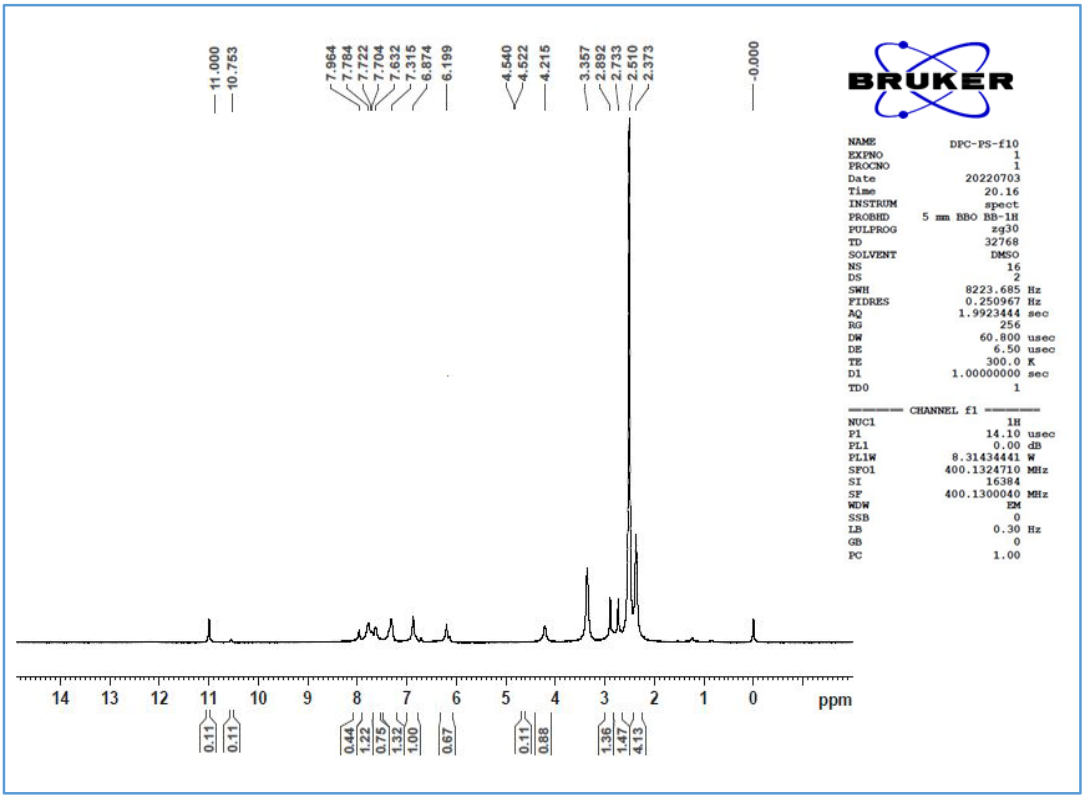

MASS Spectrum of Compound (12d-II)

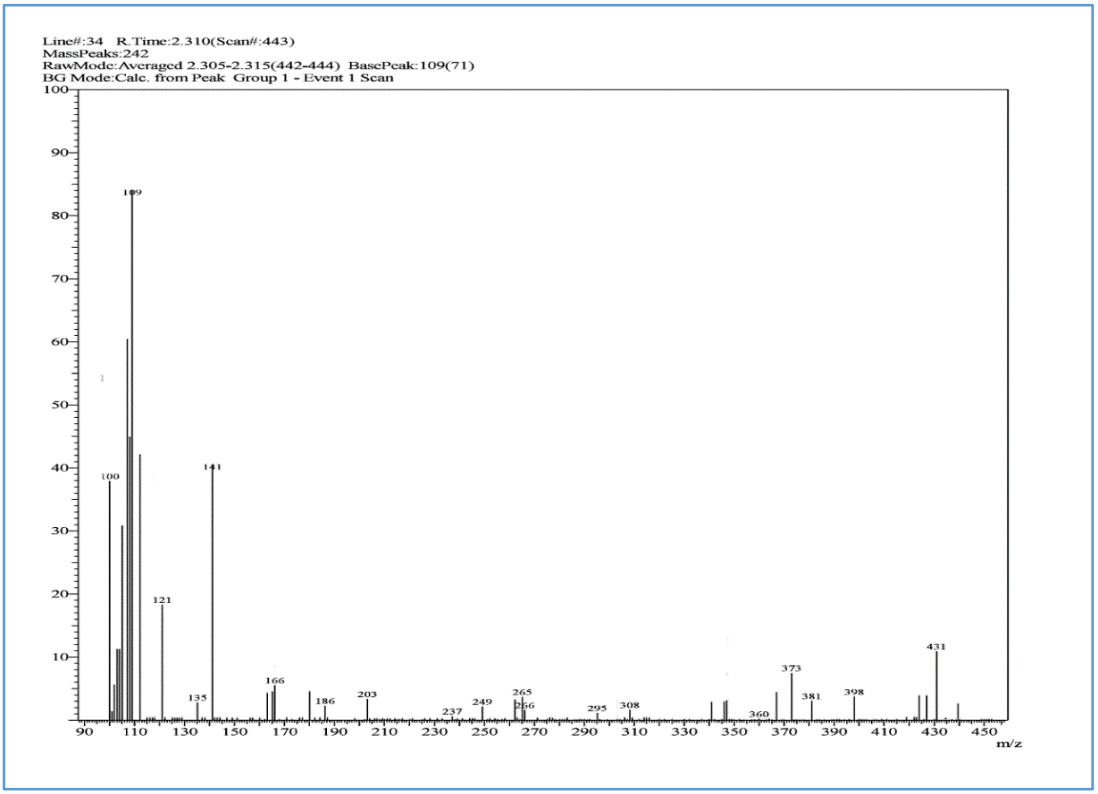

IR Spectrum of Compound (12d-IV)

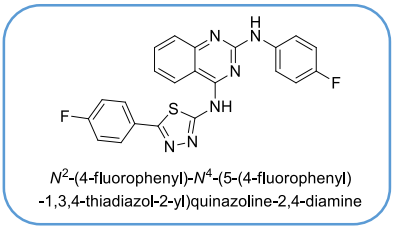

N^2-(4-fluorophenyl)-N^4-(5-(4-fluorophenyl)-1,3,4-thiadiazol-2-yl)quinazoline-2,4-diamine

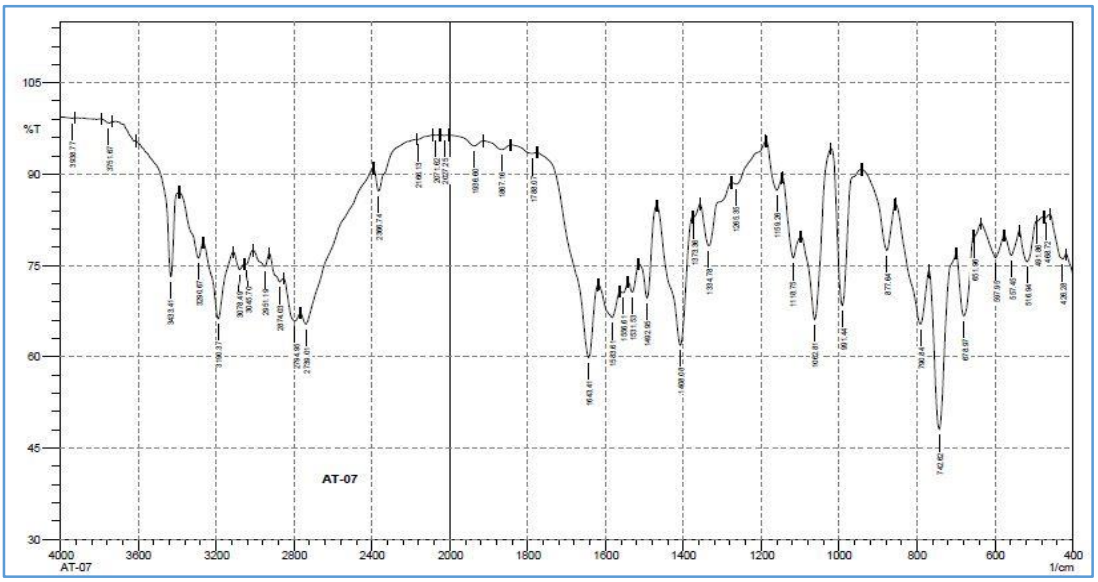

NMR Spectrum of Compound (12d-IV)

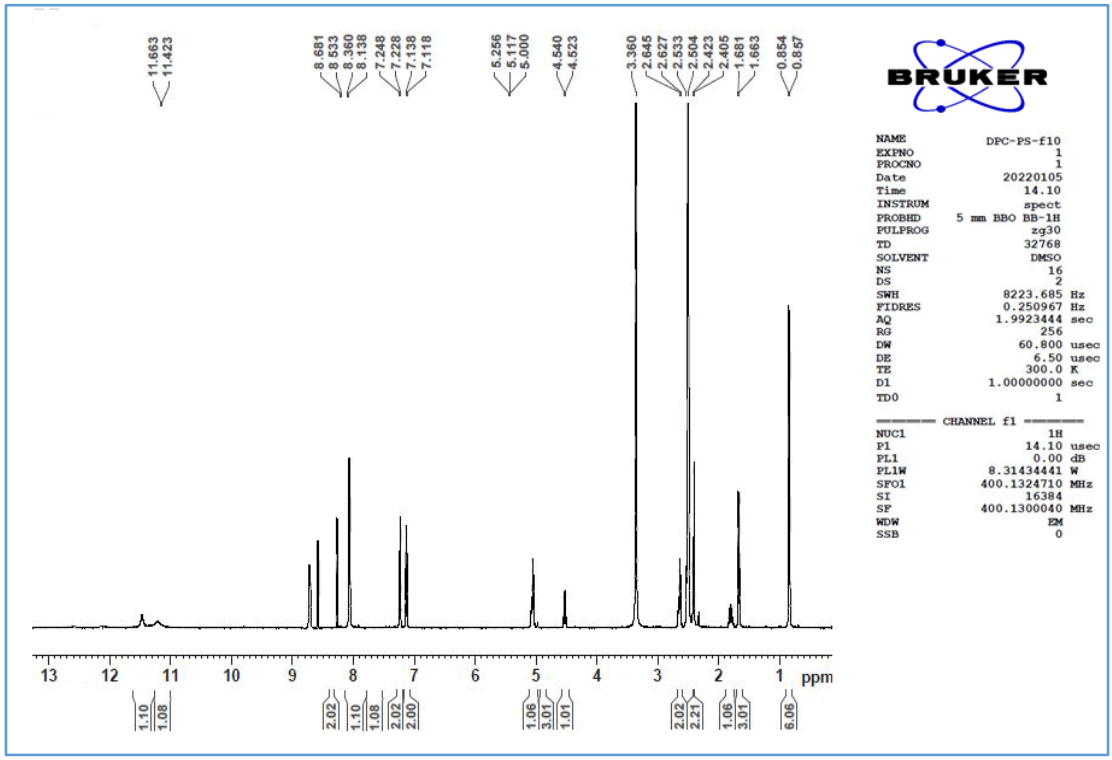

MASS Spectrum of Compound (12d-IV)

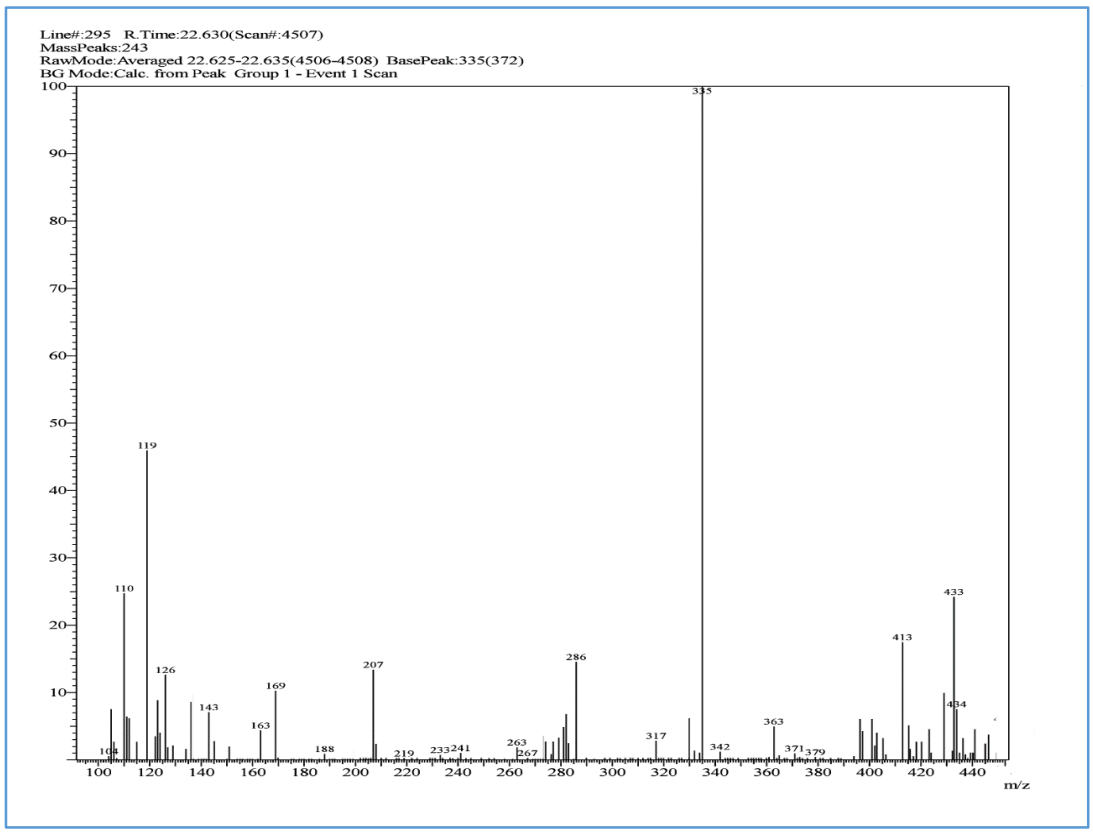

IR Spectrum of Compound (12g-IV)

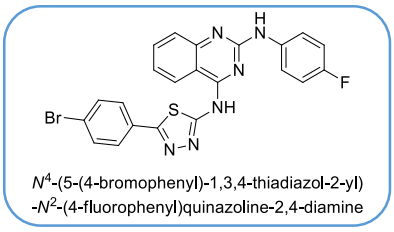

N^4-(5-(4-bromophenyl)-1,3,4-thiadiazol-2-yl) -N^2-(4-fluorophenyl)quinazoline-2,4-diamine

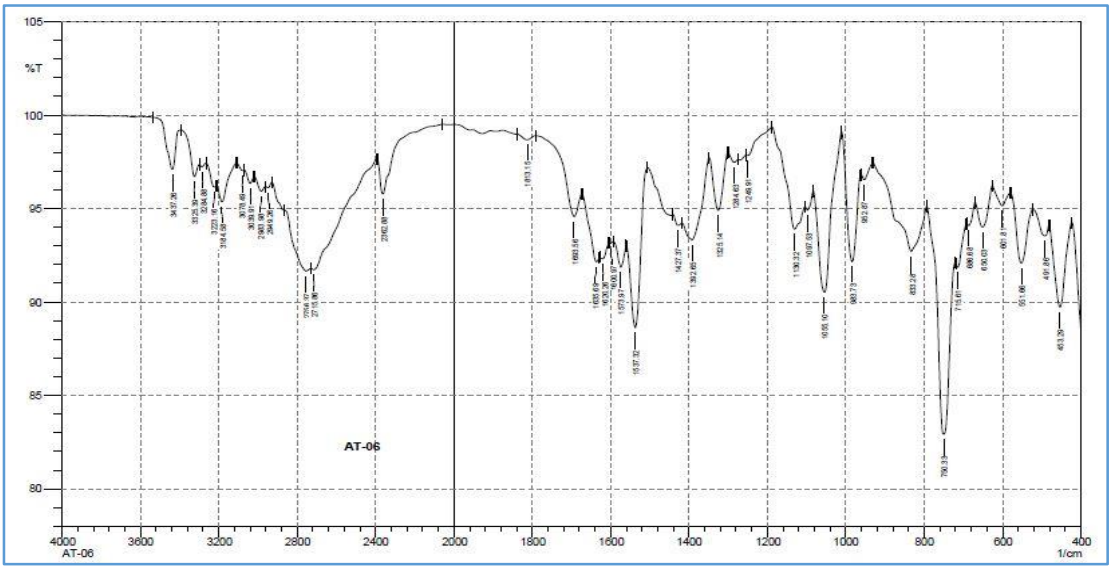

NMR Spectrum of Compound (12g-IV)

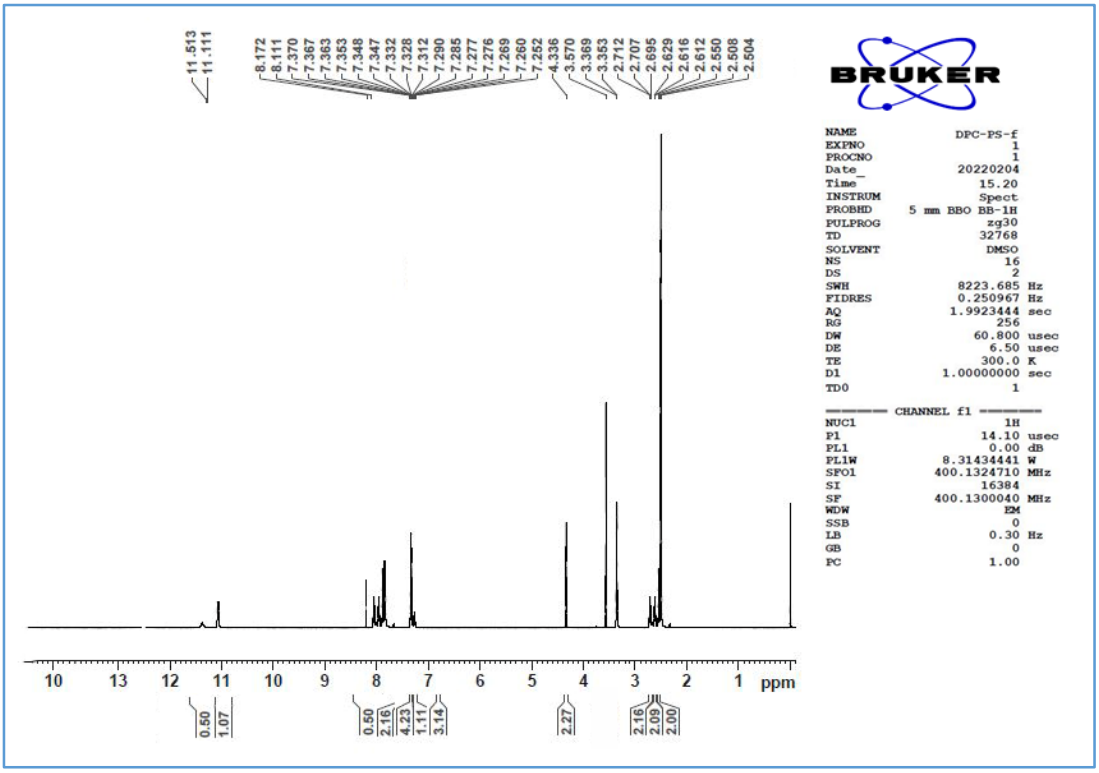

MASS Spectrum of Compound (12g-IV)

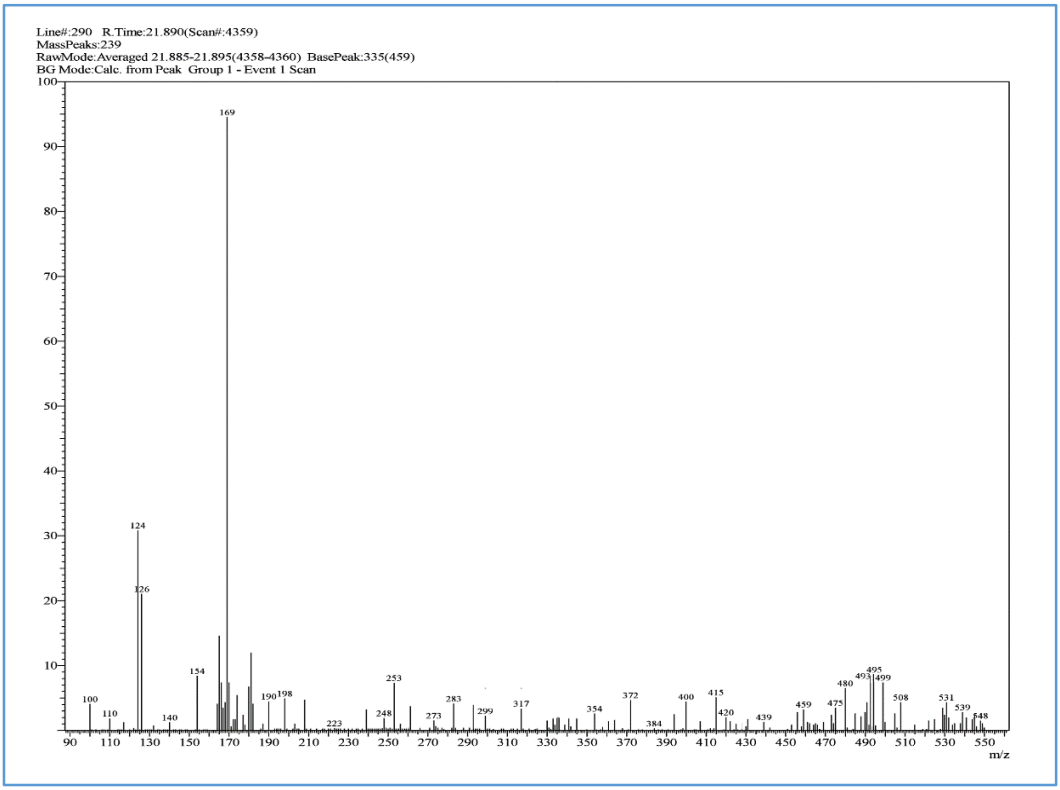

IR Spectrum of Compound (12g-V)

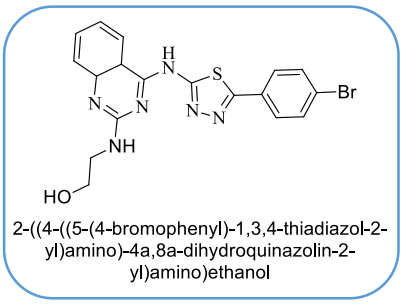

2-((4-((5-(4-bromophenyl)-1,3,4-thiadiazol-2-yl)amino)-4a,8a-dihydroquinazolin-2-yl)amino)ethanol

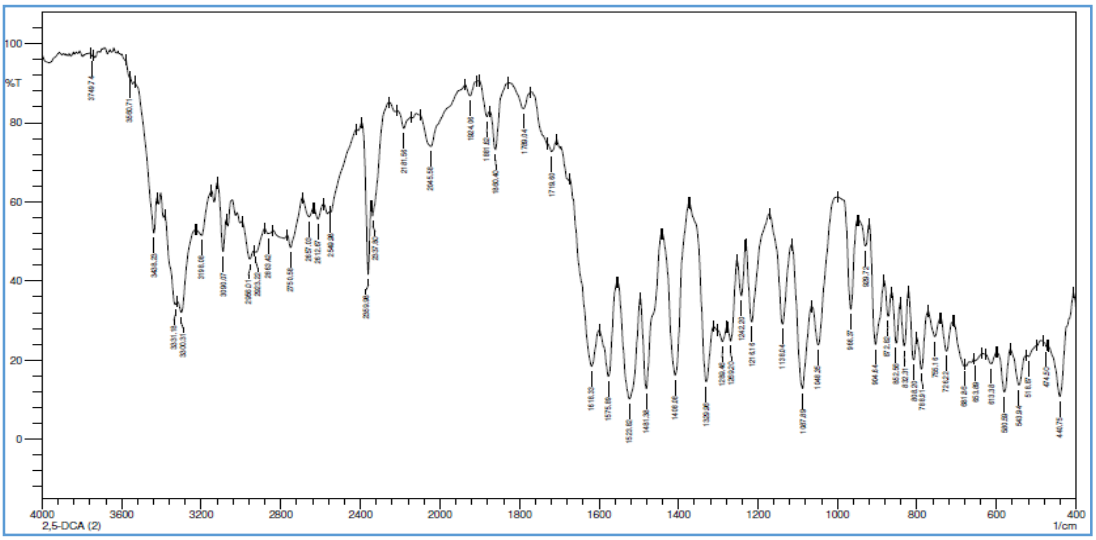

NMR Spectrum of Compound (12g-V)

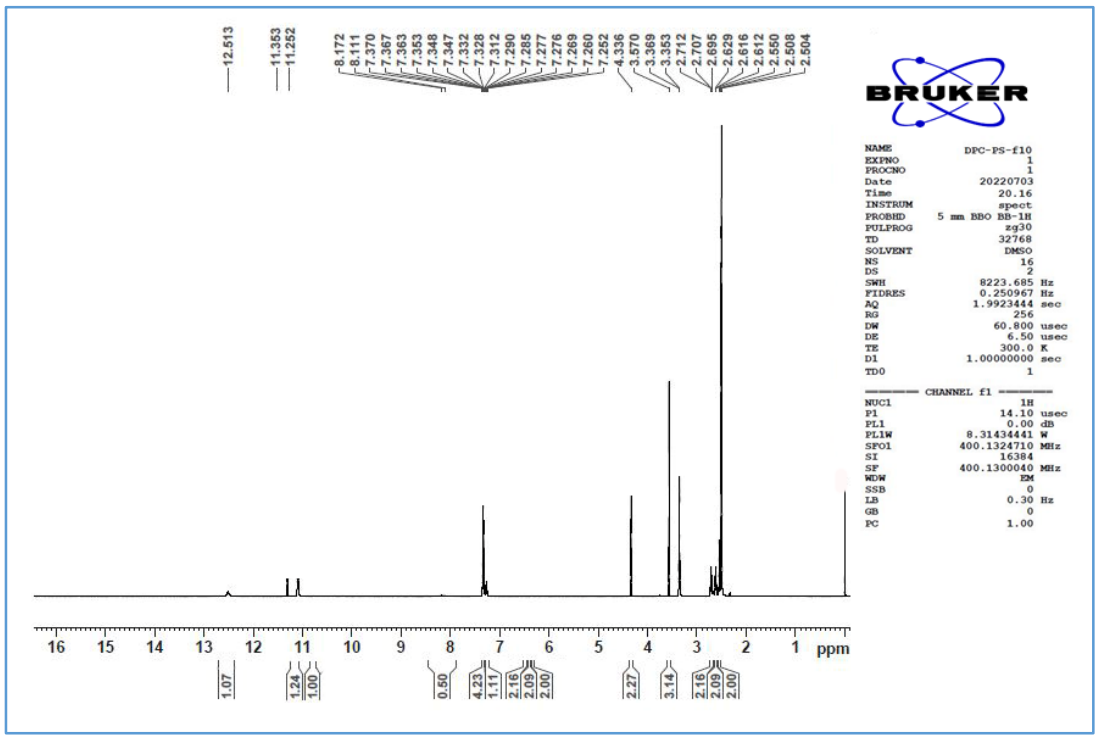

MASS Spectrum of Compound (12g-V)

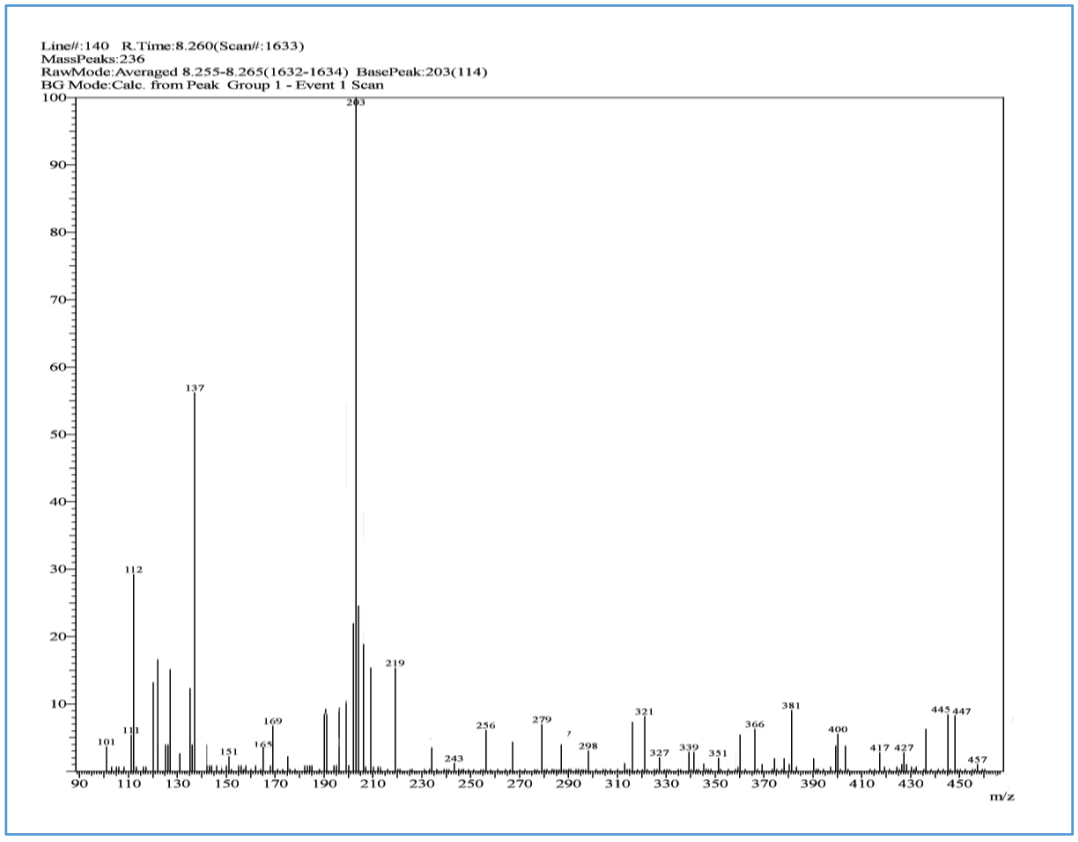

IR Spectrum of Compound (12e-IV)

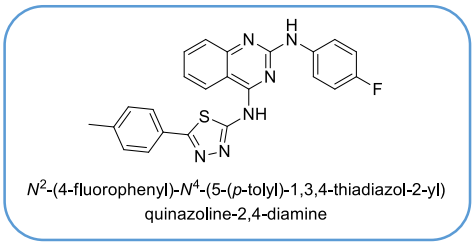

N^2-(4-fluorophenyl)-N^4-(5-(*p*-tolyl)-1,3,4-thiadiazol-2-yl) quinazoline-2,4-diamine

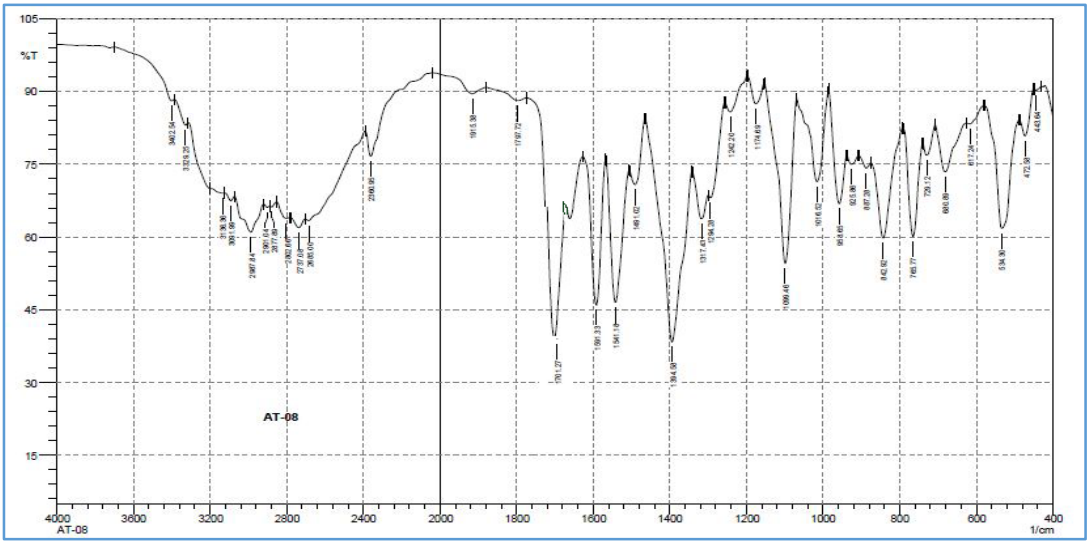

NMR Spectrum of Compound (12e-IV)

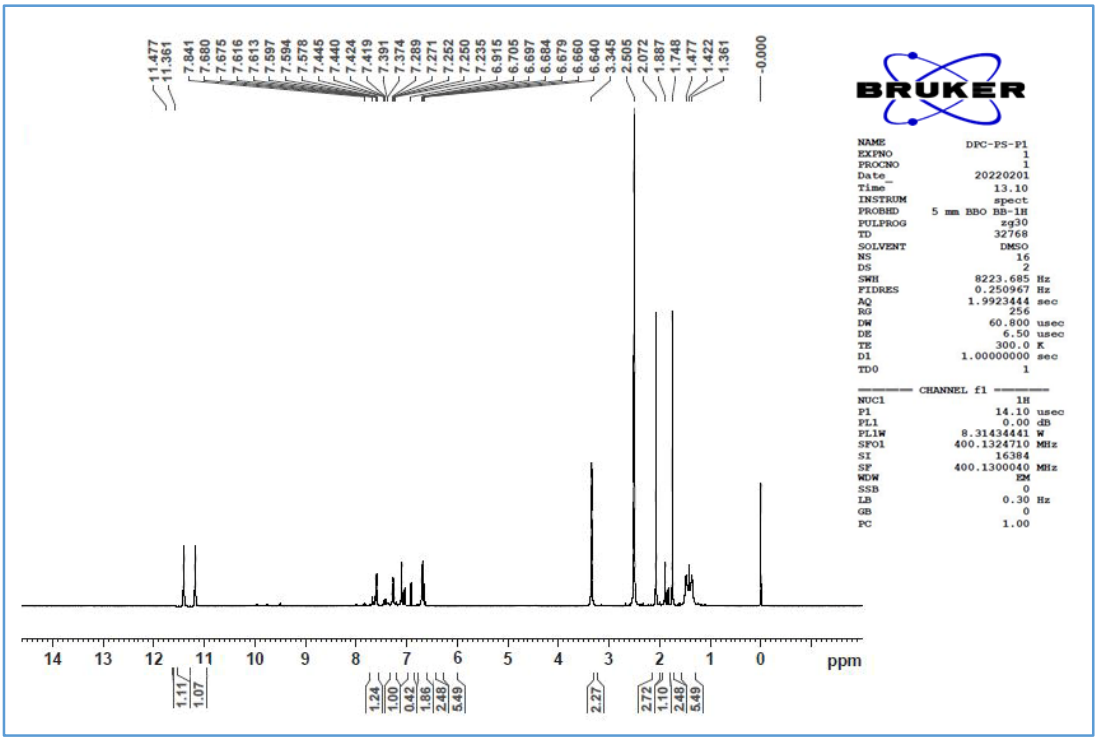

MASS Spectrum of Compound (12e-IV)

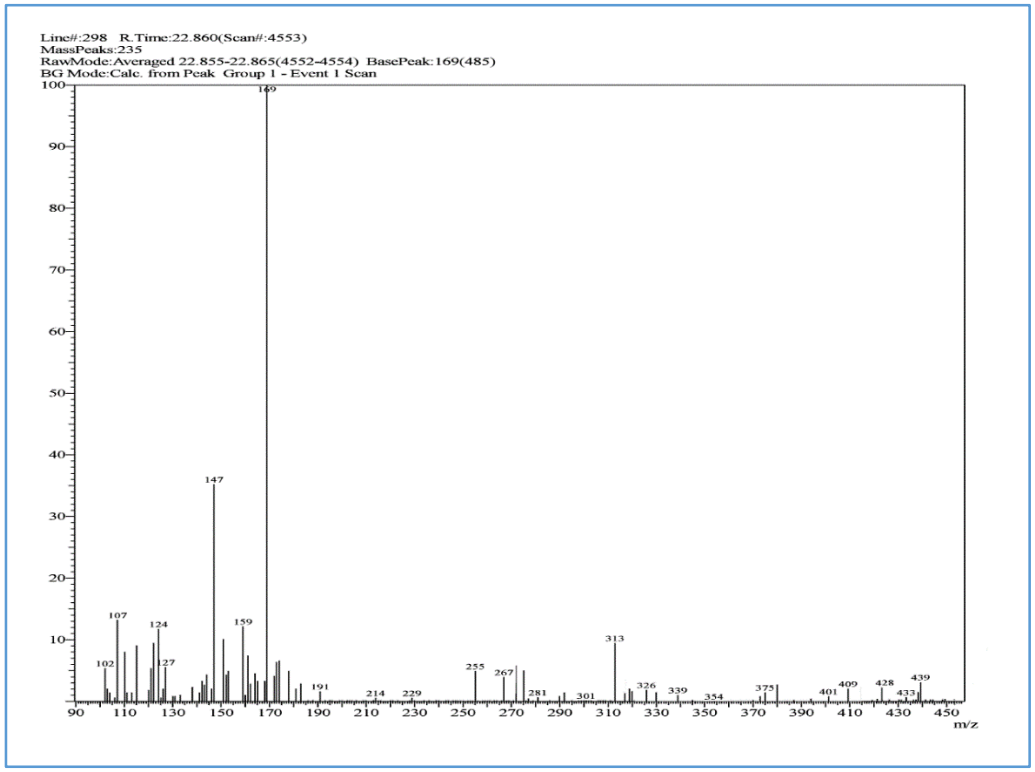

IR Spectrum of Compound (12e-V)

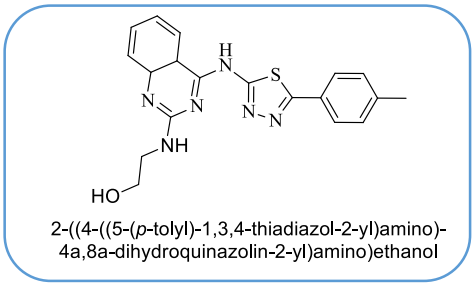

2-((4-((5-(*p*-tolyl)-1,3,4-thiadiazol-2-yl)amino)-4a,8a-dihydroquinazolin-2-yl)amino)ethanol

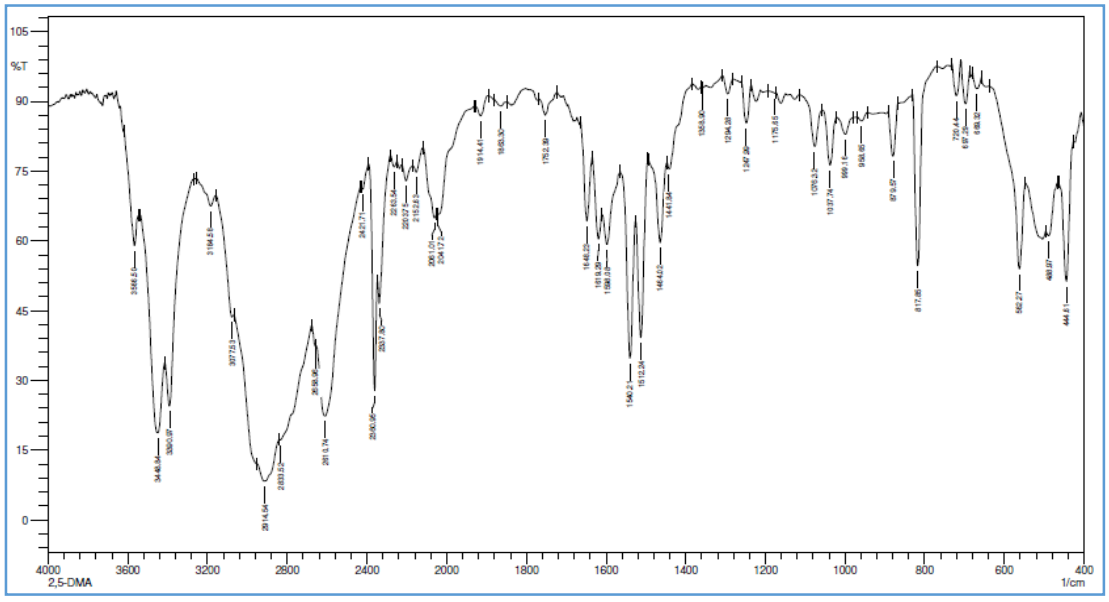

NMR Spectrum of Compound (12e-V)

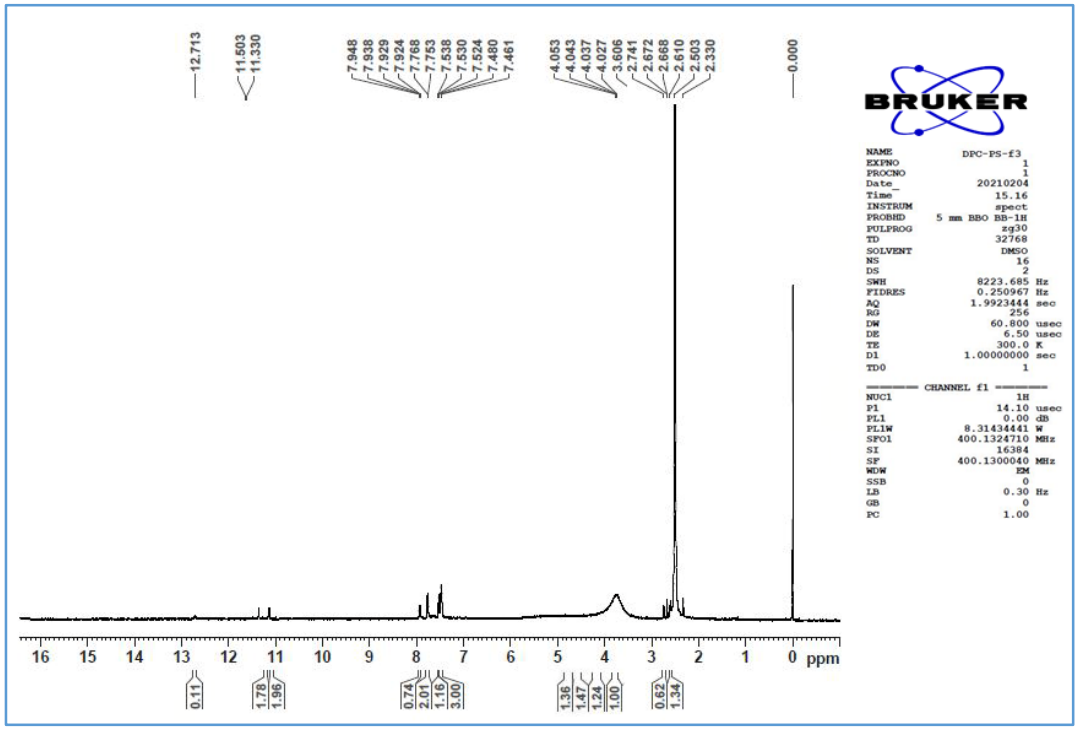

MASS Spectrum of Compound (12e-V)

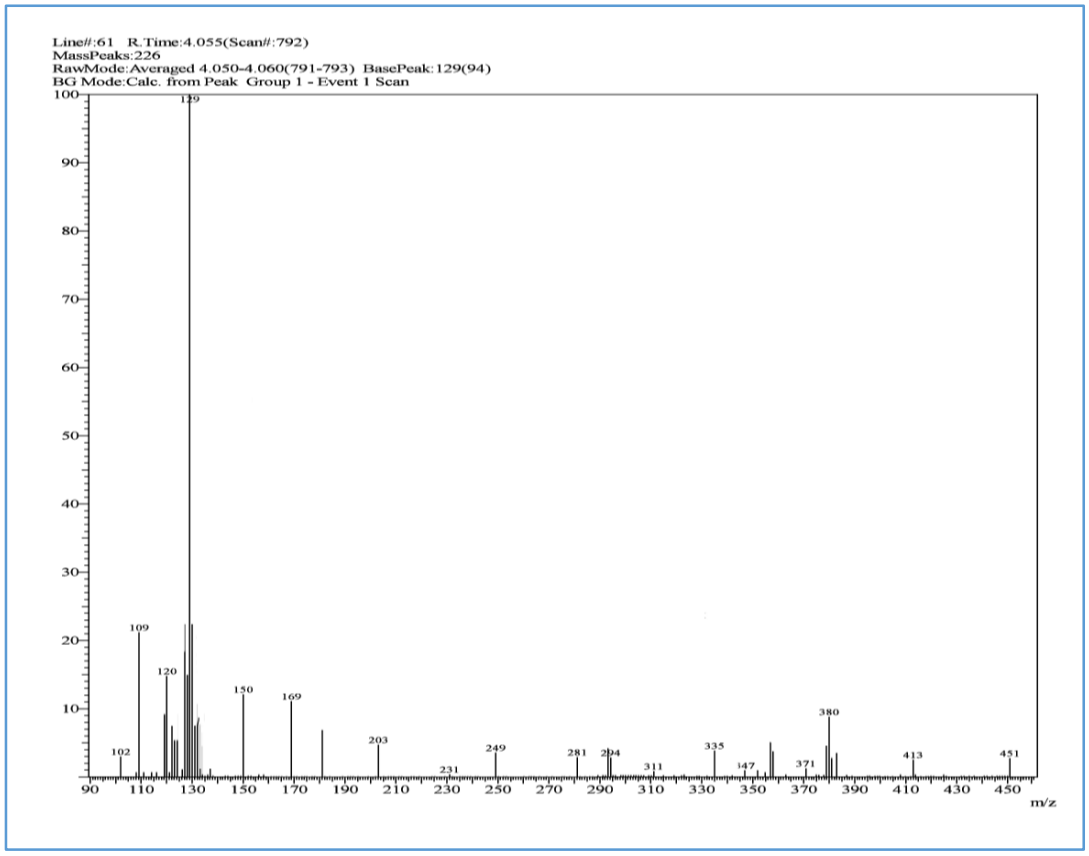

APPENDIX-B: LIST OF CHEMICALS

Sr. No.	Chemical Name	Manufacture
1	Thiosemicarbazide	Astron
2	Phosphorous Oxychloride	Spectrochem
3	Sodium Hydroxide	Rankem
4	Dimethylformmaide	Rankem
5	Methanol	Rankem
6	Chloroform	Rankem
7	Dichloro Methane	Finar
8	Dimethyl Sulfoxide	Rankem
9	N,N Diethyl isopropyl ethylamine	Rankem
10	Urea	Loba

APPENDIX-C: LIST OF EQUIPMENT AND INSTRUMENTS

Sr. No.	Name	Manufacturer/Model
1	Magnetic Stirrer	Patel Scientific Instruments
2	Magnetic Stirrer with Thermostate	Heidolph
3	Hot Plate	Patel Scientific Instruments
4	Electric Waterbath	Narang Scientific Works (NSW-129)
5	FT-IR Spectrophotometer	Shimadzu-8400S
6	Melting Point Apparatus	Veego (VMP-PM)
7	UV Cabinet	Patel Scientific Instruments
8	Digital Weighing Balance	Shimadzu AUX 220
9	Rota Evaporater	Heidolph
10	Hot Air Oven	Patel Scientific Instruments
11	^{1}H NMR	Bruker AvanceIII 400 MHz
12	MASS Spectrophotometer	Shimadzu QP 2010
13	Deep Freezer	Pooja Deep
14	Cell culture hood (i.e., laminar-flow hood or biosafety cabinet) • Incubator (humid CO2 incubator recommended) • Water bath • Centrifuge • Refrigerator and freezer (–20°C) • Cell counter (e.g., CountessR Automated Cell Counter or hemacytometer) • Inverted microscope • Liquid nitrogen (N2) freezer or cryostorage container • Sterilizer (i.e., autoclave) •Aspiration pump (peristaltic or vacuum) • pH meter • Confocal microscope • Flow cytometer	

APPENDIX-D: LIST OF ABBREVIATION

Sr. No.	Abbreviation	Full Name
1	Ar	Aromatic
2	%w/v	Percentage weight by volume
3	%w/w	Percentage weight by weight
4	^{0}C	Degree centigrade (Unit of temperature)
5	GI_{50}	50% growth inhibition
6	IC_{50}	50% inhibitory concentration
7	CCl_4	Carbon Tetrachloride
8	V	Voltage
9	Rb	Retinoblastoma
10	UV	Ultra-violate
11	DNA	Deoxyribonucleic acid
12	RNA	Ribonucleic Acid
13	SV 40	Simian Virus 40
14	ULK	Human Autophagy initiation kinase
15	TLC	Thin Layer Chromatography
16	MP	Melting Point
17	^{1}H NMR	Proton nuclear magnetic resonance
18	DIEM	N,N Diethyl isopropyl ethylamine
19	THF	Tetrahydrofuran
20	KBr	Potassium Bromide
21	ppm	Parts per Million
22	EtOH	Ethanol
23	NaOH	Sodium Hydroxide
24	µg	Microgram
25	nM	Nanometer
26	TMS	Trimethyl Silane

Publication

1. **Sidat PS,** Jaber TM, Vekariya SR, Mogal AM, Patel AM, Noolvi M. Anticancer Biological Profile of Some Heterocylic Moieties-Thiadiazole, Benzimidazole, Quinazoline, and Pyrimidine. Pharmacophore. 2022 Jul 1;13(4):59-71. (Web of Science) https://doi.org/10.51847/rT6VE6gESu

2. **Sidat P**, Noolvi M, Patil R, Rathod S. ULK1/2 Inhibitor: Essential Component of Autophagic Cell Death Machinery. Journal of Pharmaceutical Research. 2022 Jul;21(3):56. (Web of Science) https://doi.org/10.18579/jopcr/v21i3.4

3. N Noolvi Malleshappa*, **Salim Sidat Parin**, *et. al;* Exploration of Virtually Designed and Developed Thiadiazole Derivatives as ULK1/2 Inhibitors: In silico Approach, Letters in Drug Design & Discovery 2023; 20(x) (Scopus) http://dx.doi.org/10.2174/1570180820666230825103609

4. **Sidat P**, *et.al;* "Synthesis, DFT Studies, and Biological Evaluation of new quinazoline-1,3,4-thiadiazole Derivatives as anti-proliferative agents", has been accepted for publication in Chemistry Africa. (Scopus) https://www2.cloud.editorialmanager.com/chaf/default2.aspx

BHARATI VIDYAPEETH COLLEGE OF PHARMACY, KOLHAPUR

CERTIFICATE

This is to certify that **Ms. Parin Salim Sidat** of Shree Dhanvantary Pharmacy college, Kim, Gujarat has secured **1st rank** from M pharm and Phd category in **'ChemCom-2023: National level e-Poster competition'** organized by PG Department of Pharmaceutical Chemistry at Bharati Vidyapeeth College of Pharmacy, Kolhapur.

Dr.N.R.Jadhav
Vice Principal
Administration

Dr.M.S.Bhatia
Vice Principal
Academics
Convenor

Dr.H.N.More
Principal

Dr. (Mrs.) S. A. Arvindekar
Assistant professor
Co-Ordinator

Dr. P. B Choudhari
Associate professer
Chief Coordinator

NIRMA UNIVERSITY
INSTITUTE OF PHARMACY

NCIP 2019

3rd National Conference of Institute of Pharmacy
"Integrating Natural and Modern Medicines in Drug Discovery and Development"
January 24-25, 2019

CERTIFICATE

This is to certify that Dr. / Mr. / Ms. Sidat Parin S.
has attended 3rd National Conference of Institute of Pharmacy held during January 24-25, 2019 as a delegate and presented a poster entitled Design & Synthesis of VIKI/2 Inhibitor as Anticancer Agents.
co-authored by _____.

Prof. Tejal Mehta
Coordinator, Scientific Committee

Dr. Niyati Acharya
Organizing Secretary

Prof. Manjunath Ghate
Convener

Department of Biotechnology
Govt. of India

Institute of Pharmacy, Nirma University, S. G. Highway, Ahmedabad – 382481, Gujarat, INDIA

SHREE SAHKAR EDUCATION TRUST

IQAC of Shree Dhanvantary Pharmacy College, Kim-Surat organized

AICTE Sponsored 2-Days 3rd National Conference

CERTIFICATE OF APPRECIATION

This is to Certify that Dr./Mr./Ms./Mrs.

Parin Salim Sidat

has Presented Poster in AICTE Sponsored two days 3rd National Conference on "ADVANCES IN DRUG DISCOVERY AND DEVELOPMENT " held on 25th & 26th March, 2022 organized by Shree Dhanvantary Pharmacy College, Kim-Surat, On the topic Entitled In silico, mol simulation studies and synthesis of some ulkl 1/2 inhibitors as anti-cancer agents

Co-authored by Parin . Salim . Sidat , M . N Noolvi

Dr. N. D. Jivani
President

Dr. M.N. Noolvi
Convenor

International Conference on Drug Discovery

Nov. 10th & 11th 2022, BITS Pilani, K K Birla Goa Campus

ICDD 2022

Certificate

This is to certify that

Parin Salim Sidat

has successfully participated in International Conference on Drug Discovery held at BITS-Pilani K K Birla Goa Campus on 10th & 11th Nov. 2022 and presented a poster.

R. Raghu
Vice President

Suman Kundu

Prof. Suman Kundu
Director, BITS Pilani
K.K. Birla Goa Campus

Schrödinger | BITS Pilani
K K Birla Goa Campus

Bhagwan Mahavir University

Bhagwan Mahavir College of Pharmacy

Organized

One Day National Conference on

Emerging Trends & Innovation in Pharmaceutical Technology

Certificate of Participation

This certificate is awarded to

Ms. Parin Salim Sidat

in recognition of ~~his~~/her participation for the ~~Poster~~/Oral Presentation at One Day National Conference held on July 1st 2023, organized by Bhagwan Mahavir College of Pharmacy.

Mrs. Velenti Chauhan
Co-convener

Dr. Zarna Dedania
Co-convener

Dr .Vineet Jain
Convener

विज्ञान एवं प्रौद्योगिकी विभाग
DEPARTMENT OF SCIENCE & TECHNOLOGY

G20 भारत 2023 INDIA

Azadi Ka Amrit Mahotsav

Department of Science & Technology (DST) funded Training workshop under STUTI
(Synergistic Training Program Utilizing the Scientific and Technological Infrastructure)

STUTI-DST SCXRD Workshop

Celebrating International Women's Day

CERTIFICATE OF PARTICIPATION

This is to certify that Parin Salim Sidat has participated in the 7 Days Workshop on Single Crystal X-Ray Crystallography at Indian Institute of Technology Gandhinagar, Gujarat held from 15th March to 21st March, 2023.

Prof. Vijay Thiruvenkatam
Event Coordinator